

# รายงานวิจัยฉบับสมบูรณ์

โครงการ เซนเซอร์ทางเคมีโดยอาศัยสมบัติเชิงแสงของวัสดุนาโน Chemical sensors based on the optical properties of nanomaterials

โดย รองศาสตราจารย์ ดร. วิทยา เงินแท้ และคณะ

# รายงานวิจัยฉบับสมบูรณ์

โครงการ เซนเซอร์ทางเคมีโดยอาศัยสมบัติเชิงแสงของวัสดุนาโน Chemical sensors based on the optical properties of nanomaterials

รองศาสตราจารย์ ดร. วิทยา เงินแท้ ภาควิชาเคมี คณะวิทยาศาสตร์ มหาวิทยาลัยขอนแก่น

สนับสนุนโดยสำนักงานกองทุนสนับสนุนการวิจัย

(ความเห็นในรายงานนี้เป็นของผู้วิจัย สกว. ไม่จำเป็นต้องเห็นด้วยเสมอไป)

## บทคัดย่อ

**รหัสโครงการ:** RSA5780021

**ชื่อโครงการ:** เซนเซอร์ทางเคมีโดยอาศัยสมบัติเชิงแสงของวัสดุนาโน

เจ้าของโครงการ: รศ. ดร. วิทยา เงินแท้

ภาควิชาเคมี คณะวิทยาศาสตร์ มหาวิทยาลัยขอนแก่น

จดหมายอิเล็กทรอนิกส์: wittayange@kku.ac.th

ระยะเวลาของโครงการ: มิถุนายน 2557 - มิถุนายน 2560

ความก้าวหน้าล่าสุดของงานวิจัยทางนาโนเทคโนโลยีและวัสดุนาโนคือการได้นำเอามาใช้ในงานทางด้าน เคมีวิเคราะห์ในการออกแบบฟลูออเรสเซนซ์โพรบเป็นจำนวนมาก ซึ่งในงานวิจัยจะนี้มุ่งเน้นการสังเคราะห์และ ประยุกต์ใช้วัสดุนาโนที่แตกต่างกันสองชนิด ประกอบด้วย ซิลเวอร์นาโนคลัสเตอร์ (AgNCs) และ แคดเมียมซัลไฟด์ ควอนตัมดอท (CdS QDs) เพื่อสร้างเป็นเซนเซอร์เชิงแสง

งานวิจัยนี้ทำการสังเคราะห์ซิลเวอร์นาโนคลัสเตอร์โดยการใช้พอลีอิเล็กโทรไลต์ คือพอลีเมททาคลิลิค แอซิด (PMAA) ซึ่งทำหน้าที่เป็นตัวรีดิวซ์และแม่แบบในการเกิดอนุภาคนาโน จากนั้นนำไปใช้เป็นคัลเลอร์รีเมตริก และฟลูออเรสเซนซ์เซนเซอร์สำหรับการวิเคราะห์เชิงคุณภาพและปริมาณของ  $Fe^{2+}$  และ  $Co^{2+}$  ตามลำดับ การ สร้างคัลเลอร์รีเมตริกเซนเซอร์แนวทางใหม่สำหรับตรวจวัด  $Fe^{2+}$  ทำได้โดยการใช้ ซิลเวอร์นาโนคลัสเตอร์ พบว่า เมื่อสารละลายมี  $Fe^{2+}$  สีของสารละลายซิลเวอร์นาโนคลัสเตอร์จะเปลี่ยน เป็นสีส้ม และสามารถสังเกตการ เปลี่ยนแปลงนี้ได้ด้วยตาเปล่า นอกจากนั้นยังได้นำเอาซิลเวอร์นาโนคลัสเตอร์นี้ไปประยุกต์ต่อ โดยทำการปรับปรุง ซิลเวอร์นาโนคลัสเตอร์โดยใช้ซิสเตอีน (L-Cyst-AgNCs) แล้วใช้ในการตรวจวัด  $Co^{2+}$  พบว่าเมื่อสารละลายมี  $Co^{2+}$  ผสมอยู่ ความเข้มของการคายแสงฟลูออเรสเซนซ์ของ L-Cyst-AgNCs มีค่าลดลงและแปรผันตามความเข้มข้นของ  $Co^{2+}$  ที่เพิ่มขึ้น การศึกษาดังกล่าวนี้แสดงให้เห็นว่า L-Cyst-AgNCs เป็นเซนเซอร์ที่มีความจำเพาะเจาะจงต่อ  $Co^{2+}$  เมื่อเปรียบเทียบกับโลหะไอออนชนิดอื่นๆ

นอกจากนั้นแล้วงานวิจัยนี้ยังมุ่งเน้นในการสร้างเซอร์คูลาร์ไดโครอิซึมเซนเซอร์ โดยอาศัยสมบัติเชิงแสงที่ เป็นเอกลักษณ์ของผลึกนาโนของสารกึ่งตัวนำ แคดเมียมซัลไฟด์ควอนตัมดอท (CdS QDs) โดยทำการเสนอ แนวทางใหม่เพื่อตรวจวัด Ni²+ และ Co²+ โดยวัดสัญญาณการบิดระนาบแสงโพลาไรซ์ (CD) ของแคดเมียมซัลไฟด์ ควอนตัมดอทที่มีโมเลกุลปกคลุมเป็นซิสเตอีน (L-Cyst-CdS QDs) พบว่าการมี Ni²+ หรือ Co²+ จะส่งผลให้ สเปกตรัมของการบิดระนาบแสงโพลาไรซ์ของ L-Cyst-CdS QDs มีการเปลี่ยนแปลงอย่างมีนัยสำคัญ เนื่องจากเกิด สารประกอบเชิงซ้อนไครัลปกคลุมบนพื้นผิวของควอนตัมดอท นอกจากนั้นยังทำการสร้างเซนเซอร์การบิดระนาบ แสงแนวทางใหม่โดยการใช้แคดเมียมซัลไฟด์ควอนตัมดอทที่ปกคลุมด้วยซิสเตียมีน (Cys-CdS QDs) เพื่อเป็น เซนเซอร์สำหรับตรวจวัดและพิสูจน์เอกลักษณ์ใครัลของเพนนิซิลลามีน (PA) ซึ่งโดยทั่วไป D-PA และ L-PA ให้ สัญญาณการบิดระนาบแสงโพลาไรซ์ที่น้อย และ Cys-CdS QDs ไม่สามารถให้สัญญาณการบิดระนาบแสงโพลาไรซ์ของ D-PA และ L-PA สามารถทำให้มีค่าสูงขึ้นและทำ การตรวจวัดได้เมื่อมี Cys-CdS QDs อยู่ร่วมด้วย

งานวิจัยนี้ยังทำการศึกษาเพิ่มเติมในการสร้างฟลูออเรสเซนซ์เซนเซอร์โดยการใช้ CdS QDs สำหรับ ตรวจวัด Cu<sup>2+</sup>, Hg<sup>2+</sup> และ cysteamine โดยพบว่า Cys-CdS QDs สามารถนำมาใช้เป็นฟลูออเรสเซนซ์เซนเซอร์ แบบเปิดสัญญาณเพื่อตรวจวัด Cu<sup>2+</sup> และการคายแสงฟลูออเรสเซนซ์ของ Cys-CdS QDs มีการเปลี่ยนแปลงสอง แบบคือมีความเข้มการคายแสงเพิ่มขึ้นและเกิดการเลื่อนของความยาวคลื่นไปทางแสงสีแดงเมื่อมีการเติม Cu<sup>2+</sup> นอกจากนี้พบว่าค่าความเข้มของการคายแสงฟลูออเรสเซนซ์ของ Cys-CdS สามารถเปลี่ยนแปลงได้เมื่อมีการ ปรับปรุงพื้นผิวโดยการใช้ Ag<sup>+</sup> (Ag<sup>+</sup>@Cys-CdS QDs) และสามารถนำมาใช้เป็นฟลูออเรสเซนซ์เซนเซอร์ในการ ตรวจวัด Hg<sup>2+</sup> โดยการคายแสงของ Ag <sup>+</sup>@Cys-CdS QDs มีการลดลงแม้มีปริมาณ Hg<sup>2+</sup> ที่ระดับความเข้มข้นน้อย มาก เนื่องจากเกิดอันตรกิริยาแบบเมทัลโลฟิลิค ระหว่าง Hg<sup>2+</sup> และ Ag<sup>+</sup> ส่วนงานวิจัยสุดท้าย ได้นำเอาแคดเมียม ซัลไฟด์ควอนตัมดอทที่ปกคลุมพื้นผิวด้วยเพนนิซิลลามีน (DPA-CdS QDs) เพื่อใช้เป็นฟลูออเรสเซนซ์เซนเซอร์ สำหรับตรวจวัดซีสเตียมีน เมื่อในระบบมีซีสเตียมีน จะส่งผลให้ความเข้มของการคายแสงฟลูออเรสเซนซ์ของ DPA-CdS QDs มีค่าเพิ่มขึ้นตามปริมาณของซิสเตียมีนที่เพิ่มขึ้น เซนเซอร์ที่เสนอขึ้นมานี้สามารถนำมาใช้ในการตรวจวัด ซีสเตียมีนในตัวอย่างน้ำปัสสาวะอย่างมีประสิทธิภาพด้วยความแม่นที่สูง

#### Abstract

**Project Code:** RSA5780021

**Project Title:** Chemical sensors based on the optical properties of nanomaterials

Investigator: Associate Professor Dr. Wittaya Ngeontae

Department of Chemistry, Faculty of Science,

Khon Kaen University

E-mail Address: wittayange@kku.ac.th

**Project Period:** June 16, 2014 to June 16, 2017

The recent advances in nanotechnology and nanomaterials have been integrated into analytical chemistry for the design of large numbers of fluorescent chemical probes. In this work focused on the synthesis and application of two different types of nanomaterials including silver nanoclusters (AgNCs) and cadmium sulfide quantum dots (CdS QDs) for fabrication of the optical sensors.

A water-soluble AgNCs was synthesized by using polyelectrolyte poly(methacrylic acid) (PMAA) as a reducing agent and template and demonstrated to use as a selective colorimetric sensor and fluorescence sensor for qualitative and quantitative analysis of  $Fe^{2+}$  and  $Co^{2+}$ , respectively. A new colorimetric sensor for selective detection of  $Fe^{2+}$  by utilization of AgNCs was demonstrated. In the presence of  $Fe^{2+}$ , the color of AgNCs turned to orange and can be observed by the naked eye. This work was extended by the modification of AgNCs with L-Cysteine (L-Cyst-AgNCs) to be a  $Co^{2+}$  sensor. In the presence of  $Co^{2+}$ , the fluorescence intensity of L-Cyst-AgNCs was quenched as a linear function with the increasing of  $Co^{2+}$  concentration. The L-Cyst-AgNCs showed good selectivity towards the detection of  $Co^{2+}$  compared to other tested metal ions.

In addition, this work focused on the fabrication of circular dichroism sensors based on the unique optical property of the synthesized nanocrystalline semiconductor cadmium sulfide quantum dots (CdS QDs). A new approach for selective determination of Ni<sup>2+</sup> and Co<sup>2+</sup> by measuring a circular dichroism (CD) signal of CdS QDs capped with L-Cysteine (L-Cyst-CdS QDs) was demonstrated. In the presence of Ni<sup>2+</sup> or Co<sup>2+</sup>, the CD spectra of L-Cyst-CdS QDs were significantly changed due to the formation of new chiral complexes on the capping molecules. In addition, a new CD sensor based upon cysteamine capped CdS QDs (Cys-CdS QDs) was demonstrated for detection and chiral identification of penicillamine (PA). Basically, D-PA and L-PA provide very low CD signals and the Cys-CdS QDs are not optically active in the CD signal. However, the CD signals of D-PA and L-PA can be enhanced in the presence of Cys-CdS QDs.

Furthermore, the fluorescence sensors based CdS QDs were demonstrated for the detection of Cu<sup>2+</sup>, Hg<sup>2+</sup> and cysteamine. The Cys-CdS QDs can be used as a selective turn-on fluorescence sensor for Cu<sup>2+</sup> detection. The fluorescence intensity of the Cys-CdS QDs was both enhanced and red shifted in the presence of Cu<sup>2+</sup>. In addition, the fluorescence intensity of Cys-CdS QDs can be modulated with Ag<sup>+</sup> and employed as fluorescence sensors for the determination of Hg<sup>2+</sup> ion. The fluorescence intensity of the Ag<sup>+</sup> modulated Cys-CdS QDs (Ag<sup>+</sup>@Cys-CdS QDs) was significantly quenched in the presence of trace amounts of Hg<sup>2+</sup> due to high-affinity metallophilic interactions between Hg<sup>2+</sup> and Ag<sup>+</sup>. Finally, D-penicillamine capped cadmium sulfide quantum dots (DPA-CdS QDs) was proposed to be a fluorescence sensor for cysteamine detection. In the presence of cysteamine, the fluorescence intensity of the DPA-CdS QDs was enhanced proportionally with increasing cysteamine concentration. This sensor can be efficiently used for the detection of cysteamine in real urine samples with high accuracy.

# **Executive Summary**

**Project Code:** RSA5780021

**Project Title:** Chemical sensors based on the optical properties of nanomaterials

**Investigator:** Associate Professor Dr. Wittaya Ngeontae

Department of Chemistry, Faculty of Science,

Khon Kaen University

E-mail Address: wittayange@kku.ac.th

**Project Period:** June 16, 2014 to June 16, 2017

This work focused on the utilization of the special optical properties of optical nanomaterials including silver nanoclusters and nanocrystalline cadmium sulfide quantum dots for the fabrication of chemical sensors. Three types of new optical sensors were constructed including colorimetric sensor, fluorescence sensor and circular dichroism sensor. A colorimetric sensor was derived from optical property of the silver nanoclusters templated by polymethacrylic acid for the detection of ferrous ion. A novel concept of circular dichroism sensors based on chiral and achiral cadmium sulfide quantum dots were successfully demonstrated and fabricated. For the chiral quantum dots, L-Cysteine capped cadmium sulfide quantum dots, was used as a sensor probe for the detection of cobalt ion and nickel ion. In addition, achiral quantum dots, cysteamine capped cadmium sulfide quantum dots can be used as chiral identification and detection of penicillamine isomer. Finally, the new fluorescence sensors can be fabricated based on the silver nanoclusters and quantum dots. The silver nanoclusters modified with L-Cysteine can be used to selectively detect cobalt ion. The cadmium sulfide quantum dots capped with cysteamine was used to detect copper ions and can be applied for the detection of mercury ions after modification with silver ion. The cadmium sulfide quantum dots capped with ppenicillamine was utilized as a sensor probe for detection of cysteamine.

# 1. A highly selective colorimetric sensor for ferrous ion based on polymethylacrylic acid-templated silver nanoclusters

### 1. Introduction

Iron is an integral metal ion in many physiological processes involving electron transfer [1]. Basically, it can complex with hemoglobin which carries oxygen from lungs to cells and plays an equally essential role in respiratory enzymes such as cytochromes–[2]. However, accumulation of iron in the central nervous system can cause diseases such as Huntington's, Parkinson's, and Alzheimer's diseases [3]. On the other hand, iron deficiency can be a problem during infancy, pregnancy, and adolescence [4]. In order to avoid the iron deficiency disease, an adequate supply of iron is required by taking dietary supplements, which contain iron, such as multi-vitamins.

It is important to develop simple, accurate, and low cost methods for iron determination. Several methods have been proposed for quantitative analysis of iron such as spectrophotometry [5-10], digital image-based colorimetry [11], flow injection analysis [12-14], fluorescence [15-16], chemiluminescence [17], radiometric [18], ion selective electrode [19-24], voltammetry [25-27], and high performance liquid chromatography [28-30]. Furthermore, atomic absorption [31-32] and inductively coupled plasma mass spectrometry can commonly be used to determine a total concentration of iron in samples [33]. Basically, the simplest method for iron determination is based on the spectrophotometric detection after formation of a colored complex of Fe<sup>2+</sup> with a specific ligand [34]. Several organic dye-based colorimetric probes for Fe<sup>3+</sup> have recently been reported [35-40]. However, organic dyes forming color complexes with Fe<sup>2+</sup> have been rarely studied [41]. Therefore, it is still important to search for a new compound to fabricate a selective colorimetric sensor for detecting Fe<sup>2+</sup> in pharmaceuticals and food supplements [42].

Nanomaterials play an important role in the development of new chemical sensors due to excellent properties over its conventional bulk materials, especially the optical properties. Silver nanoclusters (AgNCs) are a new type of nanomaterials which consist of several to roughly a hundred atoms of silver [43]. The size of AgNCs is bigger than silver atom but smaller than silver nanoparticles resulted in hybrid properties between a single atom and nanoparticles. AgNCs possess a molecule-like property with a discrete electronic energy level [44]. Therefore, when AgNCs are excited by an appropriate light source, the nanoclusters can give fluorescence with high emission rates and large Stokes shifts [45]. Thus, the AgNCs can be used to fabricate the fluorescence sensors.

Recently, different synthetic methods have been developed to prepare water-soluble Ag nanoclusters [46-48] to improve the quality of the nanoclusters. All synthetic methods start from a Ag<sup>+</sup> precursor that must be reduced to Ag<sup>0</sup>. The key point of the nanoclusters synthesis is the use of scaffolds to prevent particle aggregation. There are several types of scaffolds used in the synthesis of AgNCs such as polyelectrolytes, polymers, DNA, and dendrimers [49-52]. In addition, a simple anionic polyelectrolyte poly(methacrylic acid) (PMAA) has been proved to function as an ideal template to generate high quality AgNCs.

The applications of the AgNCs templated by PMAA which were synthesized by different methods have been reported. Most of the reports were based on the measurement of fluorescence emission such as the AgNCs synthesis from UV irradiation process can be used as  $Cu^{2+}$  sensor by measuring the fluorescence quenching [53]. In addition, AgNCs synthesized from a microwave irradiation process were employed as a sensitive and selective fluorescence quenching sensor for  $Cr^{3+}$  [47]. Moreover, AgNCs templated by PMAA were reported as a biosensor for detecting  $\alpha$ -L-fucosidase (AFu) by measuring the fluorescence quenching [54]. From the literature reviews and our knowledge, there is no report regarding

the use of AgNCs templated by PMAA in fabricating colorimetric sensors for the detection of Fe<sup>2+</sup>.

Currently, colorimetric sensors have become popular due to their capabilities to detect target compounds by observing color changes without resorting to any expensive instruments [55]. Thus, the development of naked eye diagnostic tool for selective detection of iron is a challenge in sensor research. In this paper, we aim to fabricate a new colorimetric sensor for selective detection of Fe<sup>2+</sup> by utilization of AgNCs stabilized with PMAA. We hypothesized that in the presence of Fe<sup>2+</sup>, un-reacted Ag<sup>+</sup> in the AgNCs solution can be reduced to Ag<sup>0</sup> and deposit on the AgNCs. Therefore, the increasing particle size and the color changes are expected to be observed by the naked eye. Possible parameters affecting the color change are investigated and optimized to obtain the best sensitivity. Moreover, selectivity of the sensor towards Fe<sup>2+</sup> comparing to other metal ions is also investigated. In addition, the proposed sensor is used to determine Fe<sup>2+</sup> in iron supplement tablets.

# 2. Experimental

## 2.1 Chemicals

All reagents are of analytical grade and used without further purification. Silver nitrate, BDH, England. Poly(methacrylic acid) sodium salt, Sigma-aldrich, Germany. Ferrous ammonium sulphate, Carlo Erba Reagents, Italy. Glacial acetic acid, QRec, Thailand. Sodium hydroxide, Carlo Erba Reagents, Italy. Ferric nitrate nonahydrate, lead (II) nitrate, nickel nitrate hexahydrate and zinc nitrate hexahydrate were purchased from Fluka. Sodium acetate and sodium hydroxide were obtained from Carlo Erba Reagents. Ultrapure water (18.2 M $\Omega$ cm) was obtained from a Millipore water purification system.

## 2.2 Instrumentations

Absorbance spectra were recorded using an Agilent HP 8453 UV-Vis Fluorescence spectra were recorded using RF-5301PC spectrophotometer. spectrofluorometer (Shimadzu). The slit width used for both excitation and emission were 10 Cyclic voltammetry (CV) was carried out with an Autolab PGSTAT101 potentiostat/galvanostat. The Nova 1.7 software was used to control the system and process data. A conventional three-electrode system was used. A glassy carbon electrode was used as working electrode, while the platinum sheet was used as counter electrode and Ag/AgCl as reference electrode. The pH of solutions was measured using UB-10 Ultra Basic pH meter (Denver Instrument). Transmission electron microscopy (TEM) images of the AgNCs were recorded on Tecnai G<sup>2</sup>-20 (FEI, Netherlands) under the accelerating voltage of 200 kV. An inductively coupled plasma optical emission spectrometer (ICP-OES, Optima 2100 DV, USA) was used to determine total Fe content in the samples.

# 2.3 Synthesis of silver nanoclusters (AgNCs)

The silver nanoclusters (AgNCs) were synthesized using the procedure published previously [54] with modification. Briefly, AgNO<sub>3</sub> (0.1699 g, 12.5 mmol) was dissolved in 80 mL of deionized water in a three necked round bottom flask, and PMAA was diluted by water in the proportion of 1:20. The AgNO<sub>3</sub> and PMAA solution were sonicated about 30 min before mixing. The AgNO<sub>3</sub> solution was then heated at 90 °C under nitrogen atmosphere and 9 mL of PMAA solution was quickly added the hot AgNO<sub>3</sub> solution with stirring. The mixed solution was refluxed under nitrogen atmosphere for 270 min. The mixture gradually became colorless to light umber color and then a reddish purple color. The concentration of colloidal silver nanoclusters was calculated using the mole of AgNO<sub>3</sub> and found to be 11.25 mM. The size of the synthesized AgNCs was characterized by transmission electron microscope (TEM).

## 2.4 Absorbance measurements

Absorption spectra of AgNCs before and after adding  $Fe^{2+}$  were recorded in the 0.1 M acetic-acetate buffer solution at pH 5.0. To a 10.00 mL volumetric flask, 400  $\mu$ L of 11.25 mM AgNCs (final concentration = 0.45 mM) and 40  $\mu$ L of 10 mM ferrous ammonium sulfate hexahydrate solution (final concentration = 40  $\mu$ M) were sequentially added. The mixture was made to a final volume of 10.00 mL with 0.1 M acetic-acetate buffer pH 5.0. The mixture was then incubated at room temperature for 20 min. The absorbance was monitored at the wavelength of 447 nm. The absorbance of silver nanoclusters solution and the absorbance after adding  $Fe^{2+}$  were assigned as  $A_0$  and A, respectively. The difference of the absorbance (A-A<sub>0</sub>) was plotted versus the concentration of  $Fe^{2+}$  to obtain a calibration curve. To study the effect of incubation time, the mixed solution between AgNCs and  $Fe^{2+}$  in 0.1 M acetic-acetate buffer solution pH 5.0 was incubated at 1-60 minutes before the absorbance measurements. To study the effect of solution pH, 0.1 M acetic-acetate buffer was used to control the pH range of 4.0-6.0. The calibration curve was constructed under the optimized conditions (0.45 mM of AgNCs in 0.1 M acetic-acetate buffer pH 5.0 and incubation time of 20 min) in the presence of  $Fe^{2+}$  concentration ranging from 5 to 100  $\mu$ M.

## 2.5 Selectivity of the sensor

To evaluate the selectivity of the proposed sensors, the following procedure was carried out. An individual stock solution of various metal ions (10 mM) was prepared by dissolution of a metal salt in deionized water. To a 10 mL volumetric flask containing 400  $\mu$ L of 11.25 mM AgNCs (final concentration = 0.45 mM) was added individually 40  $\mu$ L of 10 mM stock metal ions including Na<sup>+</sup>, K<sup>+</sup>, Li<sup>+</sup>, Mg<sup>2+</sup>, Ca<sup>2+</sup>, Pb<sup>2+</sup>, Ba<sup>2+</sup>, As<sup>3+</sup>, Cr<sup>3+</sup>, Zn<sup>2+</sup>, Cd<sup>2+</sup>, Fe<sup>2+</sup>, Fe<sup>3+</sup>, Co<sup>2+</sup>, Ni<sup>2+</sup>, Cr<sup>3+</sup> and Cu<sup>2+</sup> to obtain a final concentration of 40  $\mu$ M. The mixture was diluted to the total volumetric flask with 0.1 M acetic-acetate buffer pH 5.0. The solution was mixed thoroughly and left for 20 min before recording the absorption spectrum.

# 2.6 Determination of Fe<sup>2+</sup> in real tablet samples

A ferrous sulfate tablet sample (0.0500 g) was ground to a fine powder. The obtained powder was dissolved in 200 mL of deionized water and sonicated for 30 min. The suspension was subsequently filtered through a filter paper. Then, 1 mL of the supernatant solution was added to a 10 mL volumetric flask containing 400  $\mu$ L of AgNCs and diluted with 0.1 M acetic-acetate buffer pH 5.0. The concentration of Fe<sup>2+</sup> can be calculated using the standard calibration curve. For standard addition method, the appropriate volumes of Fe<sup>2+</sup> standard solution were individually added into the mixture of 400  $\mu$ L of AgNCs and 1 mL of the sample solution. Then the mixture was diluted with 0.1 M acetic-acetate buffer pH 5.0, and left for 20 min before recording the absorption spectrum.

# 3. Results and Discussion

AgNCs are one of the most currently interesting nanomaterials and have recently been introduced to the chemical analysis approach. Since the size of the nanoclusters, between a silver atom and silver nanoparticles, results in discrete electronic levels and allows the transition of an electron from a ground state to a higher electronic state upon excitation, the fluorescence emission is a dominant characteristic of this material. On the other hand, there are a few reports about the use of the absorption property of AgNCs to fabricate chemical sensors. Based on the quantum confinement effect, the absorption change can be expected if the size of the particle is changed. Therefore, in this work we expect the color of AgNCs solution changes in the presence of Fe<sup>2+</sup> due to the increasing particle size. Parameters affecting the color changes are investigated and discussed extensively.

# 3.1. Characterization of the synthesized AgNCs

The water-soluble silver nanoclusters (AgNCs) were successfully synthesized by an assistance of PMAA which was used as both template and reducing agent in a one-pot reaction. To avoid the oxidation reaction by oxygen presented in the solution, the solution of Ag<sup>+</sup> and PMAA must be sonicated to remove the dissolved oxygen. AgNCs were obtained after heating the mixture of Ag<sup>+</sup> and PMAA solution under N<sub>2</sub> atmosphere. Characteristics of the synthesized AgNCs were investigated by TEM, UV-Vis spectrophotometer and fluorometer.

The morphology of AgNCs was elucidated by TEM as shown in Fig. 1(a). The shape of the synthesized particles was nearly spherical, and the particles have a uniform distribution without any aggregation with an average size of about 2.1±0.1 nm (N=172). This result confirms that the synthesized particles are at the nanocluster size approaching the Fermi wavelength of electrons (0.5 nm for Au and Ag) [56]. Therefore, interesting properties beyond nanopaticles, such as the discrete energy levels leading to the observation of dramatically different optical, electrical, and chemical properties, can be expected [57]. Moreover, the synthesized nanoclusters become molecular-liked species with size-dependent absorption and size-dependent fluorescent emission upon irradiation by the UV–Visible light [58].

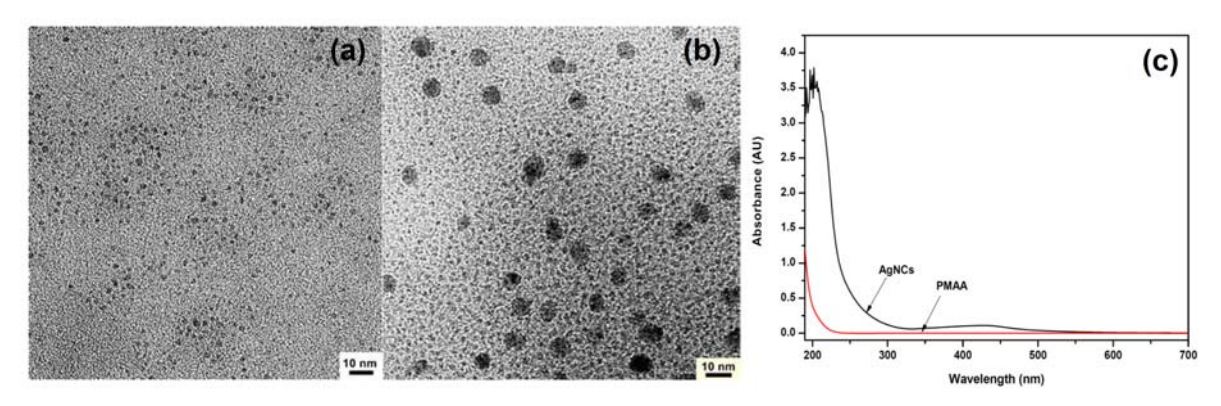


**Fig.1** TEM images of AgNCs templated PMAA (a) before adding Fe<sup>2+</sup>, the average particle size was 2.1±0.1 nm (N=172) and (b) after adding Fe<sup>2+</sup>, the average particle size was 7.4± 0.2 nm (N=32) (c) UV–Vis absorption spectra of the synthesized silver nanoclusters (AgNCs) at the concentration of 0.45 mM in deionized water and the solution of 6.0×10<sup>-3</sup> %w/v PMAA (equivalent to the concentration of 0.45 mM AgNCs).

Depending on the synthesis method and stabilizing agents, silver nanoclusters show different absorbance and fluorescence characteristics [59]. The optical properties of AgNCs were characterized and the results were shown in Fig 1(c). There was no significant plasmon band of Ag nanoparticles appeared in the range of 380-450 nm. The damping of the plasmon absorption with a respective weak and broadened absorption is typical for nanocrystal size particles (around 2 nm) [60-61].

Fluorescence emission of the synthesized particles can be used to confirm the nanocluster size of the particles due to the discrete electronic transition basically occurring in the nanocluster size level. Therefore, the fluorescence spectrum of the AgNCs was recorded and shown in Fig. S1 (ESI). The fluorescence emission maximum of AgNCs was obtained at 555 nm when exciting at 470 nm. The fluorescence spectrum showed a relatively symmetric emission band suggesting that the synthesized AgNCs were nearly homogeneous and monodisperse [62].

The absorption and fluorescence spectrum revealed that the size of obtained particles was in the nanoclusters range, and there was no silver nanoparticles in the synthesized product, which was in agreement with the result obtained from TEM. Therefore, the fabrication of colorimetric probes based on nanocluster size particles can be performed using the as-prepared AgNCs.

# 3.2. Study of the absorption spectra

Experiments were carried out in acetic-acetate buffer pH 5.0 and in the final concentration of AgNCs and metal ion at 0.45 mM and 40 µM, respectively. The absorbance of AgNCs was firstly measured and the spectrum was showed in Fig. 2. The inset in Fig. 2 depicted the corresponding color of each solution mixture. The AgNCs themselves showed very weak absorption band around 350-500 nm corresponding to a light yellow color. On the other hand, in the presence of Fe<sup>2+</sup> the absorbance at 447 nm significantly increased and the color of the mixture turned to orange. Therefore, the synthesized AgNCs can potentially be used as a naked eye colorimetric sensor for detecting Fe<sup>2+</sup>. To confirm this observation was actually resulted from the two components, Fe2+ and AgNCs, parallel experiments were performed. AgNCs were mixed with Fe<sup>3+</sup>, and the absorption spectrum was recorded. The absorbance slightly increased comparing to the original spectrum. However, Fe<sup>3+</sup> cannot significantly change the color of AgNCs. This result signifies that AgNCs can be used to differentiate Fe<sup>2+</sup> and Fe<sup>3+</sup>. In addition, to confirm the important role of AgNCs, the absorbance spectra of the mixture between Fe<sup>2+</sup>/PMAA and Fe<sup>2+</sup>/Ag<sup>+</sup> were measured. There was no significant change observed in both cases. The color change was not due to the mixture of PMAA and Fe<sup>2+</sup>. In addition, in the absence of AgNCs, the reaction of Fe<sup>2+</sup> and Ag<sup>+</sup> could not give a color change.

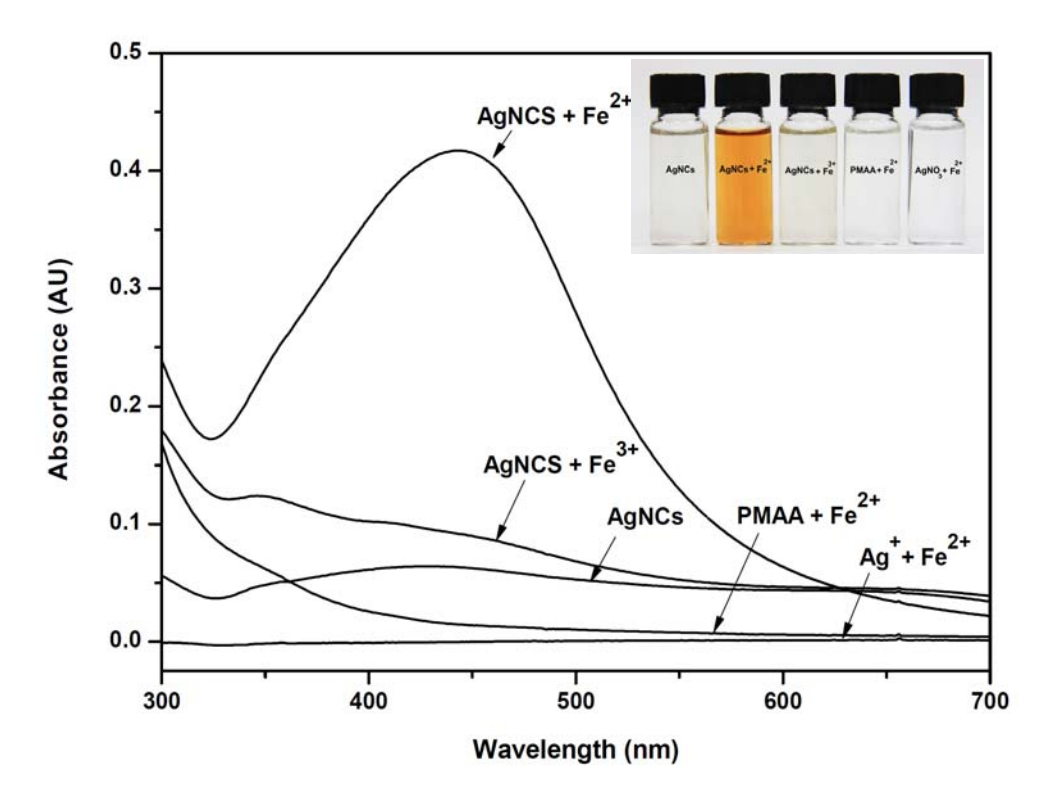


**Fig.**2 Absorption spectra of 0.45 mM AgNCs and AgNCs in the presence of  $Fe^{2+}$  and  $Fe^{3+}$  compared with the mixture between PMAA+  $Fe^{2+}$  and  $Ag^{+}+Fe^{2+}$  in 0.1 M aceticacetate buffer pH 5.0. (All of metal ion concentrations were fixed at 40  $\mu$ M).

## 3.3. Possible sensing mechanism

From the previous section, it can clearly be seen that the mixture of AgNCs and  $Fe^{2+}$  gave the orange solution with the maximum absorption at 447 nm. Actually, during the synthesis of AgNCs the reduction of  $Ag^+$  to  $Ag^0$  cannot be completed. Therefore, there is always free  $Ag^+$  remained in the solution. The cyclic voltammetry was used to confirm the presence of unreacted  $Ag^+$  and the results were shown in the Fig. S2 (ESI). Form cyclic voltammograms of the AgNCs and AgNO<sub>3</sub> solution, it can be seen that the cathodic peak ( $E_{pc}$ ) at -114 mV vs Ag/AgCl was due to the reduction of  $Ag^+$  to  $Ag^0$  and deposited on the electrode surface. Moreover, the anodic peak ( $E_{pa}$ ) at 400 mV vs Ag/AgCl was due to the oxidation of  $Ag^0$  which deposited on the electrode surface to  $Ag^+$ . This result confirmed that there were unreacted  $Ag^+$  remained in the AgNCs solution. In this work, the unreacted  $Ag^+$  may bind with the negative charge of PMAA.

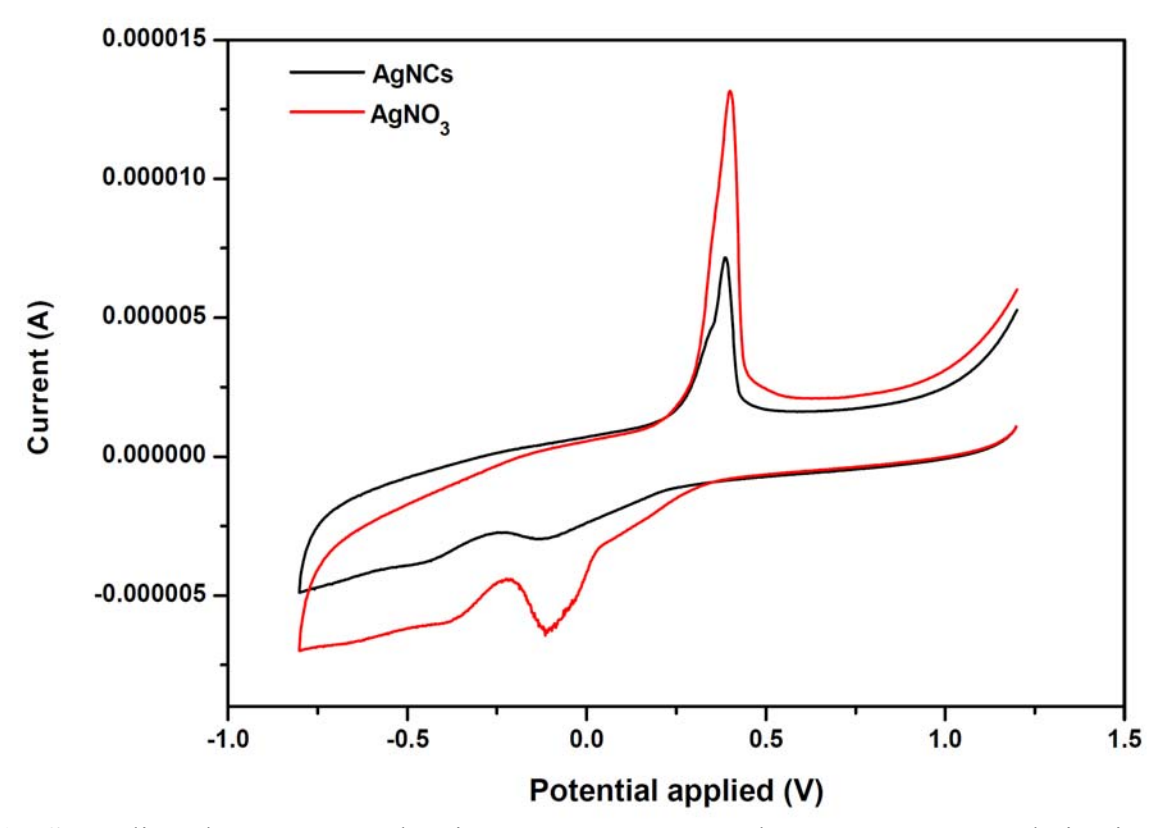


**Fig. S2**Cyclic voltammogram taken in 0.11 mM AgNCs and 0.11 mM AgNO<sub>3</sub> solution in 0.1 M acetic-acetate buffer pH 5.0 at a scan rate of 100 mV s<sup>-1</sup>

After adding  $Fe^{2+}$  into the AgNCs solution, free  $Ag^+$  on the polymer chain will be reduced by  $Fe^{2+}$  and deposited on the AgNCs. Therefore, the increasing size of the nanoclusters can be expected. The optical characteristic of the nanoclusters was reduced and the surface plasmon behavior, which is the nanoparticles characteristic, was dominated. This can be seen by the increasing of the plasmon band at around 447 nm (Fig. 2). This result agreed well with the TEM result shown in Fig. 1(b). Form the TEM image, it can be clearly seen that the average particle size of the AgNCs after mixing with  $Fe^{2+}$  was around  $7.4\pm0.2$  nm bigger than the original AgNCs  $(2.1\pm0.1 \text{ nm})$ .

In addition, the results from the fluorescence spectroscopy can also used to support this phenomenon. Basically, if the particle size is in the nanoclusters region, the discrete energy level should be dominated. On the other hand, the energy level become close together if more silver atoms are connected. It is expected that the fluorescence emission of the AgNCs should decrease with the increasing of the particle size (to be the silver nanoparticles). Therefore, the fluorescence emission of AgNCs in the absence and presence of Fe<sup>2+</sup> were measured and the results were shown in Fig. S1 (ESI). The fluorescence intensity of the AgNCs can be observed indicating the presence of the discrete energy level. On the other hand, the fluorescence intensity decreased at the same wavelength in the presence of Fe<sup>2+</sup>. This result suggests that the decreasing of the fluorescence intensity was due to the decreasing of the number of nanoclusters (fluoresce specie) and the increasing of the number of nanoparticles (non-fluoresce species).

The reduction of free  $Ag^+$  causing the increasing of the AgNCs size has also been reported by Tang, F. and coworker [54]. The growth of AgNCs was due to the reduction of the surplus  $Ag^+$  to  $Ag^0$  by  $\alpha$ -L-fucosidase, and the fluorescence intensity was quenched due to the growth of the particle size. In addition, AgNCs were required as catalysts for the growth of the particles.

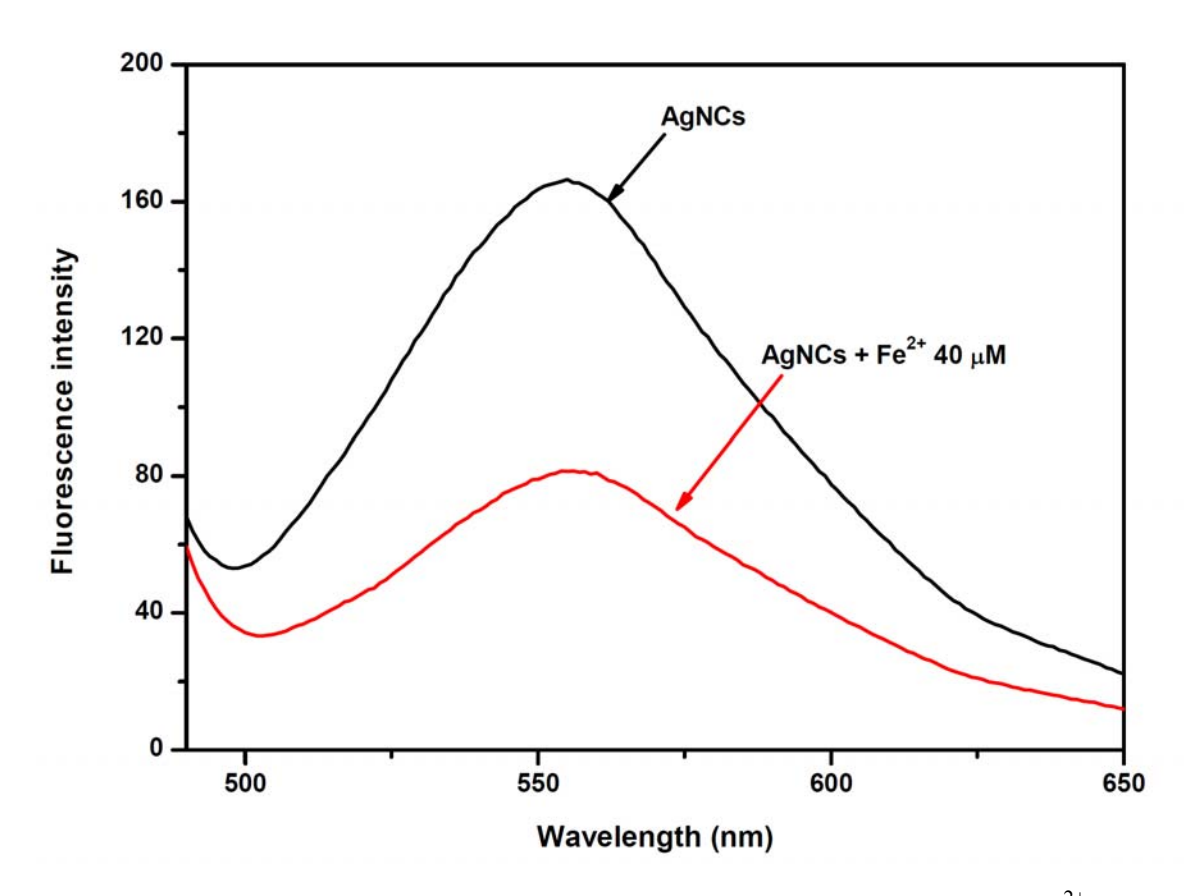


**Fig. S1** Fluorescence spectra of 0.45 mM AgNCs without and with 40  $\mu$ M Fe<sup>2+</sup> in 0.1 M acetic-acetate buffer pH 5.0

## 3.4. Selectivity of the proposed sensor

The selectivity of the sensor is the key feature of a chemical sensor because the proposed sensor must ideally respond to only one target species when other related species do not respond in the same direction. Although there are many reports on the use of organic ligands as selective probes for fabricating colorimetric sensors for Fe<sup>2+</sup>, to the best of our knowledge the use of other materials to fabricate a selective colorimetric sensor for Fe<sup>2+</sup> has not yet been reported. In this work, we proposed the colorimetric sensor using PMAA-template AgNCs for the detection of Fe<sup>2+</sup>. The interference of other cations to our proposed sensor must be investigated by measuring the absorbance change in the presence of various

cations including  $Li^+$ ,  $Na^+$ ,  $K^+$ ,  $Mg^{2+}$ ,  $Ca^{2+}$ ,  $Ba^{2+}$ ,  $Mn^{2+}$ ,  $Fe^{3+}$ ,  $Co^{2+}$ ,  $Ni^{2+}$ ,  $Cu^{2+}$ ,  $Zn^{2+}$ ,  $Cd^{2+}$ ,  $Ag^+$ ,  $Pb^{2+}$ ,  $Hg^{2+}$ ,  $Al^{3+}$  and  $Cr^{3+}$ . The absorption spectra of AgNCs in the presence of various metal ions and the corresponding absorbance changes were shown in Fig. 3(a) and Fig. 3(b), respectively. Moreover, color changes upon mixing each metal ion with AgNCs were exhibited in Fig. 4. It can be seen that the absorbance spectra of the AgNCs at 447 nm were significantly increased only in the presence of Fe<sup>2+</sup>. On the other hand, other studied metal ions especially Fe<sup>3+</sup> did not significantly affect the spectrum. In addition, as seen from Fig. 4, the color of AgNCs turned to orange only in the case of Fe<sup>2+</sup>. The slightly yellow color can be observed in the case of Fe<sup>3+</sup> possibly due to the redox equilibrium between Fe<sup>2+</sup> and Fe<sup>3+</sup>. Our proposed sensor can be used in a qualitative analysis for Fe<sup>2+</sup> using the naked eye. The interfering studies confirmed that the proposed sensor possesses the highest selectivity towards Fe<sup>2+</sup>. From the absorption spectra in Fig. S3 (ESI), it can be clearly seen that this sensor can be used to detect Fe<sup>2+</sup> in the presence of other metal ions. However, Hg<sup>2+</sup> showed a different spectrum from other metal ions, probably due to different effects to the sensor. The good selectivity of this sensor may be due to the fact that the spontaneous redox reaction can be possible only in the case of  $Fe^{2+}$ . From the standard reduction potential data [63], it can be seen that the reduction potential of  $Fe^{3+} + e^{-} \rightarrow Fe^{2+}$  equal to 0.771 V (at 298.15 K) which is less than that of  $Ag^+ + e^- \rightarrow Ag$  (s) (0.7993 V at 298.15 K). Therefore, the reduction of Ag<sup>+</sup> by Fe<sup>2+</sup> can spontaneously occur. On the other hand, other studied metal ions possess higher reduction potential than that of Ag<sup>+</sup>/Ag (cannot undergo the oxidation reaction), and the spontaneous redox reaction cannot be occurred. The selectivity of this sensor can, however, be interfered by a strong reducing agent such as Sn<sup>2+</sup>.

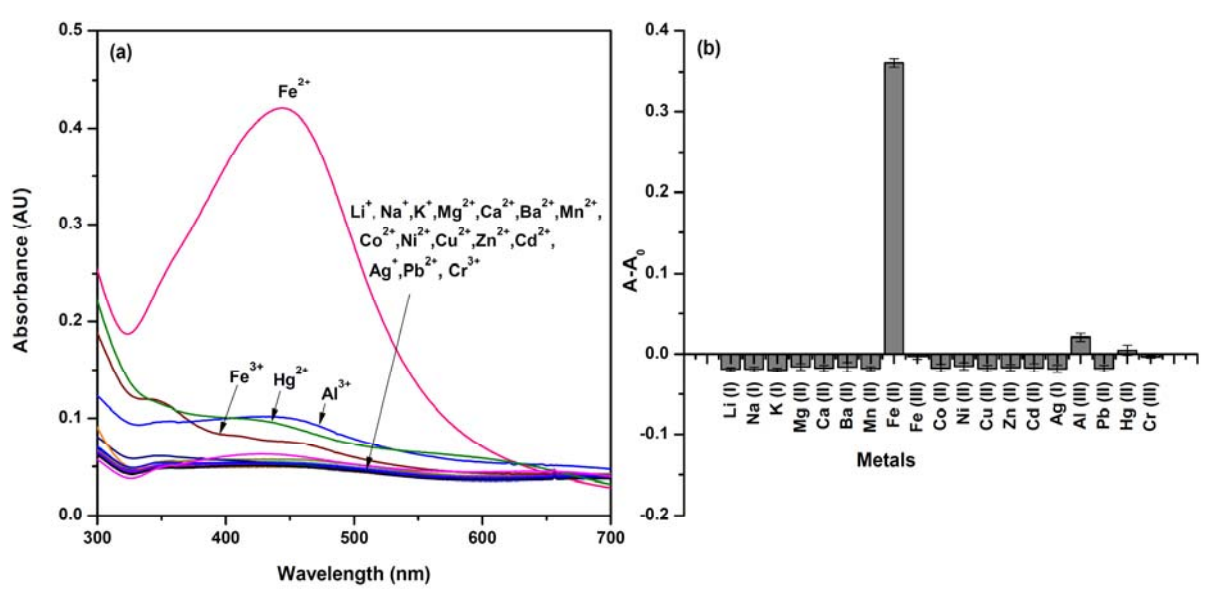


Fig.3 (a) Absorption spectra of 0.45 mM AgNCs with different metal ions in 0.1 M acetic-acetate buffer pH 5.0. (b) The corresponding absorbance difference between before  $(A_0)$  and after (A) adding various metal ions to a final concentration of 40  $\mu$ M.

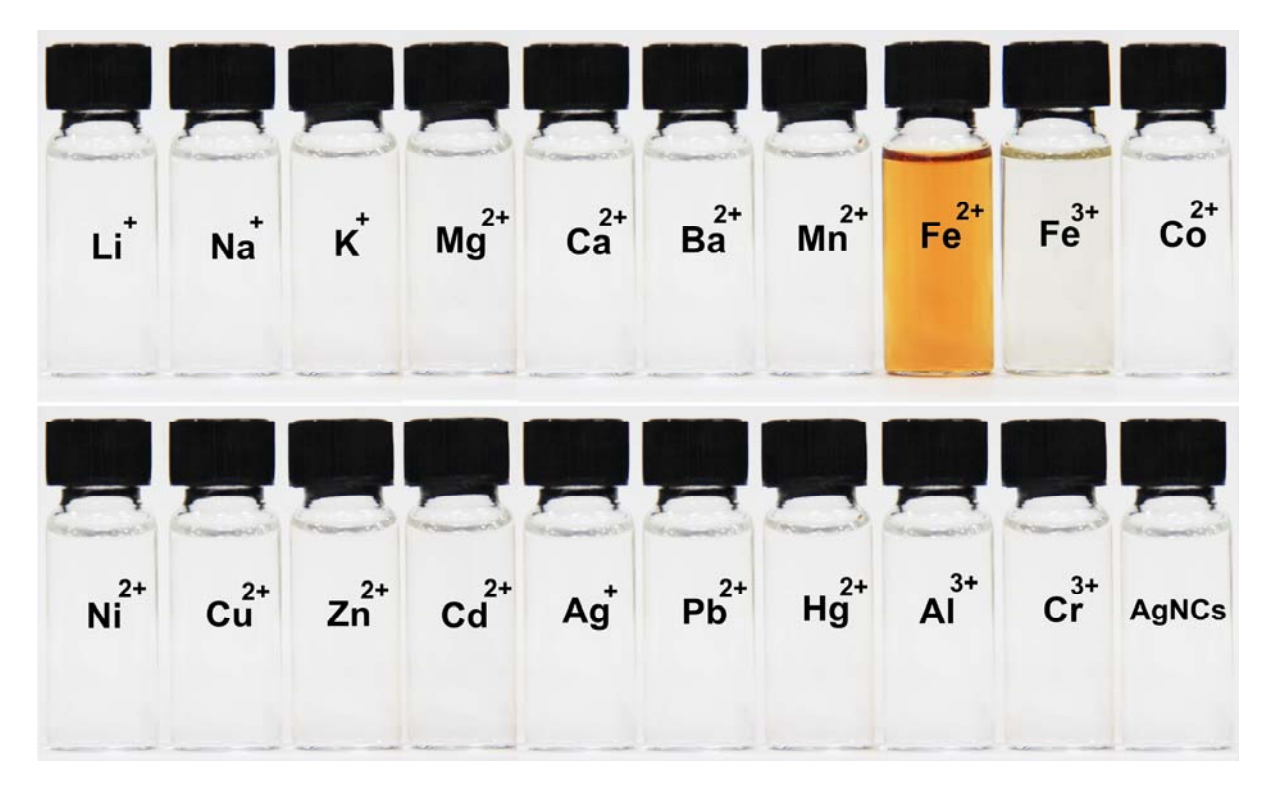
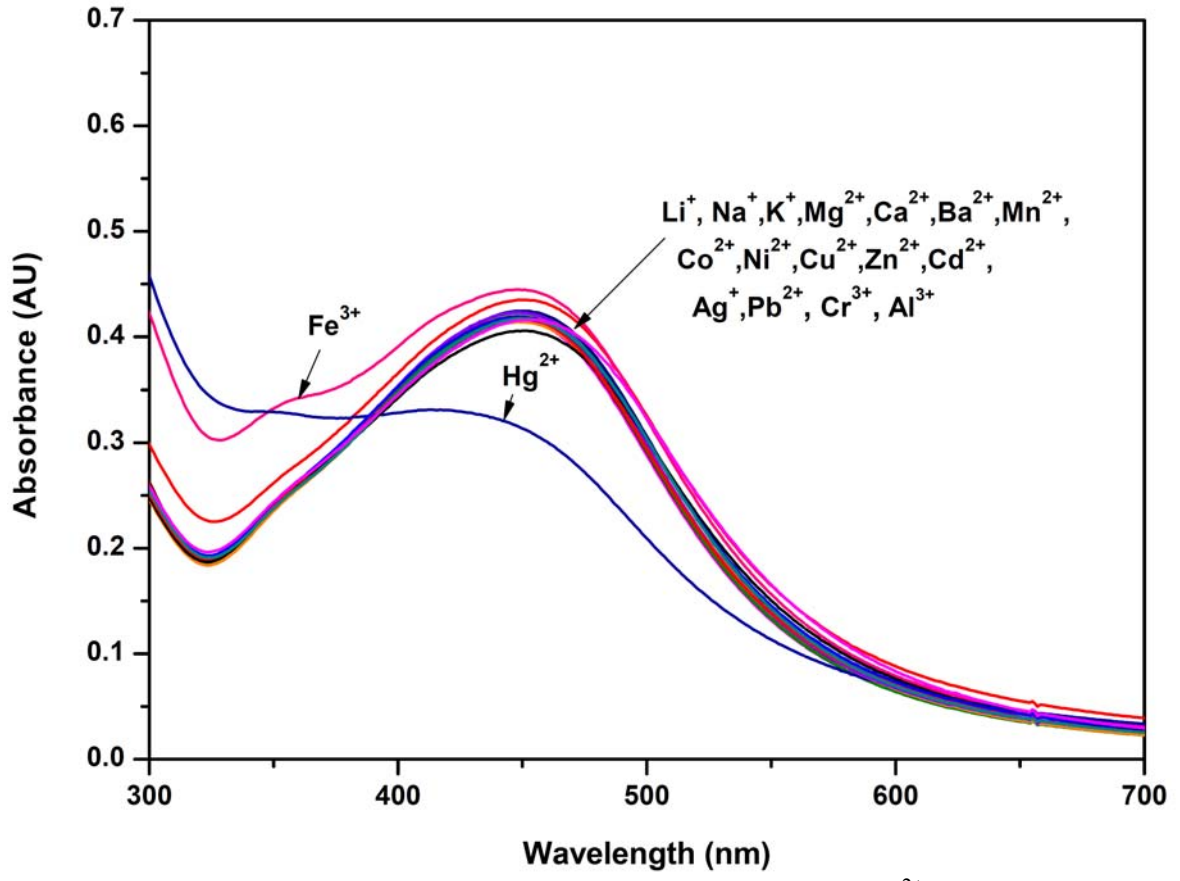


Fig.4 Photograph of 0.45 mM AgNCs solution with different metal ions in 0.1 M acetic-acetate buffer pH 5.0 when adding various metal ions to a final concentration of 40  $\mu$ M.



**Fig. S3**Absorption spectra of 0.45 mM AgNCs in the presence of Fe<sup>2+</sup> 40  $\mu$ M and 40  $\mu$ M of other metal ions in 0.1 M acetic-acetate buffer pH 5.0.

## 3.5. Effect of the solution pH

Since pH of the solution can affect the charge of PMAA, the effect of the solution pH to the absorption spectra of AgNCs and the effect of pH to the reaction of the AgNCs with Fe<sup>2+</sup> were studied. Experiments were carried out by adjusting pH of 0.1 mM acetic-acetate buffer from 3.0 to 6.5. The absorbance of AgNCs in different pHs before and after adding Fe<sup>2+</sup> were shown in Fig. S4 (ESI) and the comparison of absorbance values were plotted as a function of pH as shown in Fig. 5. As shown in Fig. S4 (a) (ESI), absorption spectra of AgNCs were depended on the solution pH. At the solution pH lower than 5.0, the significant absorption spectra can be observed at around 435 nm. On the other hand, when the solution pH was higher than 5.0 the absorbance at 435 nm was very low. At lower pH, the aggregation of AgNCs may occur due to the protonation of the carboxylate group of the PMAA reducing the repulsion between the AgNCs particles. Therefore, the characteristic of silver nanoparticles was dominated. On the other hand, at higher pH, the negative charge of PMAA may prevent the particle aggregation, and the nanoclusters form was dominated.

The effect of solution pH to the reaction of AgNCs and  $Fe^{2+}$  was shown in Fig. S4 (b) and the comparison of absorbance values was shown in Fig. 5(a). The results revealed that when adding 40  $\mu$ M of  $Fe^{2+}$  the absorbance of AgNCs at 447 nm increased and absorption spectra were not much different for all studied pHs. This may stem from the fact that after AgNCs reacted with  $Fe^{2+}$  and the particles grew bigger, the pH would no longer affect the particle aggregation. However, to obtain the best sensitivity the maximum absorbance change should be selected. Fig 5(b) showed the relationship between the difference (A-A<sub>0</sub>) of AgNCs absorbance after (A) and before (A<sub>0</sub>) adding  $Fe^{2+}$  and solution pHs. It can be seen that at the solution pH higher than 4.5 the increasing of the absorbance at 447 nm were not significantly different. Therefore, the pH 5.0 was chosen as a suitable pH and used in further experiments.

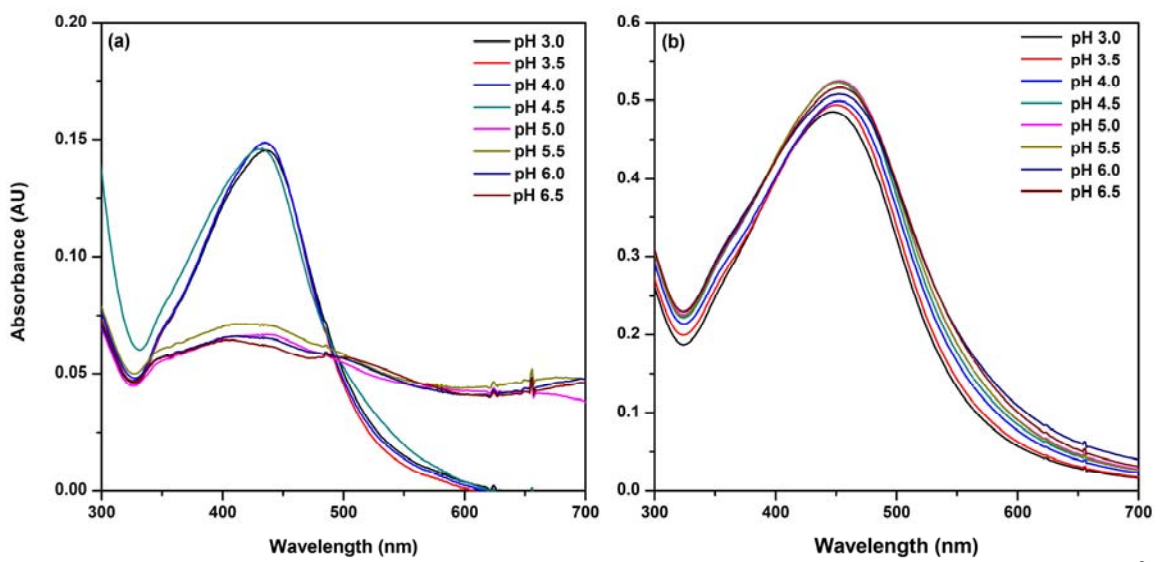


**Fig. S4**Absorption spectra of 0.45 mM AgNCs in the absence (a) and presence (b) of Fe<sup>2+</sup> 40  $\mu$ M in 0.1 M acetic-acetate buffer pH 3.0-6.5.

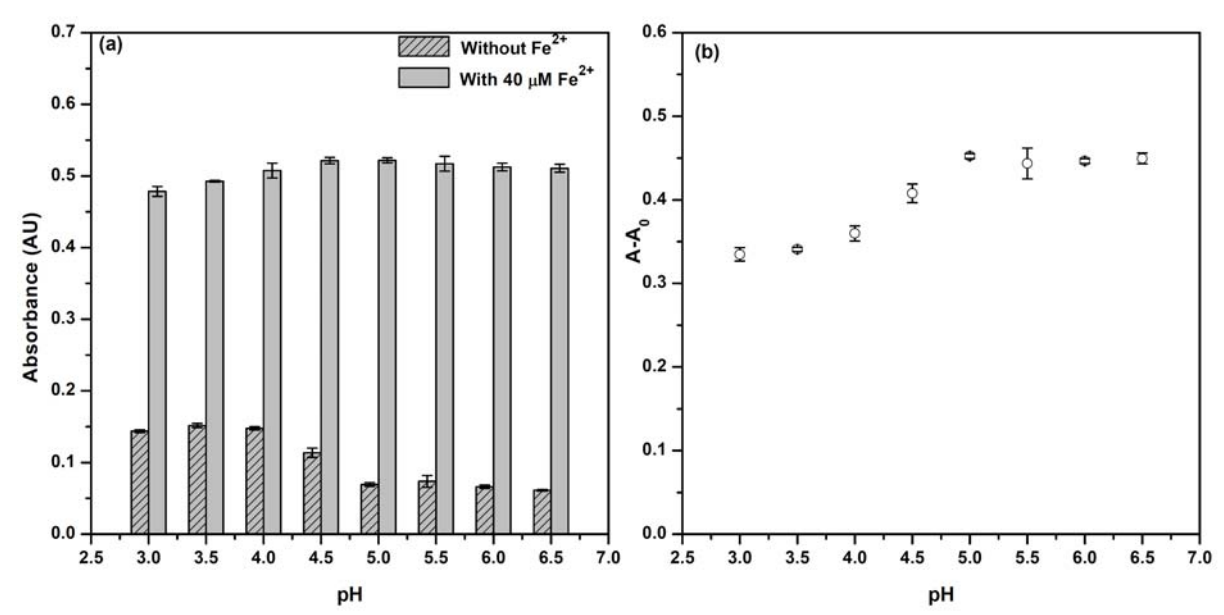


**Fig.5** Effect of the solution pH towards the absorbance of 0.45 mM AgNCs in the absence (a) and presence (b) of  $Fe^{2+}$  40  $\mu$ M in 0.1 M acetic-acetate buffer pH 3.0-6.5.

## 3.6. Effect of the incubation time

Fast response time is an ideal characteristic of chemical sensors. In this work the response time of the sensor was studied in term of the incubation time between AgNCs and Fe<sup>2+</sup> in the range of 0-60 min at the optimized condition. The absorption spectra of the mixture between AgNCs and Fe<sup>2+</sup> were recorded at different incubation time. The absorbance spectra were shown in Fig. S5 (ESI) and the plot between the absorbance values versus incubation times were depicted in Fig. 6. The results exhibited that the reaction between AgNCs and Fe<sup>2+</sup> immediately occurred after mixing. Therefore, the response time of the proposed sensor is very fast and can be used to sense Fe<sup>2+</sup> in a few seconds. For practical use, the color of AgNCs immediately changed to orange after mixing with Fe<sup>2+</sup>. Although, the reaction can immediately occur in a few minutes but the detection precision at the incubation time less than 20 minutes (as shown in Fig. 6) was not satisfied. Therefore, to obtain the best sensitive and precise sensor, we allowed the incubation time of 20 min before recording the absorbance spectra.

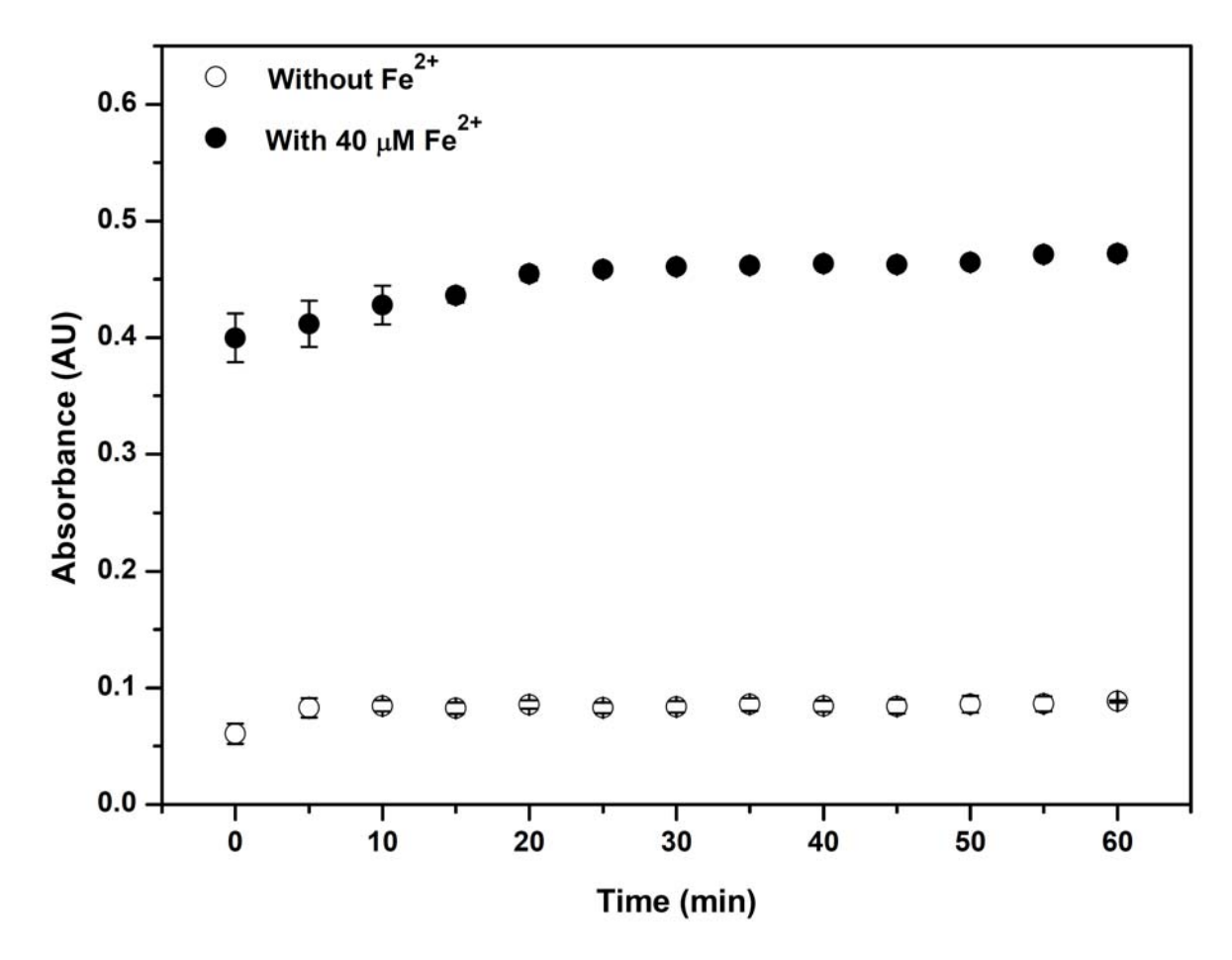


**Fig.**6 Effect of incubation time towards the absorption spectra of 0.45 mM AgNCs in presence of Fe $^{2+}$  40  $\mu$ M in 0.1 M acetic-acetate buffer pH 5.0 at the incubation time from 0-60 min.

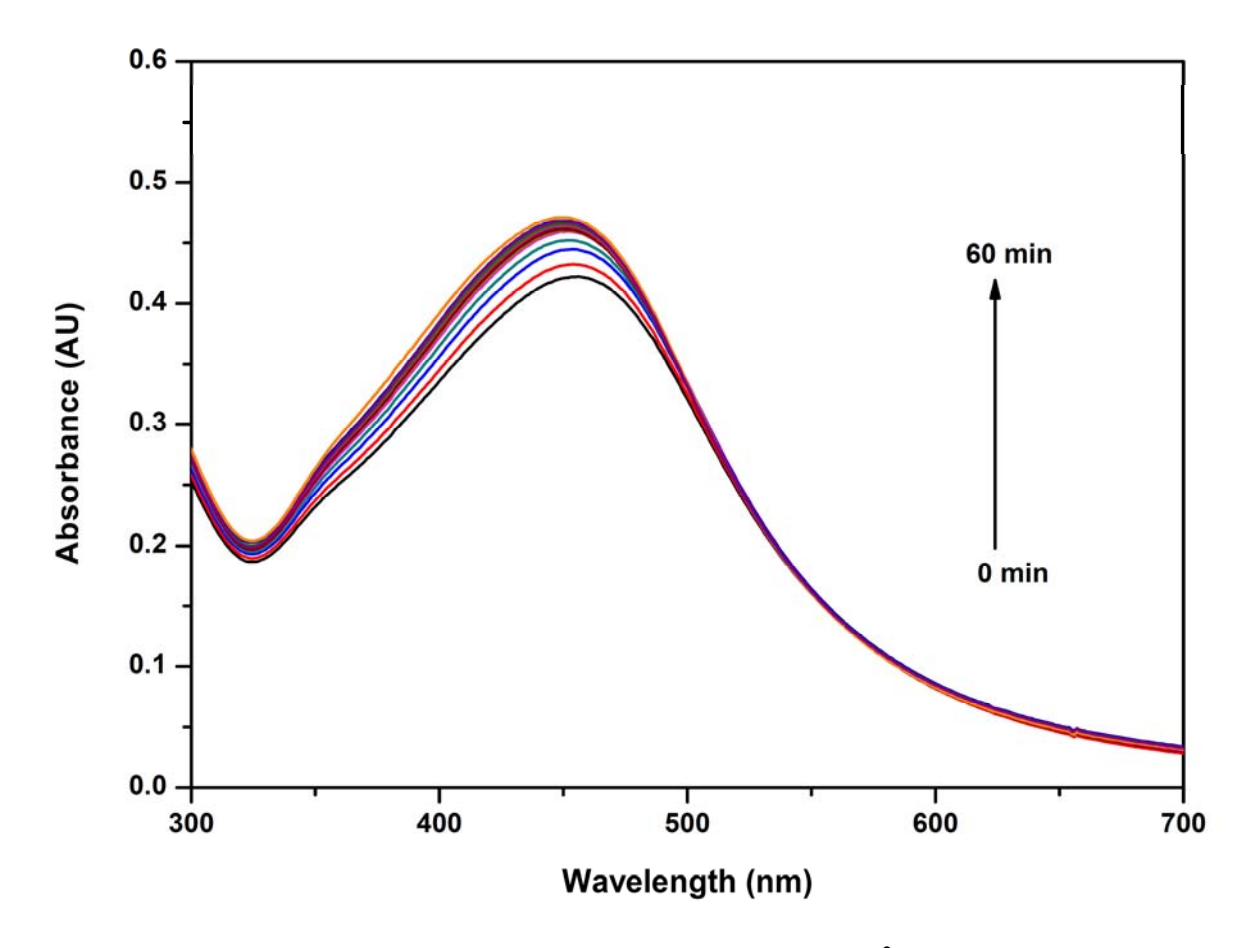


**Fig. S5**Absorption spectra of 0.45 mM AgNCs in presence of  $Fe^{2+}$  40  $\mu M$  in 0.1 M acetic-acetate buffer pH 5.0 at the incubation time from 0-60 min.

# 3.7. Effect of concentration of AgNCs on the detection of Fe<sup>2+</sup>

The effect of AgNCs concentrations to the detection sensitivity was investigated by measuring the absorbance of AgNCs at different concentrations in the presence of 40 µM Fe<sup>2+</sup>. The absorption spectra after adding Fe<sup>2+</sup> were depicted in Fig. S6 (ESI) and the plot of absorbance values versus AgNCs concentrations were shown in Fig. 7. The absorbance of AgNCs (at 447 nm) is lower than 0.1 AU at all concentrations according to the characteristic of silver nanoclusters. The low absorbance of the sensor probe at the detection wavelength is a good characteristic for the sensor fabrication because a better sensitivity can be obtained. In the presence of Fe<sup>2+</sup>, higher concentration of AgNCs provided higher absorbance value with the red shift spectrum as shown in Fig. S6 (ESI). The higher concentration of AgNCs may provide bigger particle size of silver nanoparticles. However, when looking at the increasing absorbance (A-A<sub>0</sub>) at 447 nm and comparing to the absorbance of AgNCs at the same concentration (Fig. 7(b)), the increasing of the absorbance values was found to be in the same order. Therefore, the concentrations of AgNCs in the studied range did not significantly affect the detection sensitivity. However, the concentration of AgNCs should be fixed for a comparison and the color change could be distinguished by the naked eye. Therefore, the concentration of AgNCs at 0.45 mM was selected for further investigation.

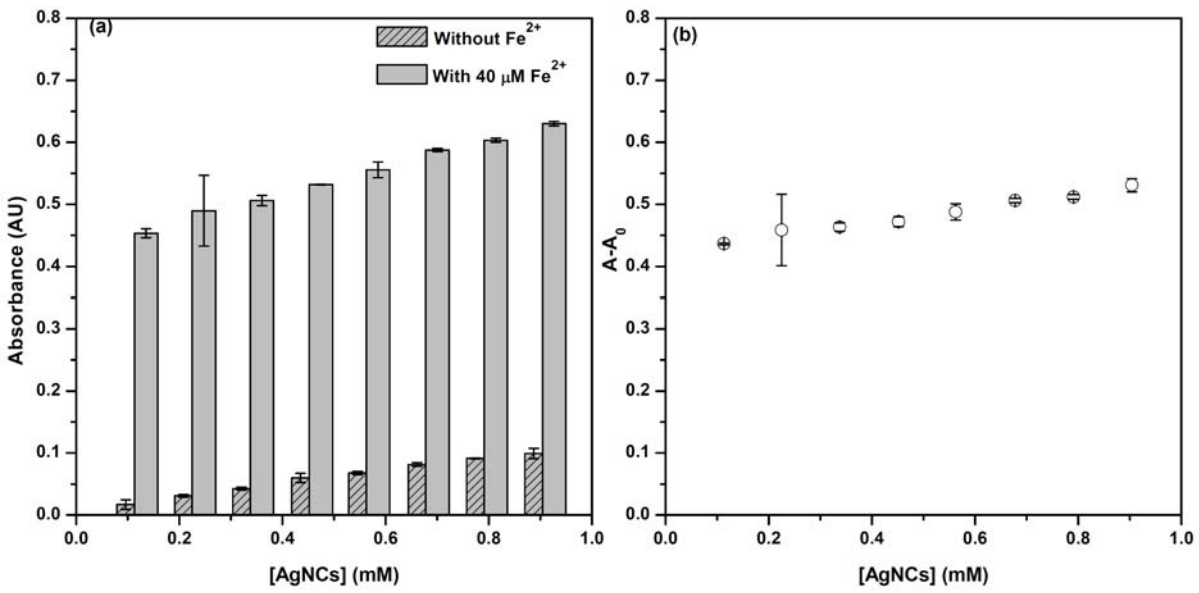


**Fig.**7 Effect of the AgNCs concentration towards the absorption spectra of AgNCs in the presence of  $Fe^{2+}$  40  $\mu M$  in 0.1 M acetic-acetate buffer pH 5.0 at the different concentration of AgNCs from 0.11-0.90 mM.

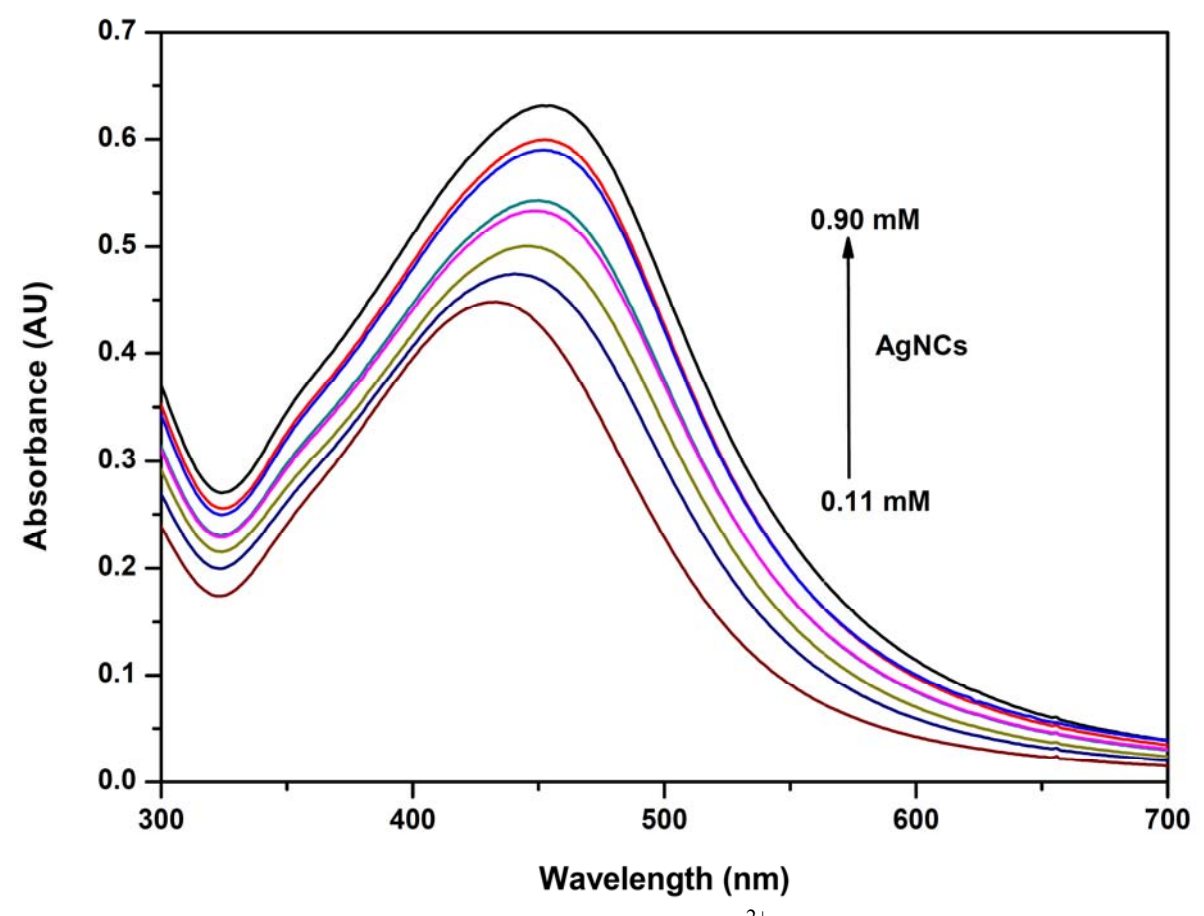


**Fig. S6**Absorption spectra of AgNCs in presence of  $Fe^{2+}$  40  $\mu M$  in 0.1 M acetic-acetate buffer pH 5.0 at the difference concentration of AgNCs from 0.11-0.90 mM.

# 3.8. Colorimetric titrations

The quantitative analysis of  $Fe^{2+}$  by the proposed sensor was studied by measuring the AgNCs absorbance upon the increment of  $Fe^{2+}$  concentrations at the optimized condition to construct a calibration curve. The absorbance spectra of AgNCs at different  $Fe^{2+}$  concentrations and the corresponding calibration curve were shown in Fig. 8. Upon the increment of  $Fe^{2+}$  concentration from 5 to 100  $\mu$ M, the absorbance at 447 nm linearly increased as a function of the increasing  $Fe^{2+}$  concentration. It should be noted that the spectrum shape did not change, and only the increasing of absorbance was observed. As shown in the inset of Fig. 8, the proposed sensor can be used in a wide linear working concentration range of 5-100  $\mu$ M, where the linear regression equation was  $(A-A_0) = 9.51 \times 10^{-3} \, [Fe^{2+}] \, (\mu M) + 0.0024$  with a correlation coefficient  $(r^2)$  of 0.9993.

The LOD was calculated as the concentration of  $Fe^{2+}$  producing the absorbance equal to  $A_0+3\times$ the standard deviation of  $A_0$ , whereas the LOQ was also calculated as the concentration of  $Fe^{2+}$  giving a absorbance equal to  $A_0+10\times$ the standard deviation of  $A_0$ . The LOD and LOQ of the proposed sensor were 76 nM and 1.96  $\mu$ M, respectively. These results indicated that the developed sensor was highly sensitive and that it could detect  $Fe^{2+}$  at very low concentration levels. There have been several reports on  $Fe^{2+}$  sensors as summarized in Table S1 (ESI). It can be seen from Table S1 that most of the detection limits obtained by colorimetric sensors are lower than micromolar range. In addition, the detection limit obtained by the proposed sensor is in nanomolar level which is better than that in the previous reports as shown in Table S1 (ESI). In addition, it should be noted that the selectivity of the proposed sensor over the detection of  $Fe^{3+}$  ion is excellent.

Furthermore, the repeatability of the proposed sensor was evaluated. The relative standard deviation from the detection of 40  $\mu M$  Fe²+ for ten replicates was found to be only 0.67%. In addition, the repeatability of the calibration curve was also evaluated. The calibration curves of Fe²+ were constructed in triplicate by using the same crop of the synthesized AgNCs, and the results were shown in Fig. S7 (ESI). The three calibration curves obtained could be superimposed almost perfectly. These results suggested that the proposed sensor exhibited very good repeatability. Furthermore, the reproducibility of the proposed sensor was also demonstrated by constructing of the Fe²+ calibration curves from different crops of synthesis and the results were shown in Fig. S8 (ESI). Three calibration curves obtained from different crops of the synthesized AgNCs exhibited insignificantly different curve. This result suggests that the proposed sensor can provide a very well reproducibility.

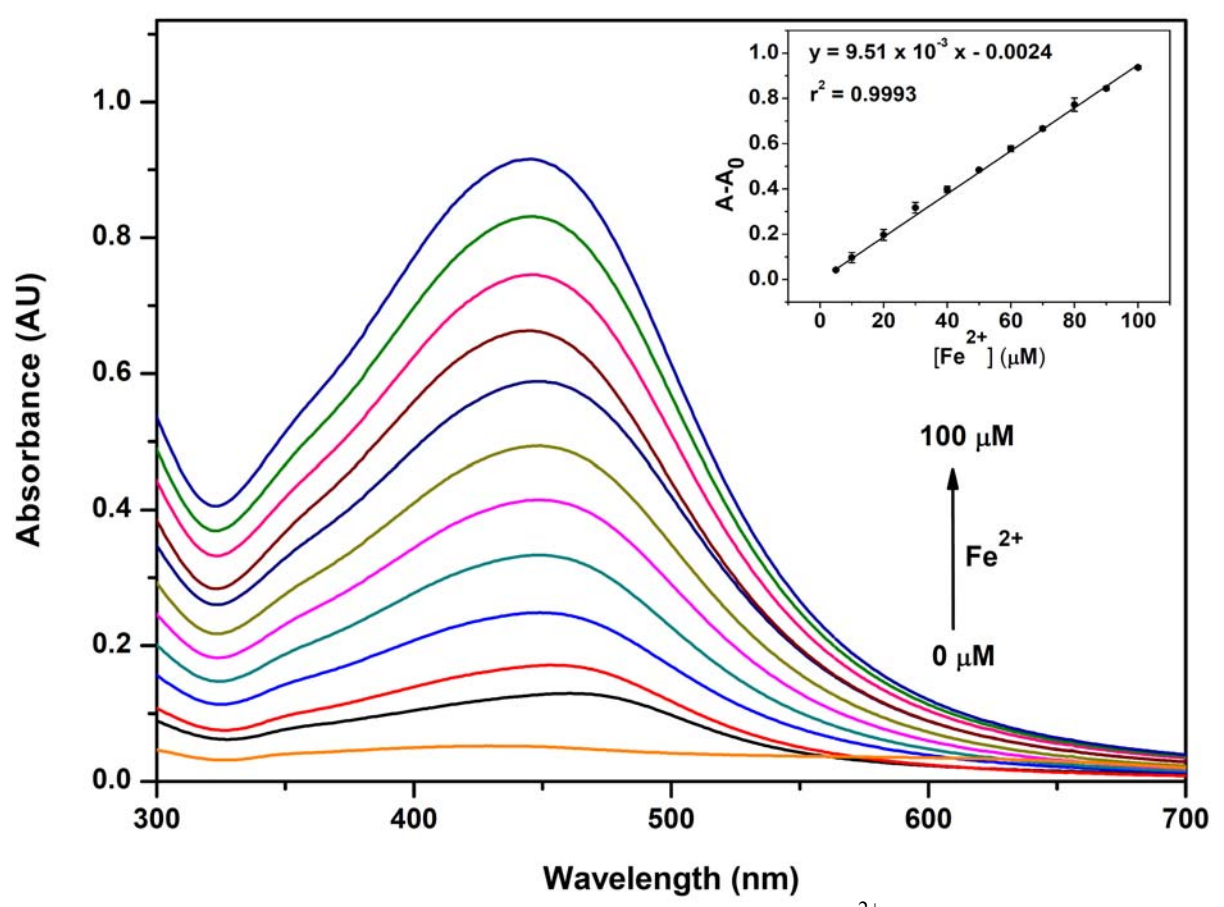


**Fig.**8 Colorimetric titration spectra of 0.45 mM AgNCs with  $\mathrm{Fe}^{2^+}$  concentration range of 0-100  $\mu$ M in 0.1 M acetic-acetate buffer pH 5.0, (inset) the corresponding calibration curve.

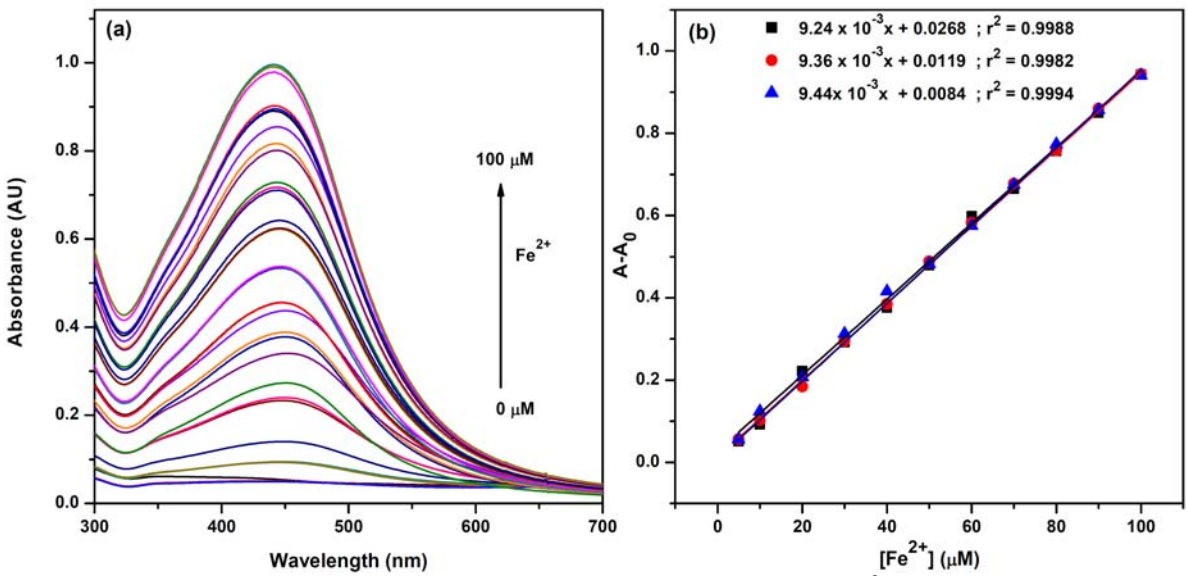


**Fig. S7**(a) Absorption spectra of 0.45 mM AgNCs in presence of  $Fe^{2+}$  40  $\mu$ M in 0.1 M acetic-acetate buffer pH 5.0 at the same lot of the synthesized AgNCs and (b) the corresponding calibration curve.

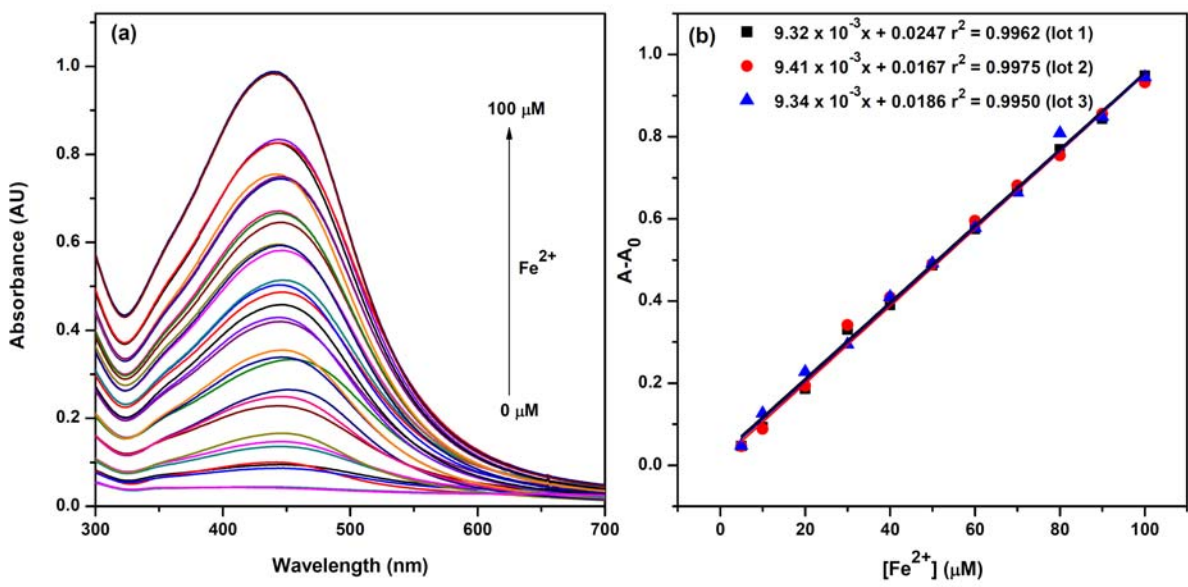


**Fig. S8**(a) Absorption spectra of 0.45 mM AgNCs (different crop) in presence of Fe<sup>2+</sup> 40 μM in 0.1 M acetic-acetate buffer pH 5.0 at the different lot of the synthesized AgNCs and (b) the corresponding calibration curve.

# 3.9. Measuring Fe<sup>2+</sup> in real tablet samples

In order to demonstrate the proposed method in real samples application, we further investigated the feasibility of the assay for the detection of Fe<sup>2+</sup> in tablet samples. Two types of the iron supplement tablets in the ferrous sulphate form were dissolved in deionized water and diluted to the appropriate concentration before the measurement. Concentrations of the Fe<sup>2+</sup> in diluted samples were directly calculated comparing to the standard calibration curve constructed by each method. Moreover, spiked samples with the standard Fe<sup>2+</sup> at two different concentration levels were also evaluated to determine the method accuracy. The amount of Fe<sup>2+</sup> in the tablet samples was also measured comparing to the 1.10-phenanthroline method. In addition, total Fe in the tablet samples were determined by using ICP-OES. The results obtained from the three methods are listed in Table 1. From Table 1, Fe<sup>2+</sup> concentrations in the sample I and sample II calculated by the three methods were not significantly different. Moreover, after spiking two different Fe<sup>2+</sup> concentration levels into the samples, the %recovery in the range of 98.6–116.8% was obtained, confirming the accuracy of the sensor. Regarding the precision aspect, %R.S.D. values of three measurements were less than 0.025%. These results showed that the proposed sensor provided a very good precision.

**Table 1** Measurements of Fe<sup>2+</sup> in iron supplement tablet samples using the proposed sensor,

1.10 phenanthroline and ICP-OES method.

Methods	Sample No	Added (µg)	Found $\pm$ SD (%W/W)	%RSD	% Recovery ± SD
This method	Sample I	-	$13.45 \pm 0.20$	0.015	-
		5.58	$16.46 \pm 0.06$	0.003	$104.9 \pm 0.4$
		16.7	$20.81 \pm 0.33$	0.016	$103.3 \pm 1.7$
	Sample II	-	$15.85 \pm 0.23$	0.014	-
		5.58	$21.12 \pm 0.53$	0.025	$116.8 \pm 2.9$
		16.7	$23.56 \pm 0.00$	0.002	98.6±0.2
1,10- Phenanthroline		-	$13.95 \pm 0.42$	0.030	-
	Sample I	5.58	$15.82 \pm 0.25$	0.016	97.8±1.5
		16.7	$20.23 \pm 0.10$	0.005	$98.0 \pm 0.5$
	Sample II	-	$16.03 \pm 0.66$	0.041	-
		5.58	$18.16 \pm 0.11$	0.006	$99.4 \pm 0.1$
		16.7	$22.50 \pm 0.00$	0.002	99.0±0.2
ICP-OES		-	$14.30 \pm 0.20$	0.014	-
	Sample I	5.58	$15.90 \pm 0.20$	0.013	96.3±1.2
		16.7	$19.80 \pm 0.49$	0.025	$94.3 \pm 2.3$
	Sample II	-	$16.43 \pm 0.07$	0.004	-
		5.58	$18.10 \pm 0.05$	0.003	$96.8 \pm 0.3$
		16.7	$22.10 \pm 0.59$	0.026	95.5±2.6

## 4. Conclusion

We have successfully demonstrated a new, selective, and rapid colorimetric sensor for the determination of  $Fe^{2+}$  using PMAA-templated AgNCs. In the presence of  $Fe^{2+}$ , the color of AgNCs turned to orange and can be observed by the naked eye. On the other hand, other studied metal ions did not alter the color of the AgNCs signifying that this sensor possesses high selectivity towards  $Fe^{2+}$ . The maximum plasmon band at 447 nm linearly increases with the increasing of  $Fe^{2+}$  concentrations due to the decreasing of silver nanoclusters form and the increasing of the silver nanoparticles form. The proposed  $Fe^{2+}$  sensor provided a wide working range of 5–100  $\mu$ M with very low detection limit of 76 nM. This sensor was applied to determine  $Fe^{2+}$  in iron supplement tablet samples with satisfactory results.

## References

- [1] J.J.R. Fraústo da Silva and R.J.P. Williams, The biological chemistry of the elements. The Inorganic Chemistry of Life, Oxford University Press, New York, 1991.
- [2] P.C.C. Oliveira, J.C. Masini, Sequential injection determination of iron (II) in antianemic pharmaceutical formulations with spectrophotometric detection. Anal. Lett. 34 (2001) 389-397.
- [3] J.R. Burdo, J.R. Connor, Brain iron uptake and homeostatic mechanisms: an overview, Biometals. 16 (2003) 63-75.
- [4] A.N. Araujo, J. Gracia, J.L.F.C. Lima, M. Poch, M. Lucia, M.F.S. Saraiva, Colorimetric determination of iron in infant fortified formulas by sequential injection analysis, Fresenius. J. Anal. Chem. 357 (1997) 1153-1156.
- [5] P.K. Tarafder, R. Thakur, Surfactant-mediated extraction of iron and its

- spectrophotometric determination in rocks, minerals, soils, stream sediments and water samples, Microchem J. 80 (2005) 39–43.
- [6] M.A. Kassem, A.S. Amin, Spectrophotometric determination of iron in environmental and food samples using solid phase extraction, Food Chem. 141 (2013) 1941–1946.
- [7] S.M. Abdel-Azeem, N.R. Bader, H.M. Kuss, M.F. El-Shahat, Determination of total iron in food samples after flow injection preconcentration on polyurethane foam functionalized with N,N-bis(salicylidene)-1,3-propanediamine, Food Chem. 138 (2013) 1641–1647.
- [8] N. Yongnian, H. Chunfang, K. Serge, Simultaneous determination of iron and aluminium by differential kinetic spectrophotometric method and chemometrics, Anal. Chim. Acta. 599 (2007) 209–218.
- [9] A.B. Tabrizi, Development of a dispersive liquid-liquid microextraction method for iron speciation and determination in different water samples, J. Hazard. Mater. 183 (2010) 688-693.
- [10] J.S. Kosse, A.C. Yeung, A.I. Gil, D.D. Miller, A rapid method for iron determination in fortified foods, Food Chem. 75 (2001) 371–376.
- [11] M.L. Firdaus, W. Alwi, F. Trinoveldi, I. Rahayu, L. Rahmidar, K. Warsito, Determination of chromium and iron using digital Image-based colorimetry, Procedia Environ Sci. 20 (2014) 298 304.
- [12] D.A. Weeks, K.W. Bruland, Improved method for shipboard determination of iron in seawater by flow injection analysis, Anal. Chim. Acta. 453 (2002) 21–32.
- [13] S. Koronkiewicz, S. Kalinowski, Application of direct-injection detector integrated with the multi-pumping flow system to photometric stop-flow determination of total iron, Talanta. 96 (2012) 68–74.
- [14] T. Watanabe, N. Teshima, S. Nakano, T. Kawashima, Flow-injection/standard subtraction method for the determination of iron(III) based on its catalytic effect and inhibition of EDTA, Anal. Chim. Acta. 374 (1998) 303-307.
- [15] S.S.M. Rodrigues, A.S. Lima, L.S.G. Teixeira, M.d.G.A. Korn, J.L.M. Santos, Determination of iron in biodiesel based on fluorescence quenching of CdTe quantum dots, Fuel. 117 (2014) 520–527.
- [16] Y. Du, M. Chen, Y. Zhang, F. Luo, C. He, M. Li, X. Chen, Determination of iron(III) based on the fluorescence quenching of rhodamine B derivative, Talanta. 106 (2013) 261–265.
- [17] P.L. Croot, P. Laan, Continuous shipboard determination of Fe(II) in polar waters using flow injection analysis with chemiluminescence detection. Anal. Chim. Acta. 466 (2002) 261-273.
- [18] A. Banerjee, D. Nayak, S. Lahiri, A new method of synthesis of iron doped calcium alginate beads and determination of iron content by radiometric method, Biochem. Eng. J. 33 (2007) 260–262.
- [19] M. Aghaie, M. Giahi, H. Aghaie, M. Arvand, M. Pournaghdy, F. Yavari, New Fe(II) ion–selective electrode based on N-phenylaza-15-crown-5 as neutral carrier in PVC matrix, Desalination. 247 (2009) 346–354.
- [20] K.R. Bandi K.S. Ashok, U. Anjali, Construction and performance characteristics of polymeric membrane electrode and coated graphite electrode for the selective determination of Fe<sup>3+</sup> ion, Mater. Sci. Eng. C. 36 (2014) 187–193.
- [21] M.H. Mashhadizadeh, I.S. Shoaei, N. Monadi, A novel ion selective membrane potentiometric sensor for direct determination of Fe(III) in the presence of Fe(II), Talanta. 64 (2004) 1048–1052.
- [22] H.A. Zamani, M.R. Ganjali, F. Faridbod, M. Salavati-Niasari, Heptadentate Schiff-base based PVC membrane sensor for Fe(III) ion determination in water samples, Mater. Sci.

- Eng. C. 32 (2012) 564-568.
- [23] W.H. Mahmoud, Iron ion-selective electrodes for direct potentiometry and potentiotitrimetry in pharmaceuticals, Anal. Chim. Acta. 436 (2001) 199–206.
- [24] A. Sil, V.S. Ijeri, A.K. Srivastava, Coated-wire iron(III) ion-selective electrode based on iron complex of 1,4,8,11-tetraazacyclotetradecane, Sens. Actuator B-Chem. 106 (2005) 648–653.
- [25] D. Merli, A. Profumo, C. Dossi, An analytical method for Fe(II) and Fe(III) determination in pharmaceutical grade iron sucrose complex and sodium ferric gluconate complex, J. Pharm. Anal. 2 (2012) 450–453.
- [26] R.K. Shervedani, A. Hatefi-Mehrjardi, A. Asadi-Farsani, Sensitive determination of iron(III) by gold electrode modified with 2-mercaptosuccinic acid self-assembled monolayer, Anal. Chim. Acta. 601 (2007) 164–171.
- [27] A. Kamal, N. Kumar, V. Bhalla, M. Kumar, R.K. Mahajan, Rhodamine-dimethyliminocinnamyl based electrochemical sensors for selective detection of iron (II), Sens. Actuator B-Chem. 190 (2014) 127–133.
- [28] M. Frankowski, Simultaneous determination of aluminium, aluminium fluoride complexes and iron in groundwater samples by new HPLC-UVVIS method, Microchem J. 101 (2012) 80–86.
- [29] P. Mytides, S. Rozou, D. Benaki, E. Antoniadou-Vyza, 2,2':6',2''- Terpyridine[hydroxypropyl-β-cyclodextrin] 1:3 complex used as chelating agent for the determination of iron with a sensitive, selective and fast liquid chromatographic method, Anal. Chim. Acta. 566 (2006) 122–129.
- [30] S. García-Marco, M.A. Cremonini, P. Esteban, F. Yunta, L. Hernández-Apaolaza, G. Placucci, J.J. Lucena, Gradient ion-pair chromatographic method for the determination of iron N,N'-ethylenediamine-di-(2-hydroxy-5-sulfophenylacetate) by high performance liquid chromatography—atmospheric pressure ionization electrospray mass spectrometry, J. Chromatogr. A. 1064 (2005) 67–74.
- [31] Y. Bakircioglu, D. Bakircioglu, N. Tokman, A novel preconcentration method for determination of iron and lead using Chromosorb-103 and flame atomic absorption spectrometry, Anal. Chim. Acta. 547 (2005) 26–30.
- [32] M. Niemelä, H. Kola, K. Eilola, P. Perämäki, Development of analytical methods for the determination of sub-ppm concentrations of palladium and iron in methotrexate, J. Pharm. Biomed. Anal. 35 (2004) 433–439.
- [33] S.E. Pepper, M. Borkowski, M.K. Richmann, D.T. Reed, Determination of ferrous and ferric iron in aqueous biological solutions, Anal. Chim. Acta. 663 (2010) 172–177.
- [34] A. Huberman, C. Perez, Nonheme iron determination. Anal. Biochem. 307 (2002) 375-378.
- [35] D. Wei, Y. Sun, J. Yin, G. Wei, Y. Du, Design and application of Fe<sup>3+</sup> probe for "naked-eye" colorimetric detection in fully aqueous system, Sens. Actuator B-Chem. 160 (2011) 1316–1321.
- [36] N.R. Chereddy, K. Suman, P.S. Korrapati, S. Thennarasu, A.B. Mandal, Design and synthesis of rhodamine based chemosensors for the detection of Fe<sup>3+</sup> ions, Dyes Pigment. 95 (2012) 606–613.
- [37] T.-B. Wei, P. Zhang, B.-B. Shi, P. Chen, Q. Lin, J. Liu, Y.-M. Zhang, A highly selective chemosensor for colorimetric detection of Fe<sup>3+</sup> and fluorescence turn-on response of Zn<sup>2+</sup>, Dyes Pigment. 97 (2013) 297-302.
- [38] H. Ozay, O. Ozay, Rhodamine based reusable and colorimetric naked-eye hydrogel sensors for Fe<sup>3+</sup> ion, Chem. Eng. J. 232 (2013) 364–371.
- [39] M. She, Z. Yang, B. Yin, J. Zhang, J. Gu, W. Yin, J. Li, G. Zhao, Z. Shi, A novel rhodamine-based fluorescent and colorimetric "off-on" chemosensor and investigation

- of the recognizing behavior towards Fe<sup>3+</sup>, Dyes Pigment. 92 (2012) 1337-1343.
- [40] Y. Zhang, G. Wang, J. Zhang, Study on a highly selective fluorescent chemosensor for Fe<sup>3+</sup> based on 1,3,4-oxadiazole and phosphonic acid, Sens. Actuator B-Chem. 200 (2014) 259-268.
- [41] S. Wang, S.-Y. Gwon, S.-H. Kim, A highly selective and sensitive colorimetric chemosensor for Fe<sup>2+</sup> based on fluoran dye. Spectrochim. Acta A. 76 (2010) 293-296.
- [42] Z.O. Tesfaldet, J.F. van Staden, R.I. Stefan, Sequential injection spectrophotometric determination of iron as Fe(II) in multi-vitamin preparations using 1,10-phenanthroline as complexing agent, Talanta. 64 (2004) 1189-1195.
- [43] H. Xu, K.S. Suslick, Water-soluble fluorescent silver nanoclusters, Adv. Mater. 22 (2010) 1078-1082.
- [44] F. Lu, S. Zhou, J.-J. Zhu, Photochemical synthesis of fluorescent Ag nanoclusters and enhanced fluorescence by ionic liquid. Int. J. Hydrogen Energy. 38 (2013) 13055-13061.
- [45] X. Yu, Q. Wang, The determination of copper ions based on sensitized chemiluminescence of silver nanoclusters, Microchim. Acta. 173 (2011) 293-298.
- [46] L. Shang, S. Dong, Facile preparation of water-soluble fluorescent silver nanoclusters using a polyelectrolyte template, Chem. Commun. 9 (2008) 1088–1090.
- [47] S. Liu, F. Lu, J.-J. Zhu, Highly fluorescent Ag nanoclusters: microwave-assisted green synthesis and Cr<sup>3+</sup> sensing, Chem. Commun. 47 (2011) 2661–2663.
- [48] H. Xu, K.S. Suslick, Sonochemical synthesis of highly fluorescent Ag nanoclusters, ACS Nano. 4 (2010) 3209–3214.
- [49] J. Zheng, R.M. Dickson, Individual water-soluble dendrimer-encapsulated silver nanodot fluorescence, J. Am. Chem. Soc. 124 (2002) 13982-13983.
- [50] P.R. O'Neill, L.R. Velazquez, D.G. Dunn, E.G. Gwinn, D.K. Fygenson, Hairpins with poly-C loops stabilize four types of fluorescent Agn:DNA. J. Phys. Chem. C. 113 (2009) 4229-4233.
- [51] X. Huang, B. Li, L. Li, H. Zhang, I. Majeed, I. Hussain, B. Tan, Facile preparation of highly blue fluorescent metal nanoclusters in organic media. J. Phys. Chem. C, 116 (2012) 448-455.
- [52] S. Huang, C. Pfeiffer, J. Hollmann, S. Friede, J.J.-C. Chen, A. Beyer, B. Haas, K. Volz, W. Heimbrodt, J.M. Montenegro Martos, W. Chang, W.J. Parak, Synthesis and characterization of colloidal fluorescent silver nanoclusters, Langmuir 28 (2012) 8915-8919.
- [53] L. Shang, S. Dong, Silver nanocluster-based fluorescent sensors for sensitive detection of Cu(II), J. Mater. Chem. 18 (2008) 4636–4640.
- [54] X. Ren, Z. Chen, X. Meng, D. Chen, F. Tang, Synthesis of fluorescent Ag nanoclusters and their application in α-L-fucosidase detection, Chem. Commun. 48 (2012) 9504–9506.
- [55] Y. Cheng, M. Zhang, H. Yang, F. Li, T. Yi, C. Huang, Azo dyes based on 8-hydroxyquinoline benzoates synthesis and application as colorimetric Hg<sup>2+</sup>-selective chemosensors, Dyes Pigment. 76 (2008). 775-783.
- [56] I. Díez, R.H.A. Ras, Fluorescent silver nanoclusters, Nanoscale. 3 (2011) 1963-1970.
- [57] J.P. Wilcoxon, B.L. Abrams, Synthesis, structure and properties of metal nanoclusters, Chem. Soc. Rev. 35 (2006) 1162.
- [58] J. Zheng, P.R. Nicovich, R.M. Dickson, Highly fluorescent noble-metal quantum dots, Annu. Rev. Phys. Chem. 58 (2007) 409-431.
- [59] S. Dhanya, V. Saumya, T.P. Rao, Synthesis of silver nanoclusters, characterization and application to trace level sensing of nitrate in aqueous media, Electrochim. Acta 102 (2013) 299–305.

- [60] M.M. Alvarez, J.T. Khoury, T.G. Schaaff, M.N. Shafigullin, I. Vezmar, R.L. Whetten, Optical absorption spectra of nanocrystal gold molecules, J. Phys. Chem. B. 101 (1997) 3706–3712.
- [61] T.G. Schaaff, M.N. Shafigullin, J.T. Khoury, I. Vezmar, R.L. Whetten, W.G. Cullen, P.N. First, C. Gutie'rrez-Wing, J. Ascensio, M.J. Jose-Yacama'n, Isolation of smaller nanocrystal Au molecules: robust quantum effects in optical spectra, J. Phys. Chem. B. 101 (1997) 7885–7891.
- [62] T. Khantaw, C. Boonmee, T. Tuntulani, W. Ngeontae, Selective turn-on fluorescence sensor for Ag<sup>+</sup> using cysteamine capped CdS quantum dots: Determination of free Ag<sup>+</sup> in silver nanoparticles solution, Talanta. 115 (2013) 849–856.
- [63] S.G. Bratsch, Standard electrode potentials and temperature coefficients in water at 2981.5 K, J. Phys. Chem. Ref. Data. 18 (1989) 1-21.

# 2. L-Cysteine modified luminescence nanomatrials as fluorescence sensor for Co<sup>2+</sup>: effects of core nanomaterials in detection selectivity

## 1. Introduction

Cobalt is a vital trace element that plays an important role in human organisms as a key component of vitamin B12 [1,2]. However, cobalt is also acutely toxic in larger doses and even long-term exposure at low level. Cobalt can give rise to adverse health effects related to various organs and tissues such as decreased cardiac output, thyroid enlargements, heart disease, and elevated red blood cells [3-5].

Numerous techniques have been used for the determination of trace Co<sup>2+</sup> such as flame atomic absorption spectrometry (FAAS) [6], inductively coupled plasma–atomic emission spectrometry (ICP-OES) [7,8], fluorometric methods [9,10], surface-enhanced raman spectroscopy [10], electrochemical techniques [12,13] and colorimetric methods [14,15]. However, these methods have their own limitations such as tedious sample treatments, time-consuming and expensive instrumentation.

Nowadays, chemical sensor is an interesting research discipline to analytical chemists. Chemical sensors fabricated from nanomaterials are currently a hot issue due to special properties of the nanometerials upon the size reduction to nanometer levels. Optical phenomena of nanomaterials such as absorption or emission have been applied to fabricate new optical chemical sensors [16]. There are many kinds of optical chemical sensors using nanomaterials for the detection of heavy metal ions such as fluorescence sensors derived from quantum dots [17-20] and carbon dots [21]. Moreover, gold nanoparticles [22,23] and silver nanoparticles [24] have been used to fabricate colorimetric sensors for metal ions. However, based on the best of our knowledge, there are no reports regarding the effect of luminescence core nanomaterials in detection selectivity toward heavy metal ions. Therefore, in this work we investigate the role of luminescence core nanomaterials towards the detection selectivity of the fabricated sensors.

Recently, silver nanoclusters (AgNCs) have been discovered as a new class of luminescent nanomaterials and have attracted a great deal of interests from analytical chemists [25-27]. AgNCs show excellent photophysical properties such as good photostability, high photoluminescence and large Stokes shift [28]. Basically, the size of silver nanoclusters is found between silver atoms and silver nanoparticles which is close to the Femi wavelength of electrons, ca. 0.5 nm [29]. Therefore, a molecular like phenomenon is dominated from discrete energy levels [30], resulting in size-dependent luminescence and exhibiting better optical properties compared to silver nanoparticles [31].

AgNCs were found to be excellent fluorophores for chemical sensing, bioimaging, bio-labels, catalysis and single-molecule studies [32]. AgNCs can be prepared from the chemical reduction [33-36],  $\gamma$ -rays irradiation [25], sonochemistry [37] or photochemical reduction [38] of silver nitrate in the presence of different template/capping molecules such as DNA [39-43], peptides and proteins [44], dendrimers [45], polymers [37], polymer microgels [46]. The as-prepared AgNCs from different synthetic methods were proposed as fluorescence probes for the detection of different specific target species such as  $\alpha$ -L-fucosidase [47],  $Cu^{2+}$  [48],  $Hg^{2+}$  [49] and  $Cr^{3+}$  [50]. However, there are a few reports regarding the fabrication of fluorescence sensors by modification of AgNCs surfaces with specific molecules to be a selective sensor for a specific target analyte.

In this work, we propose a new approach for the fabrication of the fluorescence sensor to detect  $Co^{2+}$  based on a modified surface of the luminescence nanomaterials including AgNCs and CdS QDs with L-Cysteine. AgNCs have been prepared by using poly(methacrylic acid) as both template and reducing agent and following by the reaction with L-Cysteine in a one pot reaction. There are many papers described the fluorescence sensors fabricated from L-Cysteine capped CdS QDs to detect  $Ag^+$  [51],  $Hg^{2+}$  [52] and  $Zn^{2+}$  [53]. However, there is no report regarding the use of Cyst-CdS QDs as a  $Co^{2+}$  sensor. The analogues L-Cysteine capped cadmium sulfide quantum dots (Cyst-CdS QDs) was also synthesized. Luminescence properties of the L-Cyst-AgNCs and Cyst-CdS QDs are investigated to find a suitable sensor for  $Co^{2+}$ . Circular dichroism (CD) spectroscopy is also used to observe the formation of  $Co^{2+}$  complex with L-Cysteine on the surface of both luminescence nanomaterials. Moreover, the effective sensor is applied to determine  $Co^{2+}$  in real water samples.

## 2. Experimental

# 2.1 Reagents

All chemicals were of analytical grade and used without further purification. L-Cysteine was obtained from Aldrich. AgNO<sub>3</sub> was purchased from BDH. Poly(methacrylic acid) (PMAA) was received from Carlo Erba. Cobalt nitrate was received from Fluka. Trishydroxymethyl- methylamine was obtained from Merck. Sodium hydroxide was purchased from UNIVAR. Hydrochloric acid 37% were purchased from QReC. All aqueous solutions were prepared by using deionized water with the specific resistivity of 18.2 M $\Omega$  cm from RiO<sub>s</sub> TM Type I Simplicity 185 (Millipore water). L-Cysteine capped CdS quantum dots (L-Cyst-CdS QDs) used in this work were synthesized using the previously reported procedure [54].

## 2.2 Instrumentation

Emission spectra were recorded using a RF-5301PC spectrofluorophotometer (Shimadzu). Slit widths for the excitation and emission were 5 nm. Absorption spectrum of the L-Cyst-AgNCs solution was recorded on a Agilent HP 8453 spectrophotometer (Agilent). Inductively coupled plasma optical emission spectrometer (ICP-OES, Optima 2100 DV, USA) was employed for the determination of Co<sup>2+</sup> in real water samples. Transmission electron microscopy (TEM) images of L-Cyst-AgNCs were obtained from a TecnaiG<sup>2</sup>-20 (FEI, Netherlands) under the accelerating voltage of 200 kV. Circular dichroism (CD) spectra were measured on a J-815 circular dichroism spectrometer (Jasco). The pH of solution was measured using a UB-10 UltraBasic pH meter (Denver Instrument).

## 2.3 Synthesis of L-Cysteine modified silver nanocluster (L-Cyst-AgNCs)

The L-Cysteine modified silver nanoclusters (L-Cyst-AgNCs) were synthesized by modification of the method described previously [55]. PMAA was diluted ten times by deionized water and the solution of 12.5 mM AgNO<sub>3</sub> was sonicated in ultrasonic bath for 30 minutes. Into a three neck round bottom flask, the mixtute of 11 mL of diluted PMAA and 80 mL of AgNO<sub>3</sub> was heated at 80 °C under N<sub>2</sub> atmosphere for 15 minutes. In anothor flask, L-Cysteine (0.1515 g) was dissolved in 7 mL of deionized water and 3 mL of 1.0 M NaOH. Then, the solution of L-Cysteine was quickly added to the hot solution in the three neck round bottom flask. After refluxing for 270 min, a yellow brown color of L-Cyst-AgNCs was obtained.

## 2.4 Fluorescence measurements

To study the quenching of L-Cyst-AgNCs and L-Cyst-CdS QDs emission spectrum by  $Co^{2+}$ , the following general procedures were carried out. To a 10 mL volumetric flask containing 1.5 mL of the L-Cyst-AgNCs or the L-Cyst-CdS QDs solution was added 10.0 mM of the stock solution of  $Co^{2+}$  to a given concentration level. Then, 1.0 mL of 1.0 M Tris–HCl buffer solution pH 9.5 was added to adjust the solution pH, and the mixture was diluted to a final volume of 10.00 mL with deionized water. The solution mixture was then incubated at room temperature for 10 minutes before recording the fluorescence spectrum at  $\lambda_{em}/\lambda_{ex} = 520/383$  nm and 495/330 nm for L-Cyst-AgNCs and L-Cyst-CdS QDs, respectively.

## 2.5 Interference studies

The selectivity of the proposed sensor towards  $Co^{2+}$  over other cations was evaluated by the following procedure. Each stock solution of metal ions (10 mM) was prepared by dissolution of a metal salt in deionized water. To a 10 mL volumetric flask, 50  $\mu$ L of the stock solution (to be a final concentration of 50  $\mu$ M) was mixed with 1.50 mL of the L-Cyst-AgNCs solution. Then, 1.0 mL of 1.0 M Tris–HCl buffer solution pH 9.5 was subsequently added to control the solution pH, and the mixture was diluted to a final volume of 10.00 mL with deionized water. The solution mixture was then incubated at room temperature for 10 minutes before recording the fluorescence spectrum.

## 2.6 Circular dichroism (CD) measurement

Circular dichroism spectra of L-Cystiene, and L-Cyst-AgNCs in the absence and presence of various metal ions were studied by the following procedure. To a 10 mL volumetric flask, 50 µL of 10 mM Co<sup>2+</sup> was mixed with 1.50 mL of the L-Cyst-AgNCs solution or 1.50 mL of 12.5 mM L-Cystiene. Then, 1.0 mL of 1.0 M Tris–HCl buffer solution pH 9.5 was sequentially added to adjust the solution pH, and the mixture was diluted to a final volume of 10.00 mL with deionized water. The solution mixture was then incubated at room temperature for 10 minutes and diluted 10 times with deionized water before recording the CD spectrum. The CD spectra were collected with a standard sensitivity of 100 mdeg, a data pitch of 1.0 nm, a bandwidth of 1.0 nm, a scanning speed of 200 nms<sup>-1</sup>, and a response time of 1 s using a quartz cuvette (1 cm path length). The circular dichroism spectra of L-Cyst-CdS QDs in the absensence and presence of various metal ions were studied according to our previously published paper [54].

## 2.7 Application to real water samples

In order to demonstrate the applicability of the proposed sensor, real ground water was used as representative environmentally contaminated samples. The water sample was collected with a polyethylene bottle and used immediately after filtering through a filter paper. The accuracy and precision of the proposed sensor were evaluated by the determination of spiked samples at 3 different concentrations (25, 50 and 75  $\mu$ M) under the optimized condition. The concentration of Co<sup>2+</sup> in the spiked samples were calculated using the calibration curve. The results from the proposed sensor was compared to those obtained from the ICP-OES technique.

### 3. Results and discussion

In this work, AgNCs were synthesized by using PMAA as both a reducing agent and a template, following by the modification of the AgNCs surface with L-Cysteine to obtain the as-prepared L-Cyst-AgNCs. CdS QDs capped with L-Cysteine were also synthesized in order to compare the effect of core materials. Both of the synthesized compounds were proposed as a fluorescence sensor for the detection of Co<sup>2+</sup>. The sensor characterization and parameters possibly affected the detection efficiency were studied and discussed.

# 3.1. Characteristics and optical properties of L-Cyst-AgNCs and L-Cyst-CdS QDs

The size and morphology of the as-prepared L-Cyst-AgNCs were evaluated by transmission electron microscopy (TEM). The TEM image of the L-Cyst-AgNCs was shown in Fig. 1. It can be seen from Fig. 1 that size of the synthesized product was at the nanocluster level with the average size approximately 2.2±0.5 nm. In addition, the shape of the L-Cyst-AgNCs was close to spherical. The size distribution was very narrow suggesting a well-dispersed nanomaterial. Moreover, there was no formation of larger silver nanoparticles or aggregates appeared in the image. Form the morphology results, this material should provide good optical characteristics, especially fluorescence emission.

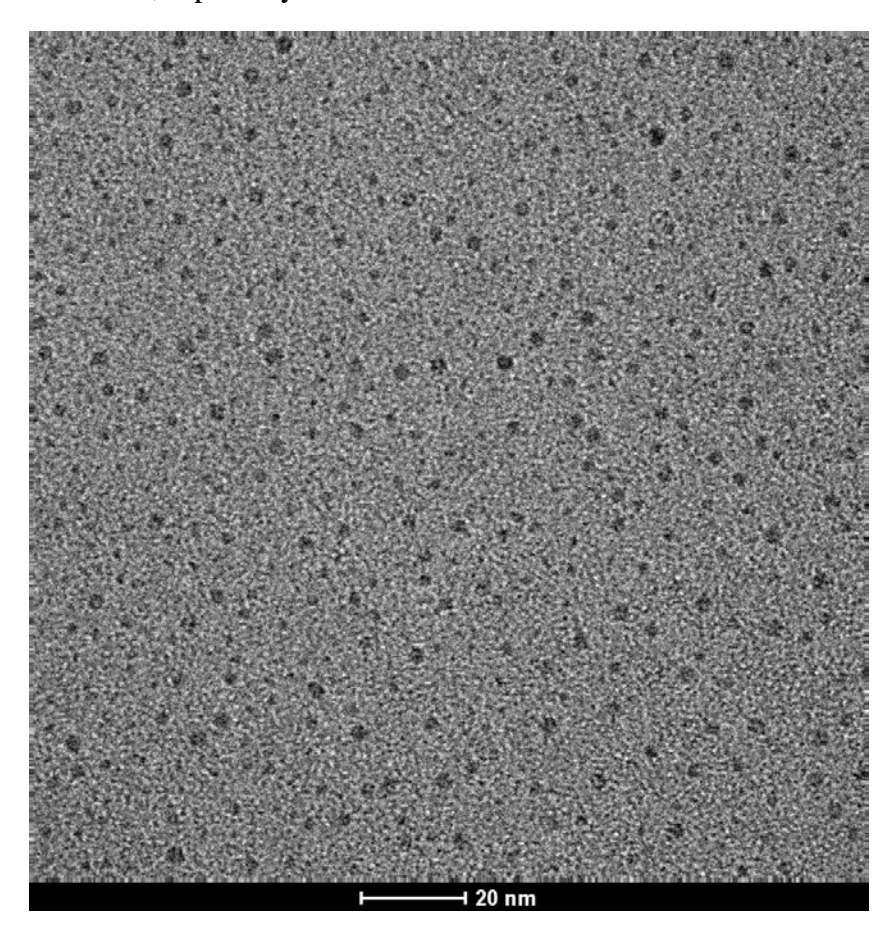
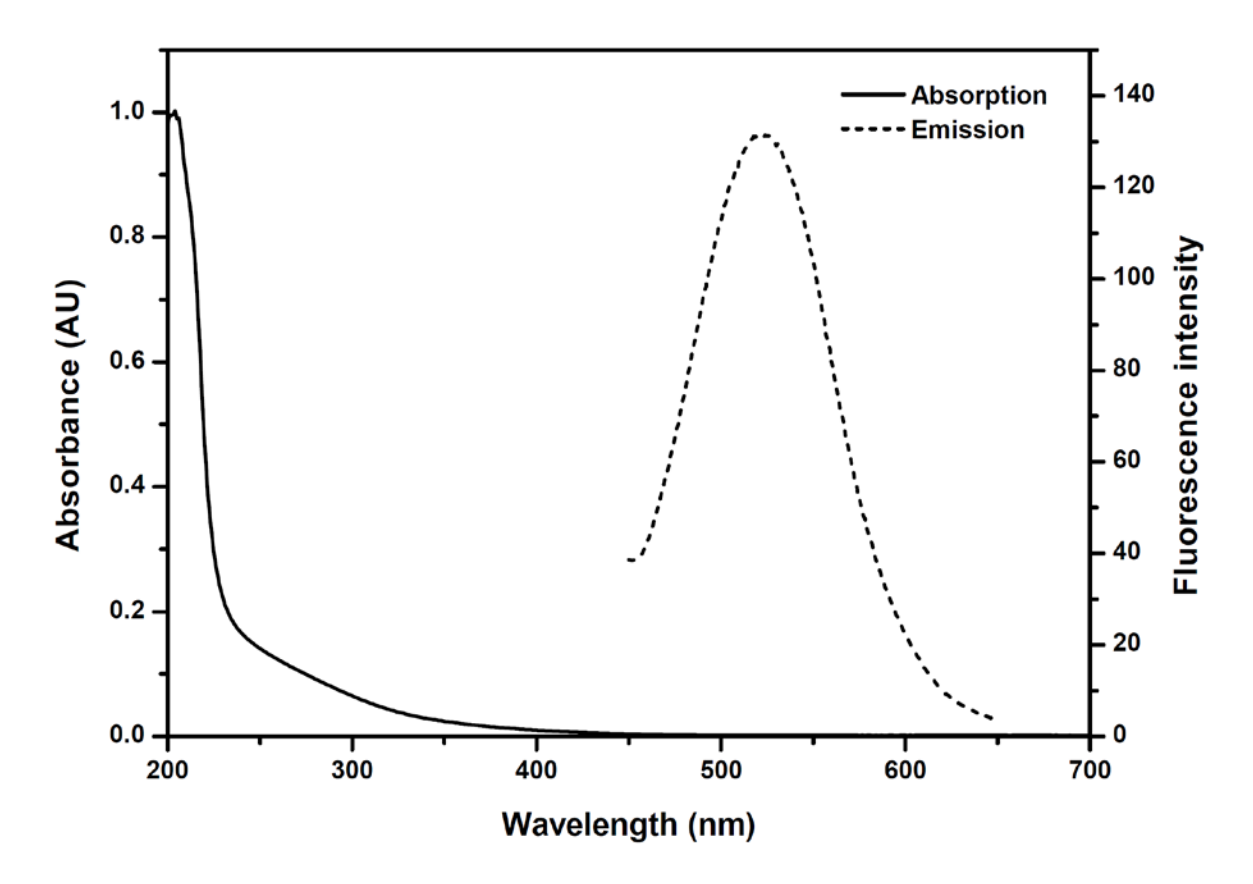


Fig. 1 The TEM image of L-Cyst-AgNCs

Optical properties of the L-Cyst-AgNCs were characterized from their absorption and emission spectra. Fig. 2 shows a UV-visible absorption spectrum and a fluorescence spectrum of the synthesized AgNCs. The L-Cyst-AgNCs showed an absorption onset at around 425 nm. However, there was no plasmon bands of Ag nanoparticles appeared around 380-450 nm. In addition, the damping and broadening of the plasmon absorption signified the unique

characteristic of silver at the nanocrystal level [56,57]. The fluorescence spectra of the asprepared L-Cyst-AgNCs are shown in Fig. 2. The strong emission of L-Cyst-AgNCs appeared at 520 nm with an excitation at 383 nm, which also indicated the formation of the silver nanoclusters. The as-prepared L-Cyst-AgNCs showed a symmetrical emission spectrum, indicating that the L-Cyst-AgNCs were monodisperse [58], agreeing well with the TEM result. Both optical and morphology studies suggested that the L-Cyst-AgNCs were successfully synthesized by the present method and possessed good optical properties for fabricating fluorescence sensors.



**Fig. 2** The absorption and fluorescence spectra of the synthesized L-Cyst-AgNCs ( $\lambda_{ex}/\lambda_{em}=383/520$  nm).

The synthesis and characterization details of L-Cyst-CdS QDs were already reported in previous publications (ESI) [54]. A typical TEM image of the Cyst-CdS QDs (Fig. S1; ESI) showed highly uniform and monodisperse nanocrystals in a narrow distribution of 2.8 ± 0.4 nm diameter. An absorption band edge was observed around 420 nm (Fig. S2 (a); ESI). In addition, a fluorescence emission band was observed at 495 nm upon exciting at 330 nm (Fig. S2 (a); ESI). Moreover, the obtained fluorescence spectrum shape was well defined and relatively symmetrical. Since the fluorescence spectrum of quantum dots is very sensitive to their size and shape, the result implies that the synthesized L-Cyst-CdS QDs are uniform in shape and naturally spherical.

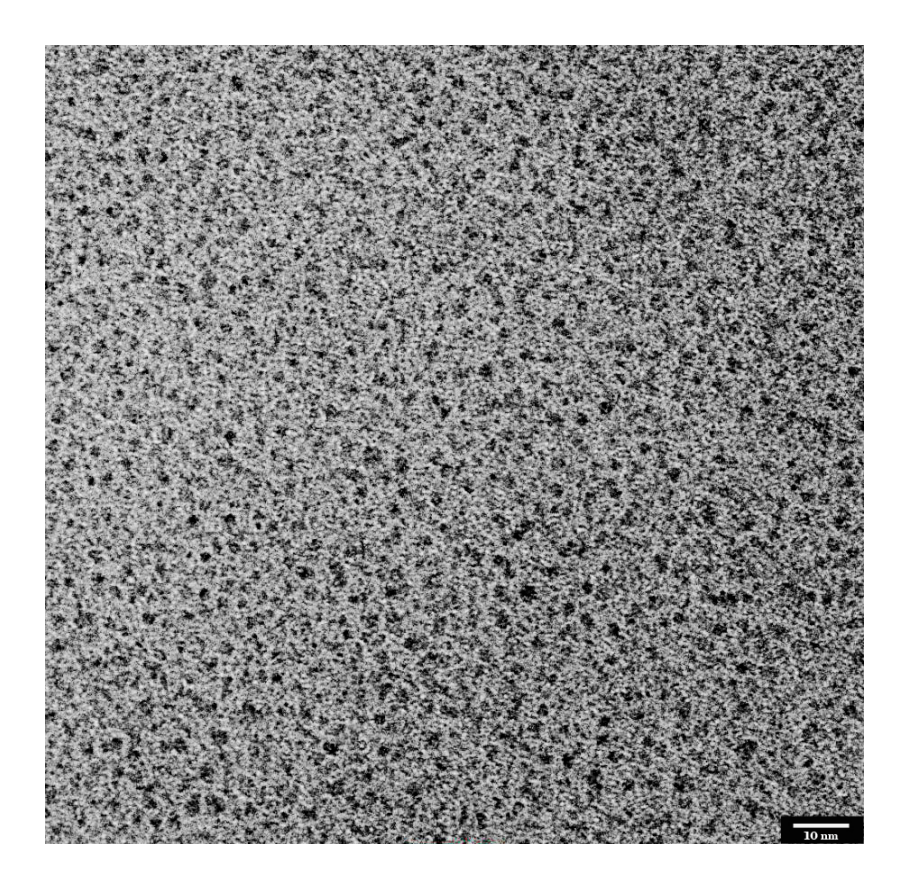


Fig. S1TEM image of the L-Cyst-CdS QDs with the average particle size of  $2.8 \pm 0.4$  nm (N=229)

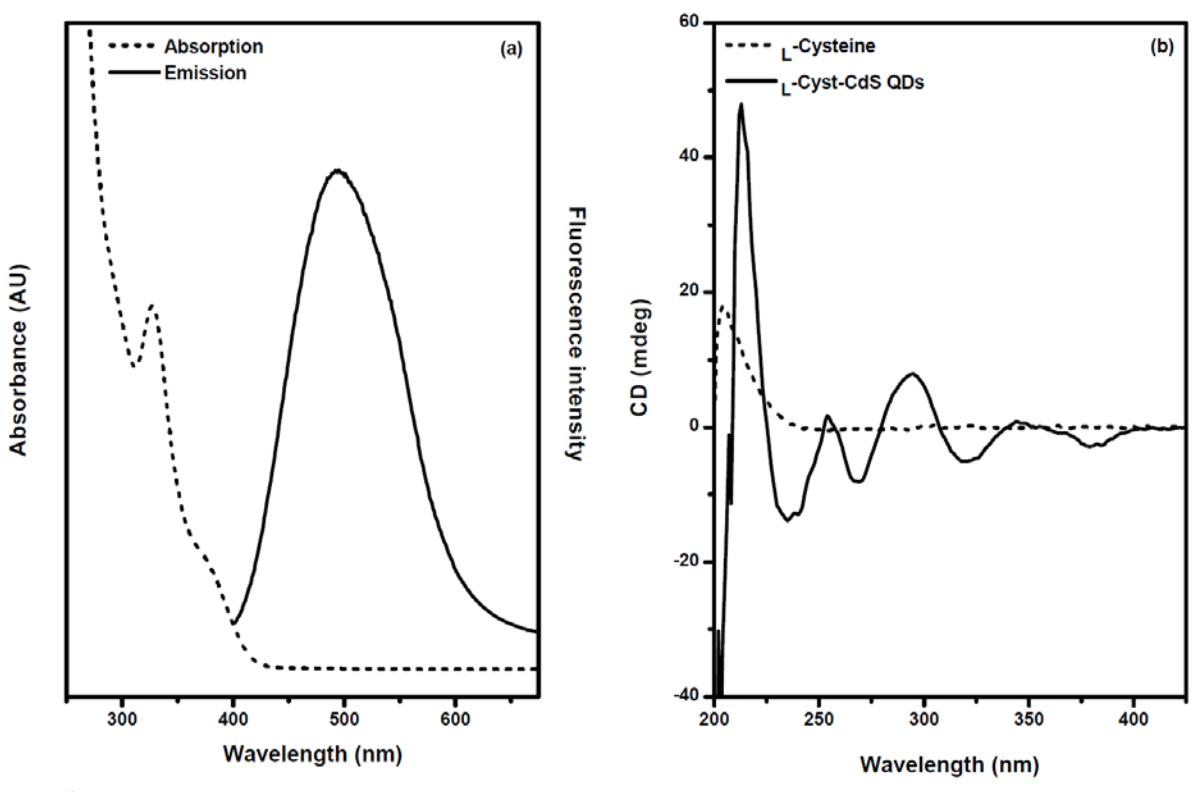
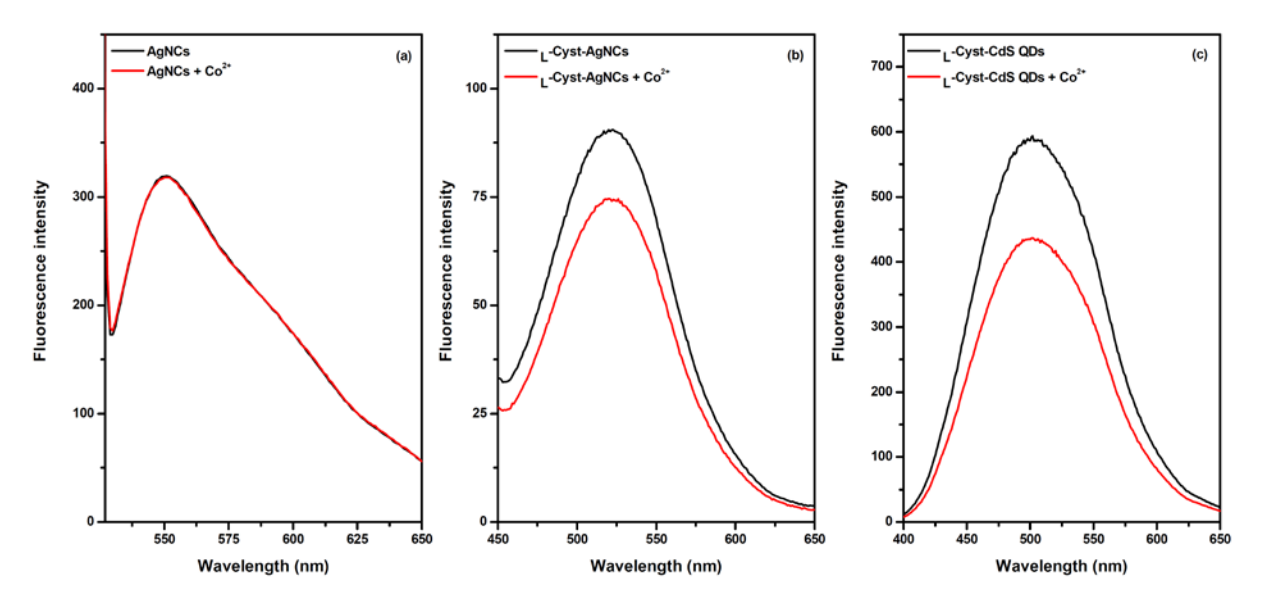


Fig. S2(a) absorption (dash line) and fluorescence (solid line) spectrum of 1.095 mM  $_{\rm L}\text{-}Cyst-CdS~QDs~(\lambda_{ex}=330~nm)$  in 0.1 M PBS pH 7.0, (b) CD spectrum of 2.50 mM  $_{\rm L}\text{-}Cysteine$  and 0.365 mM  $_{\rm L}\text{-}Cyst-CdS~QDs$  in 0.1 M PBS pH 7.0.

## 3.2. Fluorescence spectrum

The fluorescence spectrum of the PMAA templated silver nanocluster (AgNCs) and L-Cyst-AgNCs were studied to demonstrate the importance of the surface modification by using L-Cystiene. The fluorescence spectrum of PMAA-templated AgNCs, L-Cyst-AgNCs and L-Cyst-CdS QDs in the absence and presence of Co<sup>2+</sup> are shown in Fig. 3(a), Fig. 3(b), and Fig. 3(c), respectively. The fluorescence spectrum of the PMAA-templated AgNCs (Fig. 3(a)) can be observed at the maximum fluorescence emission at 575 nm when exciting at 507 nm. When adding Co<sup>2+</sup> in to the solution of PMAA-templated AgNCs, the fluorecence spectrum was slightly changed when comparing to the original spectrum. The results signified that the PMAA-templated AgNCs can not be used as a fluorescence probe for the detection of Co<sup>2+</sup>. On the other hand, the fluorescence spectrum of L-Cyst-AgNCs showed the maximum fluorescence emission at shorter wavelength of 520 nm when exciting at 383 nm signified the smaller cluster size than PMAA-templated AgNCs. In addition, the shape of the fluorescence spectrum was relatively symmetrical compared to the fluorescence spectrum of PMAA-templated AgNCs, suggesting that the L-Cyst-AgNCs had narrower size distribution. Furthermore, the fluorescence intensity of L-Cyst-AgNCs was significantly quenched in the presence of Co<sup>2+</sup>, but the spectrum maintained the same pattern. The fluorescence quenching may be due the electron transfer from core AgNCs to the Co<sup>2+</sup> which form complex with L-Cysteine moieties on the AgNCs surface. This phenomenon demonstrated the important role of L-Cystiene modified on the PMAA-templated AgNCs surface.

In addition, the same experiment has been carried out using the synthesized L-Cyst-CdS QDs as a probe and the results are shown in Fig. 3(c). The fluorescence spectrum of L-Cyst-CdS QDs can also be quenched in the presence of Co<sup>2+</sup> and the fluorescence spectrum maintains the same shape. This result revealed that Co<sup>2+</sup> may form a complex with L-Cysteine on the surface of the quantum dots and act as a good quencher. From this experiment, it can be noted that L-Cyst-AgNCs and the L-Cyst-CdS QDs can potentially be used as a fluorescence probe for the detection of Co<sup>2+</sup> by observing the degree of fluorescence quenching.



**Fig. 3** Fluorescence spectra of (a) PMAA-templated AgNCs, (b) L-Cyst-AgNCs and (c) L-Cyst-CdS QDs in 100 mM Tris–HCl buffer solution pH 9.5 in the presence and absence of  $50 \, \mu M \, \text{Co}^{2^+}$ .

## 3.3. Selectivity

Selectivity is a key index when a new chemical sensor is proposed. Ideally, the sensor must respond to only target species so that it can be used in a complex sample. The experiment has been carried out by measuring the fluorescence spectra after adding each metal ion at the same concentration level. The fluorescence spectra of the L-Cyst-AgNCs and L-Cyst-CdS QDs in the presence of various metal ions are shown in Fig. 4(a) and Fig. 4(b), respectively. It can be seen that the fluorescence spectrum of the L-Cyst-AgNCs and L-Cyst-CdS QDs are significantly quenched in the case of Co<sup>2+</sup>. However, other studied metal ions do not alter the fluorescence spectrum when using AgNCs as a luminescence core. This may due to the formation of a stable cobalt complex with the L-Cystiene moieties on the L-Cyst-AgNCs surface. Therefore, the electron transfer from the AgNCs to the cobalt complex can occur when the AgNCs are excited with an appropriate wavelength resulting in the fluorescence quenching (relaxation in the radiationless pathway).

On the other hand, when using CdS QDs as a luminescence core, other studied metal ions significantly altered the fluorescence spectrum of L-Cyst-CdS QDs (Fig. 4(b)). The poor selectivity signified that a metal ion could interact not only with the capping molecule but also with the core CdS QDs by the possible formation of a metal sulfide. From these results, it can be concluded that the type of luminescence core plays an important role in the selectivity of the sensor and use of AgNCs as a luminescence core provides better selectivity than CdS QDs.

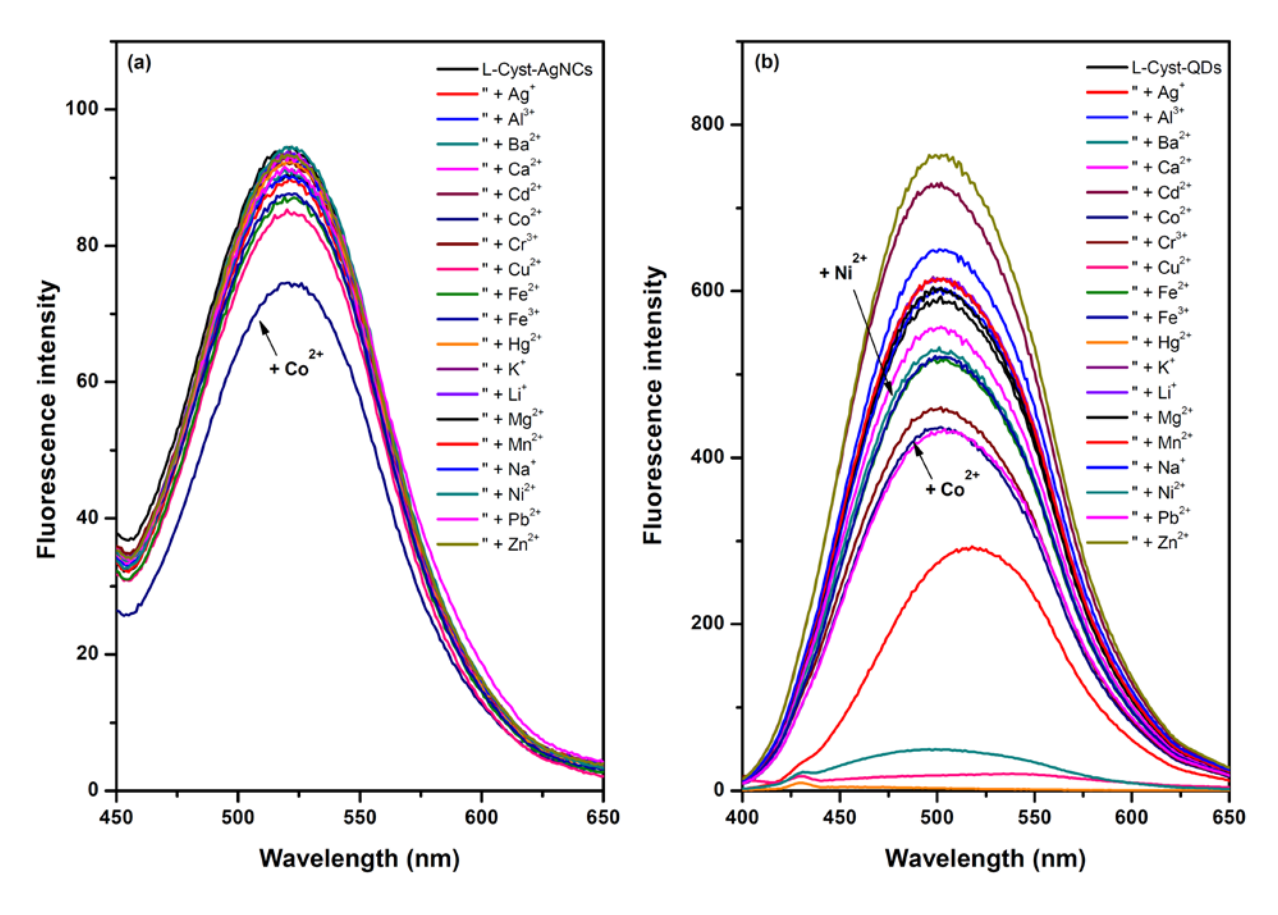


**Fig. 4**. Fluorescence spectrum of (a) 1.5 mM L-Cyst-AgNCs and (b) 0.23 mM L-Cyst-CdS QDs in the presence of 50  $\mu$ M of metal ions (reaction medium in 100 mM Tris–HCl buffer solution pH 9.5).

#### 3.4. Circular dichroism (CD) spectroscopy

Since the L-Cysteine molecule contains a chiral carbon, the L-Cyst-AgNCs should be optically active and give a CD spectrum. When Co<sup>2+</sup> complexes with L-cysteine on the surface of AgNCs to give a chiral Co<sup>2+</sup> complex, changes in the CD spectrum of L-Cyst-AgNCs can also be observed. CD spectra of L-Cyst-AgNCs and free L-Cystiene in the presence and absence of Co<sup>2+</sup> are illustrated in Fig. 5(a) and Fig. 5(b), respectively. Upon adding Co<sup>2+</sup> into the solution of free L-Cysteine and L-Cyst-AgNCs, the results in Fig. 5 showed that in the case of free L-Cysteine, the new CD band at around 275 nm was observed. The intensity of the band increased with the increasing of Co<sup>2+</sup> concentration, suggesting the formation of a chiral complex between L-Cysteine and Co<sup>2+</sup>. However, when observing the titration of L-Cyst-AgNCs with Co<sup>2+</sup>, the change in CD pattern was significantly different from the case of free L-Cysteine. In the presence of Co<sup>2+</sup>, a twist of CD spectrum at (-) 250 and (+) 296 nm can be observed. The intensity of both bands increased upon increasing Co<sup>2+</sup> concentrations. This result suggested that the chiral Co<sup>2+</sup> complex of the L-Cysteine moiety occurred on the surface of AgNCs.

Circular dichroism spectroscopy (CD) was also applied to shed light on the selectivity of the proposed sensor toward metal ions. The CD spectra of L-Cyst-AgNCs in the presence of various metal ions are shown in Fig. 5(c). The CD spectra of L-Cyst-AgNCs change to a twist shape which can be observed only in the presence of Co<sup>2+</sup>. On the other hand, the CD spectra do not change when adding other metal ions. The results implied only Co<sup>2+</sup> formed chiral complexes with the modified L-Cystiene moieties on the L-Cyst-AgNCs surface. The evidence from fluorescence and CD spectra confirmed that the proposed sensor could be a selective sensor for the detection of Co<sup>2+</sup>.

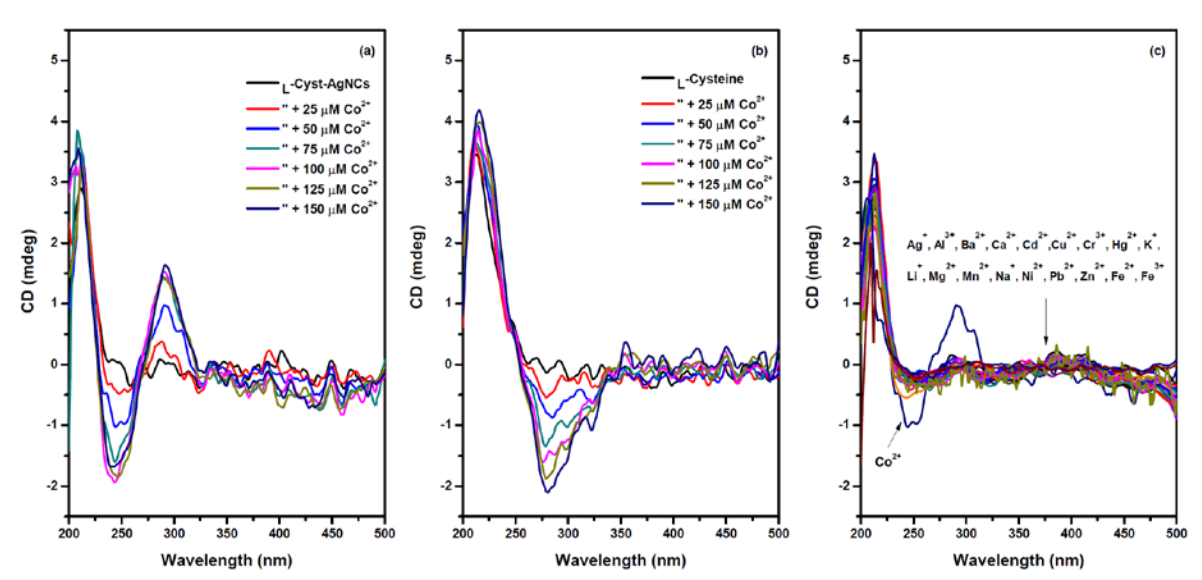


**Fig. 5** Circular dichroism spectra of (a) 0.15 mM L-Cyst-AgNCs, (b) 0.19 mM L-Cysteine and (c) 0.15 mM L-Cyst-AgNCs in the present of 5.0 μM different cations in 10 mM Tris-HCl buffer solution pH 9.5 in the presence of different concentrations of Co<sup>2+</sup>.

In the case of L-Cyst-CdS QDs, our previous work showed that the CD spectrum of L-Cyst-CdS QDs significantly changes only in the presence of Ni<sup>2+</sup> and Co<sup>2+</sup>. In the presence of only Ni<sup>2+</sup>, the CD signal at 324 nm changed to the opposite direction, while in the presence of only Co<sup>2+</sup> the intensity of the signal at 352 nm increased significantly as shown in Fig. S3 (ESI). On the other hand, other studied metal ions did not significantly affect the CD

spectrum of Cyst-CdS QDs. This experiment demonstrated that only Ni<sup>2+</sup> and Co<sup>2+</sup> were able to interact with cysteine on the CdS QDs surface to form chiral complexes.

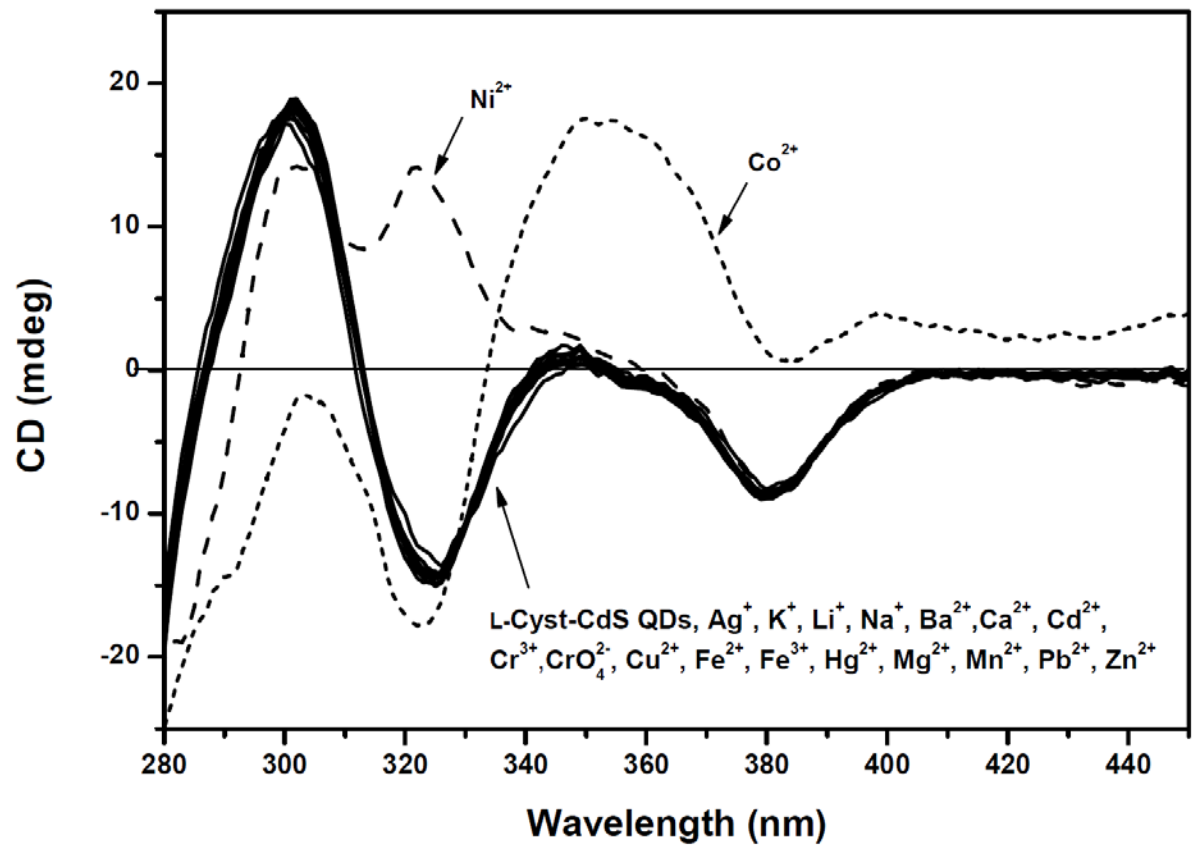


Fig. S3CD Spectrum of L-Cyst-CdS QDs in the presence of various metal ions (50  $\mu$ M) in 0.1 M PBS pH 7.0.

CD spectra of L-Cyst-AgNCs suggested that the fluorescence quenching of L-Cyst-AgNCs upon adding Co<sup>2+</sup> was due to the chiral complex formation between L-Cysteine on the nanomaterials surface and Co<sup>2+</sup> ions. However, CD spectra of L-Cyst-CdS QDs implied that the fluorescence quenching of L-Cyst-CdS QDs upon adding various metal ions was more complicated, rather than the simple coordination bonding of metal ions to the L-Cysteine moiety on the CdS QDs surface. Possibly, other metal ions interact with the core CdS QDs by formation of metal sulfides [59]. The possible metal sufide formation on the QDs surface affected the emission (fluorescence) spectum tremendously but did not affect the absorption (CD) spectrum. These results revealed the important role of the core nanomaterials in ion sensing by luminescence approaches. Thus, L-Cyst-AgNCs were definitely chosen as a suitable fluorescence sensor for the detection of Co<sup>2+</sup> and were studied in the details.

## 3.5. Effect of pH

The effect of the solution pH towards the fluorescence quenching of L-Cyst-AgNCs by  $Co^{2+}$  was studied. The experiment was carried out by adjusting 100 mM Tris-HCl buffer containing 1.0 mM L-Cyst-AgNCs and 50  $\mu$ M  $Co^{2+}$  to the desired pH. The fluorescence intensity of 1.0 mM L-Cyst-AgNCs at different solution pHs before and after adding  $Co^{2+}$  is shown in Fig. 6(a). Flouorescence intensity of L-Cyst-AgNCs increased when pH of the solution were increased from 7.5 to 9.5. At pH 9.5, the L-Cyst-AgNCs showed the highest fluorescence intensity while pHs above 9.5 the fluorescence intensity decreased. After adding

50  $\mu$ M Co<sup>2+</sup>, the fluorescence intensity of L-Cyst-AgNCs was quenched for all studied pHs. The degree of fluorescence quenching (F<sub>0</sub>-F) upon adding Co<sup>2+</sup> is shown in Fig. 6(b). The highest fluorescence quenching efficiency was found at pH 9.5. Therefore, 100 mM Tris-HCl buffer pH 9.5 was chosen as a medium solution for further studies.

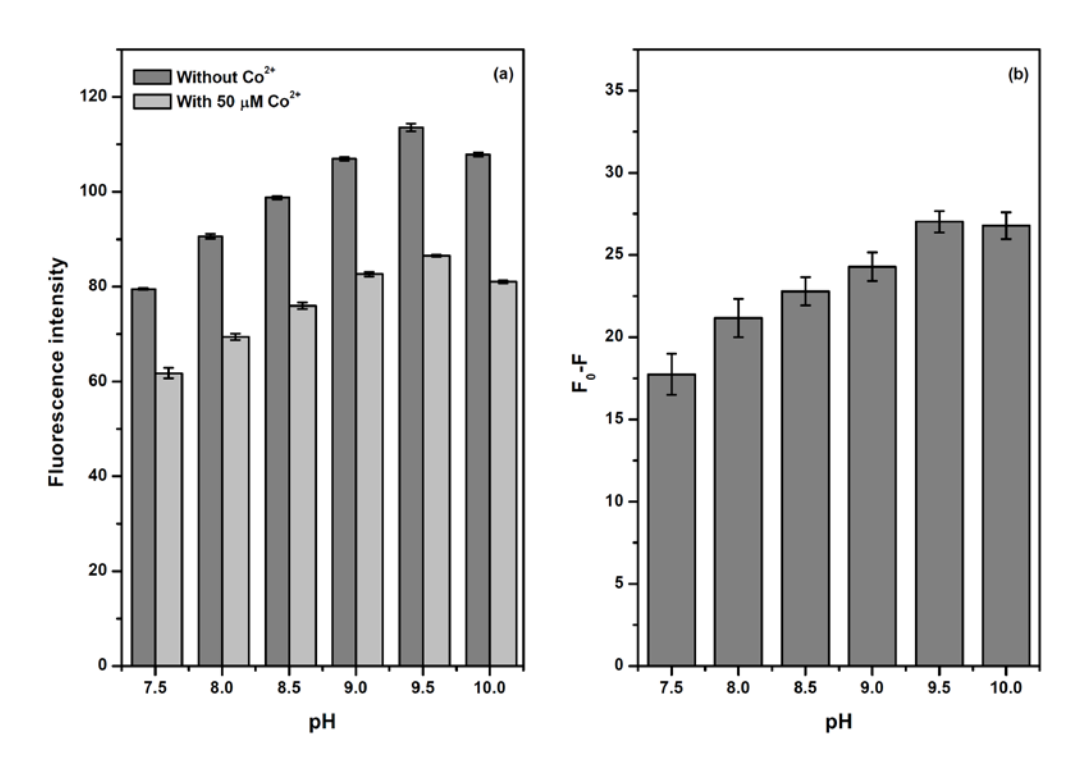


**Fig. 6** (a) Effect of the pH on fluorescence intensity of 1.0 mM L-Cyst-AgNCs, in the absence and presence of 50  $\mu$ M of Co<sup>2+</sup> in 100 mM Tris–HCl buffer solution, (b) The comparison of degree of fluorescence quenching (F<sub>0</sub>-F) at different pHs when adding 50  $\mu$ M Co<sup>2+</sup>.

## 3.6. Effect of the L-Cyst-AgNCs concentration

The effect of L-Cyst-AgNCs concentration towards the detection sensitivity was studied by varying from 0.50 to 2.00 mM and controlling the solution pH at 9.5 with 100 mM Tris-HCl buffer. Fluorescence intensities of L-Cyst-AgNCs at different concentrations in the absence and presence of  $\text{Co}^{2+}$  are exhibited in Fig. 7(a). In the absence of  $\text{Co}^{2+}$ , the fluorescence intensities increased with increasing the concentration of L-Cyst-AgNCs. In addition, when adding only 50  $\mu$ M of  $\text{Co}^{2+}$  into the solution of L-Cyst-AgNCs, the fluorescence intensities were quenched for all studied concentration of L-Cyst-AgNCs. The degree of fluorescence quenching (F<sub>0</sub>-F) upon adding  $\text{Co}^{2+}$  is compared in Fig. 7(b). The highest detection sensitivity was obtained when using 1.5 mM concentration of L-Cyst-AgNCs. Therefore, 1.50 mM concentration of L-Cyst-AgNCs was chosen in order to obtain the best detection sensitivity.

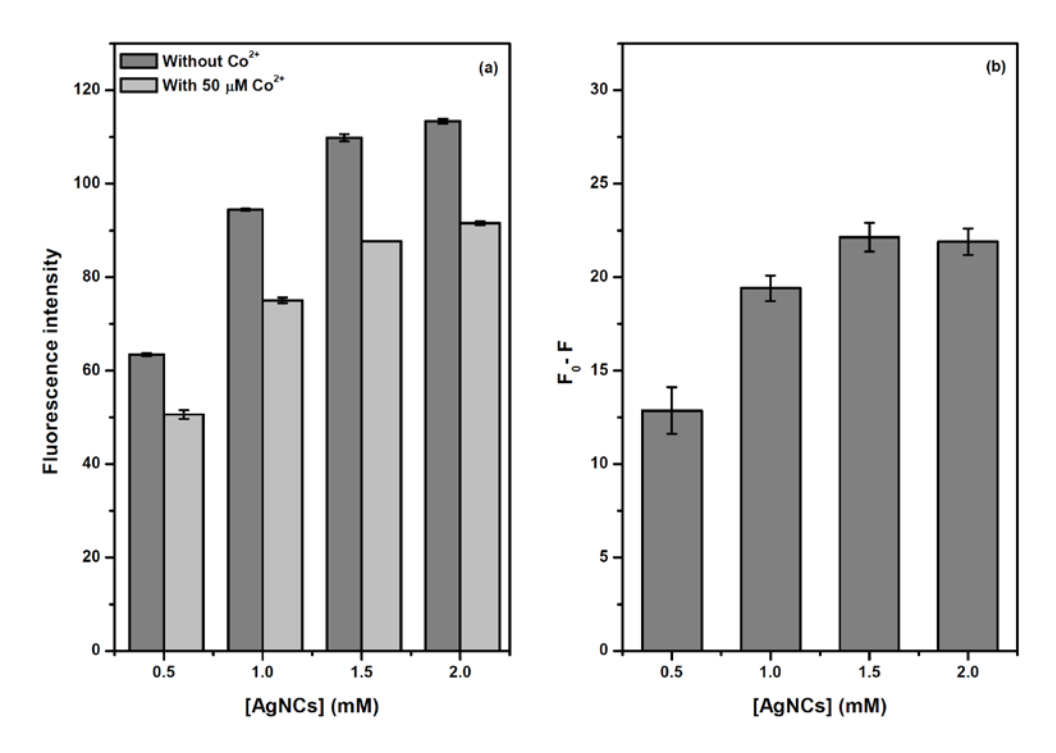


**Fig. 7** (a) Fluorescence intensity of L-Cyst-AgNCs at the different concentration, in the absence and presence of 50  $\mu$ M Co<sup>2+</sup> in 100 mM Tris–HCl buffer solution pH 9.5, (b) The comparison of degree of fluorescence quenching (F<sub>0</sub>-F) when adding 50  $\mu$ M Co<sup>2+</sup> at different L-Cyst-AgNCs concentration.

#### 3.7. Incubation time

In order to compromise between the detection sensitivity and analysis time, the effect of the incubation time was also examined. The experiment was carried out by mixing L-Cyst-AgNCs and 50 µM of Co<sup>2+</sup> in 100 mM Tris–HCl buffer solution pH 9.5 at room temperature for a period of 60 minutes, and the fluorescence spectra were recorded every 5 minutes. The fluorescence intensities of L-Cyst-AgNCs at different incubation time are shown in Fig. 8. It can be seen that the fluorescence intensity of L-Cyst-AgNCs itself was very stable through a period of the study. This result signified that the as-prepared L-Cyst-AgNCs were very stable and could be tolerant to photobleaching. After adding Co<sup>2+</sup>, it was found that the fluorescence intensities were quenched and became stable after mixing less than one minute. The results signified that the proposed sensor provided very a fast response time and did not need a long period of incubation time. In practical, the fluorescence intensity can be measured immediately after mixing Co<sup>2+</sup> with L-Cyst-AgNCs. This characteristic is one of the requirements for the fabrication of an efficient chemical sensor.

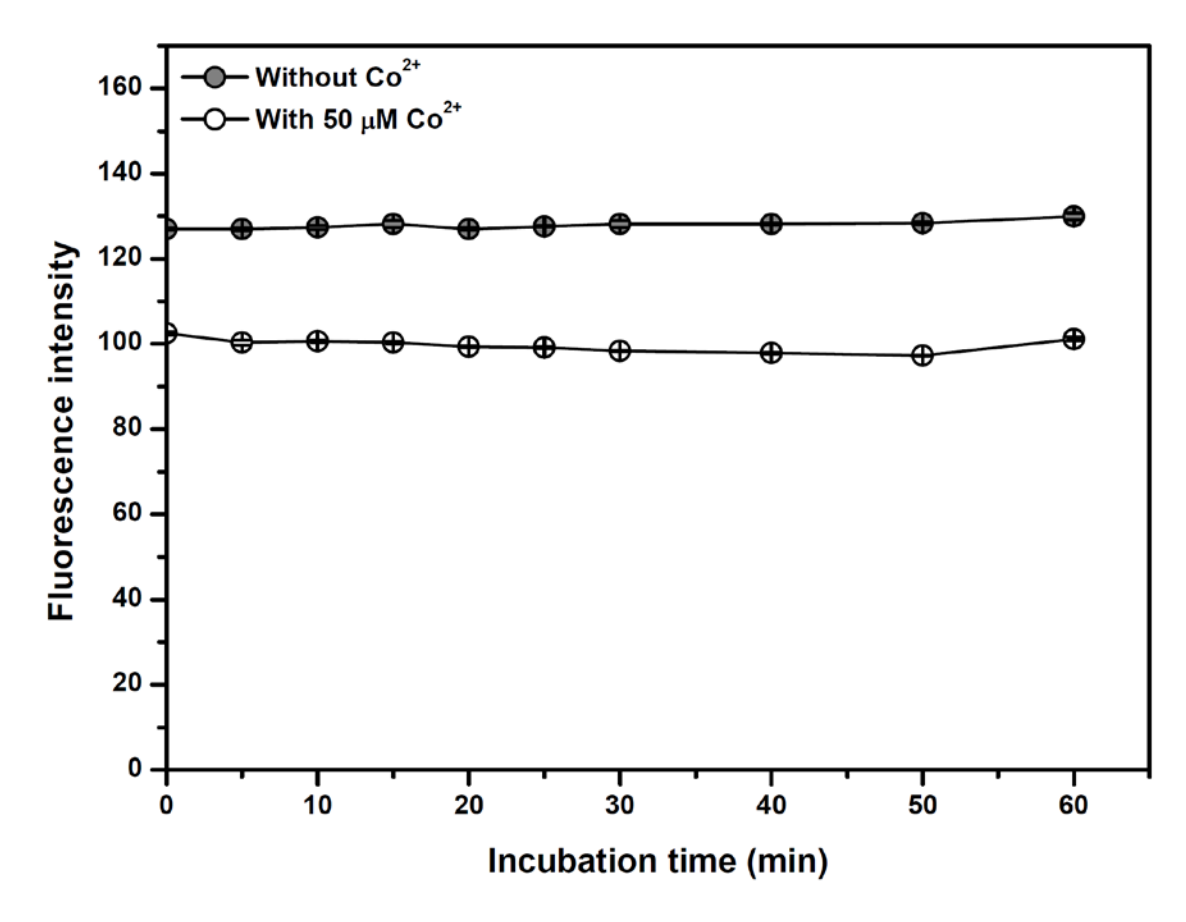


**Fig. 8** Fluorescence intensity of L-Cyst-AgNCs in the absence and presence of 50 μM Co<sup>2+</sup> in 100 mM Tris–HCl buffer solution pH 9.5 at different incubation times.

## 3.8. Analytical performance characteristic of the proposed sensor

The proposed sensor was validated to demonstrate the analytical merits under the optimized parameters. The experiment was carried out by recording the decreasing of the fluorescence intensity of the L-Cyst-AgNCs upon the addition of different concentrations of  $Co^{2+}$  under the optimized conditions. The fluorescence spectra in the presence of various concentrations of  $Co^{2+}$  and the corresponding calibration curve are shown in Fig. 9(a) and Fig. 9(b), respectively. It is obvious that the fluorescence intensities gradually decreased with the increasing of  $Co^{2+}$  from 0 to 150  $\mu M$ . Form the fluorescence spectra, it can be seen that the spectrum shape after quenching remained the same, signifying that the quenching mechanism was based on the decreasing of the fluoresce number (uncomplexed L-Cyst-AgNCs). A good linear relationship between the maximum fluorescence intensity of L-Cyst-AgNCs and  $Co^{2+}$  concentrations was obtained within the range of 0 to 150  $\mu M$ . The regression equation was found to be  $F=-0.48\times[Co^{2+},\,\mu M]+125.59$  ( $r^2=0.9945$ ). The limit of detection (LOD) and limit of quantitation (LOQ) were also evaluated to demonstrate the limitation of the sensor. The LOD and LOQ of the proposed sensor were 4.2 and 14.0  $\mu M$ , respectively.

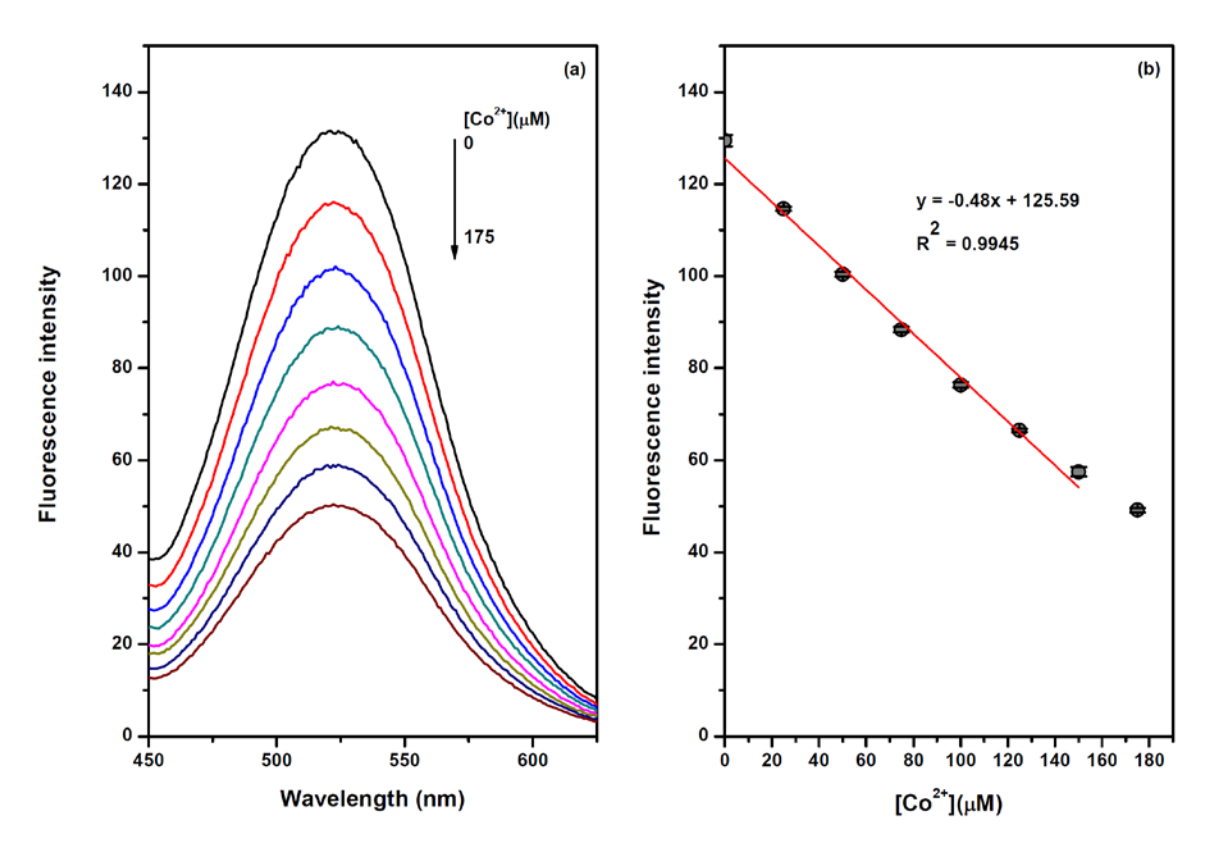


**Fig. 9** (a) The fluorescence spectra of 1.5 mM L-Cyst-AgNCs in the presence of  $Co^{2+}$  0-175  $\mu$ M in 100 mM Tris–HCl buffer solution pH 9.5 (b) The corresponding calibration curve.

## 3.9. Application to real water samples

In order to demonstrate the feasibility of the proposed sensor in real applications, determination of Co<sup>2+</sup> in a spiked ground water sample was evaluated by the proposed sensor and compared with results obtained from ICP-OES technique. The ground water sample was collected and filtered through Whatman No. 42 filter papers. Then, each of the filtered water was mixed with 100 mM Tris-HCl buffer pH 9.5 and spiked with Co2+ at three different concentration levels (25, 50 and 75 µM). The results obtained by the proposed sensor and ICP-OES method are summarized in Table 1. It can be seen that the Co<sup>2+</sup> contaminated in the water samples was not detectable by the proposed method suggested that the Co<sup>2+</sup> concentration in the water samples were lower than the LOD of this sensor. However, after spiking three different concentrations of Co<sup>2+</sup> into the water samples, the %recovery values of 104-107% can be obtained. Moreover, the water sample and its spiked sample were determined using ICP-OES. The results showed that the Co<sup>2+</sup> content obtained from the proposed sensor was in close agreement with those obtained by using the ICP-OES method. The recovery results and the results from ICP-OES can be used to confirm the accuracy of this sensor. In addition, the %R.S.D. values of three measurements were less than 5% suggested that the proposed sensor provided good precision and could be used to determine Co<sup>2+</sup> in real situation.

**Table 1.** Determination of Co<sup>2+</sup> in ground water sample by the proposed sensor and ICP-OES

Added	Proposed sensor			ICP-OES			
( <b>µM</b> )	Found $(\mu M)^a$	%Recovery	RSD (%)		$Found(\mu M)^a$	%Recovery	RSD (%)
0	n.d.	-	-		$0.80 \pm 0.00$	-	-
25	$25.88 \pm 0.84$	$104 \pm 3$	3.2		$25.94 \pm 0.17$	$101 \pm 1$	0.7
50	$52.42 \pm 2.24$	$105 \pm 5$	4.3		$50.46 \pm 0.06$	$99 \pm 1$	0.1
75	$80.15 \pm 1.27$	$107 \pm 2$	1.6		$75.54 \pm 0.17$	$100 \pm 1$	0.2

<sup>&</sup>lt;sup>a</sup> Mean  $\pm$  SD (n = 3)

n.d. = not detectable (less than  $4.2 \mu M$ )

## 4. Conclusion

In this work, the fluorescence sensor for the selective detection of Co<sup>2+</sup> was developed by using L-Cysteine modified luminescence nanomaterials including quantum dots and silver nanoclusters. The results confirmed that the L-Cysteine modified on poly(methacrylic acid) templated-AgNCs (L-Cyst-AgNCs) provided better sensor characteristics toward the detection of Co<sup>2+</sup> than the L-Cyst-CdS QDs. In the presence of Co<sup>2+</sup>, the fluorescence intensity of L-Cyst-AgNCs decreased as a linear function with the increasing of Co<sup>2+</sup> concentration due to the formation of chiral Co<sup>2+</sup> complex of the L-Cystiene moieties on the L-Cyst-AgNCs surface. The fabricated sensor showed good selectivity towards the detection of Co<sup>2+</sup> compared to other tested metal ions. This sensor can be used to detect trace Co<sup>2+</sup> in wide working concentration range with excellence accuracy and precision. The proposed sensor was demonstrated to detect Co<sup>2+</sup> in real water samples with satisfied results.

## References

- [1] D. Lindsay, W. Kerr, Cobalt close-up, Nat. Chem. 3 (2011) 494–494.
- [2] A. Maiga, D. Dlallo, R. Bye, B.S. Paulsen, Determination of some toxic and essential metal ions in medicinal and edible plants from Mali, J. Agric. Food Chem. 53 (2005) 2316–2321.
- [3] H.Y.A. Yeung, E.J. New, C.J. Chang, A selective reaction-based fluorescent probe for detecting cobalt in living cells, Chem. Commun. 48 (2012) 5268–5270.
- [4] A.I Seldén, C. Norberg, C. KarlsonStiber, C. Hel ström Lindberg, Cobalt release from glazed earthenware: observations in a case of lead poisoning, Environ. Toxicol. Pharmacol. 23 (2007) 129–131.
- [5] F.A. Abebe, C.S. Eribal, G. Ramakrishna, E. Sinn, A "Turn- on" fluorescent sensor for the selective detection of Cobalt and Nickel ions in aqueous media, Tetrahedron Lett. 52 (2011) 5554–5558.
- [6] M. Ghaedi, F. Ahmadi, A. Shokrollahi, Simultaneous preconcentration and determination of copper, nickel, cobalt and lead ions content by flame atomic absorption spectrometry, J. Hazard. Mater. 142 (2007) 272–278.
- [7] A.R. Khorrami, T. Hashempur, A. Mahmoudi, A.R. Karimi, Determination of ultra trace amounts of cobalt and nickel in water samples by inductively coupled plasma-optical emission spectrometry after preconcentration on modified C<sub>18</sub>-silica extraction disks, Microchem. J. 84 (2006) 75–79.
- [8] K. Sreenivasa Rao, T. Balaji, T. Prasada Rao, Y. Babu, G.R.K. Naidu, Determination of iron, cobalt, nickel, manganese, zinc, copper, cadmium and lead in human hair by inductively coupled plasma-atomic emission spectrometry, Spectrochim. Acta B 57

- (2002) 1333-1338.
- [9] J.X. Shi, C. Lu, D. Yan, L. Ma, High selectivity sensing of cobalt in HepG2 cells based on necklace model microenvironment-modulated carbon dot-improved chemiluminescence in Fenton-like system, Biosens. Bioelectron. 45 (2013) 58–64.
- [10] S. H. Mashraqui, M. Chandiramani, R. Betkar, K. Poonia, A simple internal charge transfer probe offering dual optical detection of Co (II) via color and fluorescence modulations, Tetrahedron Lett. 51 (2010) 1306–1308.
- [11] D. Tsoutsi, L. Guerrini, J.M. Hermida-Ramon, V. Giannini, L.M. Liz-Marzan, A. Wei, R.A. Alvarez-Puebla, Simultaneous SERS detection of copper and cobalt at ultratrace levels, Nanoscale 5 (2013) 5841–5846.
- [12] M. Morfobos, A. Economou, A. Voulgaropoulos, Simultaneous determination of nickel(II) and cobalt(II) by squarewave adsorptive stripping voltammetry on a rotating-disc bismuth-film electrode, Anal. Chim. Acta 519 (2004) 57–64.
- [13] Z. Gao, G. Wang, P. Li, Z. Zhao, Differential pulse voltammetric determination of cobalt with a perfluorinated sulfonated polymer-2,2-bipyridyl modified carbon paste electrode, Anal. Chem. 63 (1991) 953–957.
- [14] D. Badocco, P. Pastore, G. Favaro, C. Macca, Effect of eluent composition and pH and chemiluminescent reagent pH on ion chromatographic selectivity and luminol-based chemiluminescence detection of Co<sup>2+</sup>, Mn<sup>2+</sup> and Fe<sup>2+</sup> at trace levels, Talanta 72 (2007) 249–255.
- [15] Z. Liu, X. Jia, P. Bian, Z. Ma, A simple and novel system for colorimetric detection of cobalt ions, Analyst 139 (2014) 585–588.
- [16] R. Freeman, I. Willner, Optical molecular sensing with semiconductor quantum dots (QDs), Chem. Soc. Rev. 41 (2012) 4067–4085.
- [17] B. Liu, F. Zeng, G. Wu, S. Wu, Nanoparticles as scaffolds for FRET-based ratiometric detection of mercury ions in water with QDs as donors, Analyst 137 (2012) 3717–3724.
- [18] P. Wu, T. Zhao, S. Wanga, X. Hou, Semicondutor quantum dots-based metal ion probes, Nanoscale 6 (2014) 43–64.
- [19] N. Butwong, S. Srijaranai, W. Ngeontae, R. Burakham, Speciation of arsenic (III) and arsenic (V) based on quenching of CdS quantum dots fluorescence using hybrid sequential injection–stopped flow injection gas–diffusion system, Spectrochim. Acta A 97 (2012) 17–23.
- [20] K. Zhang, J. Guo, J. Nie, B. Du, D. Xu, Ultrasensitive and selective detection of Cu2+ in aqueous solution with fluorescence enhanced CdSe quantum dots, Sens. Actuat. B-Chem. 190 (2014) 279–287.
- [21] W. Lu, X. Qin, S. Liu, G. Chang, Y. Zhang, Y. Luo, A.M. Asiri, A.O. Al-Youbi, X. Sun, Economical, Green synthesis of fluorescent carbon nanoparticles and their use as probes for sensitive and selective detection of mercury(II) ions, Anal. Chem. 84 (2012) 5351–5357.
- [22] S. Anandhakumar, R. Rajaram, J. Mathiyarasu, Unusual seedless approach to gold nanoparticle synthesis: application to selective rapid naked eye detection of mercury(II), Analyst 139 (2014) 3356–3359.
- [23] Y. Zhou, H. Dong, L. Liu, M. Li, K. Xiao, M. Xu, Selective and sensitive colorimetric sensor of mercury (II) based on gold nanoparticles and 4-mercaptophenylboronic acid, Sens. Actuat. B-Chem. 196 (2014) 106–111.
- [24] P. Bian, L. Xing, Z. Liu, Z. Ma, Functionalized-tryptophan stabilized fluorescent Ag nanoclusters: synthesis and its application as Hg<sup>2+</sup> ions sensor, Sens. Actuat. B-Chem. 203 (2014) 252–257.
- [25] H. Xu, K. S. Suslick, Water-soluble fluorescent silver nanoclusters, Adv. Mater. 22 (2010) 1078–1082.

- [26] G. Maduraiveeran, R. Ramaraj, Potential sensing platform of silver nanoparticles embedded in functionalized silicate shell for nitroaromatic compounds, Anal. Chem. 81 (2009) 7552–7560.
- [27] S. Li, S.J. Dong, G.U. Nienhaus, Ultra-small fluorescent metal nanoclusters: synthesis and biological applications, Nano Today 6 (2011) 401–418.
- [28] I. Díez, R.H.A. Ras, M.I. Kanyuk, A.P. Demchenko, On heterogeneity in fluorescent few-atom silver nanoclusters, Phys. Chem. Chem. Phys. 15 (2013) 979–985.
- [29] I. Díez, R.H.A. Ras, Fluorescent silver nanoclusters, Nanoscale 3 (2011) 1963–1970.
- [30] J.P. Wilcoxon, B.L. Abrams, Synthesis, structure and properties of metal nanoclusters, Chem. Soc. Rev. 35 (2006) 1162–1194.
- [31] J. Xie, Y. Zheng, J.Y.J. Ying, Protein-directed synthesis of highly fluorescent gold nanoclusters, Am. Chem. Soc. 131 (2009) 888–889.
- [32] T.U.B. Rao, T. Pradeep, Luminescent Ag<sub>7</sub> and Ag<sub>8</sub> clusters by interfacial synthesis, Angew. Chem. Int. Ed. 122 (2010) 4017–4021.
- [33] A. Henglein, Physicochemical properties of small metal particles in solution: microelectrode reactions, chemisorption, composite metal particles, and the atom-to-metal transition, J. Phys. Chem. 97 (1993) 5457–5471.
- [34] X. Le Guével, B. Hötzer, G. Jung, K. Hollemeyer, V. Trouillet, M. Schneider, Formation of fluorescent metal (Au, Ag) nanoclusters capped in bovine serum albumin followed by fluorescence and spectroscopy, J. Phys. Chem. C 115 (2011) 10955–10963.
- [35] I. Diez, M. Pusa, S. Kulmala, H. Jiang, A. Walther, A.S. Goldmann, A.H. Muller, O. Ikkala, R.H. Ras, Color tunability and electrochemiluminescence of silver nanoclusters, Angew. Chem. Int. Ed. 48 (2009) 2122–2125.
- [36] H. Zhang, X. Huang, L. Li, G. Zhang, I. Hussain, Z. Li, B. Tan, Photoreductive synthesis of water-soluble fluorescent metal nanoclusters, Chem. Commun. 48 (2012) 567–569.
- [37] H.X. Xu, K.S. Suslick, Sonochemical synthesis of highly fluorescent Ag nanoclusters, ACS Nano 4 (2010) 3209–3214.
- [38] L. Maretti, P. Billone, Y. Liu, J.C. Scaiano, Facile photochemical synthesis and characterization of highly fluorescent silver nanoparticles, J. Am. Chem. Soc. 131 (2009) 13972–13980.
- [39] L.A. Peyser, A.E. Vinson, A.P. Bartko, R.M. Dickson, Photoactivated fluorescence from individual silver nanoclusters, Science 291 (2001) 103–106.
- [40] J.T. Petty, J. Zheng, N.V. Hud, R.M. Dickson, DNA-templated Ag nanocluster formation, J. Am. Chem. Soc. 126 (2004) 5207–5212.
- [41] B. Sengupta, C.M. Ritchie, J.G. Buckman, K.R. Johnsen, P.M. Goodwin, J.T. Petty, Toxicity of gold nanoparticles functionalized with cationic and anionic side chains, J. Phys. Chem. C 112 (2008) 18776–18782.
- [42] E. G. Gwinn, P.R. O'neill, A.J. Guerrero, D. Bouwmeester, D.K. Fygenson, Sequence-dependent fluorescence of DNA-hosted silver nanoclusters, Adv. Mater. 20 (2008) 279–283.
- [43] K. Ma, Y. Shao, Q. Cui, F. Wu, S. Xu, G. Liu, Base-stacking-determined fluorescence emission of DNA abasic site-templated silver nanoclusters, Langmuir 28 (2012) 15313–15322.
- [44] J. Yu, S.A. Patel, R.M., pH-switchable silver nanoprism growth pathways, Angew. Chem. Int. Ed. 46 (2007) 2028–2030.
- [45] J. Zheng, R.M. Dickson, Individual water-soluble dendrimer-encapsulated silver nanodot fluorescence, J. Am. Chem. Soc. 124 (2002) 13982–13983.
- [46] J.G. Zhang, S.Q. Xu, E. Kumacheva, Photogeneration of fluorescent silver nanoclusters

- in polymer microgels, Adv. Mater. 17 (2005) 2336-2340.
- [47] X. Ren, Z. Chen, X. Meng, D. Chen, F. Tang, Synthesis of fluorescent Ag nanoclusters and their application in α-L-fucosidase detection, Chem. Commun. 48 (2012) 9504–9506.
- [48] L. Shang, S. Dong, Silver nanocluster-based fluorescent sensors for sensitive detection of Cu(II), J. Mater. Chem. (2008) 18 4636–4640.
- [49] X. Yuan, T.J. Yeow, Q. Zhang, J.Y. Lee, J. Xie, Highly luminescent Ag<sup>+</sup> nanoclusters for Hg<sup>2+</sup> ion detection, Nanoscale 4 (2012) 1968–1971.
- [50] S. Liu, F. Lu, J.J. Zhu, Highly fluorescent Ag nanoclusters: microwave-assisted green synthesis and Cr<sup>3+</sup> sensing, Chem. Commun. 47 (2011) 2661–2663.
- [51] J.L. Chen, C.Q. Zhu, Functionalized cadmium sulfide quantum dots as fluorescence probe for silver ion determination, Anal. Chim. Acta 546 (2005) 147–153.
- [52] Z.X. Cai, H. Yang, Y. Zhang, X.P. Yan, Preparation, characterization and evaluation of water-soluble L-cysteine-capped-CdS nanoparticles as fluorescence probe for detection of Hg(II) in aqueous solution, Anal. Chim. Acta 559 (2006) 234–239.
- [53] Y. Chen, Z. Rosenzweig, Luminescent CdS quantum dots as selective ion probes, Anal. Chem. 74 (2002) 5132–5138.
- [54] W. Tedsana, T. Tuntulani, W. Ngeontae, A circular dichroism sensor for Ni<sup>2+</sup> and Co<sup>2+</sup> based on L-cysteine capped cadmium sulfide quantum dots, Anal. Chim. Acta (2014) DOI:10.1016/j.aca.2014.12.004.
- [55] K. Chaiendoo, T. Tuntulani, W. Ngeontae, A highly selective colorimetric sensor for ferrous ion based on polymethylacrylic acid-templated silver nanoclusters, Sens. Actuat. B-Chem. 207 (2015) 658–667.
- [56] M.M. Alvarez, J.T. Khoury, T.G. Schaaff, M.N. Shafigullin, I. Vezmar, R.L. Whetten, Optical absorption spectra of nanocrystal gold molecules, J. Phys. Chem. B 101 (1997) 3706–3712.
- [57] T. G. Schaaff, M.N. Shafigullin, J.T. Khoury, I. Vezmar, R.L. Whetten, W.G. Cullen, P.N. First, C. Gutie'rrez-Wing, J. Ascensio, M.J. Jose-Yacama'n, Isolation of smaller nanocrystal Au molecules: robust quantum effects in optical spectra, J. Phys. Chem. B 101 (1997) 7885–7891.
- [58] C.R. Tang, Z.H. Su, B.G. Lin, H.W. Huang, Y.L. Zeng, S. Li, H. Huang, Y.J. Wang, C.X. Li, G.L. Shen, R.Q. Yu, A novel method for iodate determination using cadmium sulfide quantum dots as fluorescence probes, Anal. Chim. Acta 678 (2010) 203–207.
- [59] J. Chen, A. Zheng, Y. Gao, C. He, G. Wu, Y. Chen, X. Kai, C. Zhu, Functionalized CdS quantum dots-based luminescence probe for detection of heavy and transition metal ions in aqueous solution, Spectrochim. Acta A 69 (2008) 1044–1052.

# 3. A circular dichroism sensor for $\mathrm{Ni}^{2^+}$ and $\mathrm{Co}^{2^+}$ based on L-Cysteine capped cadmium sulfide quantum dots

#### 1. Introduction

Cobalt is an essential micronutrient for biochemical metalloenzyme reactions [1,2]. It is a part of vitamin B12 structure, which is important for production of red blood cells and prevention of pernicious anemia [3]. On the other hand, cobalt can be a toxic compound at high concentrations which can cause many diseases such as slow respiration, giddiness cardiomyopathy, pulmonary disorders and hyperglycemia [4]. Nickel is an important component of the enzyme urease. It is considered to be essential for plants and some domestic animals [5, 6]. However, nickel is one of an important toxic element widely distributed in the environment that can cause nasal and lung dermatitis, asthma, malignant tumors and disorders of central nervous system [7-9].

Several analytical methods based on the atomic spectrometry have been implemented to determine the concentration level of cobalt and nickel ions such as flame atomic absorption spectrometry (FAAS) [10-12], graphite furnace atomic absorption spectrometry (GFAAS) [13, 14], and inductively-coupled plasma optical emission spectrometry (ICP-OES) [15-17]. Moreover, electrochemistry [18-20] and chromatography [21-23] techniques have also been reported. However, these techniques require sophisticated instruments and special training, making them unfriendly and cumbersome. Therefore, it is important to develop sensitive and selective methods for determination of trace amounts of cobalt and nickel.

Circular dichroism (CD) spectroscopy is one of the powerful techniques employed in a wide research area. This technique is often used to study biological rather than non-biological systems [24] such as studies of the coordination chemistry of Ca<sup>2+</sup> ions toward some amino acids located at the C-terminus of the peptide [25], the interaction between deferiprone and human serum albumin [26], the effect of etoposide on DNA, histones and DNA–histones complex in the structure of nucleosomes [27], the affinity between pheromone binding proteins (antennal special protein 1, ASP1) with a queen mandibular pheromone component (methyl-*p*-hydroxybenzoate, HOB) [28], and the interaction between polyvinylthiol-functionalized silver nanoparticles with lysozyme [29]. Furthermore, CD is a valuable tool in inorganic chemistry, particularly in the study of chirality of inorganic and organic nanomaterials [30]. This technique is not frequently used in the quantitative analysis. However, based on the principle of this technique it may provide excellent selectivity.

Nanomaterials have been introduced into the recent developments in modern analytical chemistry and become the ideal building blocks for the fabrication of chemical sensors which cannot be found from the bulk materials. This is due to their excellent optical, electrical, magnetic, and catalytic properties resulting from quantum effects and nanoscale structures [31].

Chiral nanomaterials are currently an interesting issue and used for the fabrication of selective enantiomeric sensors. The chirality of inorganic nanomaterials is basically originated from the chirality of organic molecules used as stabilizing agent. There have been some recent publications on the preparation of chiral gold nanoparticles [32, 33] and silver nanoparticles [34, 35]. In addition, chiral nanocrystalline semiconductor or quantum dots (QDs) is also an active research area with a broad range of interesting applications [36]. Thus far, CdSe and CdS QDs prepared in the presence of chiral ligands such as penicillamine [37], cysteine methylester [38], and cysteine [39] have been reported. Chiral cysteine-capped CdSe(ZnS) quantum dots were synthesized, and used for the selective recognition of carnitine enantiomers [40]. Moreover, chiral CdS QDs were synthesized by using microwave induced heating with the racemic (Rac), D- and L- enantiomeric forms of penicillamine as the stabilizers [41]. Post-synthetic ligand exchange employing chiral capping ligands represented

an appealing approach to access chiroptical QDs. The preparation of optically active CdSe QDs by post-synthetic ligand exchange on achiral CdSe using readily available D- and L-Cysteine was also proposed. Despite a number of theoretical and experimental studies on the optically active inorganic nanomaterials, the origin of chirality was still unclear [32, 33, 41-43] and allured chemists to explore further.

To the best of our knowledge, there is no report regarding the fabrication of CD sensor based on the chiral quantum dots for detection of heavy metal ions. In this work we demonstrate a new approach for the determination of some heavy metal ions by measuring the CD signal of chiral quantum dots after complexing with Co<sup>2+</sup> or Ni<sup>2+</sup>. The selectivity of the proposed sensor can be expected due to a unique optical property of the chiral complex formed on the surface of the quantum dots. The proposed sensor may be a new elegant tool to develop a highly selective and sensitive optical chemical sensor for analysis of heavy metal ions in the future.

## 2. Experimental

#### 2.1 Chemicals

All reagents were of analytical grade and used without further purification. Cadmium chloride (CdCl $_2$ ·H $_2$ O) was obtained from Riedel–deHaen. L-Cysteine was purchased from Aldrich. Sodium sulfide and Nickle (II) nitrate 6-hydrate (Ni(NO $_3$ ) $_2$ ·6H $_2$ O) were purchased from BDH. Cobalt (II) nitrate (Co(NO $_3$ ) $_2$ ) and nitric acid (65%) were purchased from CARLO ERBA. Potassium dihydrogen orthophosphate (KH $_2$ PO $_4$ ) and potassium hydrogen orthophosphate (K $_2$ HPO $_4$ ) were purchased from UNIVAR. All aqueous solutions were prepared with deionized water (DI) with the specific resistivity of 18.2 M $\Omega$  cm (Millipore water). The L-cysteine capped CdS quantum dots (Cyst-CdS QDs) used in this work were synthesized and characterized as described in the supplementary data (SD).

#### 2.2 Instrumentations

Circular dichroism was performed on a Jasco-815 CD spectropolarimeter (JASCO, Japan) using a 1 cm quartz cell cuvette, with a scanning rate at 100 nm min<sup>-1</sup>. The fluorescence spectra were recorded using a Shimadzu RF-5301PC spectrofluorometer. Excitation and emission spectra were recorded using the slit width of 5 nm. Absorption spectra were measured using an Agilent HP 8453 spectrophotometer. The pH of solutions was measured using a UB-10 UltraBasic pH meter (Denver Instrument). FT-IR spectra were recorded on a Bruker Tensor 27 FT-IR spectrometer using Pike Gladi attenuated total reflectance (ATR) cell equipped with a diamond crystal plate. Transmission electron microscopy (TEM) was carried out on Tecnai G<sup>2</sup>-20 (FEI, Netherlands) under the accelerating voltage of 200 kV. Inductively coupled plasma optical emission spectrometer (ICP-OES, Optima 2100 DV, USA) was employed for the determination of Ni<sup>2+</sup> and Co<sup>2+</sup> in real water samples.

#### 2.3 Circular Dichroism (CD) measurements

To study the circular dichroism spectra of the synthesized Cyst-CdS QDs, the following procedure was carried out. A stock solution of  $Ni^{2+}$  and  $Co^{2+}$  (10 mM) was prepared by dissolution of the nitrate salt in DI water. To a 10 mL volumetric flask, 200  $\mu$ L of the synthesized Cyst-CdS QDs (to be a final concentration of 1.095 mM) was mixed with the stock solution of  $Ni^{2+}$  or  $Co^{2+}$  to obtain the final concentration of 70  $\mu$ M for  $Ni^{2+}$  and 80  $\mu$ M for  $Co^{2+}$ . The mixed solution was made to a final volume of 10.00 mL with 0.1 M phosphate buffer pH 7.0 and incubated at room temperature for 10 min before recording the CD spectra. To study the effect of incubation time, the mixed solution of Cyst-CdS QDs and  $Ni^{2+}$  or  $Co^{2+}$  in 0.1 M phosphate buffer solution pH 7.0 was incubated at 1–30 min before the

CD measurements. To study the effect of solution pH, 0.1 M phosphate buffer was used to control the pH range of 6.5–7.0, and 0.1 M Tris-HCl buffer was used for the pH range of 7.5–9.5. The calibration curves were constructed from the optimized conditions (1.095 mM of Cyst-CdS QDs in 0.1 M phosphate buffer pH 7.0 and incubation time of 10 minutes) in the presence of  $Ni^{2+}$  or  $Co^{2+}$  (concentration ranging from 4-400  $\mu$ M). The wavelengths at 324 nm and 352 nm were monitored for  $Ni^{2+}$  and  $Co^{2+}$ , respectively.

## 2.4 Absorption and fluorescence measurements

Effects of  $Ni^{2+}$  or  $Co^{2+}$  toward the absorption and fluorescence spectrum of Cyst-CdS QDs were investigated. Into a 10.00 mL volumetric flask, 200  $\mu$ L of Cyst-CdS QDs (final concentration of 1.095 mM) was mixed with 1.0 mL of 1.0 M phosphate buffer solution pH 7.0. An appropriate volume of stock  $Ni^{2+}$  or  $Co^{2+}$  solutions was sequentially added into the mixture and diluted with DI water. The mixture was then incubated at room temperature for 10 minutes before recording the absorption spectrum or fluorescence spectrum ( $\lambda_{ex} = 330$  nm).

## 2.5 Selectivity of the sensor

To evaluate the selectivity of the proposed sensors, the following procedure was carried out. Into a 10.00 mL volumetric flask, 200  $\mu$ L of Cyst-CdS QDs (to obtain a final concentration of 1.095 mM) was mixed with 1.0 mL of 1.0 M phosphate buffer solution pH 7.0, following by adding the individual stock solution of metal ions including Li<sup>+</sup>, K<sup>+</sup>, Ba<sup>2+</sup>, Ag<sup>+</sup>, Fe<sup>2+</sup>, Hg<sup>2+</sup>, Mn<sup>2+</sup>, Pb<sup>2+</sup>, Cd<sup>2+</sup>, Zn<sup>2+</sup>, Mg<sup>2+</sup> and Cr<sup>3+</sup> to obtain the final concentration of 50  $\mu$ M. The mixture was diluted to the total volumetric flask with DI water. The solution was mixed thoroughly and left for 10 min before recording the CD spectra.

#### 2.6 Application to real water samples

In order to demonstrate the applicability of the proposed sensor, drinking water, natural pond water and tap water were used as the real samples. All water samples were analyzed immediately without storage and filtered through filter paper to remove particle matters. The accuracy and precision of each measurement were evaluated by spiking with two different concentrations of  $\mathrm{Ni}^{2+}$  (at 35.0 and 65.0  $\mu\mathrm{M}$ ) and  $\mathrm{Co}^{2+}$  (at 7.0 and 25.0  $\mu\mathrm{M}$ ) and analyzed under the optimized condition. Moreover, to confirm the accuracy of the proposed sensor, all spiked samples were also directly analyzed using the ICP-OES.

## 3. Results and Discussion

Basically, nanocrytalline quantum dots have been used for fabrication of fluorescence sensors for selective detection of various target species. However, the applications of quantum dots in the fabrication of CD sensors have rarely been demonstrated. Therefore, evaluation of the CD phenomenon of L-cysteine capped CdS QDs is still a challenging issue. The change of CD signal of the chiral nanocrystal upon complexation with some heavy metal ions is studied in details.

#### 3.1. Study of the CD spectra

The feasibility of the synthesized chiral QDs for the fabrication of CD sensor has been studied. It can be expected that the optical property of the chiral QDs should be altered if the chiral ligands on the surface of QDs complex with metal ions. Changes of the CD spectrum should correspond to the degree of complexation. Therefore, the CD spectrum of the Cyst-CdS QDs are studied by observing the change of CD signal in the absence and the presence of Ni<sup>2+</sup> or Co<sup>2+</sup>, and the results are shown in the Fig. 1.

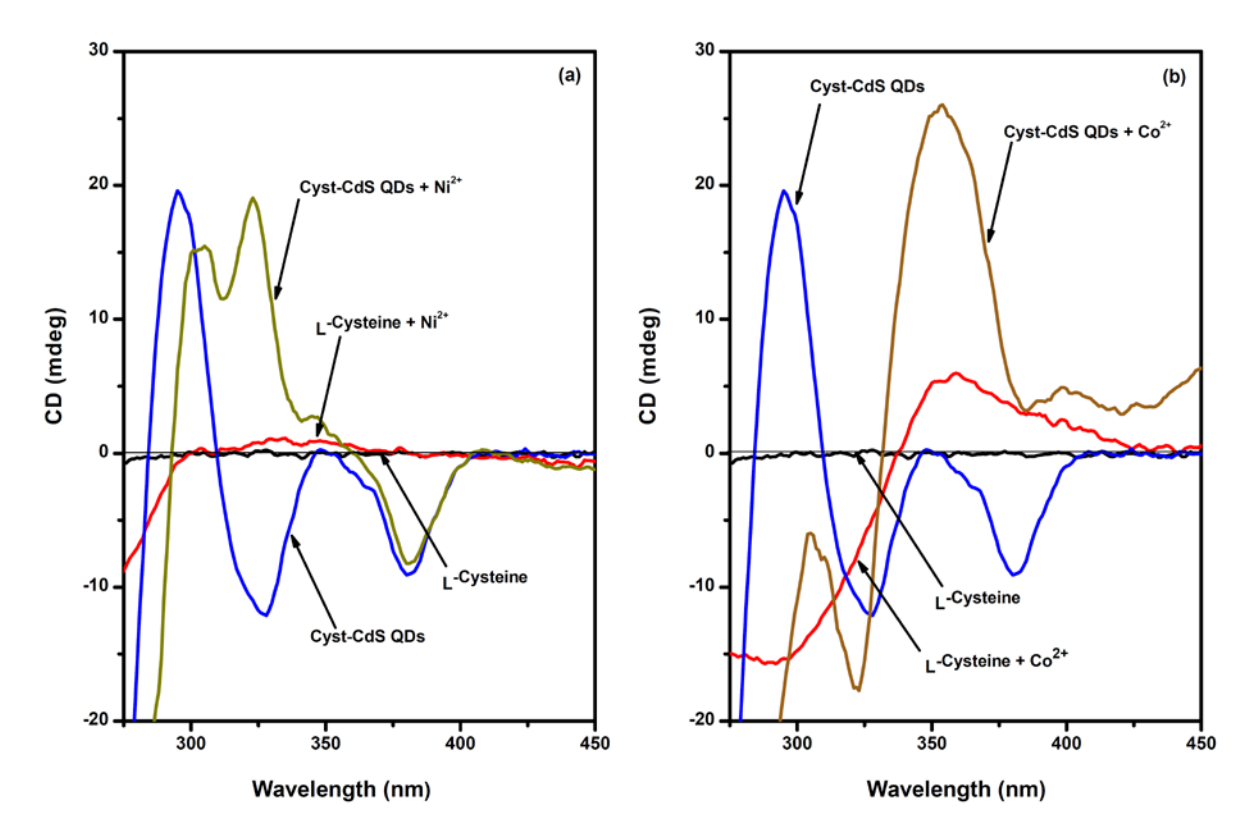


**Fig. 1** CD spectrum of 1.095 mM Cyst-CdS QDs and 2.50 mM L-Cysteine in 0.1 M PBS pH 7.0 in the absence and presence of (a) Ni<sup>2+</sup> and (b) Co<sup>2+</sup>.

After adding Ni<sup>2+</sup> or Co<sup>2+</sup> into the solution of L-Cysteine, the CD spectra show a negative change at the wavelength lower than 300 nm in the case of Ni<sup>2+</sup>. In the presence of Co<sup>2+</sup>, changes of the CD signal in the negative direction at 295 nm and positive direction at 350 nm can be observed. The changes of the CD spectrum of L-Cysteine upon the addition of Ni<sup>2+</sup> or Co<sup>2+</sup> are due to the formation of the chiral complex between L-Cysteine and Ni<sup>2+</sup> or Co<sup>2+</sup> [44]. The formation of chiral complex between L-Cysteine and Ni<sup>2+</sup> or Co<sup>2+</sup> is further investigated. The L-Cysteine solution is titrated with Ni<sup>2+</sup> or Co<sup>2+</sup> and the results are shown in Fig. S4 (in the SD). The results show that the increasing of Ni<sup>2+</sup> or Co<sup>2+</sup> concentration enhances the intensity of the CD signals. These results signify that the degree of the CD change corresponds to the number of chiral complexes formed and can be used for the quantitative analysis of Ni<sup>2+</sup> and Co<sup>2+</sup>. Comparing to the CD spectrum of Cyst-CdS QDs in the presence of Ni<sup>2+</sup> or Co<sup>2+</sup>, the CD spectrum also changes from the original CD spectrum of Cyst-CdS QDs. In the case of Ni<sup>2+</sup>, the CD signal at 324 nm exhibits significant changes to the opposite direction. Upon the addition of Co<sup>2+</sup>, the CD signal of Cyst-CdS QDs at 352 nm increases in the positive direction. It should be noted that the change of CD spectrum upon the addition of Ni<sup>2+</sup> or Co<sup>2+</sup> in the case of L-Cysteine and Cyst-CdS QDs are totally different. Therefore, the resulting chiral complexes in both cases are definitely not the same structure. In addition, Cyst-CdS QDs give more enhanced CD signals than L-Cysteine upon addition of Ni<sup>2+</sup> or Co<sup>2+</sup>. Thus, a CD sensor for the selective detection of Ni<sup>2+</sup> and Co<sup>2+</sup> can potentially be fabricated by monitoring the CD signal of Cyst-CdS QDs.

Since the principle of CD detection is based on the rotation of the polarized light by a single chiral compound, it cannot discriminate a mixture of chiral compounds. Therefore, simultaneous determination of Co<sup>2+</sup> and Ni<sup>2+</sup> was found to be a limitation of the propose sensor because there are two kinds of chiral complexes in the same sample. The optical rotation by two chiral complexes also provides a mixture of the CD spectra (Fig. S5 in the

SD), and the quantitative analysis of each analyte cannot be evaluated.

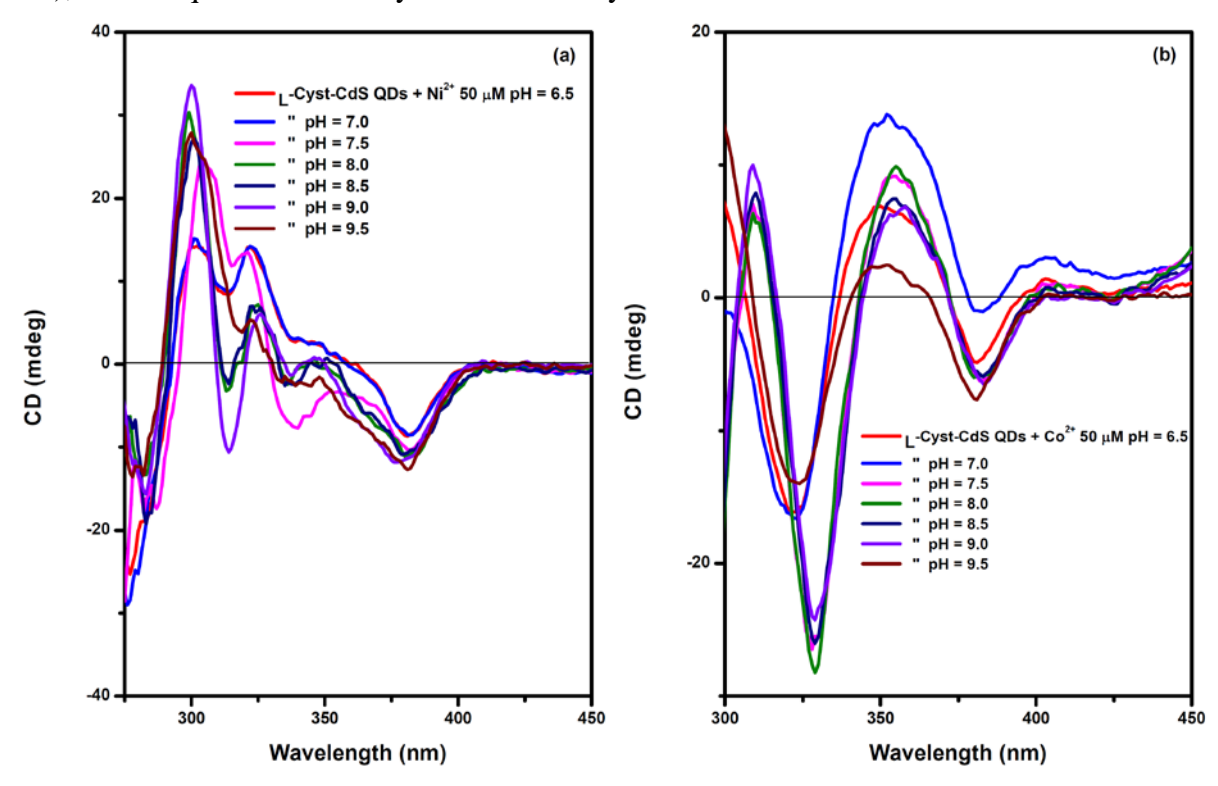


**Fig. S4**CD spectrum of 1.095 mM Cyst-CdS QDs in 0.1 M PBS (pH 6.5-7.0) or 0.1 M Tris-HCl buffer (pH 7.5-9.5) in the presence of 50  $\mu$ M (a) Ni<sup>2+</sup> and (b) Co<sup>2+</sup>.

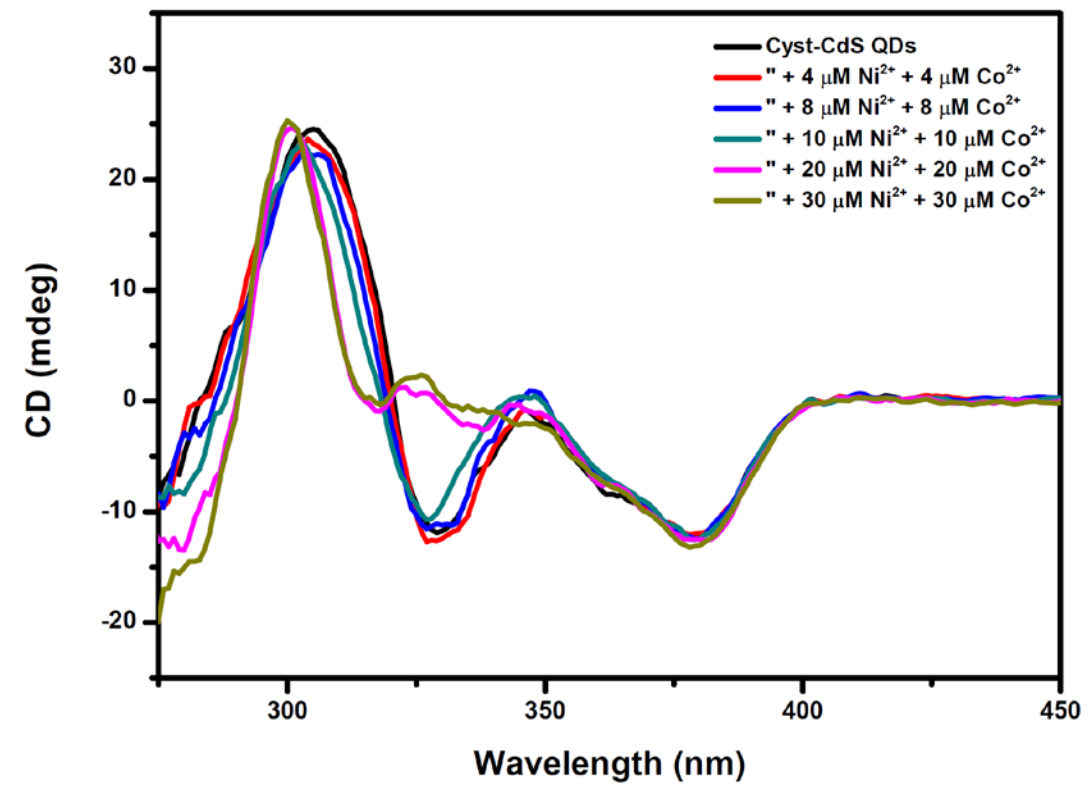


**Fig. S5** The CD spectra of 1.095 mM Cyst-CdS QDs in 0.1 M PBS pH 7.0 in the presence of Ni<sup>2+</sup> and Co<sup>2+</sup> (at the same concentration) concentration ranging 4-30  $\mu$ M.

## 3.2. Effect of the solution pH

Since L-Cysteine is an amino acid, the pH of the solution can affect the charge of L-Cysteine on the Cyst-CdS QDs and may affect the complex formation. To obtain the best sensitivity, the effect of solution pH has been explored. Experiments are carried out by adjusting the pH of the buffer solution. Phosphate buffer is used to control the pH ranging from 6.5-7.0 and Tris-HCl buffer for the pH beyond 7.0. The CD spectrum is illustrated in Fig. S4 (in the SD). The changes of mdeg upon the addition of 50 µM Ni<sup>2+</sup> and Co<sup>2+</sup> are monitored at 324 and 352 nm, and the results are shown in the Fig. 2(a) and Fig. 2(b), respectively. It can be seen that the Ni<sup>2+</sup> or Co<sup>2+</sup> can form chiral complexes with Cyst-CdS QDs for all studied pH ranges. The best sensor sensitivity is obtained when using 0.1 M PBS at pH 7.0. Therefore, this condition is applied for further investigation.

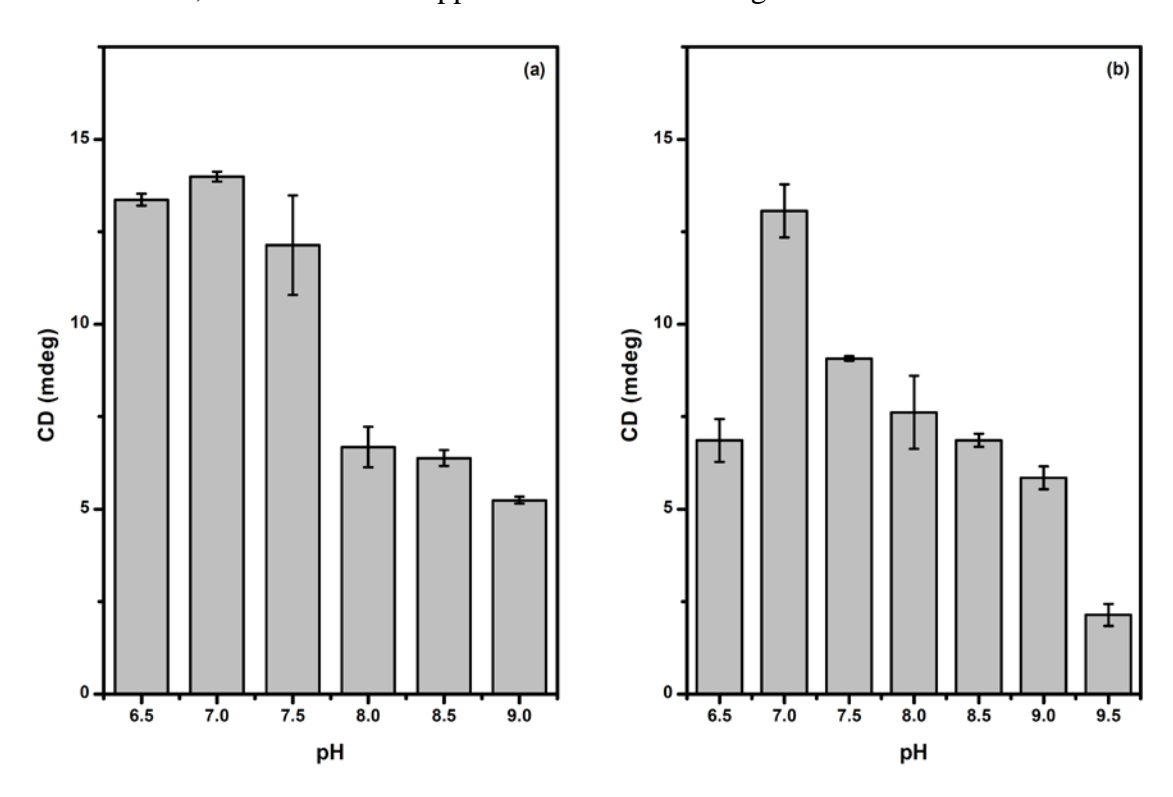


**Fig. 2** Effect of the solution pH on the CD change of 1.095 mM Cyst-CdS QDs in 0.1 M PBS (pH 6.5-7.0) or 0.1 M Tris-HCl buffer (pH 7.5-9.5) in the presence of 50  $\mu$ M (a) Ni<sup>2+</sup> (at 324 nm) and (b) Co<sup>2+</sup> (at 352 nm).

#### 3.3. Effect of the incubation time

The incubation time after mixing Cyst-CdS QDs with Ni<sup>2+</sup> or Co<sup>2+</sup> has been studied to compromise between the analysis time and the sensitivity. Actually, fast analysis time is needed for the fabrication of new efficient chemical sensors. The experiments are carried out by measuring the mdeg change after adding Ni<sup>2+</sup> or Co<sup>2+</sup> at different incubation times from 0 to 30 minutes. The CD signal of Cyst-CdS QDs is also measured for monitoring the stability of the probe. The results are shown in Fig. 3(a) and Fig. 3(b) for Ni<sup>2+</sup> and Co<sup>2+</sup>, respectively. After adding Ni<sup>2+</sup> or Co<sup>2+</sup> for only 10 minutes, the CD signal becomes stable and gives the highest sensitivity. Therefore, the mixing solution between Cyst-CdS QDs and Ni<sup>2+</sup> or Co<sup>2+</sup> needs at least 10 minutes before recording the CD spectrum and this incubation time is used as the optimized condition for further experiments.

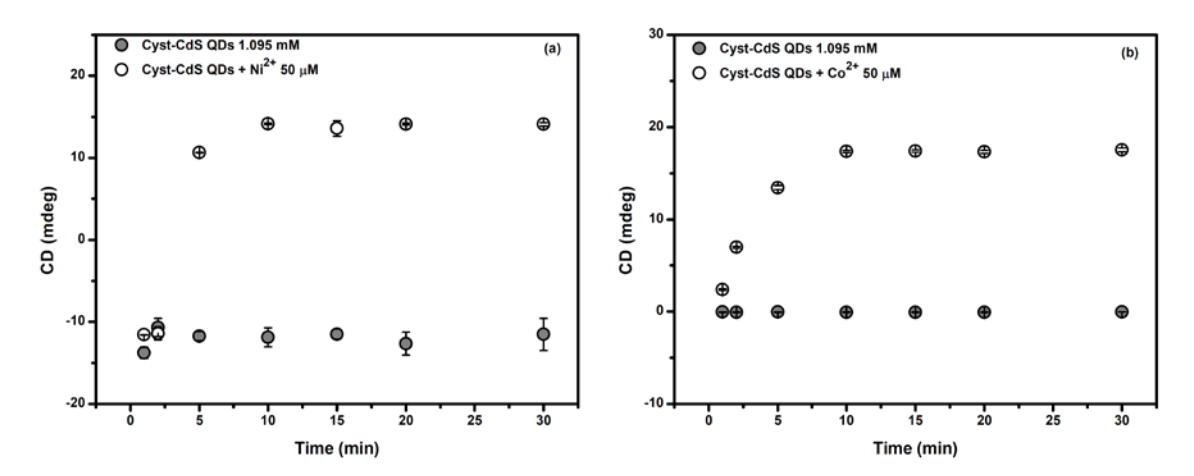


**Fig. 3** Effect of the incubation time on the CD change of 1.095 mM Cyst-CdS QDs in 0.1 M PBS pH 7.0 in the absence and presence of 50  $\mu$ M (a) Ni<sup>2+</sup> (at 324 nm) and (b) Co<sup>2+</sup> (at 352 nm).

## 3.4. Selectivity of the proposed sensor

In this work, the probe Cyst-CdS QDs possesses chiral property, and the selectivity stems from the ability of the QDs-bound L-Cysteines to complex metal ions. Previous reports have shown that L-Cysteine can form complexes with many transition [45, 46], alkali and alkaline earth metal ions [47]. Therefore, we have monitored the changes in CD spectra of Cyst-CdS QDs after adding various metal ions including Li<sup>+</sup>, Na<sup>+</sup>, K<sup>+</sup>, Ca<sup>2+</sup>, Mg<sup>2+</sup>, Ba<sup>2+</sup>, Cr<sup>3+</sup>, CrO<sub>4</sub><sup>2-</sup>, Mn<sup>2+</sup>, Fe<sup>2+</sup>, Fe<sup>3+</sup>, Cu<sup>2+</sup>, Ag<sup>+</sup>, Pb<sup>2+</sup>, Zn<sup>2+</sup>, Cd<sup>2+</sup> as well as Hg<sup>2+</sup>, and the results are shown in Fig. 4. It can be clearly seen that the CD spectrum significantly changes only in the presence of Ni<sup>2+</sup> and Co<sup>2+</sup>. In the presence of only Ni<sup>2+</sup>, the CD signal at 324 nm changes to the opposite direction. The degree of CD change monitored at 324 nm is shown in Fig. 4(b). Other studied metal ions do not respond to this sensor. In addition, this probe can also be used to detect only Co<sup>2+</sup> at the wavelength of 352 nm by monitoring the increasing of the CD signal at this wavelength, and the degree of the increasing of CD signal is shown in Fig. 4(c). On the other hand, other studied metal ions do not significantly affect the CD spectrum of Cyst-CdS QDs at this wavelength. This experiment thus confirms that the proposed sensor possesses highly selectivity toward Ni<sup>2+</sup> and Co<sup>2+</sup>.

To demonstrate the advantage of the CD sensor over the fluorescence sensor, the fluorescence titrations of Cyst-CdS QDs with Ni<sup>2+</sup> or Co<sup>2+</sup> are also studied. The fluorescence titration spectra are shown in Fig. S6 (in the SD) and Fig. S7 (in the SD) for Ni<sup>2+</sup> and Co<sup>2+</sup>, respectively. Basically, Cyst-CdS QDs can give the fluorescence emission as well as other QDs. Cyst-CdS QDs emit at the maximum emission wavelength of 495 nm when exciting at 330 nm. Upon titrating with Ni<sup>2+</sup> or Co<sup>2+</sup>, the fluorescence quenching can be observed at the same emission wavelength. The result implies that Ni<sup>2+</sup> and Co<sup>2+</sup> may form stable complexes with the QDs-bound L-Cysteines, not with the QDs surface. Based on the hard-soft acid base principle, Ni<sup>2+</sup> and Co<sup>2+</sup> ions which are modulate soft acids may form complexes with modulate soft bases of caboxylate and amine moieties. Therefore, stable complexes can be formed using donor atoms of L-Cysteines on the surface of QDs.

The fluorescence quenching data are analyzed using the Stern-Volmer equation (1) [48].

$$\frac{F_0}{F} = 1 + K_{SV}[Q] \tag{1}$$

where  $F_0$  and F are the fluorescence intensities of Cyst-CdS QDs in the absence and in the presence of  $Ni^{2+}$  or  $Co^{2+}$ , respectively.  $K_{SV}$  is the Stern-Volmer quenching constant which is related to the quenching efficiency and [Q] is the concentration of  $Ni^{2+}$  or  $Co^{2+}$ . As shown in Fig. S6 (c) and Fig. S7 (c) in the SD, a linear relationship between the ratio of  $F_0$  to F and  $Ni^{2+}$  or  $Co^{2+}$  concentration is observed in the range of 20-60  $\mu$ M and 10-80  $\mu$ M with a  $K_{SV}$  of  $3.57 \times 10^5$   $M^{-1}$  and  $1.00 \times 10^4$   $M^{-1}$  for  $Ni^{2+}$  or  $Co^{2+}$ , respectively. The remarkably high  $K_{SV}$  values suggest a high quenching efficiency of  $Ni^{2+}$  or  $Co^{2+}$ .

The results show that if the Cyst-CdS QDs probe is used as a fluorescence sensor, it cannot discriminate Ni<sup>2+</sup> and Co<sup>2+</sup>. On the other hand, it can be used as a CD sensor for selective detection of Ni<sup>2+</sup> or Co<sup>2+</sup> at different wavelength. Moreover, the improvement in term of linear working concentration range and detection sensitivity can be obtained from the proposed CD sensor.

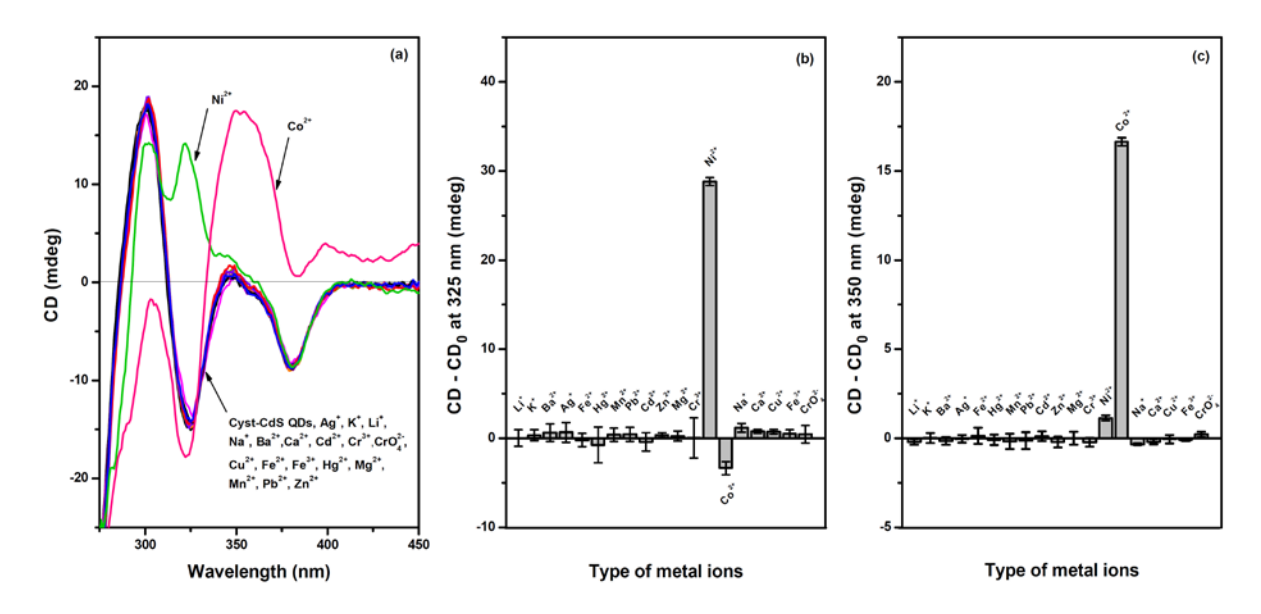


**Fig. 4** (a) Effect of the possible interfering ions on the CD spectrum of 1.095 mM Cyst-CdS QDs in 0.1 M PBS pH 7.0. The CD change upon the addition of each metal ion at 324 nm (b) and (c) at 352 nm. The concentration of each metal ion was fixed at 50 μM.

#### 3.5. Analytical performance of the proposed sensor

There are few reports regarding the application of the CD technique in the quantitative analysis of metal ions, probably due to the limit of the sensitivity. Basically, the analysis by CD needs the analyte concentration at millimolar level. However, in this work we demonstrate the CD technique for a selective determination of metal ions at the micromolar level. The lower detection sensitivity can be enhanced by the introduction of QDs nanoparticles. Therefore, our finding allows CD to be used as efficient quantitative analysis for metal ions.

The quantitative analysis is studied by constructing the calibration curve for  $Ni^{2+}$  and  $Co^{2+}$ . Under the optimized condition, the solution of Cyst-CdS QDs is titrated with the appropriate volume of the standard solution of  $Ni^{2+}$  or  $Co^{2+}$ , and the CD spectra are recorded as shown in Fig. 5. Form Fig. 5(a), it can be seen that the CD signal at the wavelength of 324 nm increases as a function of the increasing of  $Ni^{2+}$  concentration. The calibration curve of  $Ni^{2+}$  can be obtained by plotting the CD signal (mdeg) as a function of the concentration of  $Ni^{2+}$  as shown in Fig. 5(b). The working linear concentration range of the proposed sensor for detecting  $Ni^{2+}$  is found in the range of 10-60  $\mu$ M. The concentration beyond this range gives

saturate response (inset Fig. 5(b)). The regression equation is found to be CD (medg) =  $0.5757 \times [\text{Ni}^{2+}] (\mu \text{M}) - 15.234$  with the correlation coefficient (r<sup>2</sup>) of 0.9819.

For the detection of  $\text{Co}^{2+}$ , upon the increasing of  $\text{Co}^{2+}$  concentration, the CD signal at 352 nm significantly increases as a linear function of the increment of  $\text{Co}^{2+}$  concentration as shown in the Fig. 5(c). The calibration curve is also plotted between the CD signal (mdeg) at 352 nm against the concentration of  $\text{Co}^{2+}$ , and the results are shown in Fig. 5(d). It is found that this sensor provides the linear working range of 4-80  $\mu$ M. The regression equation was found to be CD (medg) =  $0.3682 \times [\text{Co}^{2+}]$  ( $\mu$ M) – 1.0153 with the correlation coefficient ( $r^2$ ) of 0.9888.

The limit of detection (LOD) and limit of quantitation (LOQ) are also determined. The LOD has been calculated as the concentration of Ni<sup>2+</sup> or Co<sup>2+</sup> giving the CD signal (mdeg) equal to CD<sub>0</sub> (mdeg)+3×standard deviation of CD<sub>0</sub>. Similarly, the LOQ is defined as the concentration of Ni<sup>2+</sup> or Co<sup>2+</sup> giving the CD signal (mdeg) equal to CD<sub>0</sub>+10×standard deviation of CD<sub>0</sub>, where CD<sub>0</sub> is the CD signal of Cyst-CdS QDs in the absence of Ni<sup>2+</sup> or Co<sup>2+</sup> at 324 or 352 nm, respectively. The LOD of the proposed sensor for the determination of Ni<sup>2+</sup> and Co<sup>2+</sup> are 7.33  $\mu$ M (0.430 ppm) and 1.13  $\mu$ M (0.066 ppm), respectively. In addition, the LOQ of the proposed sensor for the determination of Ni<sup>2+</sup> or Co<sup>2+</sup> are 11.49  $\mu$ M (0.675 ppm) and 4.19  $\mu$ M (0.247 ppm), respectively. The repeatability of the present method is also evaluated. The relative standard deviation from the detection of 50  $\mu$ M Ni<sup>2+</sup> or Co<sup>2+</sup> for five replicates is less than 1%.

Analytical characteristics of the proposed sensor confirm that the proposed sensor possesses excellence detection sensitivity, repeatability with relatively low detection limit and can be a powerful sensor for the application in real situation.

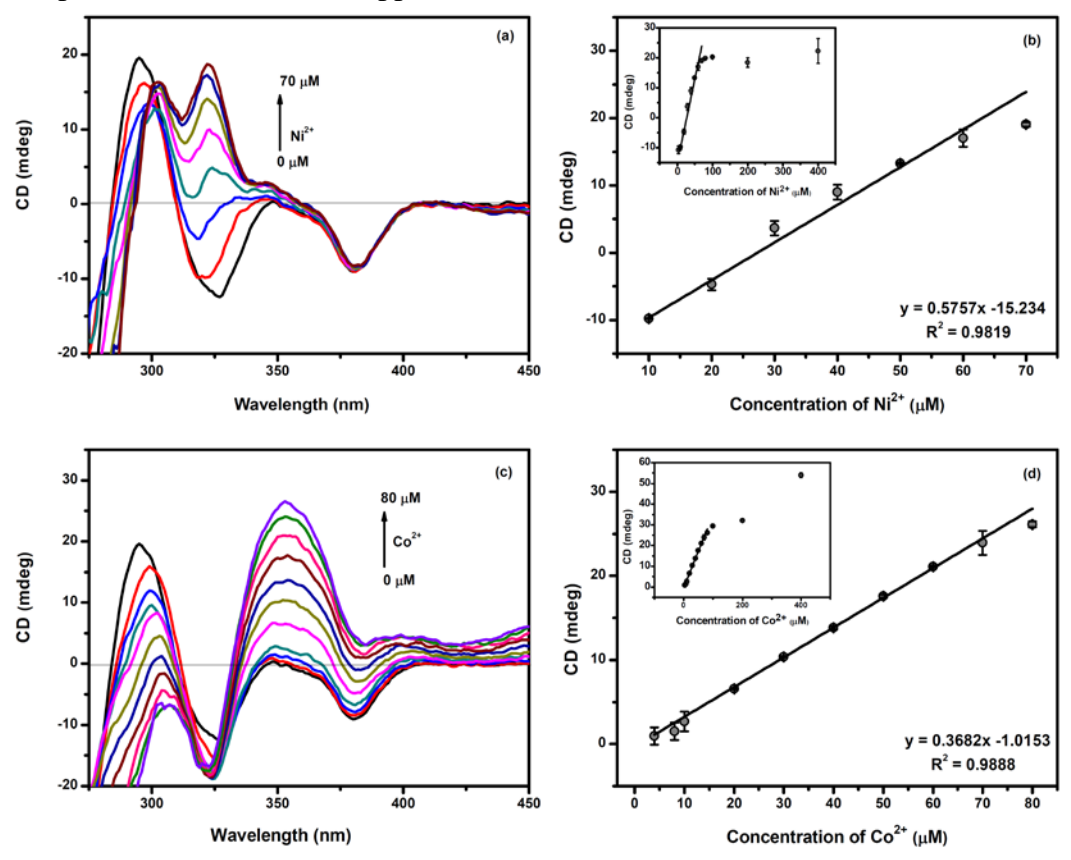


**Fig. 5** CD titration spectrum of 1.095 mM Cyst-CdS QDs in 0.1 M PBS pH 7.0 in the presence of (a)  $Ni^{2+}$  concentration ranging 10-70  $\mu$ M (b) the corresponding calibration curve (at 324 nm) and (c)  $Co^{2+}$  concentration ranging 4-80  $\mu$ M (d) the corresponding calibration curve (at 352 nm).

#### 3.6. Application to real water samples analysis

The application of the proposed sensor for the determination of  $\mathrm{Ni}^{2+}$  or  $\mathrm{Co}^{2+}$  has been demonstrated by using 3 types of real water samples. The water samples used in this work are tap water, drinking water, and pond water samples. The pond water sample has been filtered through a filter paper to remove any particulate suspension. All water samples are spiked with  $\mathrm{Ni}^{2+}$  or  $\mathrm{Co}^{2+}$  to be the final concentration of 35, and 65  $\mu\mathrm{M}$  under the optimized condition. In order to demonstrate the accuracy of the proposed sensor, the spiked samples are also directly determined by the ICP-OES. The concentrations of  $\mathrm{Ni}^{2+}$  or  $\mathrm{Co}^{2+}$  in the water samples obtained by the proposed sensor and the ICP-OES are summarized in Table 1 and Table 2 for  $\mathrm{Ni}^{2+}$  and  $\mathrm{Co}^{2+}$ , respectively. Table 1 and Table 2 show that the concentration of  $\mathrm{Ni}^{2+}$  or  $\mathrm{Co}^{2+}$  found by the proposed sensor are in good agreement with the spiked value and the recovery was in the range of 91-103%. Moreover, the concentrations of the spiked samples agree well with the results obtained from ICP-OES, confirming the accuracy of the proposed sensor. Furthermore, the %RSDs from 3 replicates are lower than 3% suggesting that the proposed sensor provides good precision. These results signify that the proposed sensor can be used in practical applications.

**Table 1.** Determination of  $Ni^{2+}$  in real water samples by using the proposed sensor (n=6) and the ICP-OES technique (n=3).

Methods	Sample	Added (µM)	Found $\pm$ SD $(\mu M)$	%RSD	% Recovery
		-	n.d.	-	-
	Tap water	35.0	$30.0 \pm 0.2$	0.6	91
		65.0	$62.2 \pm 1.0$	1.5	97
		-	n.d.	-	-
This method	Drinking water	35.0	$30.3 \pm 0.3$	1.0	92
		65.0	$63.0 \pm 1.0$	1.7	98
		-	n.d.	-	-
	Pond water	35.0	$30.0 \pm 0.2$	0.5	90
		65.0	$62.3 \pm 0.7$	1.2	98
	Tap water	-	n.d.	-	-
		35.0	$32.5 \pm 0.1$	3.7	93
		65.0	$65.4 \pm 0.1$	1.1	101
		-	n.d.	-	-
<b>ICP-OES</b>	Drinking water	35.0	$32.8 \pm 0.0$	0.4	94
		65.0	$64.8 \pm 0.1$	1.7	100
		-	n.d.	-	-
	Pond water	35.0	$32.7 \pm 0.0$	2.5	94
		65.0	$64.0 \pm 0.1$	3.7	98

<sup>\*</sup> n.d. = not detectable (less than LOD)

**Table 2.** Determination of  $Co^{2+}$  in real water samples by using the proposed sensor (n=6) and the ICP-OES technique (n=3).

Methods	Sample	Added (µM)	Found $\pm$ SD $(\mu M)$	%RSD	% Recovery
		-	n.d.	-	-
	Tap water	7.0	$7.2 \pm 0.1$	1.2	103
		25.0	$24.6 \pm 0.4$	1.6	99
		-	n.d.	-	-
This method	Drinking water	7.0	$6.7 \pm 0.1$	1.1	98
		25.0	$25.1 \pm 0.4$	1.7	100
		-	n.d.	-	-
	Pond water	7.0	$7.3 \pm 0.2$	2.6	103
		25.0	$24.9 \pm 0.3$	1.3	99
		-	n.d.	-	-
	Tap water	7.0	$7.6 \pm 0.0$	1.1	109
		25.0	$24.0 \pm 0.1$	6.9	96
		-	n.d.	-	-
<b>ICP-OES</b>	Drinking water	7.0	$7.2 \pm 0.0$	0.8	104
		25.0	$25.1 \pm 0.1$	3.9	101
		-	n.d.	-	-
	Pond water	7.0	$7.5 \pm 0.0$	6.2	108
		25.0	$24.0 \pm 0.1$	5.6	96

<sup>\*</sup> n.d. = not detectable (less than LOD)

#### 4. Conclusion

We have successfully demonstrated a new approach for the fabrication of CD sensor by using nanocrystalline quantum dots. The CdS QDs capped with L-Cysteine were used as a CD probe for selective determination of Ni<sup>2+</sup> and Co<sup>2+</sup>. The Cyst-CdS QDs showed optically active in the CD spectrum due to the chiral capping molecule. In the presence of Ni<sup>2+</sup> or Co<sup>2+</sup>, the CD spectra of Cyst-CdS QDs were significantly changed due to the formation of new chiral complexes on the capping molecules. On the other hand, other studied cations did not significantly alter the CD spectrum of Cyst-CdS QDs. The degree of the mdeg change linearly increased with increasing the concentration of Ni<sup>2+</sup> or Co<sup>2+</sup> with wide working concentration ranges. The proposed sensor provided very low detection limit of 7.33  $\mu$ M (0.430 ppm) and 1.13  $\mu$ M (0.066 ppm) for Ni<sup>2+</sup> and Co<sup>2+</sup>, respectively. The feasibility of the proposed sensor for real situation was demonstrated by using 3 types of real water samples and compared to the results obtained from ICP-OES. The results confirmed that the proposed CD sensor can be used to detect Ni<sup>2+</sup> and Co<sup>2+</sup> in real samples with good accuracy and precision.

#### References

- [1] E.J. Underwood, Trace elements in Human and Animal Nutrition, fourth ed., Academic Press, New York, 1977.
- [2] D. Purves, Trace Element Contamination of the Environments, Elsevier Science Publishers BV, Netherlands, 1985.

- [3] C.D. Klaassen, Casarett and Doull's Toxicology the Basic Science of Poisoning, sixth ed., McGraw-Hill, Medical Publishing Division, New York, 1986.
- [4] B. Venugopal, T.D. Luckey, A Metal Toxicity in Mammals, vol. 2, Plenum Press, New York, 1979.
- [5] R.K. Thauer, Nickel to the fore, Science 293 (2001) 1264–1265.
- [6] B. Zerner, Recent advances in the chemistry of an old enzyme, urease, Bioorganic. Chem. 19 (1991) 116–131.
- [7] S. Hemburg, J. Kikkane, G. Mellin, H. Lilivs, d-aminolevulinic acid dehydrase as a measure of lead exposure, Arch. Environ. Health 21 (1970) 140–151.
- [8] O.P. Kalyakina, O.N. Kononova, S.V. Kachin, A.G. Kholmogorov, Sorption preconcentration and determination of nickel in wastes of heat power industry by diffuse reflection spectroscopy, Bull. Korean Chem. Soc 24 (2003) 173–178.
- [9] J. Kristiansen, J.M. Christensen, T. Henriksen, N.H. Nielsen, T. Menne, Determination of nickel in fingernails and forearm skin (stratum corneum), Anal. Chim. Acta 403 (2000) 265–272.
- [10] M. Rajabi, S. Asemipour, B. Barfi, M.R. Jamali, M. Behzad, Ultrasound-assisted ionic liquid based dispersive liquid–liquid microextraction and flame atomic absorption spectrometry of cobalt, copper, and zinc in environmental water samples, J. Mol. Liq. 194 (2014) 166–171.
- [11] S.L.C. Ferreira, W.N.L. dos Santos, V.A. Lemos, On-line preconcentration system for nickel determination in food samples by flame atomic absorption spectrometry, Anal. Chim. Acta 445 (2001) 145–151.
- [12] J. Chen, K.C. Teo, Determination of cobalt and nickel in water samples by flame atomic absorption spectrometry after cloud point extraction, Anal. Chim. Acta 434 (2001) 325–330.
- [13] Z. Sun, P. Liang, Q. Ding, J. Cao, Determination of trace nickel in water samples by cloud point extraction preconcentration coupled with graphite furnace atomic absorption spectrometry, J. Hazard. Mater. 137 (2006) 943–946.
- [14] G. Yang, W. Fen, C. Lei, W. Xiao, H. Sun, Study on solid phase extraction and graphite furnace atomic absorption spectrometry for the determination of nickel, silver, cobalt, copper, cadmium and lead with MCI GEL CHP 20Y as sorbent, J. Hazard. Mater. 162 (2009) 44–49.
- [15] M.R. Awual, M. Ismael, T. Yaita, Efficient detection and extraction of cobalt(II) from lithium ion batteries and wastewater by novel composite adsorbent, Sens. Actuat. B—Chem. 191 (2014) 9–18.
- [16] N. Yunes, S. Moyano, S. Cerutti, J.A. Gásquez, L.D. Martinez, On-line preconcentration and determination of nickel in natural water samples by flow injection-inductively coupled plasma optical emission spectrometry (FI-ICP-OES), Talanta 59 (2003) 943-949.
- [17] S.L.C. Ferreira, C.F. Brito, A.F. Dantas, N.M.L. Araújo, A.C.S. Costa, Nickel determination in saline matrices by ICP-AES after sorption on Amberlite XAD-2 loaded with PAN, Talanta 48 (1999) 1173–1177.
- [18] D. Sancho, L. Debán, I. Campos, R. Pardo, M. Vega, Determination of nickel and cobalt in refined beet sugar by adsorptive cathodic stripping voltammetry without sample pretreatment, Food Chem. 71 (2000) 139–145.
- [19] P. González, V.A. Cortínez, C.A. Fontá, Determination of nickel by anodic adsorptive stripping voltammetry with a cation exchanger-modified carbon paste electrode, Talanta 58 (2002) 679-690.
- [20] M. Morfobos, A. Economou, A. Voulgaropoulos, Simultaneous determination of nickel(II) and cobalt(II) by square wave adsorptive stripping voltammetry on a rotating-

- disc bismuth-film electrode, Anal. Chim. Acta 519 (2004) 57–64.
- [21] Q. Zhou, A. Xing, K. Zhao, Simultaneous determination of nickel, cobalt and mercury ions in water samples by solid phase extraction using multiwalled carbon nanotubes as adsorbent after chelating with sodium diethyldithiocarbamate prior to high performance liquid chromatography, J. Chromatogr. A, 1360 (2014) 76–81.
- [22] G.-W. Cheng, C.-F. Lee, K.-C. Hsu, H.-L. Wu, Y.-L. Huang, On-line microdialysis-nano-Au/TiO<sub>2</sub>-high-performance liquid chromatography system for the simultaneous determination of cobalt and nickel in water, J. Chromatogr. A, 1201 (2008) 202–207.
- [23] V.G. Rodríguez, J.M.C. Romero, J.M.F. Solís, J.P. Iglesias, H.M.S. Lago, Simultaneous determination of cobalt and nickel by reversed-phase high-performance liquid chromatography with diethyldithiocarbamic acid, J. Chromatogr. A. 673 (1994) 291–294.
- [24] J.C. Pessoa, I. Correia, G. Gonçalves, I. Tomaz, Circular dichroism in coordination compounds, J. Argent. Chem. Soc. 97 (2009) 151–165.
- [25] E. Topchiy, T. Lehmann, Chelation of Ca<sup>2+</sup> ions by a peptide from the repeat region of the *Plasmodium falciparum* circumsporozoite protein, Malar. J. 13 (2014) 195-204.
- [26] M.S. Seyed Dorraji, V. Panahi Azar, M.H. Rasoulifard, Interaction between deferiprone and human serum albumin: Multi-spectroscopic, electrochemical and molecular docking methods, Eur. J. Pharm. Sci. 64 (2014) 9–17.
- [27] E. Chamani, A. Rabbani-Chadegani, Z. Zahraei, Spectroscopic detection of etoposide binding to chromatin components: The role of histone proteins, Spectrochim. Acta A: Mol. Biomol. Spectr. 133 (2014) 292–299.
- [28] C. Weng, Y. Fu, H. Jiang, S. Zhuang, H. Li, Binding interaction between a queen pheromone component HOB and pheromone binding protein ASP1 of *Apis cerana*, Int. J. Biol. Macromol. 72 (2015) 430–436.
- [29] M.S. Ali, H.A. Al-Lohedan, M.Z.A. Rafiquee, A.M. Atta, A.O. Ezzat, Spectroscopic studies on the interaction between novel polyvinylthiol-functionalized silver nanoparticles with lysozyme, Spectrochim. Acta A: Mol. Biomol. Spectr. 135 (2015) 147–152.
- [30] N. Berova, K. Nakanishi, R. W. Woody, Circular Dichroism: Principles and Applications, New York, 2000.
- [31] X, Zhang, J. Yin, J. Yoon, Recent advances in development of chiral fluorescent and colorimetric sensors, Chem. Rev. 114 (2014) 4918–4959.
- [32] H. Yao, K. Miki, N. Nishida, A. Sasaki, K.J. Kimura, Large optical activity of gold nanocluster enantiomers induced by a pair of optically active penicillamines, J. Am. Chem. Soc. 127 (2005) 15536–15543.
- [33] T.G. Schaaff, R.L. Whetten, Giant gold–glutathione cluster compounds: Intense optical activity in metal-based transitions, J. Phys. Chem. B 104 (2000) 2630–2641.
- [34] T. Li, H.G. Park, H.-S. Lee, S.-H. Choi, Circular dichroism study of chiral biomolecules conjugated with silver nanoparticles, Nanotechnology 15 (2004) S660–S663.
- [35] G. Shemer, O. Krichevski, G. Markovich, T. Molotsky, I. Lubitz, A.B. Kotlyar, Chirality of silver nanoparticles synthesized on DNA, J. Am. Chem. Soc. 128 (2006) 11006–11007.
- [36] Y. Xia, Y. Zhou, Z. Tang, Chiral inorganic nanoparticles: Origin, optical properties and bioapplications, Nanoscale 3 (2011) 1374–1382.
- [37] S.A. Gallagher, M.P. Moloney, M. Wojdyla, S.J. Quinn, J.M. Kelly, Y.K. Guńko, Synthesis and spectroscopic studies of chiral CdSe quantum dots, J. Mater. Chem. 20 (2010) 8350–8355.
- [38] T. Nakashima, Y. Kobayashi, T. Kawai, Optical activity and chiral memory of thiol-capped CdTe nanocrystals, J. Am. Chem. Soc. 131 (2009) 10342–10343.

- [39] Y. Zhou, M. Yang, K. Sun, Z. Tang, N.A. Kotov, Similar topological origin of chiral centers in organic and nanoscale inorganic structures: Effect of stabilizer chirality on optical isomerism and growth of CdTe nanocrystals, J. Am. Chem. Soc. 132 (2010) 6006–6013.
- [40] C. Carrillo-Carrión, S. Cárdenas, B.M. Simonet, M. Valcárcel, Selective quantification of carnitine enantiomers using chiral cysteine-capped CdSe(ZnS) quantum dots, Anal. Chem. 81 (2009) 4730–4733.
- [41] M.P. Moloney, Y.K. Guńko, J.M. Kelly, Chiral highly luminescent CdS quantum dots, Chem. Commun. 38 (2007) 3900–3902.
- [42] S.D. Elliot, M.P. Moloney, Y.K. Guńko, Chiral shells and achiral cores in CdS quantum dots, Nano Lett. 8 (2008) 2452–2457.
- [43] H. Qi, T. Hegmann, Postsynthesis racemization and place exchange reactions. Another step to unravel the origin of chirality for chiral ligand-capped gold nanoparticles, J. Am. Chem. Soc. 130 (2008) 14201–14206.
- [44] J.W. Chang, R.B. Martin, Visible circular dichroism of planar nickel ion complexes of peptides and cysteine and derivatives, J. Phys.Chem. 73 (1969) 4277–4283.
- [45] B. Herman, I. Sóvágó, Metal complexes of sulphur-containing ligands. V. interactions of cobalt(II) ion with L-Cysteine and its derivatives, Inor. Chim. Acta 80 (1983) 75–83.
- [46] B.O. Leung, F. Jalilehvand, R.K. Szilagyi, Electronic structure of transition metal-cysteine complexes from x-ray absorption spectroscopy, J. Phys. Chem. B 112 (2008) 4770–4778.
- [47] R. Shankar, P. Kolandaivel, L. Senthilkumar, Interaction studies of cysteine with Li<sup>+</sup>, Na<sup>+</sup> K<sup>+</sup>, Be<sup>2+</sup>, Mg<sup>2+</sup>, and Ca<sup>2+</sup> metal cation complexes, J. Phys. Org. Chem. 24 (2011) 553–567.
- [48] T. Noipa, S. Martwiset, N. Butwong, T. Tuntulani, W. Ngeontae, Enhancement of the fluorescence quenching efficiency of DPPH• on colloidal nanocrystalline quantum dots in aqueous micelles, J. Fluoresc. 21 (2011) 1941–1949.

## 4. Circular dichroism sensor based on cadmium sulfide quantum dots for chiral identification and detection of penicillamine

#### 1. Introduction

Penicillamine (PA) is a sulfur-containing amino acid which is generally considered to be in a family of aminothiols [1]. It is a pharmaceutically essential chiral compound which is a degradation product of penicillin [2]. It can typically be classified into two forms including D-penicillamine (DPA) and L-penicillamine (LPA). The pharmaceutical form is DPA whereas LPA is clinically toxic since it inhibits the action of pyridoxine [3]. DPA is therefore favorable in the treatment of clinical pathology [4]. Due to the toxicity of the LPA form, various analytical techniques, including high performance liquid chromatography [5], chemiluminescence, flow injection analysis [6,7],capillary electrophoresis electrochemistry [9], spectrophotometry [10], and fluorimetry [11] have been reported for identification of DPA in both pharmaceutical preparations and biological samples. All of these methods, however, cannot make an effective discrimination between D- and L-isomers. Consequently, the development of methods for analytical identification of DPA and LPA is in an early state and still a challenging issue to pursue.

Recently, chemical sensing based upon tailored nanoparticles (NPs) has attracted more and more attentions due to their unique size-dependent optical properties. Optical NPs have been widely used in a wide spectrum of practical applications such as biosensors [12], biomarkers [13], biomedical imaging [14] and optical sensors [15,16]. Recently, nanocrystalline semiconductors or quantum dots (QDs) have been efficiently used for optical sensors. The detection technique is primarily relied upon the fluorescence properties of QDs [17]. They can be designed and modified for selective fluorescence sensors by using appropriate core materials and capping molecules [18-23]. In addition to the direct sensing onto the QD surface, other indirect approaches could be used for electrochemical sensors [24].

In order to modify the fluorescence properties of QDs, various capping molecules are modified onto the QDs surface. The use of stereospecific chiral molecules as a capping agent is capable of providing a new strategy for chemical sensors [25]. Basically, chiropical activity of QDs can be induced by a chiral environment via binding of chiral organic ligands to the QDs surface [26]. The chiroptical properties of QDs can be modified by using different types of core and capping molecules. Chiroptical properties of many tailored QDs structures have been reported, for example D- and L- penicillamine capped on the CdS QDs [27], CdS nanotetrapods [28] or CdSe QDs [26,29] and chiral thiols capped CdTe QDs [30]. The distinctive properties of the surface-modified QDs can lead to the potential applications in fluorescence sensors.

However, the study on the detection of enatiomeric compounds by using fluorescence QDs is still in the early state. Very little progress has been recently reported. This is probably due to the difficulty of design of specific interactions between each isomer and the chiral probe to obtain different signals. The core/shell structure QDs, a promising candidate, has been proposed for specific enantiomeric sensors using fluorescence spectroscopy. To illustrate, cyclodextrin capped CdSe/ZnS core/shell QDs were used as chiral recognition of amino acids [31]. Chiral cysteine-capped CdSe/ZnS core/shell QDs were also proposed as a selective fluorescence sensor for quantification of carnitine enantiomers [32]. Additionally, CdSe/ZnS core/shell QDs passivated by *N*-acetyl-L-cysteine methyl ester were used as a fluorescence sensor to recognize the chirality of the non-steroidal anti-inflammatory drugs, 2-arylpropionic acid, based on the cooperative action between the QDs and their organic capping molecules [33]. To the best of our knowledge, no experimental work has so far been

published on the analysis of the QDs as a sensor for the quantitative determination of DPA and LPA.

Circular dichroism (CD) spectroscopy has been widely used to analyze chiral molecules of all types and sizes [34]. It is an essential technique to elucidate the secondary structure or conformation of macromolecules, particularly proteins. This technique can be used to observe the change of the protein secondary structure caused by the environmental changes due to interactions of amino acids. CD spectroscopy can also be used to detect interactions between QDs and biomolecules such as enzyme [35] or protein [36,37]. Nonetheless, this technique is infrequently used to observe the interactions between QDs and small chemical compounds. More specifically, this technique is seldom used as a sensor for quantitative analysis. Recently, our group demonstrated the potential application of the CD technique to detect heavy metal ions by using chiral QDs as a sensor probe [38]. The detection principle was based on the measurement of the degree of the CD signal which depends upon the formation of chiral complex on the QD surface. The proposed sensor can be utilized for the selective detection of Ni<sup>2+</sup> and Co<sup>2+</sup>. It was also found that the CD sensor based on chiral QDs provided superior sensor characteristics, compared to measuring QDs fluorescence property.

In the present work, a new CD sensor based upon cysteamine capped cadmium sulfide QDs (Cys-CdS QDs) has been proposed for detection and chiral identification of DPA and LPA. The Cys-CdS QDs are not optically active in the CD signal (achiral probe). In contrast, the CD data can be detected once Cys-CdS QDs react with DPA or LPA, resulting in a formation of chiral QDs. This phenomenon provides the possibility to apply Cys-CdS QDs as optical detection of chiral-thiol containing compounds. Interestingly, compared to the direct detection of chiral-thiol containing compounds by CD, this sensor is capable of detecting at relatively low concentration levels. Besides the capability of detecting at low concentrations, a progressive spectral change has been observed with increasing concentrations of the DPA or LPA. Thus, the quantitative analysis can also be addressed. The selectivity of the proposed sensor was comparatively observed among various forms of chiral-thiol containing compounds. Moreover, the feasibility of the proposed sensor in a practical application was demonstrated by determination of DPA and LPA in urine samples.

#### 2. Materials and Methods

#### 2.1 Chemicals

Chemical reagents used in the current work were all at least of analytical grade and used as receive. Both DPA and LPA were purchased from Aldrich. Cysteamine hydrochloride was obtained from Sigma. Sodium sulfide (Na<sub>2</sub>S) was obtained from BDH. Cadmium chloride (CdCl<sub>2</sub>·H<sub>2</sub>O), potassium dihydrogen orthophosphate (KH<sub>2</sub>PO<sub>4</sub>) and dipotassium hydrogen orthophosphate (K<sub>2</sub>HPO<sub>4</sub>) were purchased from UNIVAR. Deionized water (DI) was used for all dilutions with a specific resistivity of 18.2 M $\Omega$  cm (Millipore water). Cys-CdS QDs used in this work were prepared and characterized as previously described in our recent report [20] (see the electronic supporting information (ESI) for more information).

#### 2.2 Instrumentations

The detection and chiral identification of DPA and LPA were carried out using circular dichroism spectroscopy recorded on a Jasco-815 CD spectropolarimeter (JASCO, Japan) using a 1 cm quartz cell cuvette, with a scanning rate at 200 nm min<sup>-1</sup>. The fluorescence spectra data were collected on a Shimadzu RF-5301PC spectrofluorometer. Excitation and emission spectra were recorded with a slit width of 5 nm. Absorption spectra were investigated using an Agilent HP 8453 spectrophotometer. The pH of solutions was measured with a UB-10 UltraBasic pH meter (Denver Instrument). The transmission electron

microscope (TEM) micrograph was recorded on Tecnai G<sup>2</sup>-20 (FEI, Netherlands) operating at a 200 kV accelerating voltage.

#### 2.3 Circular dichroism measurements

The CD spectrum of PA in the presence of Cys-CdS QDs was obtained by the following procedures. DPA or LPA was dissolved in water to obtain a 10 mM stock solution. Subsequently, 100  $\mu$ L of the Cys-CdS QDs (0.04 mg mL<sup>-1</sup>) were blended with the stock solution to obtain concentrations in a range of 0-40  $\mu$ M. The mixed solution was then made to obtain a final volume of 10.00 mL with 50 mM phosphate buffer pH 7.0. Before recording the CD spectra, it was incubated at room temperature for 10 min. To investigate the effect of incubation time, the mixed solution of Cys-CdS QDs and DPA or LPA in 50 mM phosphate buffer solution pH 7.0 was incubated from 1–60 min before recording the CD spectra. The effect of solution pH on the detection and chiral identification of PA was studied by using 50 mM phosphate buffer to control pH in a range of 6.0–7.0 and 50 mM Tris-HCl buffer for the pH in a range of 7.5–10.0. Calibration curves for DPA or LPA were achieved under the optimized conditions (0.04 mg mL<sup>-1</sup> of Cys-CdS QDs in 50 mM phosphate buffer pH 7.0 and incubation time of 10 min) with a range of concentrations of DPA or LPA (0-40  $\mu$ M). The calibration curves were fitted with the CD signals at 253 nm.

## 2.4 Selectivity of the sensor

To evaluate the selectivity of the proposed sensor, the following procedures were carried out. 100  $\mu$ L of Cys-CdS QDs (to obtain a final concentration of 0.04 mg mL<sup>-1</sup>) were mixed with 500  $\mu$ L of 1.0 M phosphate buffer solution pH 7.0 in a 10.00 mL volumetric flask. Subsequently, the individual stock solution of other related compounds was added to obtain a concentration of 10  $\mu$ M. The mixture was then diluted with water. The solution was mixed and kept at room temperature for 10 min before recording CD spectra.

#### 2.5 Application to real urine samples

In order to evaluate the practical application of the proposed sensor, a urine sample from a healthy volunteer was used as a representative of clinical sample. It was prepared in the same procedure as reported previously [39]. The collection of fresh urine specimen from the healthy volunteer was done within 1 h. It was important that the urine sample was fresh when tested; therefore, it was immediately used without storing. To remove contaminated particles, the fresh urine specimen was filtered through a filter paper. A fifty-fold sample dilution was made with 50 mM phosphate buffer pH 7.0 and then equilibrated for 30 min at room temperature. The accuracy and precision of quantitative analysis were evaluated by spiking three different concentrations of DPA and LPA (5, 10 and 15  $\mu$ M) into the urine specimen under the optimized condition before the fluorescence measurement.

#### 3. Results and discussion

Surface-modified QDs have been utilized as luminescent probes for chemical determination. Herein, we demonstrate a new practical application of Cys-CdS QDs in the chiral identification and detection. This approach is based upon the CD spectroscopy technique. This technique is often used in the identification of chirality and associated CD of the chiral molecules; however, the concentrations of chiral compounds must be at a relatively high level. As a result, chiral compounds at low concentrations cannot be effectively detected. In the present work, achiral QDs are proposed as a sensor probe for detecting thiol-chiral containing compounds. It was found that the reaction between thiol-chiral containing compounds and the achiral QDs leads to optically active probe. In the following sections, the sensor characterizations and optimizations are reported and discussed in details.

## 3.1 CD response of QDs to chiral-thiol containing compounds

The CD spectra of the 0.04 mg mL<sup>-1</sup> Cys-CdS QDs in the absence and presence of PA (DPA and LPA) and cysteine were initially investigated as shown in Fig. 1 (a) and (b), respectively. The CD spectrum of Cys-CdS QDs did not show any optically active characteristics confirming that Cys-CdS QDs had no chiroptical property. Besides, it was found that concentrations of chiral-thiol containing compounds (PA and cysteine) at only 20 µM are not adequate to record the CD spectra. CD spectra of both PA and cysteine at higher concentrations were then observed as illustrated in Fig. S4 (ESI). Once the concentrations were increased, the CD spectra can be recorded and exhibited a mirror image profile of the enaniomer. It should be noted that the detection of chiral-thiol containing compounds by CD spectroscopy technique occurred at relatively high concentration levels.

To observe the CD response as a consequence of the interaction between achiral Cys-CdS QDs and chiral-thiol containing compounds, CD spectra of Cys-CdS QDs in the presence of the chiral-thiol containing compounds at the same concentration level (at only 20 μM) were recorded, and the medium of the solution was controlled. It was found that the CD spectra were significantly altered after addition of PA and cysteine as shown in Fig. 1 (a) and (b), respectively. In the presence of DPA, the CD spectrum displayed a strong trisignate CD feature with positive Cotton effects at 230 and 275 nm and a negative Cotton effect at 253 nm. The mirror image profile of LPA was also detectable. The CD spectra of Cys-CdS QDs in the existence of cysteine, as shown in Fig.1 (b), exhibit a similar pattern to that of the presence of PA but with lower intensity. It is noticeable that the CD spectrum patterns of the studied chiral-thiol containing compounds are different from their spectra at higher concentration levels ((-) 234 and (+) 234 nm for DPA and LPA, respectively). This is due to the surface modification of new chiral QDs via binding of PA (via thiol group) and Cd<sup>2+</sup> on the surface of QDs [27]. This leads to an electronic coupling between QD and chiral ligands in its proximity [26]. Organic capping ligands can be used to trigger and control interactions of optically active QDs. Therefore, the spectrum of chiral-thiol containing compounds is different from that of free PA. It should be noted that the CD spectrum of the Cys-CdS QDs after adding PA exhibited different pattern comparing with the PA capped CdS QDs as reported by Moloney et al. [27]. Moloney's work showed that the CD spectra of D- and Lpenicillamine stabilized CdS QDs are more complex than our Cys-CdS QDs after adding PA, with maxima/minima at 207  $\pm$  3, 252  $\pm$  2, 293  $\pm$  3, 320  $\pm$  2 and 345  $\pm$  2 nm. This observation suggested that hydrogen bonding interactions between the primary capping molecules (cysteamine) and PA in our case affected the CD pattern in a different manner as compared to the direct interactions of PA on the surface of CdS. However, the CD pattern obtained from both cases still showed the mirror image spectra when using the different PA isomers. More importantly, the CD signal of chiral-thiol containing compounds can be recorded at a very low concentration which cannot be detected at the same concentration level of the free PA.

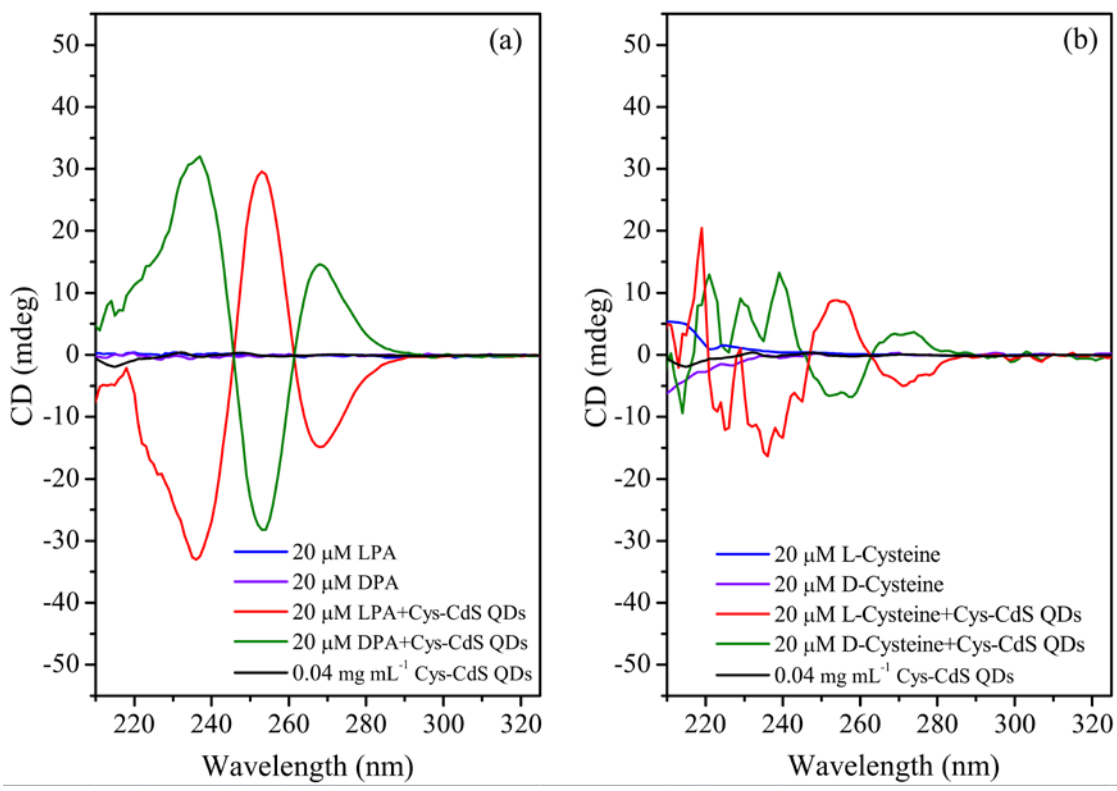


**Fig. 1** The CD spectrum of 285 μM Cys-CdS QDs in the absence and presence of 20 μM of (a) DPA and LPA and (b) <sub>D</sub>-cysteine and <sub>L</sub>-cysteine in 50 mM PBS pH 7.0.

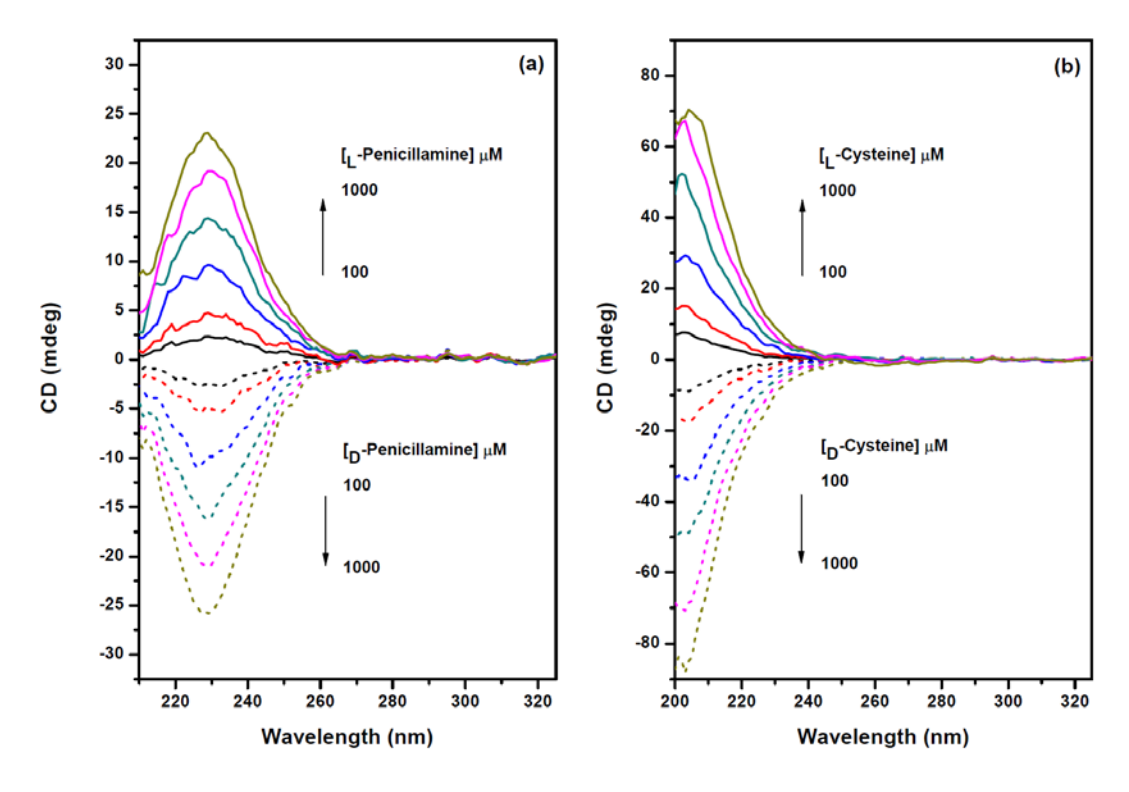


**Fig. S4**The circular dichroism spectrum of (a) D-penicillamine and L-penicillamine (b) D-cysteine and L-cysteine in 50 mM PBS pH 7.0.

#### 3.2 Possible sensing mechanism

The interaction of PA on Cys-CdS QDs was studied by investigating the absorption spectrum of Cys-CdS QDs in the presence of PA as shown in Fig. S5 (ESI). The absorbance intensity of the Cys-CdS QDs was increased without any spectrum shift after addition of PA. This indicates that the interaction between PA and QDs do not alter their sizes. In addition, PA is a strongly coordinating ligand and it is able to chelate cadmium ions on the surface of QDs providing better surface passivation [27]. This can reduce surface states and lead to strong confining potential and consequently higher luminescence efficiency.

As the fluorescence of CdS QDs is normally sensitive to the modified surface, the fluorescence spectrum of Cys-CdS QDs in the presence of various concentrations of DPA or LPA was investigated and the results are shown in Fig. S6 (ESI). There are no differences in fluorescence spectra of Cys-CdS QDs upon adding DPA or LPA. It is clearly seen that the fluorescence spectrum intensity of Cys-CdS QDs increased once PA was added. This is due to a reduction of the crystal defect at the QD surface thus reducing surface trap. However, the fluorescence intensity was not a function of the concentration of PA. Thus, the fluorescence approach can not be used to either quantitatively analyze PA or differentiate between DPA and LPA.

In order to investigate the interaction of PA on the QDs surface in details, cyclic voltammograms of the QDs in the absence and presence of PA have been recorded and the results are shown in Fig. S7 (ESI). The cyclic voltammogram of only Cys-CdS QDs showed the cathodic peak of CdS to Cd<sup>0</sup> at -1.18 V (vs Ag/AgCl) and the anodic peak at -0.95 V and -0.77 V (vs Ag/AgCl) corresponding to the oxidation of Cd<sup>0</sup> to CdS [40]. It should be noted that DPA and LPA barely showed redox waves in the studied potentials. After adding PA into the solution of Cys-CdS QDs, it can be seen in Fig. S7 (ESI) that the cathodic peak at -1.18 V (vs Ag/AgCl) significantly decreased. This may be due to the strong coordination of PA on to the surface of CdS causing less CdS to be reduced to Cd<sup>0</sup>. Consequently, the anodic peak of Cys-CdS QDs at -0.95 V (vs Ag/AgCl) increased in the presence of PA probably due to the formation of Cd(S-PA) complexes.

The results suggested that PA was attached to the surface of achiral Cys-CdS QDs resulting in novel chiral QDs. Schaaf and Whetten [41] proposed three different models accounting for a CD response from a nanocrystal with chiral ligands: (i) the core of the nanoparticle is chiral; (ii) the nanoparticle surface is chiral; (iii) only the adsorbate is chiral.

A theoretical model based on density functional theory together with experimental results of the PA capped CdS QDs showed that penicillamine ligand bound via N and S to one surface-Cd [42]. The chirality was introduced via additional bonding of carboxylate to a neighboring Cd. Due to the strong interaction between chiral ligands and, the ligands strongly distorted the outermost Cd atoms of the QDs, transmitting an enantiomeric structure to the surface layers. Nevertheless, there is little distortion of CdS geometry in the inner of QDs core. Thus, the CD signals stemmed from near-surface Cd atoms that were enantiomerically distorted by penicillamine ligands, agreeing with model (ii) proposed by Schaaf and Whetten.

Very recently, Pawar et al. [43] reported the detection of DPA using 3-mercaptopropionic acid capped CdS QDs by following the enhancement of fluorescence intensity of QDs upon the addition of DPA. In this system, the thiol (–SH) groups of DPA can bind with Cd<sup>2+</sup> on the surface of QDs which leads to the removal of local trap states and resulting in the fluorescence enhancement. Pawar's results agree well with our fluorescence and cyclic voltammetry results. Therefore, the fluorescence sensing mechanism of our work should be pertinent to model (iii) proposed by Schaaf and Whetten.

According to this phenomenon, the detection of chiral-thiol containing compounds in the presence of Cys-CdS QDs provides more sensitivity. In the light of this result, achiral Cys-CdS QDs can be used to identify chiral-thiol containing compounds. Moreover, the CD signals obtained from both PA enantiomers showed higher intensity than that obtained from cysteine. Therefore, Cys-CdS QDs can be potentially used as selective CD sensor for the detection and chiral identification of PA.

According to the basic principle of CD spectroscopy, the CD spectrum can be generated due to the different absorption of the left- and right-circularly polarized light [44]. This phenomenon would only in the case of the polarized light pass through the chiral compound. The different in the absorption of circularly polarized light can be expressed in equation (1).

$$\Delta A = A_L - A_R = b.c.\Delta \varepsilon \tag{1}$$

where  $A_L$  and  $A_R$  are the absorbance of the left- and right circularly polarized light by the chiral sample, respectively. It should be noted that there is no difference in  $A_L$  and  $A_R$  for achiral compounds. Thus, the degree of absorption can be well explained by the classical Beer–Lambert Law. Therefore, the abbreviation b, c,  $\Delta\epsilon$  are defined as a path length of the sample cell in centimeters, molar concentration and molar extinction coefficient of the sample at the specified wavelength, respectively. It can be seen from the equation (1) that the value of b is a constant parameter (in the case of using the same container) and  $\Delta\epsilon$  is also a constant value as long as measuring at the same wavelength. Therefore, the degree of  $\Delta A$  would be linearly dependent on the concentration of chiral samples. In this work, since the probe is achiral compound, the  $\Delta A$  would depend on the number of PA interacting with cysteamine on the surface of QDs. Thus, our Cys-CdS QDs can be used in a quantitative analysis of PA.

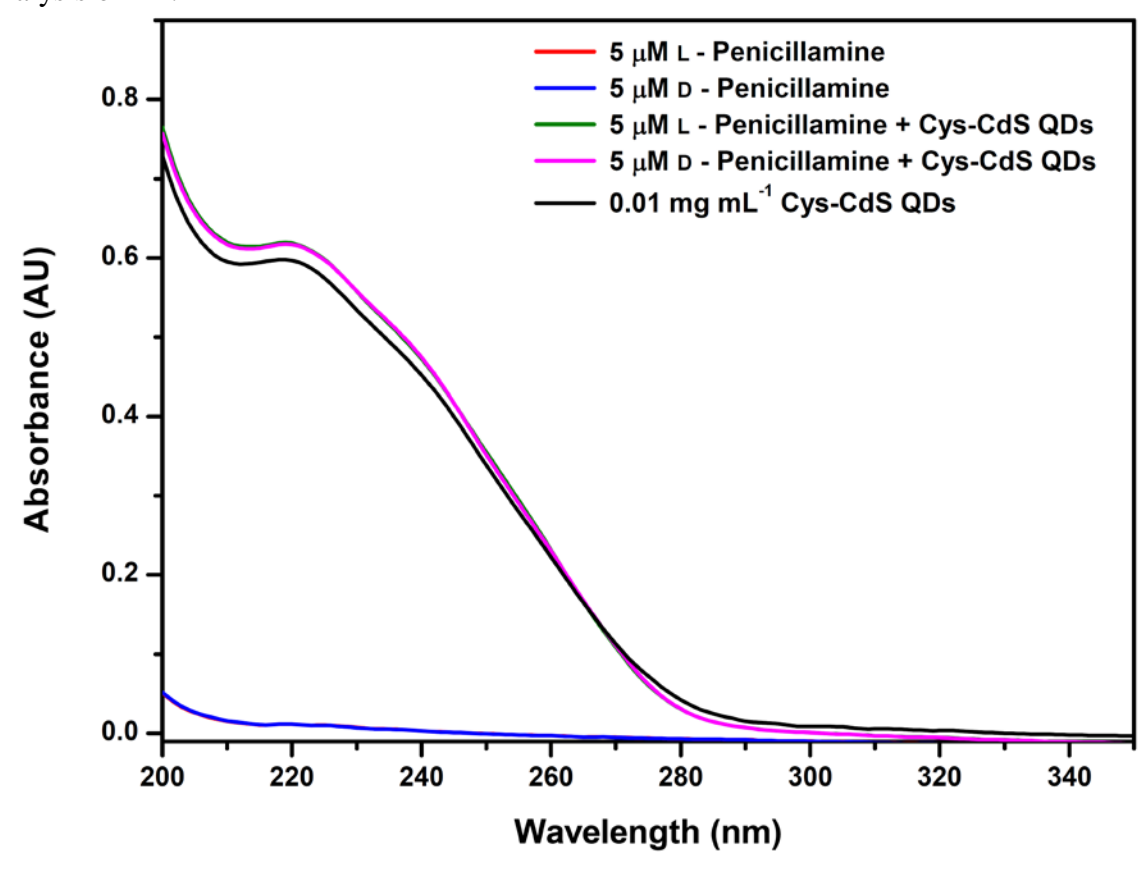


**Fig. S5**The absorption spectra of D-penicillamine, L-penicillamine before and after modified with Cys-CdS QDs in 50 mM PBS pH 7.0 (dilute 4 times from the fluorescence experiment)

#### 3.3 Effect of the solution pH

From the previous section, the CD signal of PA at low concentrations can be detected after the reaction between PA and the Cys-CdS QDs yielding new chiral QDs. Thus, the pH of the medium has to be initially optimized to obtain the best reaction condition between PA and Cys-CdS QDs. To evaluate the optimum pH, phosphate buffer solution was applied to control the pH of solution in a range of 6.0 - 7.0. In the meanwhile, tris-HCl buffer solution was introduced for a pH range of 7.5-10.0. The CD spectrum of Cys-CdS QDs in the presence of DPA and LPA at different solution pHs are illustrated in Fig. 2(a) and Fig. 2(c), respectively. In addition, the corresponding CD signal of DPA and LPA at 253 nm as a function of the solution pHs are shown in Fig. 2(b) and Fig. 2(d), respectively.

It was found that after adding either DPA or LPA into the Cys-CdS QDs, low intensity CD signals were obtained provided that the pH of the solution was lower than 7.0. In contrast, the CD signals were, after adding both DPA and LPA, significantly increased when the solution pHs were as high as 7.0 indicating the presence of a more number of PA molecules. This suggested that the binding between thiol (-SH) group of PA and the surface of Cys-CdS QDs affected by the solution pH. The binding of the S-Cd bond (thiol group of PA and CdS core QDs) at the neutral pH was more favorable than in the acidic pHs. Nonetheless, once the solution pH became more alkaline, PA may form disulfide compound by itself, thus decreasing the number of PA on the QDs. In the light of this reaction condition, the solution pH of 50 mM PBS was adjusted to 7.0 in order to obtain the optimum detection sensitivity.

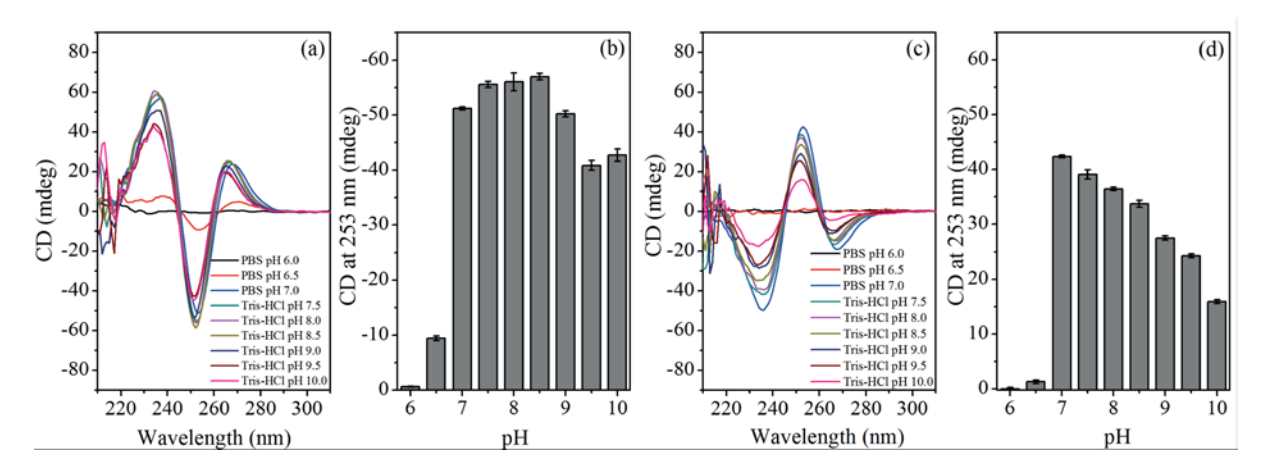


**Fig. 2** CD spectrum of 285  $\mu$ M Cys-CdS QDs in the presence of 40  $\mu$ M (a) DPA and (c) LPA in different solution pHs in 50 mM buffered solution and the corresponding CD signal of (b) DPA and (d) LPA at a wavelength of 253 nm as a function of the solution pHs (n=3).

#### 3.4 Effect of Cys-CdS QD concentration

The detection sensitivity can basically be affected by the concentration of the sensor probe. Therefore, the effect of the Cys-CdS QD concentration on the detection sensitivity was investigated in 50 mM PBS at pH 7.0 by increasing concentrations in the range of 0-0.08 mg mL<sup>-1</sup> in the presence of 40 µM of PA. After the solution was well mixed, the CD spectrum was recorded. As shown in Fig. 3, a significant role of Cys-CdS QDs in the detection can be clearly seen. Apparently, the CD signals of DPA and LPA in the absence of Cys-CdS QDs cannot be detected. In constrast, once 0.02 mg mL<sup>-1</sup> of Cys-CdS QDs was mixed into the solution the CD spectra can be observed for both DPA and LPA, as illustrated in Fig. 3 (a)

and (c), respectively. However, the fluctuation of CD spectra at wavelengths lower than 240 nm was observed once the concentrations of Cys-CdS QDs were higher than 0.04 mg mL<sup>-1</sup>, and the spectra are not well defined. This phenomenon is a result of energy absorption of Cys-CdS QDs in a range of the studied wavelengths, which can disturb the CD spectrum. Therefore, the increase of achiral probes did not improve the detection sensitivity. This suggests that fuctionalized PA onto the limited number of Cyst-CdS QDs provides better sensor characteristics than more amount of the probes. In the light of this result, 0.04 mg mL<sup>-1</sup> of Cys-CdS QDs was chosen for further studies.

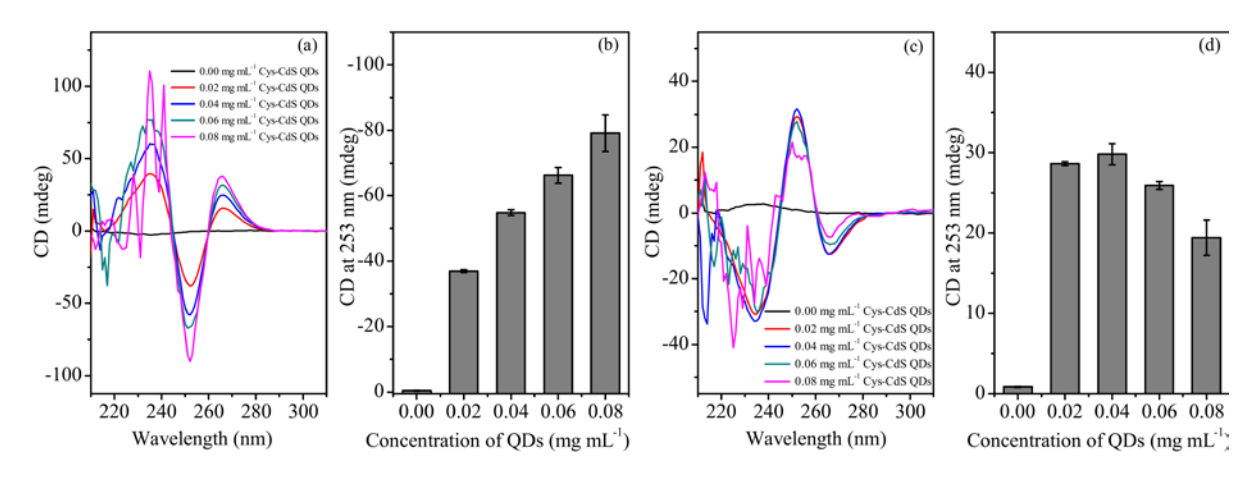


**Fig. 3** CD spectrum of Cys-CdS QDs in 50 mM PBS at pH 7.0 in a range of concentration of Cys-CdS QDs between 0-570  $\mu$ M in the presence of 40  $\mu$ M (a) DPA and (c) LPA and the corresponding CD signal of (b) DPA and (d) LPA at 253 nm as a function of the concentration of Cys-CdS QDs (n=3).

#### 3.5 Selectivity of the proposed sensor

In principle, the CD technique is capable of detecting only the compounds which manifest chiral property. Therefore, the proposed sensor is a very promising candidate for detecting PA enantiomers. The experiments were carried out by adding possible interfering compounds into the sensor probe under the optimum condition as discussed in the previous section. The CD spectrum of the Cys-CdS QDs in the existence of each interfering compound was individually recorded as shown in Fig. 4. It can be clearly seen that CD spectra developed once the Cys-CdS ODs were in the presence of chiral-thiol containing compounds including DPA, LPA, D-cysteine and L-cysteine. It is also notable that the CD signals of Cys-CdS QDs in the presence of D-cysteine and L-cysteine show lower sensitivity than that of DPA and LPA. In addition to DPA, LPA, D-cysteine and L-cysteine, several chiral compounds were also investigated including L-alanine, L-arginine, L-asparagine, L-aspartic acid, L-glutamic acid, D,L-glutamine, L-histidine, L-isoleucine, L-leucine, D,L-methionine, Dphenylalanine, L-phenylalanine, L-proline, L-threonine, L-tryptophan, L-tyrosine, L-serine and L-valine. It is noticeable that these chiral compounds have no thiol group (-SH) and they exhibit no spectrum change as illustrated in Fig. 4. This result can be used to confirm the importance of the thiol group on the detection using this novel approach. Besides, we also investigated the detection of certain compounds containing thiol group including cysteamine thioglycolic methyl-3-mercaptopropionate, 4,5-dihydro-thiazole-2-thiol, and acid. thioglycolic acid and mercaptoethanol. Although these compounds contains thiol group, they show no appearance of CD spectra. The spectral selectivity of this sensor over other thiol containing compounds is due to the basic principle of the CD technique which is capable of detecting only the chiral optically active compounds. It should be noted that a low concentration of each compound was used in the experiment in order to control the concentration level of the tested compounds for the comparison. In addition, compared with the direct detection of PA, the proposed sensor is able to detect PA at the lower concentration. This result reveals the advantages of the CD technique over conventional techniques especially the spectrofluorometry. Taking into account of these factors, our proposed sensor is capable of providing an excellent spectral selectivity on the detection of DPA and LPA.

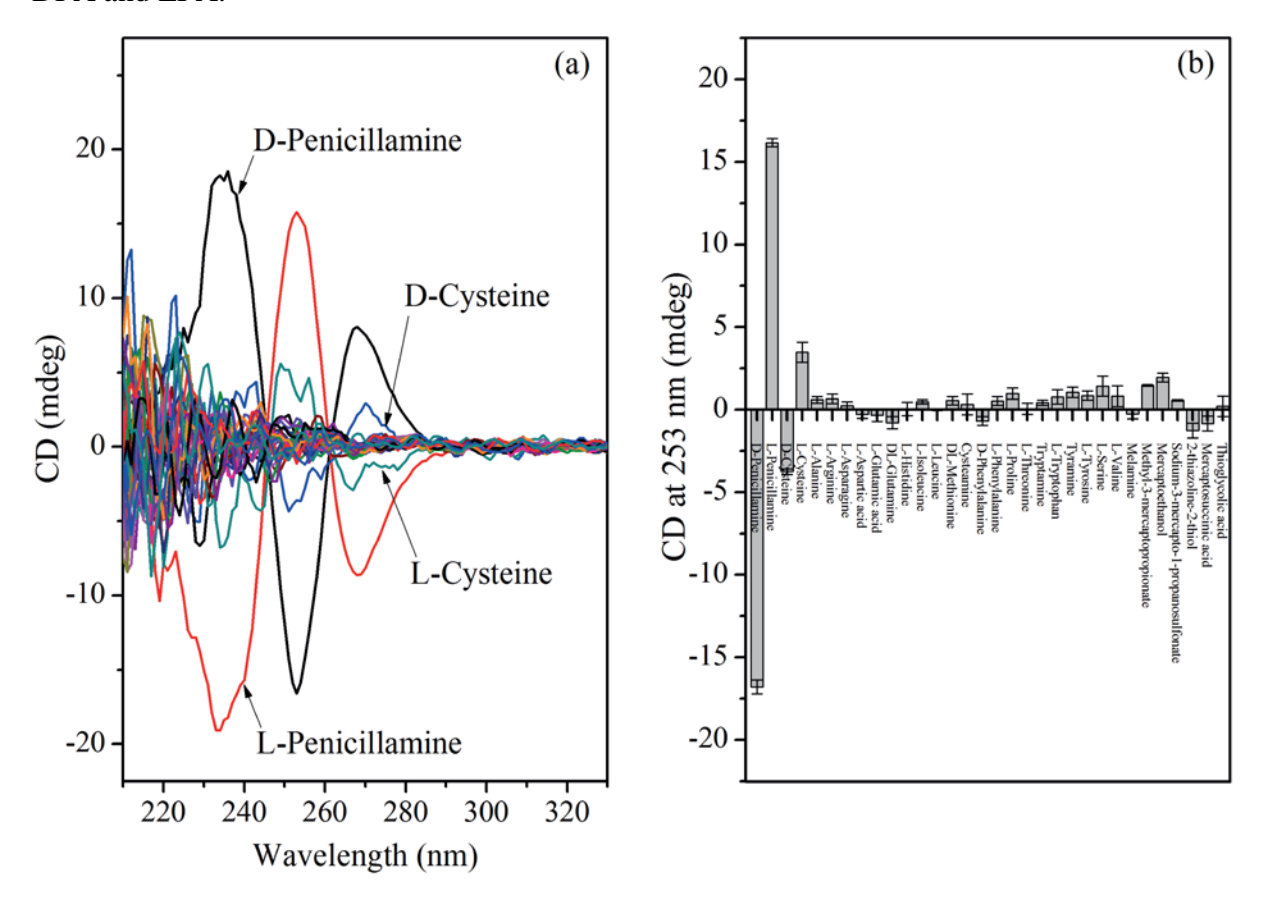


**Fig. 4** (a) CD spectrum of 285 μM Cys-CdS QDs in 50 mM PBS at pH 7.0 in the presence of 10 μM of DPA, LPA and possible interfering compounds (b) the corresponding CD signals of DPA, LPA and possible interfering compounds at 253 nm (n=3).

#### 3.6 Analytical merits of Cys-CdS QD-based CD sensor

The CD technique is not typically used as quantitative analysis approach due to the relatively high detection limit compared with other molecular spectroscopy techniques. However, our group recently demonstrated the application of CD technique in a quantitative analysis of some heavy metal ions by using chiral CdS QDs [38]. As discussed in the previous section, the CD spectrum of free PA cannot be detected provided that the concentrations of the solution are relatively low. However, the use of Cys-CdS QDs as a sensor probe allows not only chiral identification but also the quantitative analysis of PA at micromolar level. Thus, an analytical performance of the proposed sensor was thoroughly investigated.

The calibration curves for the quantitative determination of DPA and LPA were obtained by using the optimized condition as discussed in the previous section. The appropriate volumes of stock PA solutions were added into the solution of Cys-CdS QDs containing 50 mM PBS at pH 7.0 to gain the final concentrations ranging from 0 to 40  $\mu$ M. The CD spectra

of Cys-CdS QDs in the presence of different concentrations of DPA and LPA were recorded as shown in Fig. 5(a). Based on the intensity of CD spectra, the corresponding calibration curves can be obtained as illustrated in Fig. 5(b). As one can see, the CD signals of Cys-CdS QDs were increased with increasing DPA and LPA concentrations. The development of the CD spectrum upon the increase of PA amount exhibits a progressive spectral change without any significant shift. The mirror image profile of its enantiomer can also be observed. This result demonstrates that the increase of CD intensity is due to the increasing amount of PA on the surface of CdS QDs. The proposed CD sensor provides a good linear relationship between the CD signal (mdeg) and the concentration of DPA and LPA at 253 nm. The regression equations were found to be CD (mdeg) =  $-1.375 \times [DPA, \mu M] - 0.536$  ( $r^2 = 0.9896$ ) and CD (mdeg) =  $1.380 \times [LPA, \mu M] + 0.531$  (r<sup>2</sup> = 0.9920) with a range of concentrations between 1–35 µM. The concentration of PA beyond 35 µM showed the saturation of the CD signal which may be due to the limited space of the surface of the Cyst-CdS QDs (as shown in Fig. S8, ESI). The calibration equation was obtained once all possible affected parameters were optimized. As a result, the different calibration regression equation will be achieved provided that the different QD concentration is used. The detection sensitivity, however, will be less than that of the optimized condition. From a practical point of view, the concentration of the probe in both the standard and sample solution must be controlled in order to keep away from the effect of probe concentration.

The direct measurement of PA by CD technique was carried out in order to compare with the counterpart experiment. The CD spectra of DPA and LPA at the same concentration range (without Cys-CdS QDs) and medium were recorded. As shown in Fig. 5(b), the relationships between CD signals and PA concentration are plotted. Obviously, the CD signal was not significantly changed with increasing PA concentrations. This confirms that the detection sensitivity of the proposed sensor is superior to the direct CD measurement. The detection limits (LOD) of the proposed sensor was also evaluated. It is defined as the concentration of PA giving the CD signal  $CD_0 + (3\times \text{standard deviation of } CD_0)$  (at 253 nm), where  $CD_0$  is the baseline CD signal of the Cys-CdS QDs. It was found that the LOD of DPA and LPA was 0.49 and 0.74  $\mu$ M, respectively.

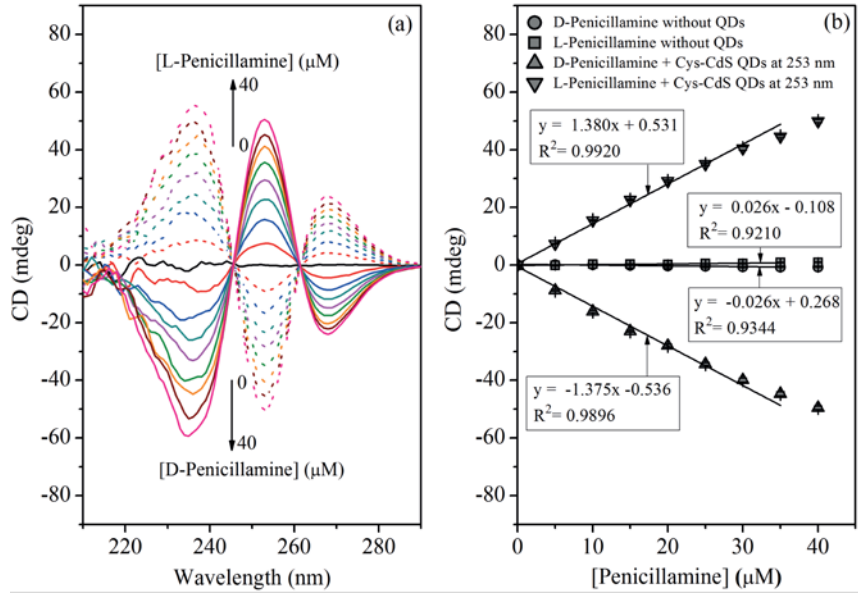


**Fig. 5** (a) The CD spectrum of 285  $\mu$ M Cys-CdS QDs in the presence of different concentrations of DPA and LPA in a range of 0-40  $\mu$ M in 50 mM PBS buffer at pH 7.0 and (b) the corresponding calibration curve (at 253 nm) and calibration curve of the direct CD measurement of DPA and LPA (at 230 nm).

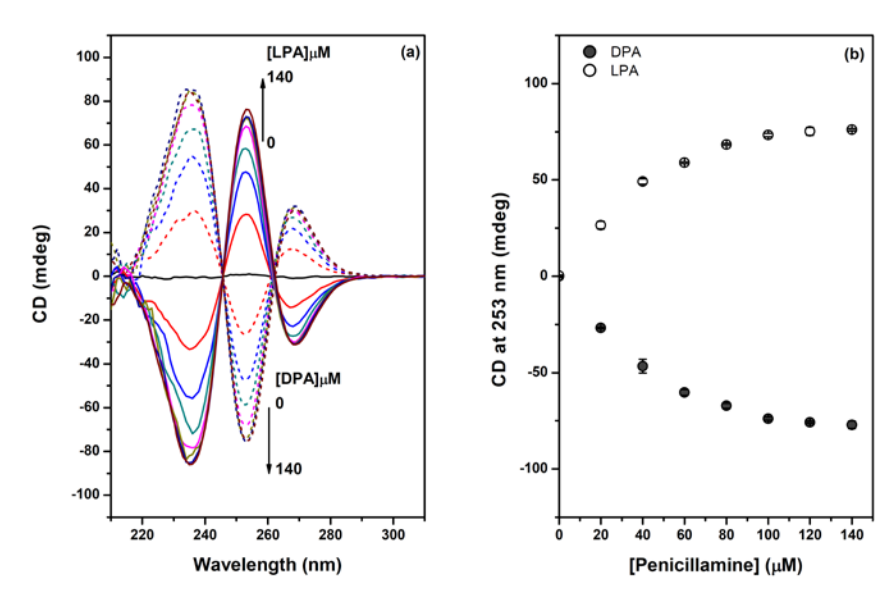


**Fig S8** (a) The CD spectrum of 0.04 mg mL<sup>-1</sup> Cys-CdS QDs in the presence of different concentrations of DPA and LPA in a range of 0-140 μM in 50 mM PBS buffer at pH 7.0 and (b) the corresponding calibration curve in a range of 0-140 μM (at 253 nm).

## 3.7 Application of the proposed sensor in real urine samples

In order to demonstrate whether the proposed sensor can be used for the detection of PA in a real situation, the urine samples from a healthy volunteer was used as a clinical sample model. The standard solutions of DPA or LPA were spiked into the urine sample to obtain the concentrations of 5, 10 and 15  $\mu$ M. The CD spectra of the spiked samples were recorded and the concentration of PA can be simply interpreted by the corresponding calibration curve. The calculated amount of PA in real urine sample and spiked samples are summarized in Table 1. Excellent recoveries are in a range from 94 to 106 % with the relative standard deviations (%RSD) lower than 6.0%. From the experiments, it can be confirmed that the proposed detection technique is reliable and can be utilized in a broad range of applications.

**Table 1.** Concentrations of DPA and LPA in real urine sample measured by the proposed sensor (n=3).

Spiked	• ,		%Recov	$\mathbf{ery} \pm \mathbf{SD}$	RSD (%)		
$(\mu M)$			DPA LPA		DPA	LPA	
-	n.d.	n.d.	-	-	-	-	
5	$5.27 \pm 0.13$	$4.94 \pm 0.25$	$105.5 \pm 2.7$	97.5±4.9	2.6	5.0	
10	$9.52\pm0.36$	9.66±0.17	95.2±3.6	96.0±1.7	3.8	1.8	
15	15.83±0.18	$14.27 \pm 0.36$	105.5±1.2	94.7±2.4	1.1	2.5	

<sup>\*</sup>n.d. = not detectable

#### 4. Conclusion

We found that thiol containing chiral molecules conjugated with CdS QDs can lead to new CD signals. The CD signal-generating phenomena of thiol containing chiral molecules can provide a novel strategy for the PA detection. The CD spectrum of DPA and LPA obtained from this approach also show mirror image profile; therefore, it can be used to identify the absolute chirality of PA. In addition, the CD signal (mdeg) from this approach depends on the concentrations of PA leading to the possible quantitative analysis. The proposed sensor allows the detection sensitivity of the PA at a micromolar range. Compared with conventional analysis, this technique provides many advantages and can overcome the primary limitations of the CD. Moreover, with reliable results this sensor can be potentially applied in practical realizations especially in detection of PA in physiological urine samples.

## References

- [1] F.E.O. Suliman, Z.H. Al-Lawati, S.M.Z. Al-Kindy, A spectrofluorimetric sequential injection method for the determination of penicillamine using fluorescamine in the presence of β-cyclodextrins, J. Fluoresc. 18 (2008), 1131–1138.
- [2] J. M.Walshe, The story of penicillamine: a difficult birth, Mov. Disord. 18 (2003) 853–859.
- [3] L. Song, Z. Guo, Y. Chen, Separation and determination of chiral composition in penicillamine tablets by capillary electrophoresis in a broad pH range, Electrophoresis 33 (2012) 2056–2063.
- [4] M. Zeeb, M.R. Ganjali, P. Norouzi, S.R. Moeinossadat, Selective determination of penicillamine by on-line vapor-phase generation combined with Fourier transform infrared spectrometry, Talanta 78 (2009) 584–589.
- [5] R. Saetre, D.L. Rabenstein, Determination of penicillamine in blood and urine by high performance liquid chromatography, Anal. Chem. 50 (1978) 276–280.
- [6] Z.D. Zhang, W.R.G. Baeyens, X.R. Zhang, G. Van Der Weken, Chemiluminescence determination of penicillamine via flow injection applying a quinine–cerium(IV) system, Analyst 121 (1996) 1569–1572.
- [7] M. Catalá Icardo, O. Armenta Estrela, M. Sajewicz, J.V García Mateo, J. Martínez Calatayud, Selective flow-injection biamperometric determination of sulfur-containing amino acids and structurally related compounds, Anal. Chim. Acta 438 (2001) 281–289.
- [8] X. Yang, H. Yuan, C. Wang, X. Su, L. Hu, D. Xiao, Determination of penicillamine in pharmaceuticals and human plasma by capillary electrophoresis with in-column fiber optics light-emitting diode induced fluorescence detection, J. Pharm. Biomed. Anal. 45 (2007) 362–366.
- [9] A.A.J. Torriero, H.D. Piola, N.A. Martinez, N.V. Panini, J. Raba, J.J. Silber, Enzymatic oxidation of tert-butylcatechol in the presence of sulfhydryl compounds: Application to the amperometric detection of penicillamine, Talanta 71 (2007) 1198–1204.
- [10] F.E.O. Suliman, H.A.J. Al-Lawati, S.M.Z. Al-Kindy, I.E.M. Nour, S.B. Salama, A sequential injection spectrophotometric method for the determination of penicillamine in pharmaceutical products by complexation with iron(III) in acidic media, Talanta 61 (2003) 221–231.
- [11] V. Cavrini, R. Gatti, P. Roveri, M.R. Cesaroni, Use of 4-(6-methylnaphthalen-2-yl)-4-

- oxobut-2-enoic acid as a reagent for the spectrophotometric and fluorimetric determination of aliphatic thiol drugs, Analyst 113 (1988) 1447–1452.
- [12] L.Z. Hu, S. Han, S. Parveen, Y.L. Yuan, L. Zhang, G.B. Xu, Highly sensitive fluorescent detection of trypsin based on BSA-stabilized gold nanoclusters, Biosens. Bioelectron. 32 (2012) 297–299
- [13] D.H. Tian, Z.S. Qian, Y.S. Xia, C.Q. Zhu, Gold nanocluster-based fluorescent probes for near-infrared and turn-on sensing of glutathione in living cells, Langmuir 28 (2012) 3945–3951.
- [14] J. Ai, W.W. Guo, B.L. Li, T. Li, D. Li, E.K. Wang, DNA G-quadruplex-templated formation of the fluorescent silver nanocluster and its application to bioimaging, Talanta 88 (2012) 450–455.
- [15] X.X. Wang, P. Wu, Y. Lv, X.D. Hou, Ultrasensitive fluorescence detection of glutaraldehyde in water samples with bovine serum albumin-Au nanoclusters, Microchem. J. 99 (2011) 327–331.
- [16] L. Shang, G.U. Nienhaus, Gold nanoclusters as novel optical probes for in vitro and in vivo fluorescence imaging, Biophys. Rev. 4 (2012) 313–322.
- [17] W. Bian, J. Ma, W. Guo, D. Lu, M. Fan, Y. Wei, Y. Li, S. Shuang, M.M.F. Choi, Phosphorescence detection of L-ascorbic acid with surface-attached *N*-acetyl-L-cysteine and L-cysteine Mn doped ZnS quantum dots, Talanta 116 (2013) 794–800.
- [18] T. Noipa, K. Ngamdee, T. Tuntulani, W. Ngeontae, Cysteamine CdS quantum dots decorated with Fe<sup>3+</sup> as a fluorescence sensor for the detection of PPi, Spectrochim. Acta A 118 (2014) 17–23.
- [19] W. Tedsana, T. Tuntulani, W. Ngeontae, A highly selective turn-on ATP fluorescence sensor based on unmodified cysteamine capped CdS quantum dots, Anal. Chim. Acta 783 (2013) 65–73.
- [20] T. Khantaw, C. Boonmee, T. Tuntulani, W. Ngeontae, Selective turn-on fluorescence sensors for Ag<sup>+</sup> using cysteamine-capped CdS quantum dots: Determination of free Ag<sup>+</sup> in silver nanoparticles solution, Talanta 115 (2013) 849–856.
- [21] T. Noipa, T. Tuntulani, W. Ngeontae, Cu<sup>2+</sup>-modulated cysteamine-capped CdS quantum dots as a turn-on fluorescence sensor for cyanide recognition, Talanta 105 (2013) 320–326.
- [22] N. Butwong, T. Noipa, R. Burakham, S. Srijaranai, W. Ngeontae, Determination of arsenic based on quencing of CdS quantum dots fluorescence using the gas-diffusion flow injection method, Talanta 85 (2011) 1063–1069.
- [23] T. Noipa, S. Martwiset, N. Butwong, T. Tuntulani, W. Ngeontae, Enhancement of the fluorescence quenching efficiency of DPPH• on nanocrystalline quantum dots in aqueous micelles, J. Fluoresc. 21 (2011) 1941–1949.
- [24] S. Boonchiangma, S. Srijaranai, T. Tuntulani, W. Ngeontae, A highly selective electrochemical sensor for 1-tryptophan based on a screen-printed carbon electrode modified with poly-*p*-phenylenediamine and CdS quantum dots, J. Appl. Polym. Sci. 131 (2014) 40356–40363.

- [25] A.O. Govorov, Y.K. Gun'ko, J.M. Slocik, V.A. Gérard, Z. Fan, R.R. Naik, Chiral nanoparticle assemblies: circular dichroism, plasmonic interactions, and exciton effects, J. Mater. Chem. 21 (2011) 16806–16818.
- [26] U. Tohgha, K.K. Deol, A.G. Porter, S.G. Bartko, J.K. Choi, B.M. Leonard, K. Varga, J. Kubelka, G. Muller, M. Balaz, Ligand induced circular dichroism and circularly polarized luminescence in Cdse quantum dots, ACS Nano 7 (2013) 11094–11102.
- [27] M.P. Moloney, Y.K. Gun'ko, J.M. Kelly, Chiral highly luminescent CdS quantum dots, Chem. Commun. 38 (2007) 3900–3902.
- [28] J.E. Govan, E. Jan, A. Querejeta, N.A. Kotov, Y.K. Gun'ko, Chiral luminescent CdS nano-tetrapods, Chem. Commun. 46 (2010) 6072–6074.
- [29] S.A. Gallagher, M.P. Moloney, M. Wojdyla, S.J. Quinn, J.M. Kelly, Y.K. Gun'ko, Synthesis and spectroscopic studies of chiral CdSe quantum dots, J. Mater. Chem. 20 (2010) 8350–8355.
- [30] T. Nakashima, Y. Kobayashi, T. Kawai, Optical activity and chiral memory of thiol-capped CdTe nanocrystals, J. Am. Chem. Soc. 131 (2009) 10342–10343.
- [31] C. Han, H. Li, Chiral recognition of amino acids based on cydodextrin capped quantum dots, Small 4 (2008) 1344–1350.
- [32] C. Carrillo-Carrión, S. Cárdenas, B.M. Simonet, M. Valcárcel, Selective quantification of carnitine enantiomers using chiral cysteine-capped CdSe(ZnS) quantum dots, Anal. Chem. 81 (2009) 4730–4733.
- [33] T. Delgado-Pérez, L.M. Bouchet, M. de la Guardia, R.E. Galian, J. Pérez-Prieto, Sensing chiral drugs by using CdSe/ZnS nanoparticles capped with *N*-Acetyl-L-cysteine methyl ester, Chem. Eur. J. 19 (2013) 11068–11076.
- [34] T. Li, H.G. Park, H.-S. Lee, S.-H. Choi, Circular dichroism study of chiral biomolecules conjugated with silver nanoparticles, Nanotechnology 15 (2004) S660–S663.
- [35] H. Sun, B. Yang, E. Cui, R. Liu, Spectroscopic investigations on the effect of *N*-Acetyl-L-cysteine-capped CdTe quantum dots on catalase, Spectrochim. Acta A 132 (2014) 692–699.
- [36] P. Liu, Y. Liu, Q. Wang, Studies on the interaction of CdTe QDs with bovine serum albumin, J Chem. Technol. Biotechnol. 87 (2012)1670–1675.
- [37] Q. Wang, X. Zhang, X. Zhou, T. Fang, P. Liu, P. Liu, X. Min, X. Li, Interaction of different thiol-capped CdTe quantum dots with bovine serum albumin, J. Lumin. 132 (2012) 1695–1700.
- [38] W. Tedsana, T. Tuntulani, W. Ngeontae, A circular dichroism sensor for Ni<sup>2+</sup> and Co<sup>2+</sup> based on L-Cysteine capped cadmium sulfide quantum dots, Anal. Chim. Acta 31 (2015) 1-8.
- [39] W. Li, Z. Nie, X. Xu, Q. Shen, C. Deng, J. Chen, S. Yao, A sensitive, label free electrochemical aptasensor for ATP detection, Talanta 78 (2009) 954–958.

- [40] S.K. Haram, B.M. Quinn, A.J. Bard, Electrochemistry of CdS nanoparticles: A correlation between optical and electrochemical band gaps, J. Am. Chem. Soc. 123 (2001) 8860–8861.
- [41] T.G. Schaaff, R.L. Whetten, Giant gold–glutathione cluster compounds: Intense optical activity in metal-based transitions, J. Phys. Chem. B 104 (2000) 2630–2641.
- [42] S.D. Elliott, M.P. Moloney, Y.K. Gun'ko, Chiral shells and achiral cores in CdS quantum dots. Nano Lett. 8 (2008) 2452–2457.
- [43] S.P. Pawar, A.H. Gore, L.S. Walekar, P.V. Anbhule, S.R. Patil, G.B. Kolekar, Turn-on fluorescence probe for selective and sensitive detection of D-penicillamine by CdS quantum dots in aqueous media: Application to pharmaceutical formulation, Sens. Actuators B 209 (2015) 911–918.
- [44] S. Li, Z. Peng, R.M. Leblanc, Method to determine protein concentration in the protein–nanoparticle conjugates aqueous solution using circular dichroism spectroscopy, Anal. Chem., DOI: 10.1021/acs.analchem.5b01451.

# 5. Cysteamine capped CdS quantum dots as a fluorescence sensor for the determination of copper ion exploiting fluorescence enhancement and long-wave spectral shifts

#### 1. Introduction

It is well known that copper is one of the heavy metals and essential elements for many living organisms [1-2]. However, it also becomes toxic at high levels. It causes liver damage in infants [3]. Recently, it has been suggested that copper deficiency can increase the risk of developing coronary heart disease [4]. Thus, the determination of copper in the environment and biological samples is of tremendous interest and importance for analytical chemists.

Basically, a large number of traditional methods including atomic absorption spectroscopy (AAS) [5-6], inductively coupled plasma emission mass spectroscopy (ICP-MS) [7], electrochemical methods [8-9], and ion chromatography [10] have been reported and used successfully for the determination of Cu<sup>2+</sup> in environmental samples. However, these methods need sophisticated and high operation cost, and the procedures used in these methods are requiring long operating times. Furthermore, they can not be used for on-site measurements. Therefore, the development of new methods for determination of Cu<sup>2+</sup> is still one of the most important goals.

Chemical sensors are currently attractive to chemists due to their high sensitivity, selectivity, and simplicity. A variety of organic fluorophore-based sensors have been proposed for the detection of Cu<sup>2+</sup> due to their relatively high sensitivity [11-14]. However, organic fluorophore often suffer from the nature of organic molecules such as non-resistance to photobleaching, giving narrow excitation bands, and emitting broad spectra. In order to overcome the drawbacks of organic fluorophore-based sensors, nanocrystalline quatum dots (QDs) have attracted widespread attention in diverse research fields [15-19] due to many excellent optical properties, such as high quantum yield, tunable size-dependent emission, narrow emission peaks, and resistance to photobleaching. These properties provide important advantages over organic dyes in fluorescent applications, resulting in the increasing use of QDs as the fluorescent probe in analytical chemistry [20].

Recently, various reports have been published on the using of QDs for determination of Cu<sup>2+</sup> via analyte-induced changes in fluorescence intensity. The concentration of Cu<sup>2+</sup> can be measured based on the change of fluorescence intensity of QDs caused by the interactions between QDs surface and Cu<sup>2+</sup>. Chen and Rosenzweig [21] reported for the first time that Zn<sup>2+</sup> and Cu<sup>2+</sup> can be determined by utilizing fluorescence CdS QDs capped by different ligands such as polyphosphate, L-cysteine and thioglycerol. Similarly, Asfura et al. [22] utilized peptide-coated CdS QDs as a fluorescence probe for Cu<sup>2+</sup> and Ag<sup>+</sup> ions. Later, CdSe-ZnS QDs modified with bovine serum albumin were also investigated for the determination of copper [23]. The water-soluble CdSe QDs surface modified either with 2-mercaptoethane sulphonic acid or with 2-mercaptoacetic acid were prepared and used for determination of Cu<sup>2+</sup> in aqueous solutions. Koneswaran and Narayanaswamy [24] developed L-cysteinecapped ZnS QDs as a novel fluorescence nanosensor for Cu<sup>2+</sup> ion in aqueous medium. The fluorescence sensor was based on the fluorescence quenching of L-cysteine-capped ZnS QDs. Moreover, mercaptosuccinic acid (MSA)-capped CdSe ODs were successfully synthesized in aqueous medium and directly applied to sensitive and selective detection of Cu<sup>2+</sup> in the presence of other physiologically relevant cations [25]. According to these reviews, it can be seen that most of the QDs sensors for the detection of Cu<sup>2+</sup> were based on the fluorescence quenching.

Basically, sensing mechanisms of fluorescence sensors using QDs as probe are based on turn-on or turn-off strategies with or without the spectrum shift. If interactions between QDs and a target analyte induce changing of the particle size, the shift of the fluorescence spectrum would be observed. For analysis purpose, the large Stokes shift to the longer

wavelength can provide better analytical merits such as sensitivity and selectivity. However, the fluorescence sensors based on the changing of the size of quantum dots have not frequently reported. Akshya et al. reported that the CdS ODs functionalized with N-(2hydroxybenzyl)-cysteine, showing a fluorescence emission at 542 nm. In the presence of Cu<sup>2+</sup> the fluorescence spectra was quenched and shifted to 600 nm. In addition, this sensor also responded to Hg<sup>2+</sup> by the fluorescence quenching mechanism [26]. Liu et al. used aptamer-programmed self assembly of ODs for sensitive fluorescent sensing of adenosine and thrombin. The aptamer was split into two flexible single strand deoxyribonucleic acid (ssDNA) fragments and modified on the QDs surface. In the presence of a target analyte, the QDs probe were assembled together, lead to fluorescence quenching and red shift of the emission peak [27]. Furthermore, Yuan fabricated fluorescence Hg<sup>2+</sup> sensor using CdSe-ZnS quantum dots functionalized with 2-hydroxyethyldithiocarbamate (HDTC). The fluorescence intensity of the sensor can be selectively and efficiently quenched by  $\mathrm{Hg}^{2+}$  through a surface chelating reaction between HDTC and Hg<sup>2+</sup>. They reported that the fluorescence maxima wavelength shifted from 596 to 603 nm due to the formation of a thin shell of a mercurycontaining compound on the CdSe cores upon the increasing concentration of Hg<sup>2+</sup> [28]. In addition, Wang et al. reported that the red-shift of the emission band of thioglycolic acidcapped CdTe ODs was used as a sensing mechanism for the detection of Ag<sup>+</sup>. However, the shift of the fluorescence spectrum was due to the stabilization of a charge-transfer state, but not due to the aggregation induced by Ag<sup>+</sup> ion [29].

Herein, we reported a new fluorescence turn-on sensor for selective detection of copper ions (Cu<sup>2+</sup>) based on the unmodified cysteamine capped CdS quantum dots (Cys-CdS QDs). Fluorescence intensity was enhanced and a red-shift in emission was observed in the presence of Cu<sup>2+</sup>. Parameters affecting the increasing ability of Cu<sup>2+</sup> were studied and optimized. Moreover, the selectivity of the sensor towards other metal ions was also investigated. In addition, the proposed sensor was used to determine Cu<sup>2+</sup> in real water samples.

## 2. Experimental

## 2.1 Chemicals

All reagents used were of analytical grade and used without further purification. Cadmium chloride (CdCl<sub>2</sub>·H<sub>2</sub>O) was obtained from Riedel-deHaen. Cysteamine hydrochloride was purchased from Sigma. Sodium sulfide (Na<sub>2</sub>S·xH<sub>2</sub>O) was recieved from BDH. Mercuric chloride was obtained from Merck. Potassium nitrate, barium nitrate, magnesium nitrate and calcium nitrate were received from Univar. Ferric nitrate nonahydrate, lead (II) nitrate, nickel nitrate hexahydrate and zinc nitrate hexahydrate were purchased from Fluka. Copper (II) nitrate hexahydrate, silver nitrate, sodium hydroxide, cobalt nitrate, chromium chloride, manganese nitrate and sodium nitrate were obtained from Carlo Erba. Tris-hydroxymethyl-methylamine was recieved from Ajax. Ultra pure water (18.2 M $\Omega$  cm) was obtained from a Millipore water purification system. Cys-CdS QDs used in this work were prepared and characterized as previously described in our recent report [30]. The concentration of the QDs was calculated based on the original cadmium source and found to be 0.076 M.

#### 2.2 Instrumentations

Fluorescence spectra were recorded using a RF-5301PC spectrofluorometer (Shimadzu). The slit width used for both excitation and emission were 5 nm. Absorption spectra of the quantum dots solution was measured on an Agilent HP 8453 UV-Vis spectrophotometer. The transmission electron microscopy (TEM) images of the Cys-CdS QDs were carried out on Tecnai G<sup>2</sup>-20 (FEI, Netherlands) under the accelerating voltage of 200 kV. Cyclic voltammetry was carried out by using an Autolab PGSTAT 101

potentionstat-galvanostat with Nova 1.7 software program (Ecochemie, The Netherlands) equipped with three electrodes: a bare glassy carbon electrode (GCE; diameter 3 mm) as the working electrode, a Ag/AgCl electrode as the reference electrode, and a platinum sheet as the counter electrode. Inductively coupled plasma optical emission spectrometer (ICP-OES, Optima 2100 DV, USA) was used for the determination of Cu<sup>2+</sup> on the Cys-CdS QDs and in real water samples. pH measurements were carried out using a UB-10 UltraBasic pH meter (Denver Instrument).

## 2.3 General procedure for Cu<sup>2+</sup> detection

In order to determine Cu<sup>2+</sup> using Cys-CdS QDs, the following general procedures were carried out. A stock solution of 1 mM Cu(NO<sub>3</sub>)<sub>2</sub>·6(H<sub>2</sub>O) was prepared. A 100 μL of Cys-CdS QDs, 8.0 mL of 0.05 M Tris-HCl buffer solution pH 9.0 and a certain amount of Cu<sup>2+</sup> were sequentially added to a 10.00 mL volumetric flask. The mixture was diluted to the final volume of 10.00 mL with 0.05 M Tris-HCl buffer solution pH 9.0 and was then incubated at room temperature for 10 min. The fluorescence intensity of the solution was measured at an excitation wavelength of 360 nm.

## 2.4 Interference studies

To investigate the selectivity of Cys-CdS QDs to  $Cu^{2+}$ , the following procedure was performed. An individual stock solution of various metal ions (1.0 mM) was prepared by dissolution of a metal ion salt in ultra pure water. A 100  $\mu$ L of Cys-CdS QDs, 500  $\mu$ L of 1.0 M Tris-HCl buffer pH 9.0 and stock of various metal ions solution with an appropriate volume were sequentially added to a 10-mL volumetric flask. The final concentration of interference metal ion was 10  $\mu$ M for Li<sup>+</sup>, Na<sup>+</sup>, K<sup>+</sup>, Ba<sup>2+</sup>, Mg<sup>2+</sup>, Ca<sup>2+</sup> and 5  $\mu$ M for Co<sup>2+</sup>, Cr<sup>3+</sup>, Cd<sup>2+</sup>, Mn<sup>2+</sup>, Ni<sup>2+</sup>, Pb<sup>2+</sup>, Zn<sup>2+</sup>, Hg<sup>2+</sup>, Ag<sup>+</sup>, Fe<sup>3+</sup>, respectively. Then the mixture was diluted to the mark with ultrapure water. The fluorescence intensity was recorded after equilibrating for 10 min.

## 2.5 Application to real water samples

Natural pond water sample from Khon Kaen Province was collected and filtered through filter paper. Then, the filtered water sample was mixed with Tris-HCl buffer and spiked with Cu<sup>2+</sup> at two different concentration levels. The sensor probe was added to the water sample and incubated prior to the fluorescence measurement. The concentrations of Cu<sup>2+</sup> in the water sample were calculated according to the calibration curve. The results from the proposed sensor was compared to those obtained from the ICP-OES technique.

## 3. Results and Discussion

According to our previous reports [30], fluorescence intensity of Cys-CdS QDs can be enhanced in the presence of  $Ag^+$  without the spectrum shift. Moreover, the fluorescence intensity of Cys-CdS QDs can be modulated by  $Cu^{2+}$  and used to fabricate a selective cyanide sensor based on the formation of  $Cu^{2+}$ -cyanide complex [31]. In the later report, when studying of the effect of  $Cu^{2+}$  on the fluorescence intensity of Cys-CdS QDs, the unexpected result showed that the fluorescence intensity of Cys-CdS QDs was enhanced at low  $Cu^{2+}$  concentration ( $Cu^{2+} < 10 \,\mu\text{M}$ ) with a large red shift. However, the fluorescence intensity was inversely quenched at high  $Cu^{2+}$  concentration ( $Cu^{2+} > 20 \,\mu\text{M}$ ). However, this behavior was not found in the case of other cations. In the presence of  $CN^-$ , the fluorescence intensity can be recovered again, however it can not restore to the original spectrum (before adding  $Cu^{2+}$ ). From this observation, we hypothesized that there are two different kinds of  $Cu^{2+}$  on the Cys-CdS QDs surface. At higher concentration of  $Cu^{2+}$ ,  $Cu^{2+}$  may form a reversible complex on the capping ligand which can quench the fluorescence intensity of the Cys-CdS QDs. On the

other hand, at lower concentration of Cu<sup>2+</sup>, Cu<sup>2+</sup> may deposit on the CdS crystal. Therefore, it can be used this phenomenon to fabricate a highly selective Cu<sup>2+</sup> sensor. The selectivity and sensitivity of the sensor fabricated from this strategy can be better than other QDs-based fluorescence sensors.

## 3.1 Fluorescence enhancement of Cys-CdS QDs by Cu<sup>2+</sup>

Recently, there are various publications reported the use of quantum dots having different capping molecules as selective Cu<sup>2+</sup> sensors. However, most of the reports were based on the fluorescence quenching mechanism. Generally, the interaction between the cation and quantum dots surface may influence the efficiency of the electron-hole recombination process. This phenomenon may reduce the probability of the electron-hole recombination and cause the fluorescence quenching. Therefore, in this work, the detection of Cu<sup>2+</sup> ions based turn-on fluorescence intensity of Cys-CdS QDs was proposed.

When adding Cu<sup>2+</sup> into the Cys-CdS QDs solution, the unexpected results showed that the fluorescence intensity of Cys-CdS QDs was enhanced with spectrum shift to the longer wavelength at low concentration of Cu<sup>2+</sup> as shown in Fig. 1(a). Moreover, the fluorescence intensity increased with increasing the concentration of Cu<sup>2+</sup>. The fluorescence enhancement after adding small amount of Cu<sup>2+</sup> may stem from the decreasing of small crystal defect on the surface of quantum dots by Cu<sup>2+</sup> ions. Therefore, the electron-hole recombination efficiency was enhanced, and consequently the fluorescence intensity increased. Meanwhile, a large red shift of fluorescence spectra was observed after adding Cu<sup>2+</sup>. This result implied, according to the quantum confinement effect, the increasing the particle size of the Cys-CdS ODs possibly due to the formation of CuS on the defect crystal of Cys-CdS ODs.

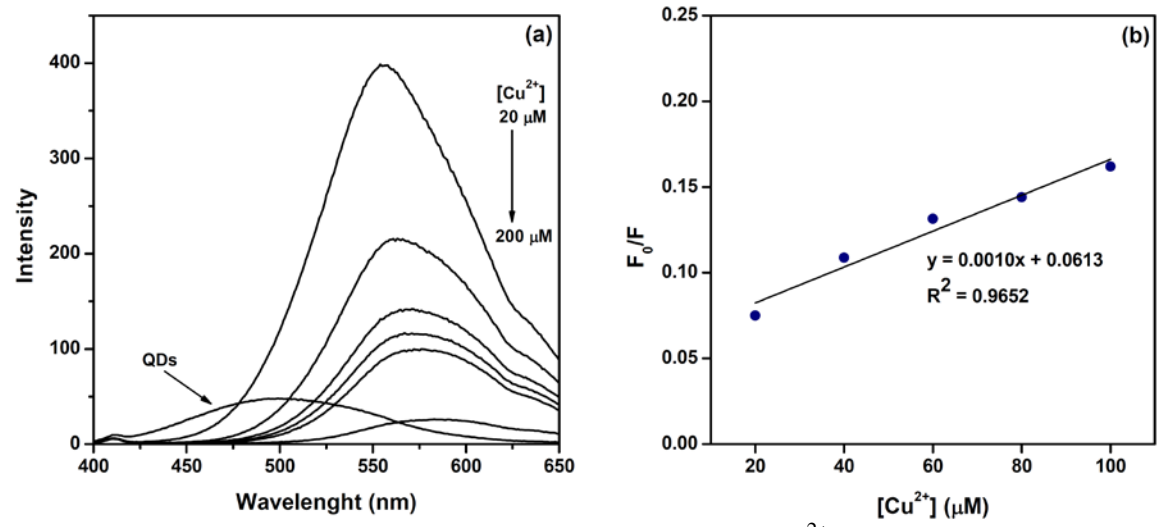


**Fig. 1** Fluorometric titration of Cys-CdS QDs at the higher  $Cu^{2+}$  concentration (20-200  $\mu$ M) (a). The corresponding linear plot by Stern-Volmer analysis (b). (Medium: [Cys-CdS QDs] = 0.76 mM, 0.05 M Tris-HCl buffer pH 9.0).

The increasing of the particle size can be confirmed by TEM images. The TEM image of the Cys-CDS QDs before and after adding 10  $\mu$ M of Cu<sup>2+</sup> was shown in Fig. 2(a) and Fig. 2(b), respectively. The average size of the particles significantly increased from 2.6±0.9 nm to 4.2±0.5 nm. The observed red shift of the fluorescence spectrum agreed well with the results obtained from the TEM images. In order to confirm the presence of Cu on the Cys-CdS QDs, the EDX spectrum of the precipitated Cys-CdS QDs after adding Cu<sup>2+</sup> was recorded. The result was shown in the Fig. S4 of the ESI. The EDX spectrum clearly exhibited the Cu signal on the Cys-CdS QDs, supporting the presence of Cu on the surface of Cys-CdS QDs.

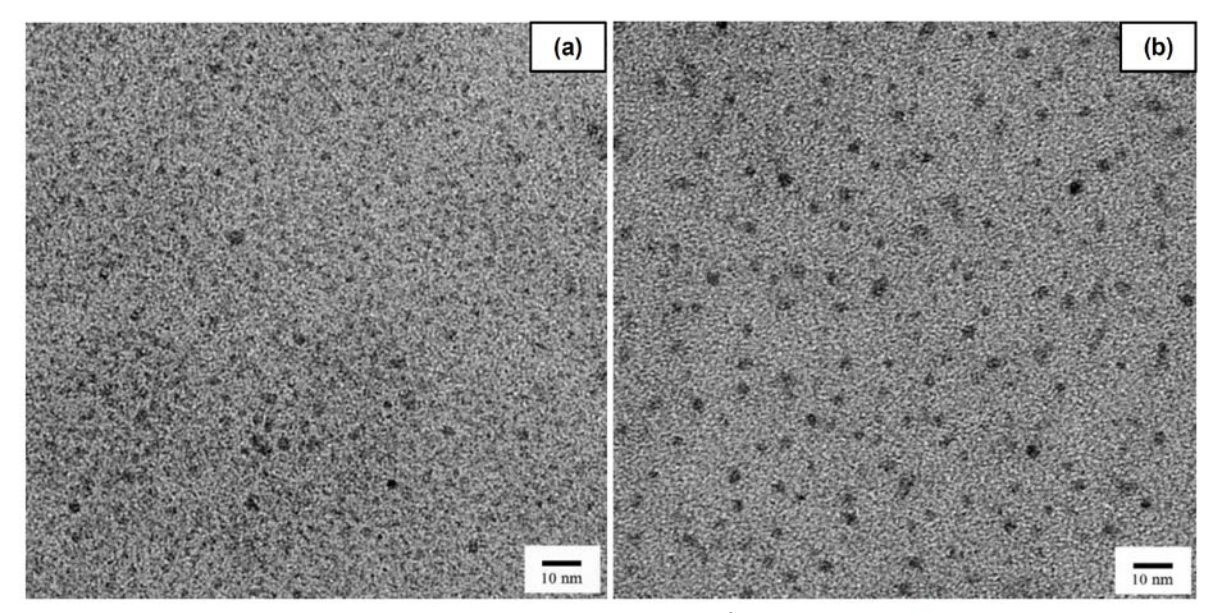


**Fig. 2** TEM images of Cys-CdS QDs before adding  $Cu^{2+}$  (a), the average particle size was  $2.6\pm0.9$  nm (N = 95) and after adding  $Cu^{2+}$  (b), the average particle size was  $4.2\pm0.5$  nm (N = 66).

On the other hand, the fluorescence intensity of Cys-CdS QDs was further quenched upon increasing the concentration of  $Cu^{2+}$  (20-200  $\mu M$ ) in conjunction with a large red shift of emission spectra (up to 70 nm) as shown in Fig. 1(a). However, the quenching efficiency of  $Cu^{2+}$  on Cys-CdS QDs did not relate to the concentration of  $Cu^{2+}$ . The fluorescence quenching data were analyzed by Stern–Volmer equation as following equation.

$$\frac{F_0}{F} = 1 + K_{SV}[Q] \tag{1}$$

where  $F_0$  and F are the fluorescence intensities of Cys-CdS QDs in the absence and in the presence of  $Cu^{2+}$ , respectively.  $K_{SV}$  is the Stern-Volmer quenching constant which is related to the quenching efficiency and [Q] is the concentration of  $Cu^{2+}$ . As shown in Fig. 1(b), a linear relationship between the ratio of  $F_0$  to F and  $Cu^{2+}$  concentration was observed in the range of 20-100  $\mu$ M with a  $K_{SV}$  of  $1.0\times10^{-3}$  M<sup>-1</sup>. The remarkably low  $K_{SV}$  value suggested a poor quenching efficiency of  $Cu^{2+}$ . The fluorescence quenching observed at high concentration of  $Cu^{2+}$  may be due to the complexation between  $Cu^{2+}$  and amine group on the surface of quantum dots [32]. The presence of  $Cu^{2+}$  complex linked to the QDs surface can cause the quenching of fluorescence intensity of Cys-CdS QDs due to the electron transfer mechanism.

From our previous report, the  $Cu^{2+}$  at higher concentration (more than 10  $\mu$ M) can be removed by the formation of the cyanide complex. However, the fluorescence spectrum did not restore to the original spectrum (before adding  $Cu^{2+}$ ) [31]. This phenomenon implied that  $Cu^{2+}$  at low concentration may form an irreversible compound (cause the particle size increased) on the QDs which cannot be removed by cyanide ions. From these observations support that there are two types of the  $Cu^{2+}$  on the Cys-CdS QDs. However, in order to develop fluorescence turn-on  $Cu^{2+}$  sensor, we are interested in the phenomenon at low concentration level of  $Cu^{2+}$  (less than 10  $\mu$ M).

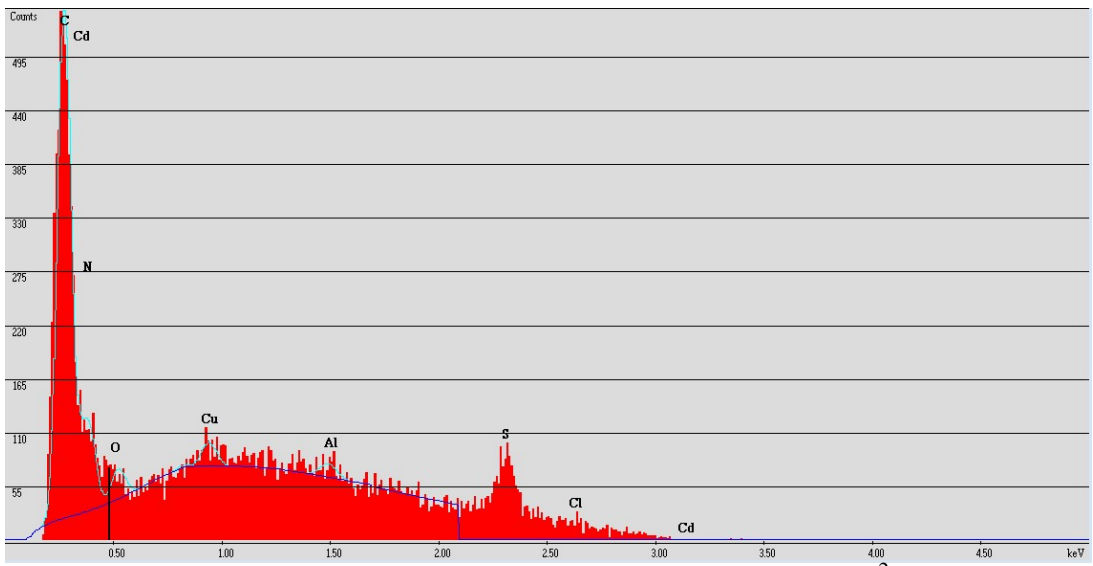


Fig. S4 EDX spectrum of the precipitated Cys-CdS QDs after adding Cu<sup>2+</sup>.

## 3.2 Cyclic voltammetry studies

In order to study the interaction between Cys-CdS QDs with Cu<sup>2+</sup>, cyclic voltammetry technique was examined. The cyclic votammogram of individual compound including Cu<sup>24</sup> solution at 10 µM (represent of Cu<sup>2+</sup> at low concentration) and 100 µM (represent of Cu<sup>2+</sup> at high concentration), Cys-CdS QDs were firstly recorded to investigate the electrochemical behavior of each compound. Then the cyclic voltammogram of the mixture solution of Cys-CdS QDs and 10  $\mu$ M or 100  $\mu$ M Cu<sup>2+</sup> were recorded and the results showed in the Fig. 3. It can be seen that the anodic peaks of Cys-CdS ODs at -0.82 and -0.63 V (vs Ag/AgCl) decreased with the same pattern after adding 10 µM of Cu<sup>2+</sup> as shown in Fig. 3(a). This result signified that the surface of the Cys-CdS QDs was changed after adding Cu<sup>2+</sup>. In addition, the cyclic voltamogram of the Cys-CdS ODs in the presence of 100 uM was recorded and the results showed in the Fig 3(b). The resulting voltammogram showed a significant difference from the former case. The anodic peak of the Cys-CdS QDs was shifted from -0.63 V to -0.58 V (vs Ag/AgCl). Furthermore, the new oxidation peaks at -0.35 V and 0.19 V (vs Ag/AgCl) can be observed which may be due to the formation of copper complex on the capping cysteamine. From the cyclic voltammetry studies, it can be concluded that there are two types of Cu<sup>2+</sup> exist on the Cys-CdS QDs, which supported the fluorescence results mentioned previously.

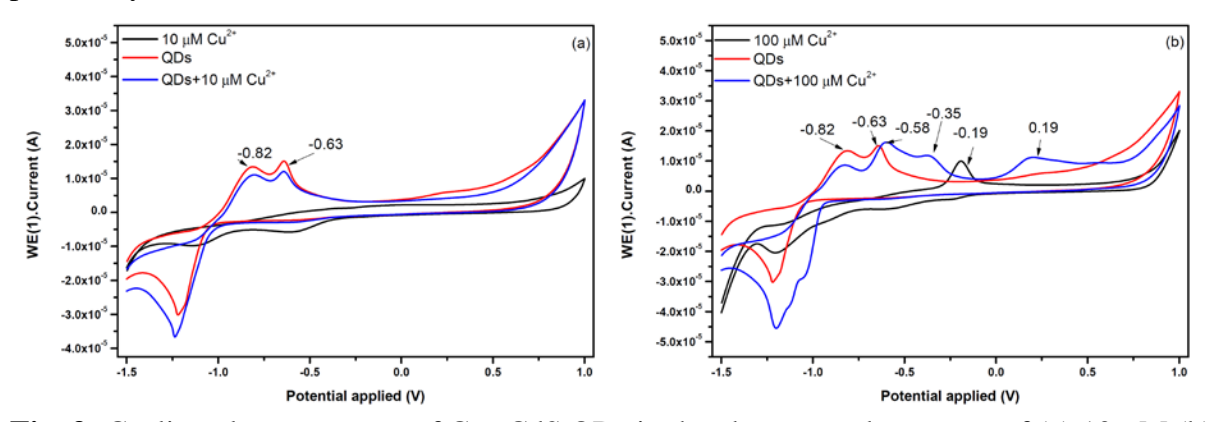
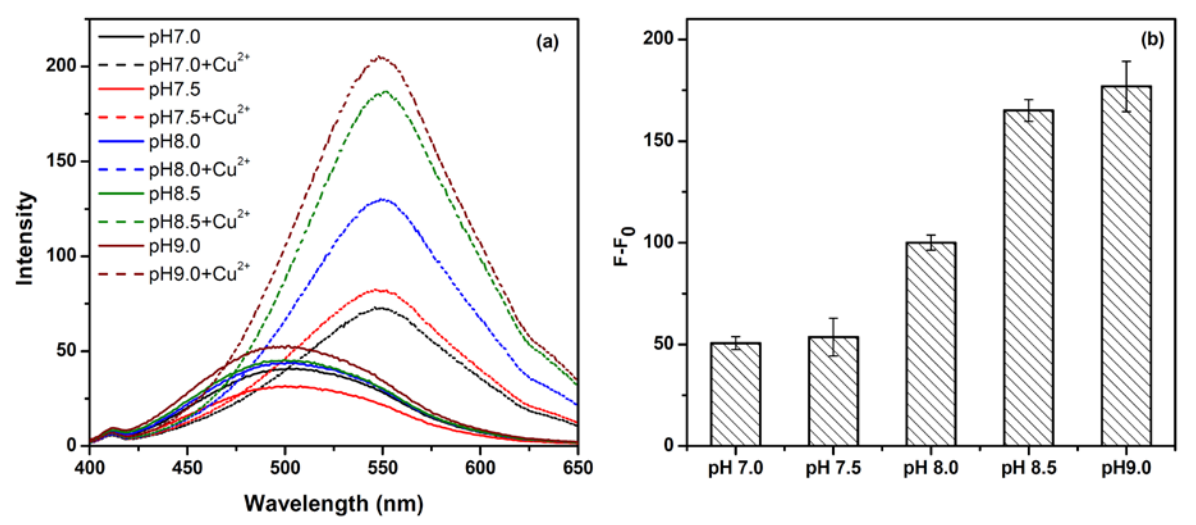


Fig. 3 Cyclic voltammograms of Cys-CdS QDs in the absence and presence of (a) 10  $\mu$ M (b) 100  $\mu$ M of Cu<sup>2+</sup> in 0.05 M Tris-HCl buffer pH 9.0.

## 3.3 Effect of pH on the fluorescence enhancement by Cu<sup>2+</sup>

Basically, the pH of the solution plays an important role in the interaction of ODs with other molecules [33]. In this work, the capping molecule is a weak base (primary amine). The charge on the surface of the QDs would depend on the degree of protonation of the amine groups and may affect to the electron-hole recombination process which corresponded to the fluorescence intensity of the QDs. Thus, the effect of the solution pH towards the fluorescence enhancement of Cys-CdS QDs by  $Cu^{2+}$  was studied in the range of 7.0 - 9.0. The pHs of solution were varied by adjusting the pH of 0.05 M Tris-HCl buffer. The fluorescence spectrum of Cys-CdS QDs in the absence and the presence of Cu<sup>2+</sup> at different pH were shown in Fig. 4(a). The fluorescence intensities of Cys-CdS QDs were enhanced in the presence of Cu<sup>2+</sup> at all solution pHs. Meanwhile, the large red shift spectra were observed. The fluorescence intensity of Cys-CdS QDs was enhanced with the increasing of solution pH (as shown in Fig. 4(b)). These results showed that the interaction between Cys-CdS QDs and Cu<sup>2+</sup> was strongly influenced by the pH of the solution. The enhancement of fluorescence intensity when increasing solution pH may be due to the deprotonation of amine group on capping molecule. Therefore, Cu<sup>2+</sup> ions can enter through the Cys-CdS QDs surface and possibly form the CuS complex at the crystal defect. This resulted in the decreasing of crystal defect and reduced trap state. Therefore, the electron-hole recombination process was enhanced and the fluorescence intensity of the Cys-CdS QDs increased with a large red shift. The maximum fluorescence enhancement was observed at pH 9.0. Therefore, 0.05 M Tris-HCl buffer solution of pH 9.0 was selected to obtain the best sensitivity.



**Fig. 4** Effect of pH on the fluorescence intensity of 0.76 mM Cys-CdS QDs in the absence and the presence of 5  $\mu$ M Cu<sup>2+</sup> (a) and the fluorescence intensity enhancement by 5  $\mu$ M Cu<sup>2+</sup> (b). (By adjusting the pH of 0.05 M Tris-HCl buffer).

## 3.4 Effect of concentration of Cys-CdS QDs on the determination of Cu<sup>2+</sup>

Basically, the concentration of quantum dots plays an important role in the detection sensitivity. To obtain the highest sensitivity and the widest linear range of the calibration curve, the effect of the Cys-CdS QDs concentration on the degree of fluorescence enhancement (F-F<sub>0</sub>) was investigated. The concentration of Cys-CdS QDs was varied from 0.38–3.8 mM in 0.05 M Tris–HCl buffer pH 9.0. As shown in Fig. 5(a), the fluorescence intensity of Cys-CdS QDs increased with the increasing of Cys-CdS QDs concentration from 0.38 to 0.76 mM. However, when further increasing the concentration of Cys-CdS QDs, the fluorescence intensities inversely decreased. The decreasing of fluorescence intensity when increasing of the concentration may be due to self absorption phenomenon.

Furthermore, the effect of Cys-CdS QDs concentration on the fluorescence enhancement in the presence of  $Cu^{2+}$  was also studied in the solution of 0.05 M Tris–HCl buffer pH 9.0 to obtain the highest detection sensitivity. The degree of fluorescence enhancement (F-F<sub>0</sub>) at each Cys-CdS QDs concentration ranging from 0.38 to 3.8 mM in the presence of 5  $\mu$ M  $Cu^{2+}$  was measured and the results were shown in Fig. 5(b). The highest fluorescence enhancement was obtained at 0.76 mM concentration of Cys-CdS QDs. Therefore, 0.76 mM was chosen for further experiments.

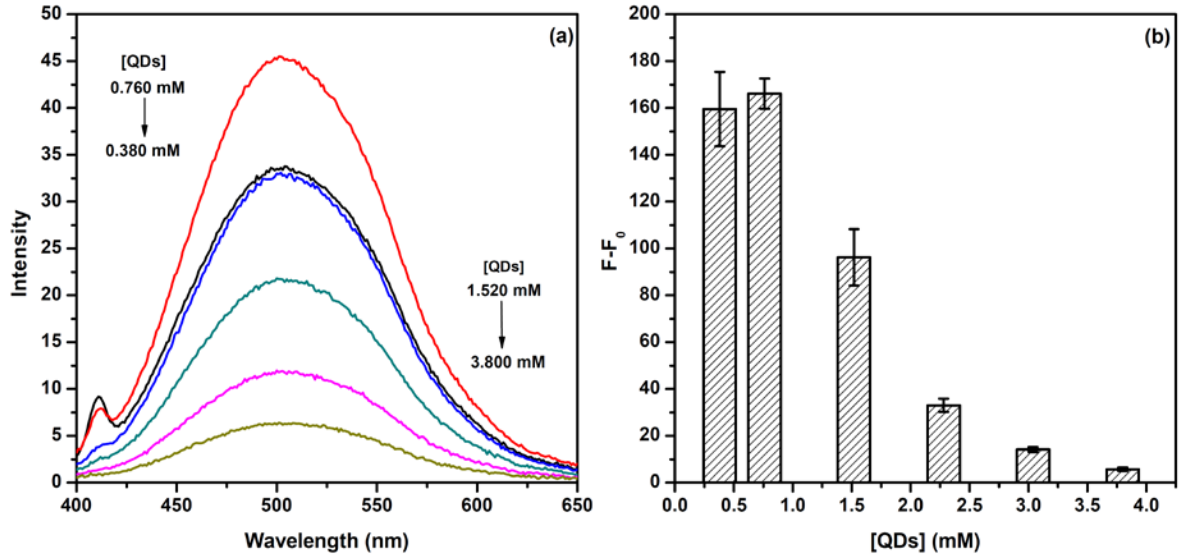


**Fig. 5** (a) Fluorescence spectra of Cys-CdS QDs at difference concentrations in 0.05 M Tris-HCl buffer pH 9.0 (b) Effect of the Cys-CdS QDs concentration on fluorescence enhancement by  $5 \,\mu\text{M} \,\text{Cu}^{2+}$  in 0.05 M Tris-HCl buffer pH 9.0.

## 3.5 Selectivity of the proposed sensor

Generally, selectivity is a key parameter for the fabrication of new chemical sensors. Ideally, the sensor should respond only to the target analyte without interfering from other species. Thus, selectivity of the sensors is still a challenging subject. In this work, the proposed sensor was based on the direct interaction of Cu<sup>2+</sup> on the surface of quantum dots. From this reaction, the crystals defect on the surface was repaired and resulting in the enhancement of fluorescence intensity of Cys-CdS QDs. Therefore, to evaluate the selectivity of Cys-CdS QDs for Cu<sup>2+</sup>, the response from other metal ions including Li<sup>+</sup>, Na<sup>+</sup>, K<sup>+</sup>, Ba<sup>2+</sup>, Mg<sup>2+</sup>, Ca<sup>2+</sup>, Co<sup>2+</sup>, Cr<sup>3+</sup>, Cd<sup>2+</sup>, Mn<sup>2+</sup>, Ni<sup>2+</sup>, Pb<sup>2+</sup>, Zn<sup>2+</sup>, Hg<sup>2+</sup>, Ag<sup>+</sup> and Fe<sup>3+</sup> to the fluorescence spectrum of the Cys-CdS QDs were studied. The fluorescence spectra of Cys-CdS QDs before and after adding cation and the comparison of the fluorescence intensity of Cys-CdS QDs in the absence and the presence of interfering ions were shown in Fig. 6(a) and Fig 6(c), respectively. It was clearly seen that the fluorescence spectra of the Cys-CdS QDs can be enhanced with large red shift spectrum only in the presence of Cu<sup>2+</sup>. On the other hand, the fluorescence spectra did not show any significant change from the original spectrum when adding other cations. As a result, the Cys-CdS QDs can be used as a selective probe for Cu<sup>2+</sup> by the fluorescence turn-on approach.

However, according to our previous reported [30], Cys-CdS QDs can also be used as the sensor for the detection of  $Ag^+$  by fluorescence turn-on approach. As shown in Fig. 6(b), when adding  $Ag^+$  the fluorescence spectrum of Cys-CdS QDs was increased with slightly red shift spectrum. This result signifies that  $Ag^+$  is an important interfering ion in the detection of  $Cu^{2+}$  by this sensor. However, if there is no  $Ag^+$  contaminated in the sample solution, this sensor can provide many interesting advantages due to the red shift spectra. For example, the qualitative analysis of  $Cu^{2+}$  can be easily obtained by observing the large red shift spectrum.

In addition, a high Stokes shift between the excitation and emission wavelengths (around 190 nm,  $\lambda_{ex}$ =360 nm,  $\lambda_{em}$ =550 nm) providing a simplified fluorescence measurement, lower interference species and higher detection sensitivity.

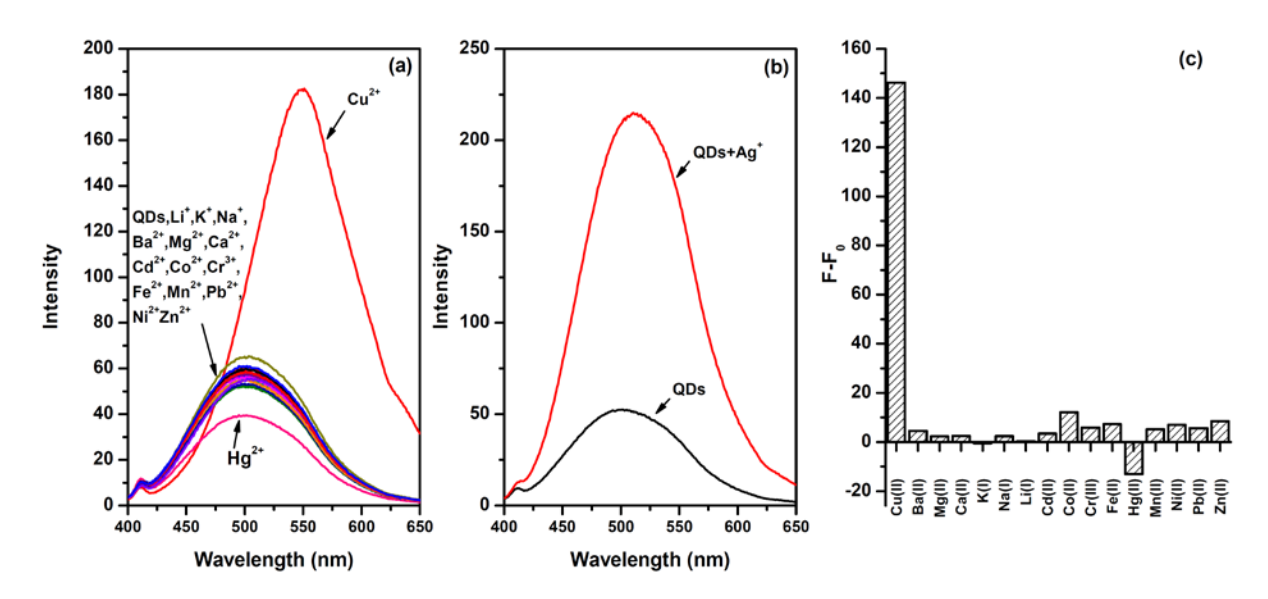


**Fig. 6** Fluorescence spectra of Cys-CdS QDs in the presence of various cations (a) and in the presence of  $Ag^+$  (b). Comparison of the degree of fluorescence enhancement (F-F<sub>0</sub>) in the presence of each cation (c). (Medium: [Cys-CdS QDs] = 0.76 mM, 0.05 M Tris-HCl buffer pH 9.0, [M<sup>n+</sup>] = 10  $\mu$ M (Li<sup>+</sup>, Na<sup>+</sup>, K<sup>+</sup>, Ba<sup>2+</sup>, Mg<sup>2+</sup>, Ca<sup>2+</sup>) and 5  $\mu$ M for the rest).

## 3.6 Analytical performance of the proposed sensor

In order to apply the proposed sensor for the quantitative analysis of  $Cu^{2+}$ , the analytical parameters were then evaluated. The fluorescence spectra of Cys-CdS QDs in the presence of different concentrations of  $Cu^{2+}$  were recorded and the results were shown in Fig. 7. From Fig. 7(a), it can be seen that the fluorescence intensity increased with a large spectrum red shift when increasing the concentration of  $Cu^{2+}$ . A good linear relationship between F-F<sub>0</sub> and the concentration of  $Cu^{2+}$  was obtained as shown in Fig. 7(b). The regression equation was found to be F-F<sub>0</sub> = 34.46[ $Cu^{2+}$  ( $\mu$ M)] – 41.41 ( $r^2$  = 0.9951) with a working concentration range of 2 – 10  $\mu$ M.

The limit of detection (LOD) and limit of quantitation (LOQ) were also determined to demonstrate the limitation of the sensor. The LOD was measured as the concentration of analyte giving the fluorescence intensity equal to  $3\times$ standard deviation of  $F_0$ , while the LOQ was calculated as the concentration of an analyte giving the fluorescence intensity equal to  $10\times$ standard deviation of  $F_0$ . The LOD and LOQ of the proposed sensor were found to be 1.5 and 1.6  $\mu$ M, respectively. These results suggested that this sensor has a potential to detect  $Cu^{2+}$  at very low concentration levels.

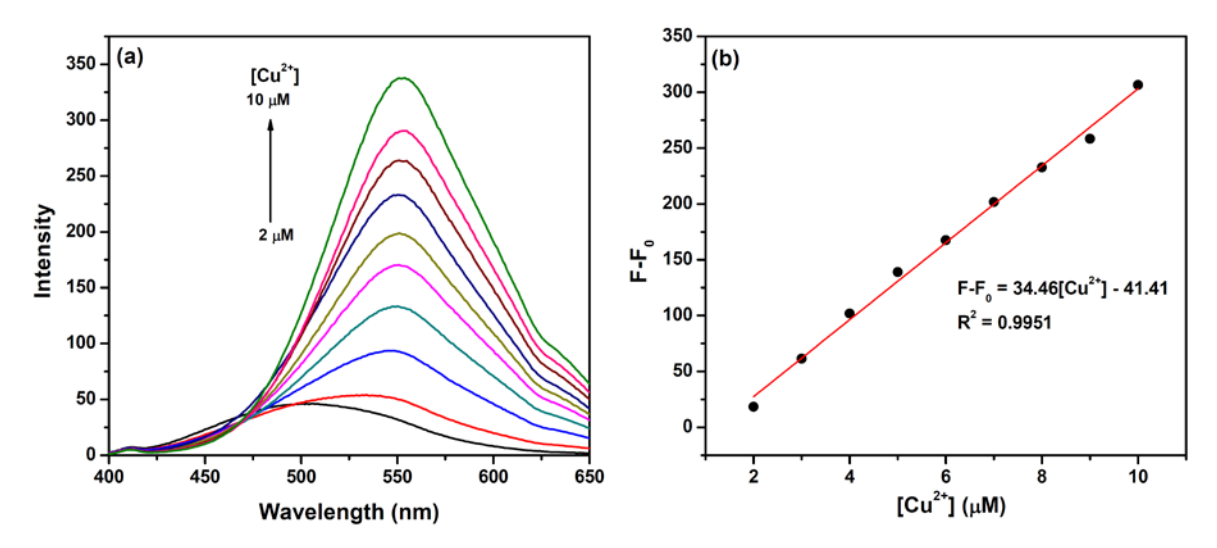


**Fig. 7** (a) Fluorescence emission spectra of Cys-CdS QDs in the presence of different concentrations of  $Cu^{2+}$  (0-10  $\mu$ M). (b) The calibration curve for  $Cu^{2+}$ . (Medium: [Cys-CdS QDs] = 0.76 mM, 0.05 M Tris-HCl buffer pH 9.0).

## 3.7 Application of the proposed sensor for detection of Cu<sup>2+</sup> in real water sample

To demonstrate the feasibility of the proposed sensor in real applications, the natural pond water sample was used as a representative sample and compared with results obtained from ICP-OES technique. The real natural pond water sample from Khon Kaen Province was collected and filtered through a Whatman No. 42 filter. Then, the filtered wastewater sample was mixed with 50 mM Tris-HCl buffer pH 9.0 and spiked with Cu2+ at two different concentration levels (3 and 6 µM). The sensor probe was added to the sample and incubated for 10 minutes prior to the fluorescence measurement. The resulting concentrations were calculated using the calibration curve and the concentration of Cu<sup>2+</sup> obtained from ICP-OES technique are summarized in Table 1. Furthermore, the fluorescence spectra of the Cys-CdS QDs in the presence of real treatment wastewater sample and after spiking with 3 µM or 6 μM Cu<sup>2+</sup> are shown in Fig. 8. It can be seen from Fig. 8 that the fluorescence spectrum of Cys-CdS QDs in the presence of natural pond water sample showed a slightly blue shift from original Cys-CdS QDs, whereas the fluorescence intensity at 550 nm was lower than that of the Cys-CdS QDs. This result suggested that the Cu<sup>2+</sup> concentration in the real sample was lower than the LOD. However, after spiking Cu<sup>2+</sup> at two levels, the % recovery values of 96-103% were obtained. Moreover, the natural pond water sample and its spiked sample were determined using ICP-OES. The results showed that the concentration of Cu<sup>2+</sup> found from the proposed sensor was in close agreement with those obtained by using the ICP-OES method. The recovery results and the results from ICP-OES can be used to confirm the accuracy of this sensor. The precision of the proposed sensor was also evaluated and reported as %R.S.D. values of the three measurements. The obtained %R.S.D. values were lower than 3%. These results confirm that the method is precise and can be applied to the determination of Cu<sup>2+</sup> in real samples.

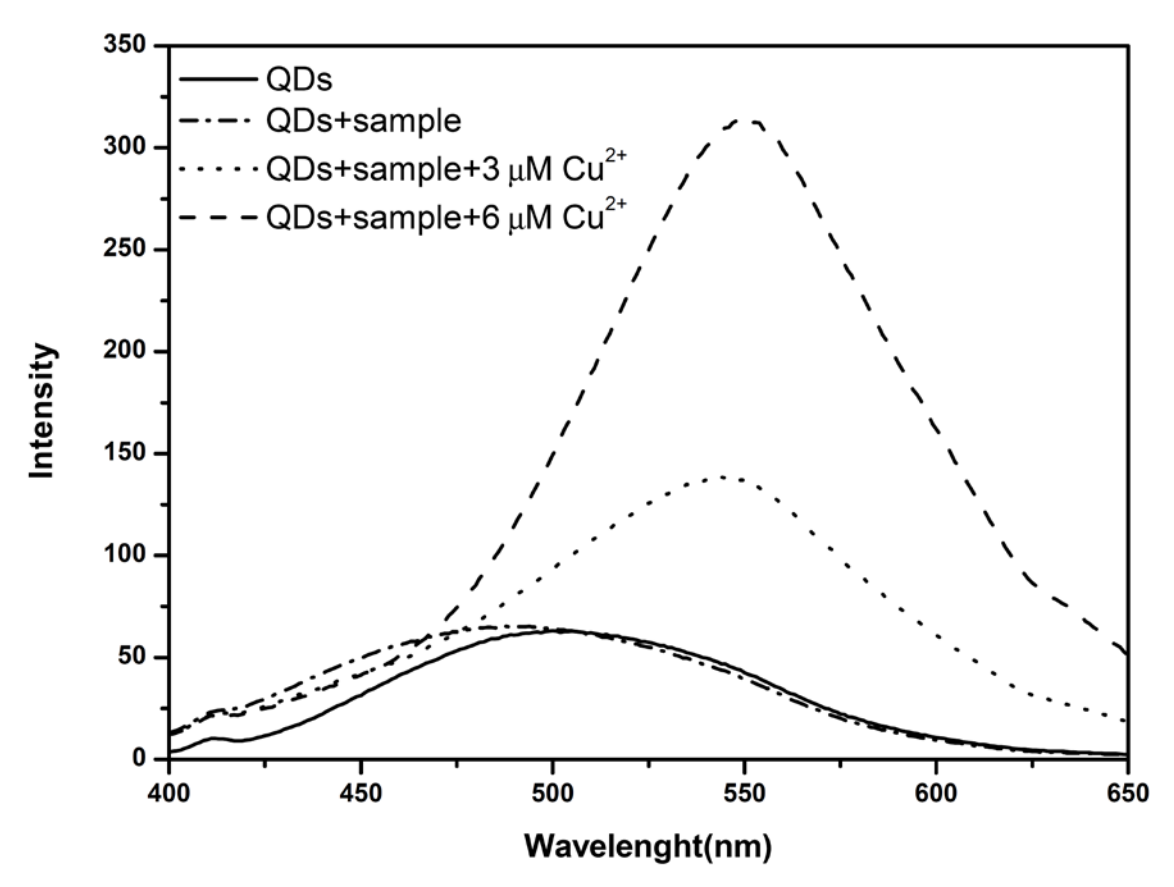


**Fig. 8** Fluorescence spectra of the Cys-CdS QDs in the presence of natural pond water sample and after spiking with 3  $\mu$ M or 6  $\mu$ M Cu<sup>2+</sup>. (Medium: [Cys-CdS QDs] = 0.76 mM, 0.05 M Tris-HCl buffer pH 9.0).

**Table 1.** Measurements of Cu<sup>2+</sup> in natural pond water sample using the proposed sensor and ICP-OES

Added	Proposed sensor			ICP-OES		
$(\mu M)$	Found (µM) <sup>a</sup>	%Recovery	RSD (%)	Found $(\mu M)^a$	%Recovery	RSD (%)
0	n.d.	-	-	n.d.	-	-
3.0	$3.1 \pm 0.1$	$103.2 \pm 1.6$	1.6	$3.2 \pm 0.1$	$108.2 \pm 0.3$	0.3
6.0	$5.8 \pm 0.2$	$96.7 \pm 2.5$	2.6	$6.3 \pm 0.1$	$105.8 \pm 0.8$	0.7

<sup>&</sup>lt;sup>a</sup> Mean  $\pm$  SD (n = 5)

n.d. = not detectable

## 3.8 Comparison the analytical merits to other Cu<sup>2+</sup> sensors based QDs

Fluorescence sensors based quantum dots for selective detection of Cu<sup>2+</sup> is an interesting research topic because they provide ultrahigh sensitive and selective assays. Several types of core quantum dots with different capping molecules were synthesized and used to fabricate the Cu<sup>2+</sup> sensors as summarized in Table 2. Fluorescence quenching was the most frequently reported mode of detection, but this work relied on the fluorescence enhancement mode. Most of the reported Cu<sup>2+</sup> sensors based QDs were potentially interfered from Fe<sup>3+</sup> and Ag<sup>+</sup>. Although the detection sensitivity of the proposed sensor was not better than other related sensors based fluorescence QDs, it can be used to detect Cu<sup>2+</sup> in the same order of magnitude (micromolar range). In addition, selectivity and simplicity of the proposed method are quite remarkable.

**Table 2** Comparison the analytical merits of the Cu<sup>2+</sup> sensors based fluorescence nanomaterials

Type of core QDs	Type of capping molecules	Mode of detection	Possible interference	Linear range (µM)	Detection limit (µM)	Ref.
CdS QDs	Thioglycerol	Fluorescence quenching	Fe <sup>3+</sup>	0.1-1200	0.1	[21]
CdS QDs	Peptide	Fluorescence quenching	Fe <sup>3+</sup>	0.5-2.0	<0.5	[22]
CdSe-ZnS QDs	Bovine Serum Albumin (BSA)	Fluorescence quenching	$Ag^+$	0.01-2.0	0.01	[23]
ZnS QDs	<sub>L</sub> -Cysteine	Fluorescence quenching	Ag <sup>+</sup> , Fe <sup>3+</sup>	0-260	7.1	[24]
CdSe QDs	Mercaptosuccinic acid	Fluorescence quenching	Not reported	0.02-2.0	0.0034	[25]
Cys-CdS QDs	Cysteamine	Fluorescence enhancement	Ag <sup>+</sup>	2.0-10.0	1.5	This work

#### 4. Conclusion

In summary, the fluorescence sensor for detection of  $Cu^{2+}$  using unmodified Cys-CdS QDs was successfully developed. After adding  $Cu^{2+}$  into the solution of Cys-CdS QDs, the change of the fluorescence spectrum can be observed. At low concentration level (less than  $10~\mu\text{M}$ ), the fluorescence intensity of Cys-CdS QDs was enhanced as a linear function of  $Cu^{2+}$  concentration at low micromolar level with a large red shift spectrum. Electrochemical studies and ICP-OES suggested that  $Cu^{2+}$  deposited on the Cys-CdS QDs surface. On the other hand, fluorescence intensity of Cys-CdS QDs was quenched when further increasing the  $Cu^{2+}$  concentration due to the formation of  $Cu^{2+}$  and Cysteamine complex. Thus, the Cys-CdS QDs can be potentially be used as a sensitive sensor for the detection of trace  $Cu^{2+}$  by turn on fluorescence strategy. The calibration plot was linear in the range between 2 and 10  $\mu$ M. The detection limit of this sensor is 1.5  $\mu$ M. Moreover, Cys-CdS QDs were directly applied to sensitive and selective detection of  $Cu^{2+}$  in the presence of other physiologically relevant cations with satisfactory results. The feasibility of the proposed sensor was demonstrated by determining the  $Cu^{2+}$  content in spiked real natural pond water sample with satisfactory results.

## References

- [1] U. Fostener, G.T. Wittmann, Metal pollution in aquatic environment, Springer, Berlin, Heidelberg, New York, 1981, pp. 8–12.
- [2] E. Merian, Metals and their compounds in the environment, VCH, Weinheim, 1991, pp. 893–898.
- [3] C. Bo, Z. Ping, Anal. Bioanal. Chem. 381(2005) 986–992.
- [4] D.Y. Sasaki, D.R. Shnek, D.W. Pack, F.H. Arnold, Angew. Chem. Int. Ed. 34 (1995) 905–907.
- [5] J.A. Sweileh, Microchem. J. 65 (2000) 87–95.
- [6] M.S. Chan, S.D. Huang, Talanta 51 (2000) 373–380.
- [7] C.N. Ferrarello, M.M. Bayon, J.I.G. Alonso, A. Sanz-Medel, Anal. Chim. Acta 429 (2001) 227–235.
- [8] O. Chailapakul, S. Korsrisakul, W. Siangproh, K. Grudpan, Talanta 74 (2008) 683–689.
- [9] C.W.K. Chow, S.D. Kolev, D.E. Davey, D.E. Mulcahy, Anal. Chim. Acta 330 (1996) 79–87.
- [10] L.E. Vanatta, J.C. Vanatta, J. Riviello, J. Chromatogr. A 884 (2000) 143–150.
- [11] I.S. Balogh, M. Ruschak, V. Andruch, Y. Bazel', Talanta 76 (2008) 111–115.
- [12] K. Rurack, M. Kollmannsberger, U. Resch-Genger, J. Daub, J. Am. Chem. Soc. 122 (2000) 968–969.
- [13] J.I. Vlugt, T.B. Rauchfuss, C.M. Whaley, S.R. Wilson, J. Am. Chem. Soc. 127 (2005)

- 1612-1613.
- [14] S. Khatua, S.H. Choi, J. Lee, J.O. Huh, Y. Do, D.G. Churchill, Inorg. Chem. 48 (2009) 1799–1801.
- [15] W.C.W. Chan, S.M. Nie, Science 281 (1998) 2016–2018.
- [16] M. Bruchez, M. Moronne, P. Gin, S. Weiss, A.P. Alivisatos, Science 281 (1998) 2013– 2016.
- [17] R. Freeman, I. Willner, Chem. Soc. Rev. 41 (2012) 4067–4085.
- [18] W.R. Algar, K. Susumu, J.B. Delehanty, I.L. Medintz, Anal. Chem. 83 (2011) 8826–8837.
- [19] R. Freeman, T. Finder, L. Bahshi, R. Gill, I. Willner, Adv. Mater. 24 (2012) 6416–6421.
- [20] X. Michalet, F.F. Pinaud, L.A. Bentolila, J.M. Tsay, S. Doose, J.J. Li, G. Sundaresan, A.M. Wu, S.S. Gambhir, S. Weiss, Science 307 (2005) 6416–6421.
- [21] Y. Chen, Z. Rosenzweig, Anal. Chem. 74 (2002) 5132–5138.
- [22] K.M.G. Asfura, R.M. Leblanc, Chem. Commun. 21 (2003) 2684–2685.
- [23] H.Y. Xie, J.G. Liang, Z.L. Zhang, Y. Liu, Z.K. He, D.W. Pan, Spectrochim. Acta Part A Mol. Biomol. Spectrosc. 60 (2004) 2527–2530.
- [24] M. Koneswaran, R. Narayanaswamy, Sens. Actuators B Chem. 139 (2009) 104–109.
- [25] S. Chen, X. Zhang, Q. Zhang, X. Hou, Q. Zhou, J. Yan, W. Tan, J. Lumin. 131 (2011) 947–951.
- [26] S. Akshya, P.S. Hariharan, V.V. Kumar, S.P. Anthony, Spectrochim. Acta Part A Mol. Biomol. Spectrosc.135 (2015) 335–341.
- [27] J. Liu, Y. Liu, X. Yang, K. Wang, Q. Wang, H. Shi, L. Li, Anal. Chem. 85 (2013) 11121–11128.
- [28] C. Yuan, K. Zhang, Z. Zhang, S. Wang, Anal. Chem. 84 (2012) 9792–9801.
- [29] J. Wang, J. Liang, Z. Sheng, H. Han, Microchim. Acta 167 (2009) 281–287.
- [30] T. Khantaw, C. Boonmee, T. Tuntulani, W. Ngeontae, Talanta 115 (2013) 849–856.
- [31] T. Noipa, T. Tuntulani, W. Ngeontae, Talanta 105 (2013) 320–326.
- [32] A.G. Kumbhar, K. Kishore, Radiat. Phys. Chem. 66 (2003) 275–280.
- [33] J.G. Liang, X.P. Ai, Z.K. He, D.W. Pang, Analyst 129 (2004) 619–622.

## 6. Silver ion modulated CdS quantum dots for highly selective detection of trace Hg<sup>2+</sup>

## 1. Introduction

The acute and/or chronic toxicity to biological organisms of mercury ions is well-known [1]. Mercury exists in multiple forms such as inorganic salts, and as organic complexes with the most common and stable form of mercury in water being the solvated divalent mercuric ion  $(Hg^{2+})$  [2]. The toxicity of mercury is primarily associated with this divalent species, with absorption, tissue distribution and biotransformation all influenced significantly by the valence state of the metal [3].  $Hg^{2+}$  produces toxic effects by protein precipitation, enzyme inhibition, and generalized corrosive action. Thus, the detection of  $Hg^{2+}$  in water samples is a serious concern because of its harmful effects on the environment and human health.

Hg<sup>2+</sup> is normally quantitatively analyzed by spectroscopic techniques such as cold vapor atomic absorption spectrometry (AAS) [4], inductively coupled plasma mass spectrometry (ICP-MS) [5], atomic fluorescence spectrometry (AFS) [6], an X-ray fluorescence spectrometry (XRF) [7, 8]. Electrochemical techniques such as anodic stripping voltammetry (ASV) [9] are also popular for Hg<sup>2+</sup> detection. Although these techniques offer high selectivity and sensitivity, they posses some drawbacks such as high operating cost, and being labor-intensive, and time-consuming. Therefore, low cost, simple, and rapid assays for Hg<sup>2+</sup> detection are highly desired.

Chemical sensors for toxic heavy metal ions based on optical nanomaterials continue to move interesting research directions [10-12]. The optical characteristics of materials at the nanometer scale differ from those of their bulk counterpart including absorption [13], fluorescence emission [14], and circular dichroism [15]. There have been several reports utilizing nanomaterials as optical chemical sensors for selective detection of Hg<sup>2+</sup>, for instance using gold nanoparticles (AuNPs) [16], silver nanoparticles (AgNPs) [17], gold nanoclusters (AuNCs) [18, 19], and silver nanoclusters (AgNCs) [20]. Colorimetric sensors for detection of Hg<sup>2+</sup> using AuNPs [21] and AgNPs [22] as sensor probes have been reported most frequently. The color change of the sensor probe in the presence of Hg<sup>2+</sup> was due to the change of the particle size, such as crystal growth [23] or aggregation/antiaggregation mechanisms [22, 24]. In addition, fluorescence sensors based metal nanoclusters including AuNCs [18] and AgNCs [25] for the detection of Hg<sup>2+</sup> have also been reported. Moreover, a dual functional fluorescence sensor for the detection of Ag<sup>+</sup> and Hg<sup>2+</sup> was proposed using cytidine stabilized AuNCs [18].

Nanocrystalline semiconductors or quantum dots (QDs) are another type of optical nanomaterial frequently used to fabricate fluorescence sensors for sensing Hg<sup>2+</sup> and other heavy metal ions. The selectivity of the sensor towards specific target metal ions can be based on several detection mechanisms. The direct interaction/reaction between metal ions and QDs surface/capping ligands are the most common detection mechanism. This mechanism can provide excellent selectivity towards the specific metal ions [26, 27]. The sensing signal may be followed by the degree of fluorescence quenching (turn-off mode) [28] or fluorescence enhancement (turn-on mode) [29]. However, this approach requires the design of a specific capping ligand for the reaction between metal ions and the QD surface. Therefore, in order to design more versatile Hg<sup>2+</sup> and heavy metal ion sensors based QDs which are not limited by the specific interaction/reaction on the QDs surface, a two-step fluorescence change strategy (turn-on-off/turn-off-on) is proposed [30-33]. For this approach, the fluorescence intensity of the QDs is firstly modulated by an appropriate conjugated compound (such as organic compounds or some metal ions). Then, the fluorescence intensity of the modulated QDs can

inversely be changed in the presence of the target metal ions due to a specific interaction between the conjugated compound and the target metal ion. The two-step fluorescence change approach can improve the selectivity of the sensor due to the specific interaction/reaction of the conjugated compound and the target species. Ideally, we can design the selective sensor for several metal ions by changing the conjugated compound (by using the same QDs as a fluorescence probe).

In this paper, we aim to fabricate a fluorescence sensor based cysteamine capped cadmium sulfide quantum dots (Cys-CdS QDs) for selective determination of  $Hg^{2+}$  via the two-step fluorescence change strategy (turn-on-off) having  $Ag^+$  as the conjugated species. The fluorescence intensity of the Cys-CdS QDs was firstly modulated by the addition of  $Ag^+$  (turn-on). Based on a strong metallophilic interaction between  $Ag^+$  and  $Hg^{2+}$ , the modulated fluorescence intensity of Cys-CdS QDs can efficiently be quenched in the presence of  $Hg^{2+}$  (turn-off). The degree of fluorescence quenching can be related to the concentration of  $Hg^{2+}$ . The parameters that may affect the detection sensitivity were studied and optimized. Finally, the feasibility of the proposed sensor in real samples application was demonstrated and compared to the results of cold vapor atomic absorption spectrometry.

## 2. Experimental

## 2.1 Chemicals

All reagents were of analytical grade and used without further purification. Cadmium chloride (CdCl<sub>2</sub>·H<sub>2</sub>O) was obtained from Riedel-deHaen. Cysteamine hydrochloride and mercury (II) chloride monohydrate were purchased from Sigma. Sodium sulfide (Na<sub>2</sub>S·H<sub>2</sub>O) and silver nitrate were received from BDH. Sodium hydroxide was obtained from Carlo Erba Reagents. Glacial acetic acid was purchased from QRec. Ultrapure water (18.2 M $\Omega$  cm) was obtained from a Millipore water purification system. Cys-CdS QDs used in this work were prepared and characterized as described in our recent report [34] (see the electronic supporting information (ESI) for more information).

## 2.2 Instrumentations

Fluorescence spectra were recorded using a RF-5301PC spectrofluorometer (Shimadzu). The slit width used for both excitation and emission was 5 nm. The transmission electron microscopy (TEM) images of the Cys–CdS QDs were carried out on a Tecnai G<sup>2</sup>-20 (FEI, Netherlands) under an accelerating voltage of 200 kV. Optical absorption spectra were recorded on an Agilent HP 8453 spectrometer. Measurements of solution pH were carried out using a UB-10 UltraBasic pH meter (Denver Instrument).

## 2.3 Fluorescence enhancement of Cys-CdS QDs by Ag<sup>+</sup>

The Cys-CdS QDs solution (volume 75  $\mu$ L) was added to a 10.00 mL volumetric flask. The appropriate volume of stock AgNO<sub>3</sub> solution (1.0 mM) was then added to the same flask. The mixture was then diluted to 10.00 mL with 0.1 M acetic-acetate buffer pH 4.0. The solution was then incubated at room temperature for 10 minutes before measuring fluorescence spectra using the excitation wavelength ( $\lambda_{ex}$ ) of 372 nm.

# 2.5 Fluorescence quenching of $Ag^+@Cys\text{-CdS}\ QDs\ by\ Hg^{2+}$

The Cys-CdS QD solution (volume 75  $\mu$ L) and 100  $\mu$ L of 1.0 mM AgNO<sub>3</sub> were added to a 10.00 mL volumetric flask and incubated for 10 min. The appropriate volume of stock Hg<sup>2+</sup> solution (1.0 mM) was then added together to the same volumetric flask. Then, the solution was diluted to 10.00 mL with 0.1 M acetic-acetate buffer pH 4.0. The solution

was then incubated at room temperature for 15 minutes before measuring the fluorescence spectrum using an excitation wavelength ( $\lambda_{ex}$ ) of 372 nm.

## 2.6 Selectivity of the sensor

The Cys-CdS QDs solution (volume of 75  $\mu$ L) and 100  $\mu$ L of 1.0 mM AgNO<sub>3</sub> were added to a 10.00 mL volumetric flask and incubated for 10 min. Then, 30  $\mu$ L of 1.0 mM stock solution of various metal ions was added (giving a final concentration of 3  $\mu$ M) including Li<sup>+</sup>, Na<sup>+</sup>, K<sup>+</sup>, Mg<sup>2+</sup>, Ca<sup>2+</sup>, Ba<sup>2+</sup>, Pb<sup>2+</sup>, Al<sup>3+</sup>, Zn<sup>2+</sup>, Cd<sup>2+</sup>, Mn<sup>2+</sup>, Ni<sup>2+</sup>, Cr<sup>3+</sup>, Co<sup>2+</sup>, Cu<sup>2+</sup>, Fe<sup>2+</sup>, Fe<sup>3+</sup> and Hg<sup>2+</sup>. The solution was then diluted to 10.00 mL with 0.1 M acetic-acetate buffer pH 4.0 and incubated at room temperature for 15 minutes before measuring the fluorescence spectrum using an excitation wavelength ( $\lambda_{ex}$ ) of 372 nm.

## 2.7 Application of the sensor for determination of Hg<sup>2+</sup> in drinking water

The sensor probe was prepared by mixing 75  $\mu L$  of Cys-CdS QDs solution and 100  $\mu L$  of 1.0 mM AgNO<sub>3</sub> in a 10.00 mL volumetric flask containing 1.0 mL of 1.0 M acetic-acetate buffer pH 4.0. Water samples spiked with Hg<sup>2+</sup> were then added into the sensor probe to a final volume of 10.00 mL and incubated for 15 minutes before recording fluorescence spectra. The concentration of Hg<sup>2+</sup> was then extracted using a standard calibration curve. The accuracy and precision of each measurement was evaluated by spiking three different concentrations of Hg<sup>2+</sup> (0.2, 0.4 and 0.6  $\mu$ M) into the water samples under the optimized condition.

#### 3. Results and discussion

## 3.1 Detection concept and the sensor response

In previous work, we showed that Cys-CdS QDs can be used as selective fluorescence sensors for the detection of  $Ag^+$  [34]. In that work, the fluorescence intensity of Cys-CdS QDs was enhanced (turn-on) in the presence of trace amounts of  $Ag^+$ . This is due to the coordination of  $Ag^+$  with the thiol moieties on the surface of QDs which result in the creation of more radiative centers at the CdS/Ag–SR complex microheterojunctions and stimulate blocking of nonradiative  $e^-/h^+$  recombination defect sites on the surface of QDs. If the  $Ag^+$  sensitized fluorescence can inversely be quenched by further specific interaction, a selective fluorescence sensor via two-step fluorescence change is obtained. Here, metallophilic interactions between  $Hg^{2+}$  and  $Ag^+$  are expected to quench the fluorescence of the  $Ag^+$  modulated Cys-CdS QDs ( $Ag^+$ @Cys-CdS QDs), constituting an efficiently and selective  $Hg^{2+}$  sensor.

The fluorescence spectrum of the Cys-CdS QDs in the absence and presence of  $Ag^+$  are shown in Fig. 1. In acidic solution (0.1 M acetic-acetate buffer pH 4.0), the fluorescence intensity of Cys-CdS QDs was relatively weak due to the protonation of the amine groups on capping moieties. Interestingly, in the presence of only 10  $\mu$ M of  $Ag^+$ , the fluorescence intensity of the Cys-CdS QDs is significantly enhanced with the same spectrum shape and a relatively small red shift. The improved fluorescence characteristics are due to the decrease of nanocrystal defects by the formation of  $Ag^+/RS^-$  adsorbed on the surface of CyS-CdS QDs [35, 36].

To demonstrate the Hg<sup>2+</sup> sensor concept, Hg<sup>2+</sup> was added to the solution of Ag<sup>+</sup>@CyS-CdS QDs and the fluorescence compared to the original CyS-CdS QDs solution (without Ag<sup>+</sup>) and the results are shown in Fig. 1. Fluorescence quenching phenomenon is observed for both systems. For the system containing only CyS-CdS QDs, fluorescence quenching (25 %) with a small red shift in the spectrum is observed. This may be due to HgS

deposition on the surface of the CyS-CdS QDs [37]. On the other hand, the fluorescence quenching when using Ag<sup>+</sup>@CyS-CdS QDs as a sensor probe showed better quenching efficiency (around 60%) upon addition of Hg<sup>2+</sup>. This behavior may be due to the well-known metallophilic interaction between Hg<sup>2+</sup> and Ag<sup>+</sup> (formation of a strong metallophilic bond between their d<sup>10</sup> centers) on the Cys-CdS QDs surface [18, 38]. The results signify that the formation of Hg<sup>2+</sup>–Ag<sup>+</sup> on the Cys-CdS QDs is a more efficient quencher than Hg<sup>2+</sup> alone. It should be noted that the fluorescence spectrum after adding Hg<sup>2+</sup> exhibits a relatively red shift of the spectrum (from 545 nm to 550 nm), indicating increasing particle size.

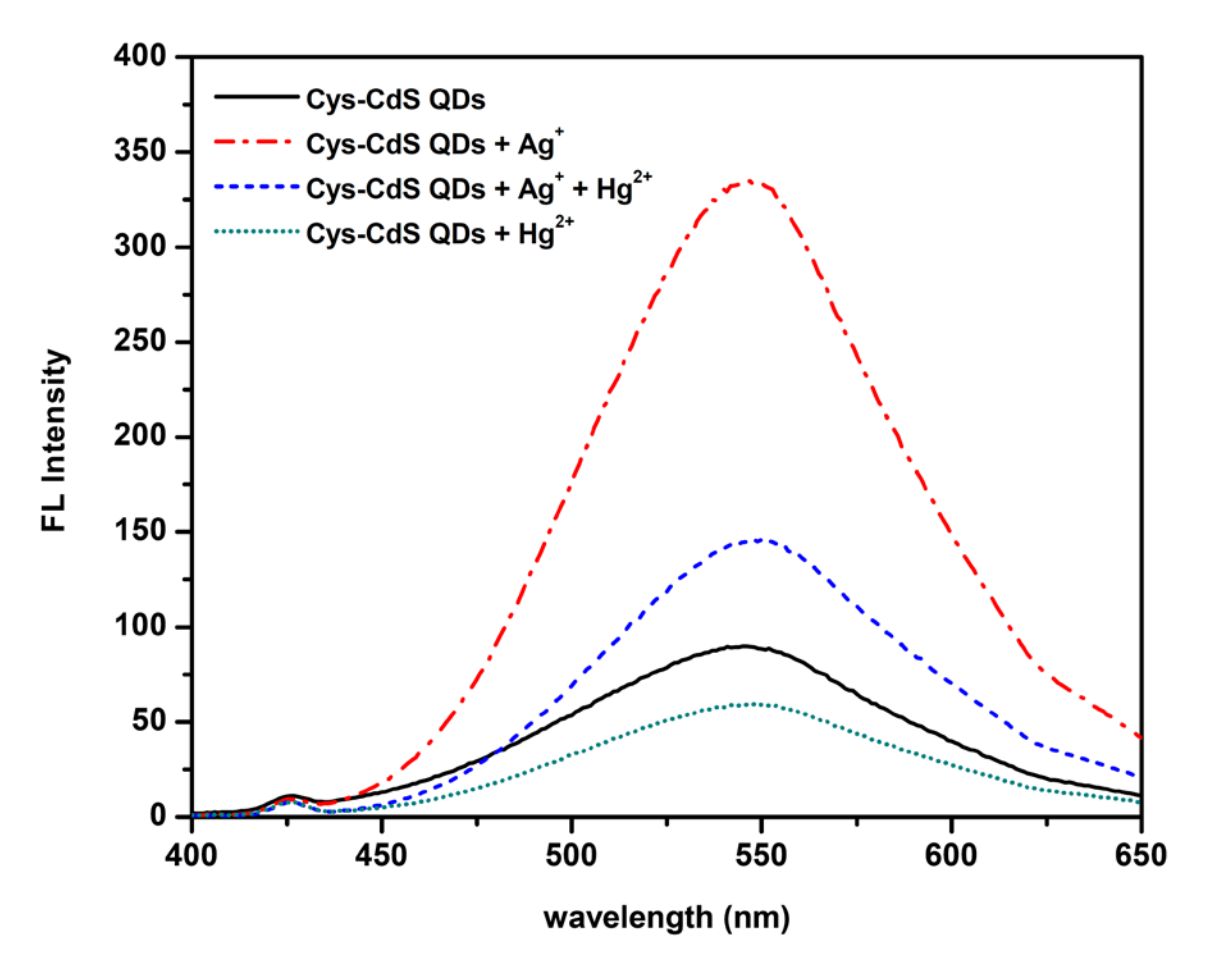


**Fig. 1** Fluorescence spectrum of 0.06 mg mL<sup>-1</sup> Cys-CdS QDs in the absence and presence of 10 μM Ag<sup>+</sup> and the effect of 3 μM Hg<sup>2+</sup> to the fluorescence spectrum of Cys-CdS QDs and Ag<sup>+</sup>@Cys-CdS QDs in 0.1 M acetic-acetate buffer pH 4.0.

The change of the particle size upon addition of Ag<sup>+</sup> and following by Hg<sup>2+</sup> was investigated by TEM. The TEM image of the Cys-CdS QDs is shown in Fig. 2 (a). The morphology of the Cys-CdS QDs is a spherical with an average diameter of 3.3±0.8 nm. No aggregation of the particles and a narrow particle size distribution were observed corresponding well with the narrow and symmetrical fluorescence spectra. From Fig. 2(b), the size of the Cys-CdS QDs after adding Ag<sup>+</sup> (3.5±0.6 nm) was relatively close to the size of the original Cys-CdS QDs (Fig. 2(a)), corresponding to the relatively small red shift observed in the fluorescence studies. The size of the QDs after adding Ag<sup>+</sup> did not change significantly because a very small amount of Ag<sup>+</sup> was used to modulate the sensor. On the other hand, the particle size significantly increased (to be around 4.6±1.4 nm) after adding Hg<sup>2+</sup> to the solution of Ag<sup>+</sup>@CyS CdS QDs as shown in Fig. 2(c). This result confirms the formation of

Hg<sup>2+</sup>-Ag<sup>+</sup> on the Cys-CdS QDs, corresponding to the significant red shift observed in the fluorescence studies.

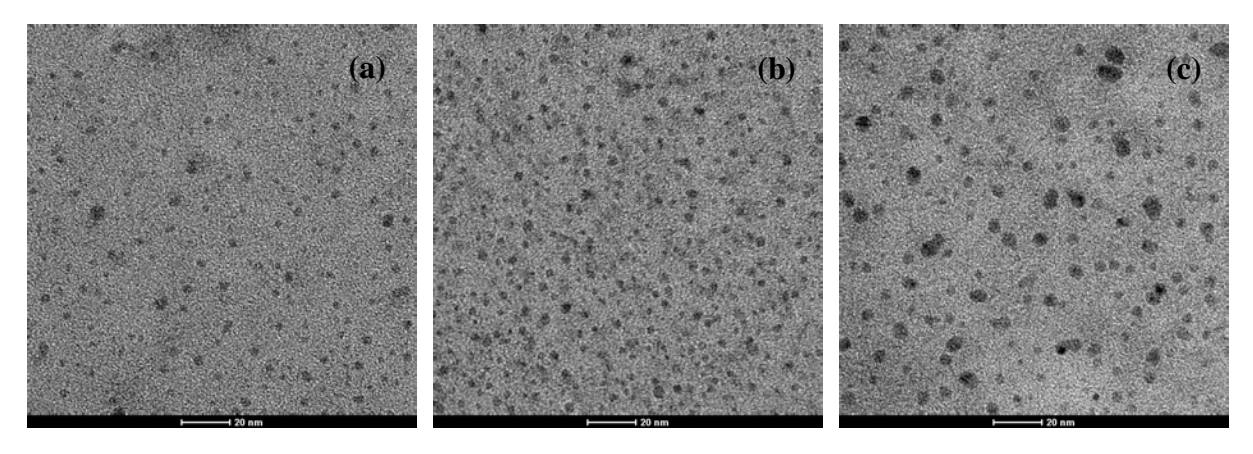


**Fig. 2** TEM images of (a) Cys-CdS QDs, (b) Ag<sup>+</sup>@Cys-CdS QDs and (c) Hg<sup>2+</sup>-Ag<sup>+</sup>@Cys-CdS QDs.

## 3.3 Effect of Ag<sup>+</sup> concentration on the fluorescence enhancement

The fluorescence spectra of Cys-CdS ODs in the presence of various concentrations of Ag<sup>+</sup> from 0 to 20 µM were recorded and shown in Fig. 3. The fluorescence intensity of Cys-CdS QDs increased gradually with increasing Ag+ can be observed until the concentration of Ag<sup>+</sup> reached 10 µM, and then was relatively constant beyond that concentration level. This may be due to the limited adsorption surface, as can be elucidated by a Langmuir-type binding isotherm [35, 36]. In order to obtain the best sensor sensitivity, the amount of Ag<sup>+</sup> used to modulate the fluorescence emission of Cys-CdS QDs was optimized. The stock solution of Hg<sup>2+</sup> (3 µM) was added to the Ag<sup>+</sup>-modulated Cys-CdS QDs. The degrees of fluorescence quenching ( $\Delta F = F_0 - F$ ) observed is shown in Fig. 3(b). The results reveal that quenching efficiency can be increased when increasing the concentration of Ag<sup>+</sup> up to 10 µM and then is relatively constant beyond that. This result suggests that excess Ag<sup>+</sup> (after the adsorption on the QDs surface) is not necessary and does not affect the fluorescence quenching efficiency by Hg<sup>2+</sup>. In addition, the fluorescence quenching was due to the interaction between Ag<sup>+</sup> deposited on the surface of Cys-CdS QDs and Hg<sup>2+</sup>. To obtain the maximum quenching efficiency (for Hg<sup>2+</sup> detection), 10 µM of Ag<sup>+</sup> was used to modulate the fluorescence intensity of the Cys-CdS QDs.

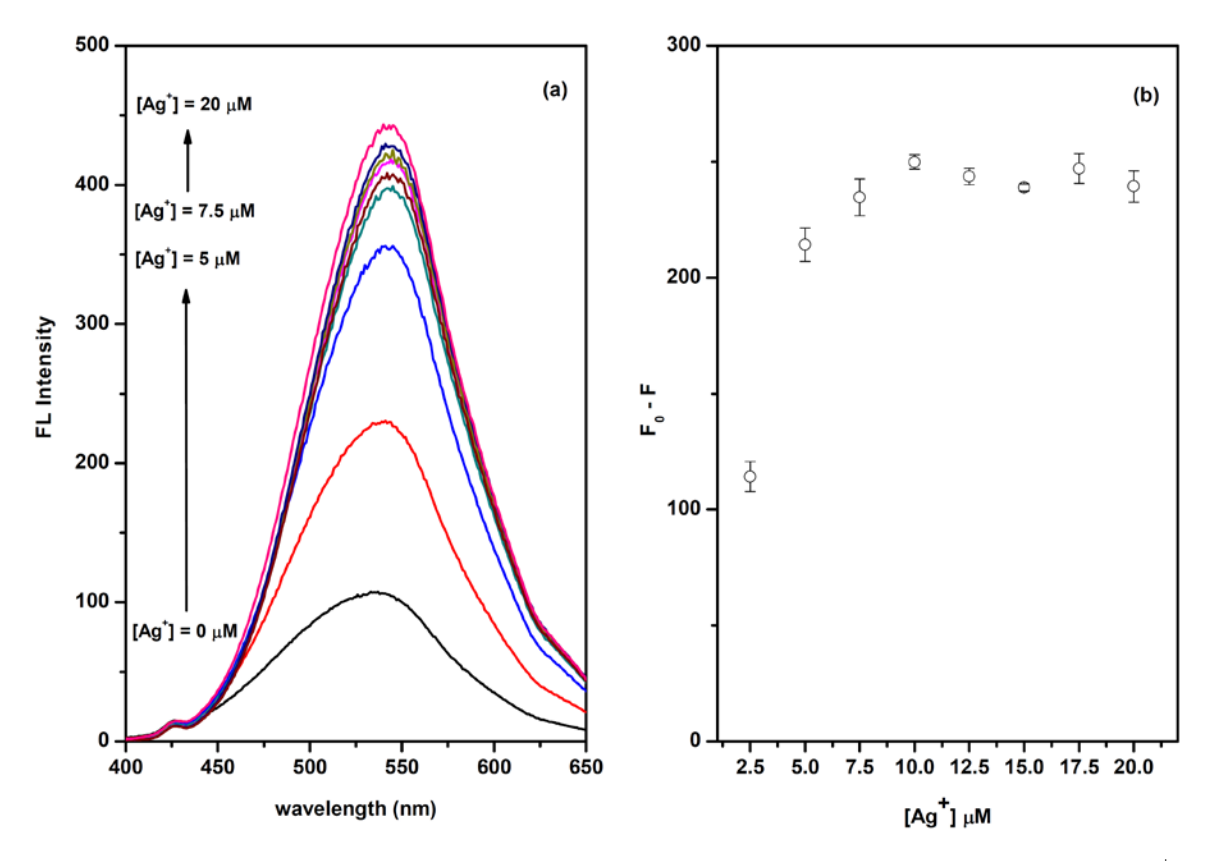


**Fig. 3** (a) Fluorescence spectrum of the Cys-CdS QDs in the presence of 0-20  $\mu$ M Ag<sup>+</sup> and (b) degree of fluorescence quenching caused by the addition of 3  $\mu$ M Hg<sup>2+</sup> at the given Ag<sup>+</sup> concentrations in 0.1 M acetic-acetate buffer pH 4.0.

## 3.4 Effect of the solution pH on the sensor preparation and detection of Hg<sup>2+</sup>

It is well-known that the photoluminescence of colloidal ODs is very sensitive to the solution pH change. Moreover, the solution pH may affect the interaction/reaction between the sensor probe and the target analyte. In this context, the Cys-CdS QDs possess a primary amine as a capping molecule, and the pH of the solution can affect the charge on the capping molecule. Moreover, the solution pH may also affect the reaction between Hg<sup>2+</sup> and Ag<sup>+</sup>. The effect of the solution pH was, therefore, studied by adjusting the pH of 0.1 M acetic-acetate buffer in the range of 3.0 to 6.0, and the results are shown in Fig. 4. For preparation of the sensor probe, Ag<sup>+</sup> (10 μM) was added to 0.08 mg mL<sup>-1</sup> Cys-CdS QDs at each solution pH. The results showed that the fluorescence intensities of the Cys-CdS ODs increased upon increasing the solution pH (Fig. 4(a)) and then decreased beyond pH 4.5. This result revealed that the pH of the solution affected the reaction between Ag<sup>+</sup> and RS<sup>-</sup> on the surface of the Cys-CdS QDs. Moreover, the effect of the solution pH towards the detection of Hg<sup>2+</sup> was also studied. The degree of fluorescence quenching as a function of the solution pH is shown in Fig. 4(b). In the presence of 3.0  $\mu M$  Hg<sup>2+</sup>, the solution pH significantly affected the fluorescence quenching efficiency. High fluorescence quenching can be observed at solution pH less than 4.0. On the other hand, the quenching efficiency above pH 4.0 was significantly decreased. It is signified that the reaction between Hg<sup>2+</sup> and Ag<sup>+</sup> is pH dependent and more efficient in acidic media. Thus, to obtain the best quenching efficiency, the pH value of 4.0 was chosen as the running assay solution throughout these studies.

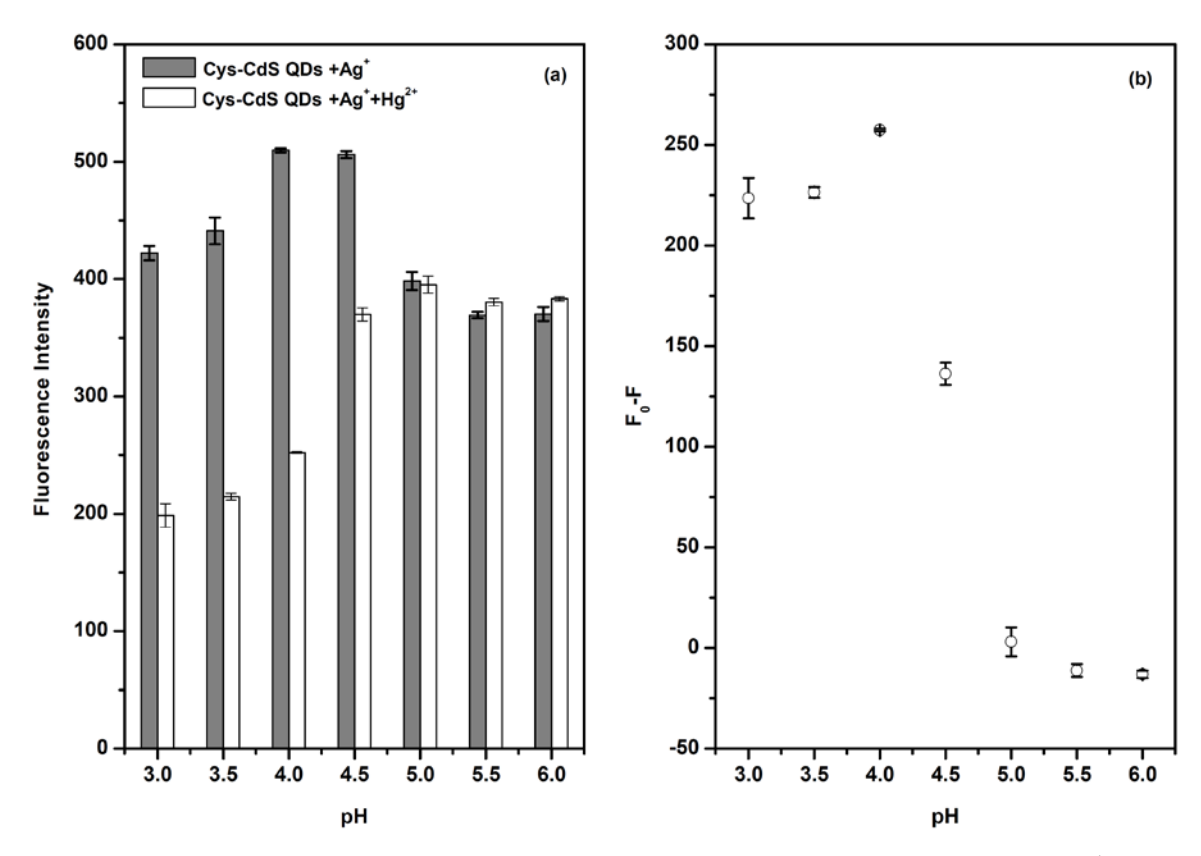


**Fig. 4** (a) Effect of the solution pH on the fluorescence intensities of 0.08 mg mL<sup>-1</sup> Cys-CdS QDs in the presence of 10 μM Ag<sup>+</sup> and the fluorescence intensities after the addition of 3 μM Hg<sup>2+</sup> in 0.1 M acetic-acetate buffer pH 4.0 (b) degree of the fluorescence quenching (F<sub>0</sub>-F) upon the addition of 3 μM Hg<sup>2+</sup> to the sensor probe (Ag<sup>+</sup>@Cys-CdS QDs) as a function of the solution pH.

## 3.5 Effect of the Cys-CdS QDs concentration on the detection of Hg<sup>2+</sup>

The detection sensitivity of optical sensors based on QDs can be affected by the number of the sensor probe. When using low QD concentrations, the fluorescence intensity of the sensor probe can be expected to be low, affecting assay sensitivity. On the other hand, at higher QD concentration, fluorescence self-absorption by particles of different sizes may occur. Therefore, the effect of Cys-CdS QDs concentration used to fabricate the Hg<sup>2+</sup> sensor was optimized. Concentrations of Cys-CdS QDs were varied in the range of 0.02-0.12 mg mL<sup>-1</sup> by fixing the amount of Ag<sup>+</sup> (10 μM) and the results were showed in Fig. 5(a). The fluorescence intensities of the Cys-CdS QDs in the presence of 10 µM Ag<sup>+</sup> increased with increasing Cys-CdS QD concentration and was then relatively constant for QD concentrations beyond 0.08 mg mL<sup>-1</sup>. This behavior stems from the increasing the number of efficiently fluorescing particles (Ag<sup>+</sup>@Cys-CdS QDs) in solution. In addition, it should be noted that no spectral shift can be observed, signifying that the particle size remains the same, but the number of similar-sized fluorescent species increases. The fluorescence quenching of the Ag<sup>+</sup>@Cys-CdS QDs caused by Hg<sup>2+</sup> at the given Cys-CdS QDs concentration was then investigated and the results are shown in Fig. 5(b). The degree of fluorescence quenching (F<sub>0</sub>-F) depended on the concentration of Cys-CdS QDs. The quenching efficiency increased with increasing Cys-CdS QDs concentration from 0.02 to 0.06 mg mL<sup>-1</sup>. This may be due to the limited number of sensor probes, with the 3 µM Hg<sup>2+</sup> saturating available biding sites and

thus also the sensor signal. Furthermore, fluorescence quenching efficiency decreased at higher QD concentrations due to the limited capacity of  $Hg^{2+}$  to quench excessive concentrations of the QD sensor probe. Hence, to obtain the best detection sensitivity, 0.06 mg mL<sup>-1</sup> Cys-CdS QDs solution was chosen for the fabrication of the  $Hg^{2+}$  sensor.

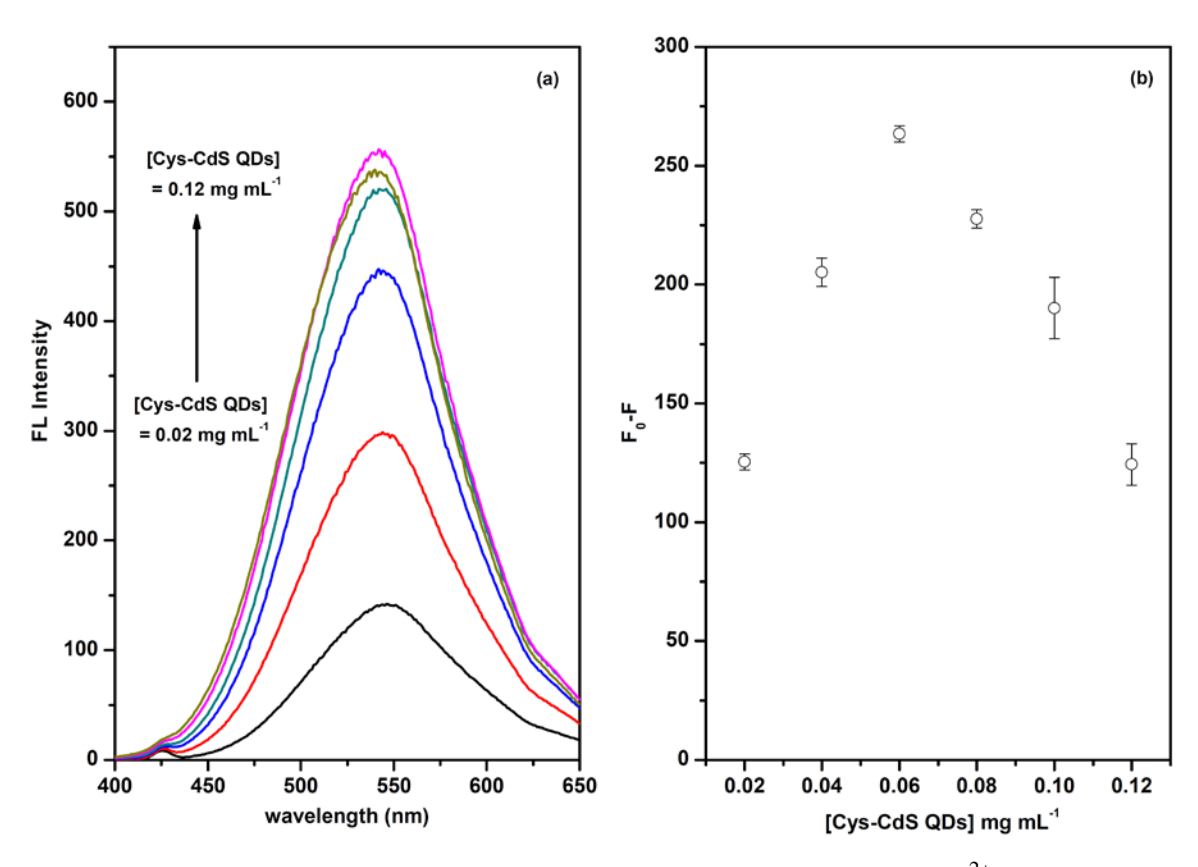


**Fig. 5** Effect of Cys-CdS QDs concentration to the detection of  $Hg^{2^+}$  (a) fluorescence spectrum of Cys-CdS QDs at various concentrations in the presence of 10  $\mu$ M  $Ag^+$  in 0.1 M acetic-acetate buffer pH 4.0 (b) Degree of the fluorescence quenching (F<sub>0</sub>-F) upon the addition of 3  $\mu$ M  $Hg^{2^+}$  to the sensor probe ( $Ag^+$ @Cys-CdS QDs) as a function of Cys-CdS QDs concentrations.

## 3.6 Effect of the incubation time

In this work, the incubation time (the time allowed for the reaction to complete) can affect sensor performance. Therefore, the effect of the incubation time was studied in detail. For the sensor preparation step, the appropriate volume of  $Ag^+$  solution (10  $\mu M$ ) was added into 0.06 mg mL $^{-1}$  of Cys-CdS QDs, and the fluorescence intensity was measured every 5 minutes for 1 hour. The results of the effect of incubation time on the sensor preparation step are shown in Fig. 6(a). The fluorescence intensity of Cys-CdS QDs in the presence of  $Ag^+$  increased with increasing incubation time but only slightly increased after incubating for 10 min. Thus, an incubation time of only 10 min was sufficient for the sensor preparation step. This result reveals that the reaction between  $Ag^+$  and  $RS^-$  on the surface of Cys-CdS QDs requires some incubation time to complete the reaction before being used as a sensor for  $Hg^{2+}$ . Next, the incubation time needed to obtain the best  $Hg^{2+}$  detection sensitivity was investigated. The experiment was carried out by the addition of the appropriate volume of  $Hg^{2+}$  (3  $\mu M$ ) to the 10 min incubated  $Ag^+$ @Cys-CdS QDs. The fluorescence intensities of  $Ag^+$ @Cys-CdS QDs after adding  $Hg^{2+}$  as a function of incubation time are shown in Fig.

6(b). The results showed that the reaction between  $Hg^{2+}$  and the sensor probe can reach equilibrium after 15 min. Therefore, in  $Hg^{2+}$  sensing experiments, the reaction was left for 15 min before recording the fluorescence spectra.

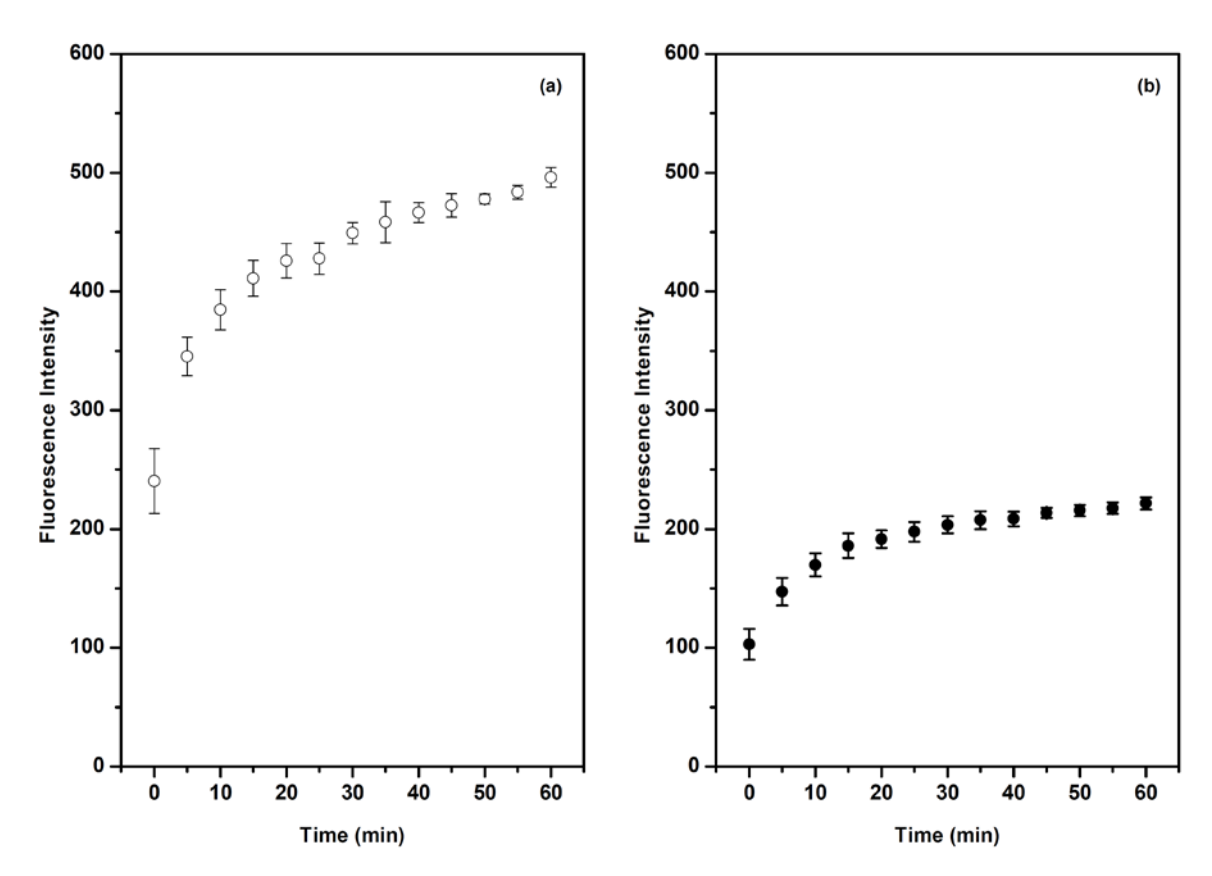


**Fig. 6** (a) Effect of incubation time on the sensor preparation (Ag<sup>+</sup>@Cys-CdS QDs) using 0.06 mg mL<sup>-1</sup> of Cys-CdS QDs and 10 μM of Ag<sup>+</sup> in 0.1 M acetic-acetate buffer pH 4.0. (b) Effect of incubation time on the detection of 3 μM Hg<sup>2+</sup> by the proposed sensor (after adding 10 μM of Ag<sup>+</sup> into 0.06 mg mL<sup>-1</sup> of Cys-CdS and incubated for 15 min in 0.1 M acetic-acetate buffer pH 4.0).

## 3.7 Response of the sensor toward other possible interfering cations

The selectivity of the proposed sensor was evaluated by testing the sensor probe (Ag<sup>+</sup>@Cys-CdS QDs) with other cations. In our previous report [34], the Cys-CdS QDs itself responded to heavy metal ions. Silver ions had the highest effect on the fluorescence spectrum of the Cys-CdS QDs in the fluorescence enhancement mode. In addition, long wavelength fluorescence shifts can be observed when adding Cu<sup>2+</sup> (less than 10 μM) to the Cys-CdS QDs. Cu<sup>2+</sup> can react with the CdS core and form CuS on the surface of the Cys-CdS QDs, resulting in the increase of particle size [39]. Moreover, the Cys-CdS QDs themselves can respond to the Hg<sup>2+</sup> in the quenching direction, however, it a relatively high concentration is required. In this work, when adding various cations to the sensor probe (Ag<sup>+</sup>@Cys-CdS QDs), the fluorescence spectrum was significantly quenched (as shown in Fig. 7) with a relatively red shift of fluorescence spectra only in the case of Hg<sup>2+</sup> and Cu<sup>2+</sup> while other cations exhibited no significant spectral or intensity changes. It may be noted that the fluorescence quenching in the case of Cu<sup>2+</sup> was due to a chemical reaction such as the formation of CuS on the surface of Cys-CdS QDs [40]. Except Cu<sup>2+</sup>, Hg<sup>2+</sup> was the only cation that significantly quenched the fluorescence of the sensor probe. The selectivity of this

sensor stems from the metallophilic interaction between  $Hg^{2+}$  and  $Ag^{+}$  (on the surface of Cys-CdS QDs), acting as the efficient quencher while other metal ions cannot undergo such a reaction. These results confirm that the proposed sensor possesses good selectivity towards  $Hg^{2+}$ .

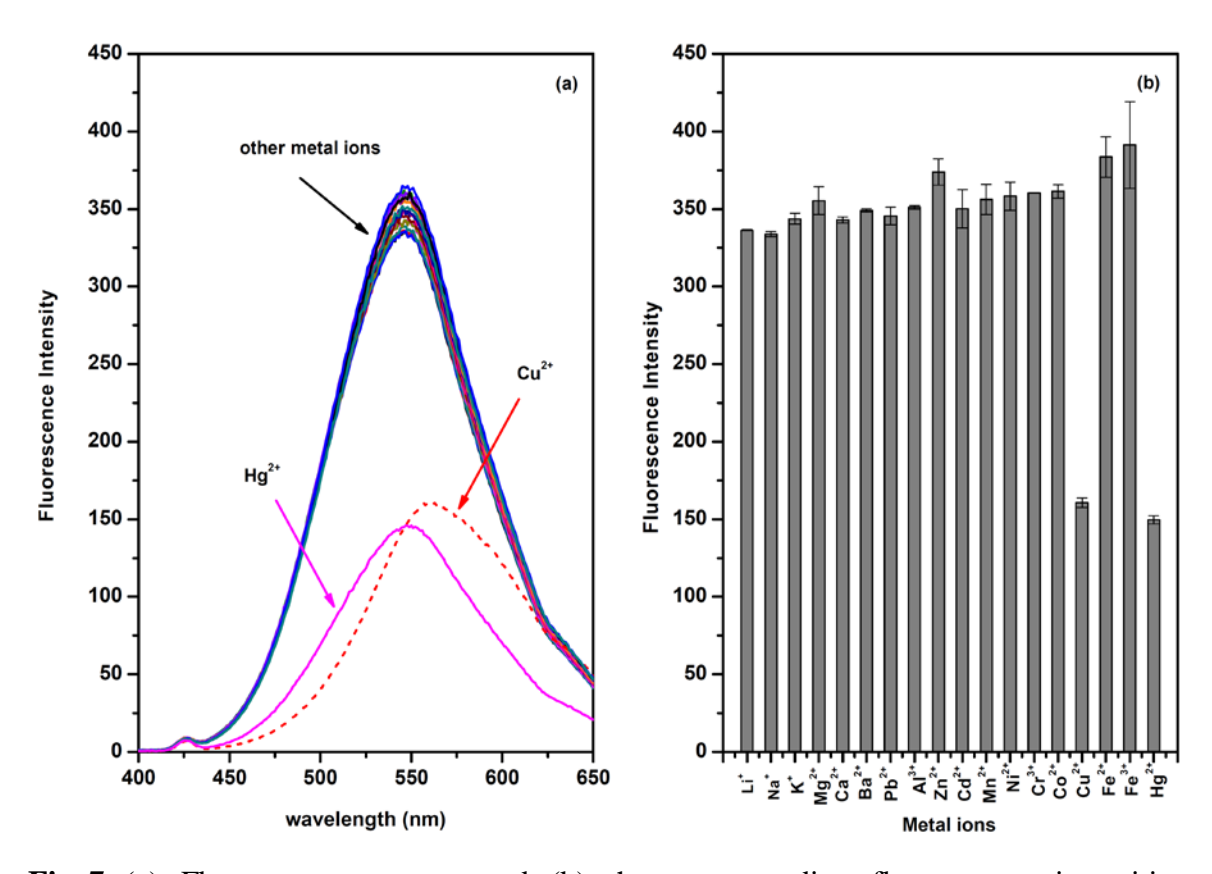


**Fig. 7** (a) Fluorescence spectra and (b) the corresponding fluorescence intensities of  $Ag^+@Cys\text{-}CdS\ QDs\ (0.06\ mg\ mL^{-1}\ of\ Cys\text{-}CdS\ QDs\ in\ the\ presence\ of\ 10\ \mu M\ of\ each\ tested\ metal\ ions.$ 

## 3.8 Analytical performance of the Hg<sup>2+</sup> detection by the proposed sensor

Since the selectivity of the proposed sensor is based on the metallophilic interaction between  $Hg^{2+}$  and  $Ag^+$  (on the Cys-CdS QDs surface), that the proposed sensor should be tolerant to possible interfering species in real samples. Therefore in principle, a sensitive and low detection limit sensor can be expected. Fluorescence titrations of the sensor probe by  $Hg^{2+}$  were carried out at the optimized conditions. The fluorescence spectra at various concentrations of  $Hg^{2+}$  ranging from 0 to 3.5  $\mu$ M are shown in Fig. 8(a). With increasing  $Hg^{2+}$  concentration, the fluorescence intensity of the sensor probe at 545 nm is quenched. A calibration curve of  $Hg^{2+}$  can be obtained by plotting the degree of fluorescence quenching at 545 nm ( $F_0$ -F; when  $F_0$  and F were the fluorescence intensity in the absence and in the presence of  $Hg^{2+}$ , respectively) as a function of the concentration of  $Hg^{2+}$  as shown in Fig. 8(b). The working linear concentration range of the proposed sensor for detecting  $Hg^{2+}$  was found to be in the range of 0-3.5  $\mu$ M.  $Hg^{2+}$  concentrations beyond this range provided the saturated response (data not shown). The regression equation was found to be  $F_0 - F = 63.25 \times [Hg^{2+}]$  ( $\mu$ M) + 9.14 with the correlation coefficient ( $r^2$ ) of 0.9826. The limit of detection (LOD) was calculated as the concentration of  $Hg^{2+}$  producing the degree of

fluorescence quenching equal to  $F_0$ -3×the standard deviation of  $F_0$ . The sensor exhibited a very low detection limit of 0.09  $\mu$ M for  $Hg^{2+}$  sensing. In addition, the fluorescence spectra showed a red shift (from 545 to 550 nm) when the concentration of  $Hg^{2+}$  was increased, signifying increased of the particle size. The experimental results show that the degree of fluorescence quenching allows for the quantitative analysis of  $Hg^{2+}$ . From the obtained analytical performance parameters, it can be confirmed that the proposed sensor possesses excellent detection sensitivity with relatively low detection limit and may be a powerful sensor for the application in a real situation.

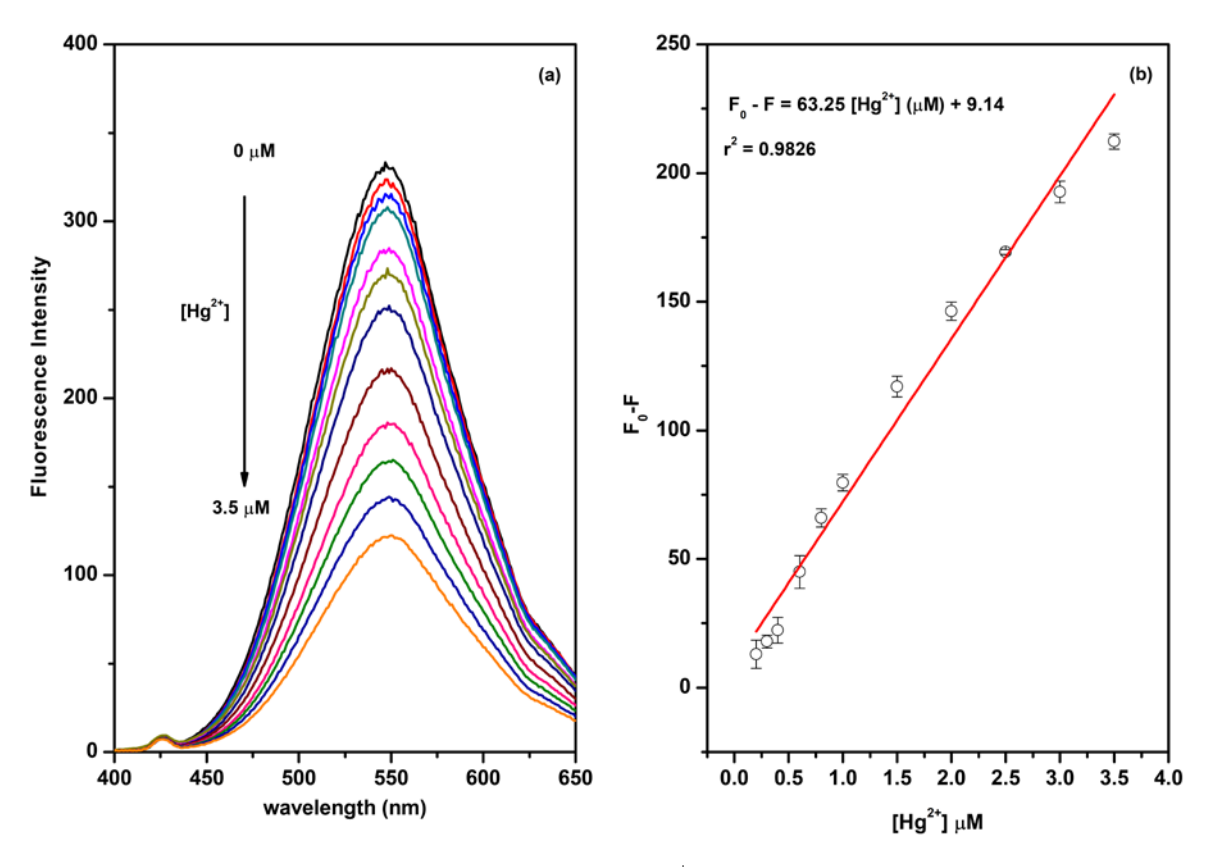


**Fig. 8** (a) Fluorescence titration spectra of  $Ag^+@Cys\text{-CdS}$  QDs upon the addition of different concentrations of  $Hg^{2+}$ . (b) The corresponding calibration curve (the solution containing 0.06 mg mL $^{-1}$  Cys-CdS QDs + 10  $\mu$ M  $Ag^+$  in 0.1 M acetic-acetate buffer pH 4.0).

## 3.9 Application of the sensor for detection of $\mathrm{Hg}^{2+}$ in drinking water samples

In order to demonstrate the application of the fabricated sensor in real samples, the detection of  $Hg^{2+}$  in samples of drinking water was evaluated. The drinking water was used without any pretreatment steps. The concentration of  $Hg^{2+}$  in drinking water was estimated by comparison with the standard calibration curve constructed by using a standard solution of  $Hg^{2+}$  in deionized water, and the results are shown in Table 1. From Table 1, the concentration of  $Hg^{2+}$  in the drinking water sample cannot be detected, signifying that the concentration of  $Hg^{2+}$  was less than the detection limit of the proposed sensor (less than 0.09  $\mu$ M). Therefore, spiked drinking water samples with the standard solution of  $Hg^{2+}$  at three different concentration levels were evaluated to determine the sensor accuracy. The concentration of  $Hg^{2+}$  in the drinking water sample and spiked samples were also measured by cold-vapor atomic absorption spectrometry, and the results are also listed in Table 1. It can

be seen that after spiking three different Hg<sup>2+</sup> concentration levels into the water samples, %recoveries in the range of 100-105% were obtained. Also, the concentrations of the spiked samples determined by our sensor agree well with the results obtained from cold-vapor atomic absorption spectrometry (CV-AAS). Furthermore, %RSDs from three replicates were lower than 10% suggesting that the proposed sensor provides good precision. These results show that the proposed sensor can potentially be used in practical applications.

**Table 1** Determination of  $Hg^{2+}$  in real drinking water samples by the proposed sensor and cold-vapor atomic absorption spectrometry (CV-AAS) (n = 3)

Addad	Proposed sensor			CV-AAS		
Added (µM)	Found (µM) <sup>a</sup>	%Recovery (%)	RSD (%)	Found (µM) <sup>a</sup>	%Recovery (%)	RSD (%)
0.00	n.d.	-	-	n.d.	-	-
0.20	$0.24\pm0.02$	$105.3 \pm 10.7$	10.2	$0.206 \pm 0.004$	$103 \pm 2$	1.8
0.40	$0.44 \pm 0.03$	101.9±6.9	6.8	$0.402 \pm 0.002$	$101 \pm 1$	0.6
0.60	$0.63\pm0.03$	$100.2\pm5.4$	5.4	$0.598 \pm 0.005$	$100 \pm 1$	0.9

<sup>&</sup>lt;sup>a</sup> Mean  $\pm$  SD (n = 3)

n.d. = not detectable

# 3.10 Comparison of the sensors merits of the ${\rm Hg}^{2+}$ sensor fabricated from various type of nanomaterials

The various reported methods of detections of  $Hg^{2+}$  using the optical properties of nanomaterials are summarized in Table 2. The  $Hg^{2+}$  sensors can be fabricated by using the different type of nanomaterials with several sensing mechanisms. Most methods have detection limits of the same order. Although the detection limit of our proposed sensor is not better than that found in previous reports, its selectivity due to the metallophilic interaction is quite remarkable.

**Table 2** Comparison of the sensors merits of the Hg<sup>2+</sup> sensor fabricated from various type of nanomaterials

Probe <sup>a</sup>	Linear range	LOD	Ref.
	(µM)	(µM)	
CA-Au NPs	0.05 - 3	0.03	[1]
Cytidine stabilized Au NCs	0.03 - 16	0.03	[18]
BSA-Au NCs	0.20 - 60 0.03		[19]
Citrate stabilized Au NPs	0.01 - 2	0.005	[21]
Ag NPR	0.005 - 10	0.0002	[23]
(E)- <i>N</i> , <i>N</i> '-bis(4-(Z)-2-(4-	0 - 3.0	0.24	[41]
butoxyphenyl)-1-			
cyanovinylphenyl)-1,4-			
benzenebismethaneimine			
L-cysteine-CdS QDs	-	0.001	[42]
CS@3D-rGO@DNA	0.001-0.01	0.001-0.01 0.000016	
FRET FB vs TGA-CdTe QDs	1.6-160	0.132	[44]
This work	0.10 - 3.5	0.09	-

<sup>&</sup>lt;sup>a</sup>Abbreviations: CA, cysteamine; BSA, bovine serum albumin; FB, Fluorescent brightener; CS@3D-rGO@DNA, DNA-modified nanocomposite of three-dimensional reduced graphene oxide and chitosan particle

## 4. Conclusion

In conclusion, we have developed a facile fluorescence sensor for  $\mathrm{Hg}^{2+}$  with high sensitivity and selectivity via the turn-on-off fluorescence emission strategy. The sensor was fabricated by using  $\mathrm{Ag}^+$  modulated Cys-CdS QDs to provide the fluorescence enhancement (turn-on). The fabricated sensor can be used to detect  $\mathrm{Hg}^{2+}$  based on the high-affinity metallophilic reaction with  $\mathrm{Ag}^+$  (on the surface of the QDs). In the presence of only small amount of  $\mathrm{Hg}^{2+}$ , the fluorescence quenching (turn-off) can be observed. The degree of fluorescence quenching was a linear function of the  $\mathrm{Hg}^{2+}$  concentration, allowing the quantitative analysis of  $\mathrm{Hg}^{2+}$  at trace levels. The sensor showed very good detection sensitivity and relatively low detection limit which was comparable to the CV-AAS technique. More importantly, according to the response mechanism, excellent selectivity towards the sensing of  $\mathrm{Hg}^{2+}$  can be obtained.

## References

- [1] Y. Ma, L. Jiang, Y. Mei, R. Song, D. Tian, H. Huang, Analyst 138 (2013) 5338.
- [2] J. Du, M. Liu, X. Lou, T. Zhao, Z. Wang, Y. Xue, J. Zhao, Y. Xu, Anal. Chem. 84 (2012) 8060.
- [3] V. V. Kumar, S. P. Anthony, Sens. Actuator. B-Chem. 225 (2016) 413.
- [4] N. Pourreza, K. Ghanemi, J. Hazard. Mater. 216 (2009) 982.
- [5] X. Chen, C. Han, H. Cheng, Y. Wang, J. Liu, Z. Xu, L. Hu, J. Chromatogr. A. 1314 (2013) 86.
- [6] L. Wu, Z. Long, L. Liu, Q. Zhou, Y.I. Lee, C. Zheng, Talanta 94 (2012) 146.
- [7] L. Bennun, J. Gomez, Spectrochim. Acta B 52 (1997) 1195.
- [8] M. Gräfe, E. Donner, R. N. Collins, E. Lombi, Anal. Chim. Acta 822 (2014) 1.
- [9] E. Punrat, S. Chuanuwatanakul, T. Kaneta, S. Motomizu, O. Chailapakul, J. Electroanal. Chem. 727 (2014) 78.
- [10] Y. Qiao, Y. Zhang, C. Zhang, L. Shi, G. Zhang, S. Shuang, C. Dong, H. Ma, Sens. Actuator. B-Chem. 224 (2016) 458.
- [11] Y. Su, B. Shi, S. Liao, Y. Qin, L. Zhang, M. Huang, S. Zhao, Sens. Actuator. B-Chem. 225 (2016) 334.
- [12] T.W. Sung, Y.L. Lo, I.L. Chanh, Sens. Actuator. B-Chem. 202 (2014) 1349.
- [13] A.V. Isarov, J. Chrysochoos, Langmuir 13 (1997) 3142.
- [14] J.M. Costa-Fernádez, R. Pereiro, A. Sanz-Medel, TrAC. Trends. Anal. Chem. 25 (2006) 207.
- [15] U. Tohgha, K.K. Deol, A.G. Porter, S.G. Bartko, J.K. Choi, B.M. Leonard, K. Varga, J. Kubelka, G. Muller, M. Balaz, ACS. Nano 7 (2013) 11094.
- [16] H. Chen, W. Hu, C.M. Li, Sens. Actuator. B-Chem. 215 (2015) 421.
- [17] L. Rastogi, R.B. Sashidhar, D. Karunasagar, J. Arunachalam, Talanta 118 (2014) 111.
- [18] Y. Zhang, H. Jiang, X. Wang, Anal. Chim. Acta 870 (2015) 1.
- [19] Y.W. Wang, S. Tang, H.H. Yang, H. Song, Talanta 146 (2016) 71.
- [20] J.L. MacLean, K. Morishita, J. Liu, Biosens. Bioelectron. 48 (2013) 82.
- [21] Y.L. Li, Y.M. Leng, Y.J. Zhang, T.H. Li, Z.Y. Shen, A.G. Wu, Sens. Actuator. B-Chem. 200 (2014) 140.
- [22] J. Duan, H. Yin, R. Wei, W. Wang, Biosens. Bioelectron. 57 (2014) 139.
- [23] S. Chen, J. Tang, Y. Kuang, L. Fu, F. Ma, Y. Yang, G. Chen, Y. Long, Sens. Actuator. B-Chem. 221 (2015) 1182.
- [24] X. Xu, J. Wang, K. Jiao, X. Yang, Biosens. Bioelectron. 24 (2009) 3153.
- [25] M. Xu, Z. Gao, Q. Wei, G. Chen, D. Tang, Biosens. Bioelectron. 79 (2016) 411.
- [26] P. Wu, T. Zhao, S. Wang, X. Hou, Nanoscale 6 (2014) 43.

- [27] N.B. Brahim, N.B.H. Mohamed, M. Echabaane, M. Haouari, R.B. Chaâbane, M. Negrerie, H.B. Ouada, Sens. Actuator. B-Chem. 220 (2015) 1346.
- [28] L. Zi, Y. Huang, Z. Yan, S. Liao, J. Lumines. 148 (2014) 359.
- [29] W. E. Mahmoud, Sens. Actuator. B-Chem. 164 (2012) 76.
- [30] Z. Liu, S. Liu, P. Yin, Y. He, Anal. Chim. Acta 745 (2012) 78.
- [31] H. Xu, R. Miao, Z. Fang, X. Zhong, Anal. Chim. Acta 687 (2011) 82.
- [32] P. Wu, X.P. Yan, Chem. Commun. 46 (2010) 7046.
- [33] S. Liu, W. Na, S. Pang, X. Su, Biosens. Bioelectron. 58 (2014) 17.
- [34] T. Khantaw, C. Boonmee, T. Tuntulani, W. Ngeontae, Talanta 115 (2013) 849.
- [35] J.L. Chen, C.Q. Zhu, Anal. Chim. Acta 546 (2005) 147.
- [36] L. Wang, A.N. Liang, H.Q. Chen, Y. Liu, B.B. Qian, J. Fu, Anal. Chim. Acta 616 (2008) 170.
- [37] J. Chen, A. Zheng, Y. Gao, C. He, G. Wu, Y. Chen, X. Kai, C. Zhu, Spectrochim. Acta A 69 (2008) 1044.
- [38] X. Yuan, T. J. Yeow, Q. Zhang, J. Y. Lee, J. Xie, Nanoscale 4 (2012) 1968.
- [39] T. Noipa, T. Tuntulani, W. Ngeontae, Talanta 105 (2013) 320.
- [40] S. Akshya, P.S. Hariharan, V. V. Kumar, S. P. Anthony, Spectrochim. Acta A 135 (2015) 335.
- [41] W. Fang, G. Zhang, J. Chen, L. Kong, L. Yang, H. Bi, J. Yang, Sens. Actuator. B-Chem. 229 (2016) 338.
- [42] M. L. Satnami, S. K. Vaishanav, R. Nagwanshi, K. K. Ghosh, J. Disper. Sci. Technol. 37 (2016) 196.
- [43] Z. Zhang, X. Fu, K. Li, R. Liu, D. Peng, L. He, M.a Wang, H. Zhang, L. Zhou, Sens. Actuator. B-Chem. 225 (2016) 453.
- [44] H. Tao, X. Liao, M. Xu, S. Li, F. Zhong, Z. Yi, J. Lumin. 146 (2014) 376.

# 7. Fluorescence sensor based on D-penicillamine capped cadmium sulfide quantum dots for the detection of cysteamine

## 1. Introduction

Cysteamine is a low-molecular weight aminothiol that distributes in organisms. Natural levels of free cysteamine in human plasma and rodent tissues are very low [1]. Cysteamine can however be introduced to treat nephropathic cystinosis, generating cysteine-cysteamine mixed disulfide species that allow cysteine to be released from cells [2]. Recently, the accurate measurement of cysteamine levels in the body is becoming more important for clinical studies, in the pharmaceutical industry, and in related research [3]. There are several methods that are currently used to detect cysteamine, for instance, electrochemical [4-12], high performance liquid chromatography (HPLC) [13-16], and gas chromatography (GC) [17, 18]. Generally, in chromatographic methods, samples must be passed through derivatization and extraction steps before injection into the analytical column. As such, these methods require expensive reagents and equipment, and significant time for the procedure. As an alternative, a spectrophotometric method was reported to detect cysteamine by following the absorption properties of *p*-benzoquinone (PBQ) after reaction with cysteamine [19].

Recently, developments in analytical chemistry have shown that nanomaterials can be ideal building blocks for the fabrication of chemical sensors. These nanomaterials display useful properties that are unique with respect to their bulk counterparts. Particularly, they allow fine control of optical, electrical, magnetic, and catalytic properties by subtle nanoscale structural changes due to quantum confinement effects [20]. Broad application of nanoparticles to chemical sensing derives not only from the use of different types of core nanomaterial [21-22] but also from the type of capping molecule bound at the particle surface. Recently, chiral nanomaterials have been shown to be attractive for the generation of enantiometric sensors. The chirality of nanoparticles can originate from the chirality of organic molecules used as capping agents (though there are a few reports of gold nanoparticles [23-24] and silver nanoparticles that are intrinsically chiral due to twisted structures). Chiral nanocrystalline semiconductors, or quantum dots (QDs), are also generating interest for a broad range of applications [25-27]. For example, the effect of the chiral amino acid cysteine on the optical properties of CdTe QDs has been investigated [28-29]. Furthermore, chiral cysteine-capped CdSe(ZnS) QDs were synthesized and used for selective recognition of carnitine enantiomers [30]. Recently, our group reported the synthesis of chiral cysteine-capped CdS QDs and their sensing of Ni<sup>2+</sup> and Co<sup>2+</sup> [31]. Gallagher et al. synthesized penicillamine capped CdSe QDs by microwave irradiation but did not report on the application of this material for sensing [32]. Finally, chiral CdS QDs have been synthesized using microwave heating and racemic (Rac), D- and L-enantiomeric forms of penicillamine as the stabilizers [33].

To the best of our knowledge, there is no report regarding the fabrication of fluorescence sensors based on CdS QDs for the detection of cysteamine. In this work, we synthesized **D**-penicillamine bound to cadmium sulfide quantum dots (DPA-CdS QDs) via a simple one-pot reaction. We then employed the nanomaterial as a sensor to detect cysteamine by measuring the fluorescence intensity of the DPA-CdS QDs. The selectivity and sensitivity of the proposed sensor is due to the coordination of cysteamine with available Cd<sup>2+</sup> ions on the surface of the QDs, resulting in enhanced QD fluorescence emission. Our proposed sensor may be an excellent new tool for the efficient and selective fluorescence sensing of cysteamine or related species.

## 2. Experimental

## 2.1 Reagents

All reagents were of analytical grade and used without further purification. Cysteamine hydrochloride was purchased from Sigma. D-Penicillamine was purchased from Aldrich. Sodium sulfide was purchased from BDH. Cadmium chloride (CdCl<sub>2</sub>·H<sub>2</sub>O) was purchased from Riedel-de Haën. All aqueous solutions were prepared with deionized water with specific resistivity of 18.2 M $\Omega$ .cm from RiO<sub>s</sub> TM Type I Simplicity 185 (Millipore water).

## 2.2 Instrumentation

Emission spectra were recorded using a RF-5301PC spectrofluorophotometer (Shimadzu). Absorption spectra of DPA-CdS QD solutions were recorded using an Agilent HP 8453 spectrophotometer. Transmission electron microscopy (TEM) images of DPA-CdS QDs were taken using a TecnaiG<sup>2</sup>-20 (FEI, Netherlands) under an accelerating voltage of 200 kV. Circular dichroism spectra were recorded on a Jasco-815 CD spectropolarimeter (JASCO, Japan) using a 1 cm quartz cell cuvette, with a scanning rate of 200 nm.min<sup>-1</sup>. Solution pH was measured with a UB-10 UltraBasic pH meter (Denver Instrument).

# 2.3 Synthesis of D-penicillamine capped cadmium sulfide quantum dots (DPA-CdS QDs)

The **D**-penicillamine capped cadmium sulfide quantum dots (DPA-CdS QDs) were synthesized and characterized using a previously published procedure with some modifications [34]. Briefly, CdCl<sub>2</sub>·H<sub>2</sub>O (0.0427 g, 0.212 mmol,) was dissolved in 50 mL of DI water in a three-necked round bottom flask. D-penicillamine (0.0558 g, 0.3750 mmol) was dissolved in 5 mL of DI water and added to the solution of CdCl<sub>2</sub>·H<sub>2</sub>O with stirring. After stirring the mixture under nitrogen atmosphere for 2 h, the solution pH was carefully adjusted to 10.5 using 1 M aqueous NaOH. In a different flask, Na<sub>2</sub>S·H<sub>2</sub>O (0.0146 g, 0.1875 mmol) was dissolved in 10 mL of deionized water. The Na<sub>2</sub>S solution was subsequently added into the reaction mixture under nitrogen atmosphere. After refluxing at 80 °C under nitrogen atmosphere for 2 h, the concentration of colloidal quantum dots was calculated using the original cadmium source and found to be 301.3 mg L<sup>-1</sup>.

## 2.4 Fluorescence measurements

To study the fluorescence enhancement of DPA-CdS QDs due to cysteamine binding, the following general procedures were carried out. A stock solution of 1.0 mM cysteamine was prepared by dissolving cysteamine hydrochloride in deionized water. To a 10 mL volumetric flask, 100  $\mu$ L of the DPA-CdS QDs solution was added followed by the addition of stock solution of cysteamine to a given concentration level. Then, 0.50 mL of 1.0 M Tris–HCl buffered solution pH 9.0 was added to adjust the solution pH. The mixture was made to a final volume of 10.00 mL with deionized water and then incubated at room temperature for 15 minutes. The fluorescence intensity was then measured at  $\lambda_{em}/\lambda_{ex} = 475/343$  nm. The slit widths for the excitation and emission were 5 and 10 nm, respectively.

#### 2.5 Interference studies

To evaluate the selectivity of the proposed sensor, individual stock solutions of various interference species (1.0 mM) were prepared by dissolution in deionized water. To a 10 mL volumetric flask containing 100  $\mu L$  of the DPA-CdS QDs solution was added 100  $\mu L$  of 1.0 mM of the interference species (final concentration of 10  $\mu M$ ). Then, 0.50 mL of 1.0 M Tris–HCl buffered solution pH 9.0 was added to adjust pH of the solution. The mixture was

made to a final volume of 10.00 mL with deionized water. The solution mixture was then incubated at room temperature for 15 minutes before recording the fluorescence spectrum.

## 2.6 Circular dichroism (CD) measurements

To study the circular dichroism of **D**-penicillamine, **D**-penicillamine complexed with cadmium ion ( $Cd^{2+}$ ) and DPA-CdS QDs, the following procedure was carried out. Stock solutions of **D**-penicillamine and  $Cd^{2+}$  ion (10 mM) were prepared by dissolution of **D**-penicillamine and cadmium salt in DI water. The **D**-penicillamine solution was prepared by adding 576  $\mu$ L of stock solution of **D**-penicillamine into a 10 mL volumetric flask. Then, 0.50 mL of 1.0 M Tris–HCl buffered solution pH 9.0 was added to adjust pH of the solution. The mixture of D-penicillamine and  $Cd^{2+}$  solution was prepared by adding 576  $\mu$ L of stock solution of D-penicillamine following by 267  $\mu$ L of stock  $Cd^{2+}$  solution (10 mM) into 10 mL volumetric flask. Then, 0.50 mL of 1.0 M Tris–HCl buffered solution pH 9.0 was added to adjust the pH of the solution. Finally, the DPA-CdS QDs solution was made up from 100  $\mu$ L of the synthesized DPA-CdS QDs solution (267  $\mu$ M) in a 10 mL volumetric flask with 0.50 mL of 1.0 M Tris–HCl buffered solution pH 9.0 added to adjust solution pH. All mixtures were made to a final volume of 10.00 mL with deionized water and incubated at room temperature for 10 min before recording the CD spectra.

## 2.7 Application to urine samples

In order to evaluate the applicability of the proposed sensor, two urine samples from healthy volunteers were used as representative clinical samples. Urine samples were prepared following the method reported previously [35]. Fresh urine samples were obtained from healthy volunteers and tested within 1 h following filtering (11  $\mu$ m pore size filter paper) to remove particulate matter. The samples were diluted 50 fold with 50 mM Tris-HCl buffer pH 9.0 and then equilibrated for 30 min at room temperature. In order to demonstrate the accuracy and precision of the proposed sensor, a standard solution of cysteamine with appropriate volume was spiked into the urine samples to give a final concentration of 2  $\mu$ M under the optimized conditions before recording the fluorescence spectrum. The concentration of the sample and spiked sample were calculated by comparison with the calibration curve. The accuracy and precision of the proposed sensor were demonstrated by the %recovery of the spiked standard and %RSD of three measurements, respectively.

## 3. Results and discussion

## 3.1. Characteristics and optical properties of DPA-CdS QDs

The optical properties of the DPA-CdS QDs were characterized by their absorption and emission properties as shown in Fig. 1(a). The DPA-CdS QDs show an absorption onset at about 275 nm which is related to the band gap energy of 4.51 eV. This result confirms that the synthesized particles are different from the corresponding bulk material (CdS). The emission spectrum of the DPA-CdS QDs following 343 nm excitation is narrow and symmetrical with a maximum at 475 nm. This suggests that the prepared DPA-CdS QDs are nearly homogeneous and monodisperse [36]. A large Stokes shift between the maximum absorption and emission wavelengths can be observed. This characteristic can be useful for ultra-sensitive analytical fluorescence measurements due to the elimination of spectral overlap and resulting self-absorption. Furthermore, the chiroptical properties of Dpenicillamine on QDs were evaluated in aqueous solution as compared to a solution of Dpenicillamine in the presence and absence of Cd<sup>2+</sup> ions as shown in Fig. 1(b). The spectra show that the CD spectrum of **D**-penicillamine alone exhibits only one band in the negative direction at 235 nm which decreases in the presence of Cd2+ ions. On the other hand, the CD spectrum of the DPA-CdS QDs shows a strong feature with a positive Cotton effect at 225 nm and a negative Cotton effect at 245 nm. This result indicates that the **D**-penicillamine is

capped on the surface of CdS QDs [37] (the CdS QDs alone show no CD signal). The UV-Vis, photoluminescence and CD spectra all suggest that the synthesized QDs possess good morphological and optical characteristics and might potentially be used as a sensor for specific target analytes.

The size and morphology of DPA-CdS QDs were determined by transmission electron microscopy (TEM). A TEM image of the synthesized DPA-CdS QDs is shown in Fig. 2, revealing that the DPA-CdS QD nanocrystals are near-spherical with average diameters of ca.  $3.2 \pm 0.5$  nm (n = 189).

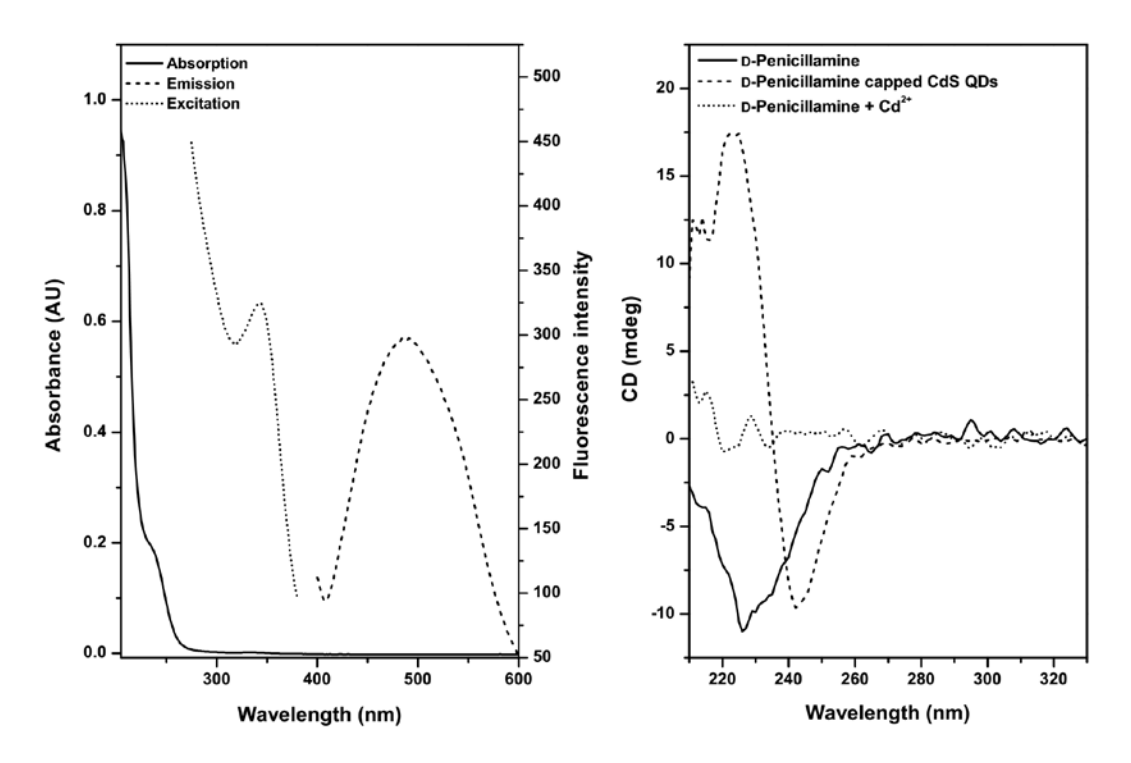


**Fig. 1** (a) The absorption and fluorescence spectra of the synthesized DPA-CdS QDs  $(\lambda_{ex}/\lambda_{em}=343/475 \text{ nm})$  (b) The circular dichroism spectra of **D**-penicillamine, **D**-penicillamine in the presence of Cd<sup>2+</sup>, and DPA-CdS QDs.

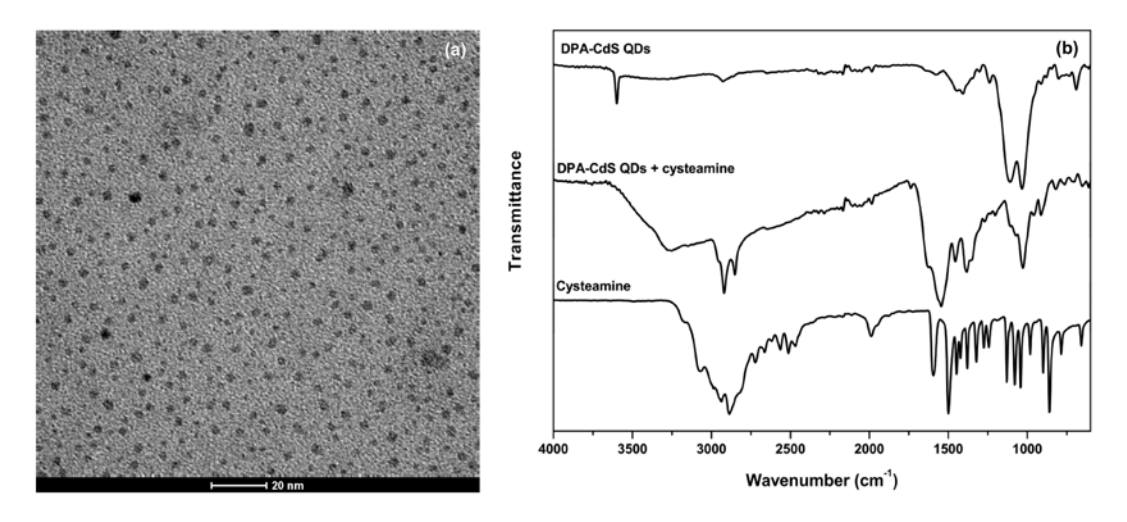


**Fig. 2** (a) The TEM image of the synthesized DPA-CdS QDs  $(3.2 \pm 0.5 \text{ nm}; n = 189)$  (b) FT-IR spectra of the precipitate of DPA-CdS QDs, cysteamine+DPA-CdS QDs and cysteamine.

## 3.2. Fluorescence enhancement of DPA-CdS QDs by cysteamine

In this work, we aim to fabricate a 'turn-on' fluorescence sensor based on the DPA-CdS QDs for the detection of cysteamine. It is well known that the fluorescence emission of nanocrystalline QDs is controlled by the rate of radiative recombination of electron—hole pairs upon band gap excitation and is sensitive to the presence of surface trap states [38]. Reports suggest that the removal of surface imperfections and dangling bonds due to binding of analytes to the QDs surface reduces surface traps, resulting in fluorescence enhancement [39-40]. The enhancement of CdS fluorescence intensity following addition of thiol molecules has been examined extensively by Pawar et al. [38] and Wang et al. [41]. They suggested that the fluorescence enhancement is due to both the lability of capping molecules and the strong affinity of thiols for the surface of CdS QDs. As seen in Fig. 3, an increase in fluorescence intensity of DPA-CdS QDs occurs after addition of cysteamine. This result implies that cysteamine plays a similar role to thiol species in previous studies [38, 41], binding to and passivating traps at the surface of DPA-CdS QDs. This further indicates that the DPA does not fully cover the CdS OD surface, there still being available Cd<sup>2+</sup> sites to form a coordinate bond with cysteamine as depicted in Scheme 1. The DPA-CdS QDs are clearly efficient fluorescence probes for detecting the presence of cysteamine.

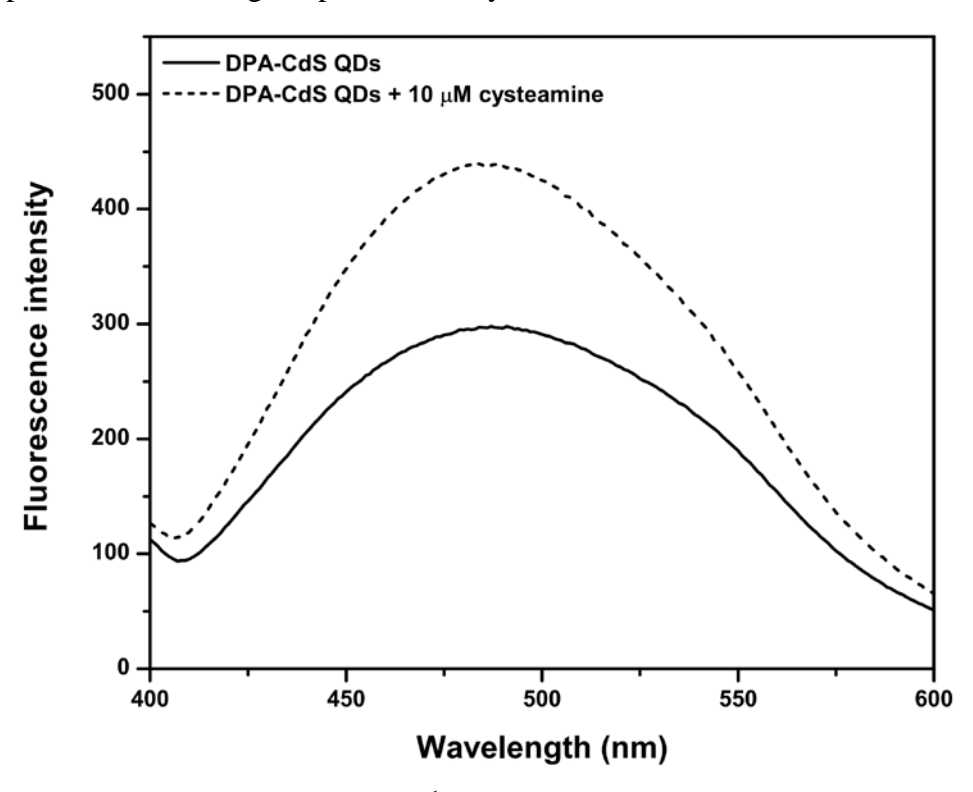
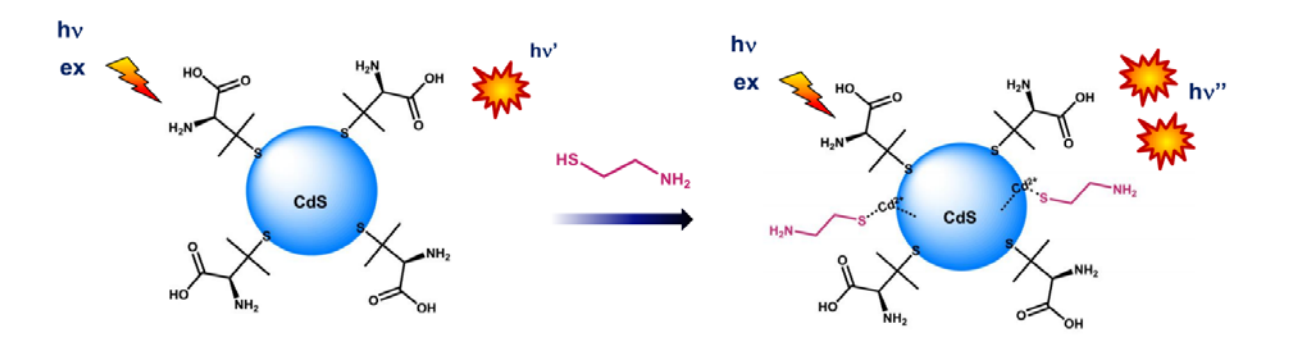


**Fig. 3** Fluorescence spectra of 15.0 mg L<sup>-1</sup> DPA-CdS QDs in 50 mM Tris–HCl buffer solution pH 9.0 in the presence and absence of 10 μM cysteamine.

To further confirm the binding of cysteamine onto the surface of the DPA-CdS QDs, the FT-IR spectra of the precipitated DPA-CdS QDs, cysteamine+DPA-CdS QDs and cysteamine were recorded as shown in Fig. 2(b). The spectra show that the characteristic peaks of cysteamine are diminished or eliminated after reaction with DPA-CdS QDs. This is

evidence for a strong interaction between the CdS QD surface and cysteamine. Importantly, the characteristic S-H stretching mode at around 2500–2600 cm<sup>-1</sup> disappeared from the FT-IR spectra of DPA-CdS QDs suggesting strong covalent binding of the cysteamine thiol to the surface of the CdS QDs [42].



**Scheme 1** Schematic illustration of a plausible mechanism for turn-on fluorescence sensing of cysteamine by DPA-CdS QDs.

## 3.4. Effect of pH

The D-penicillamine that is used as a capping molecule in this work is an  $\alpha$ -amino acid metabolite of penicillin, therefore, the pH of the solution can affect the charge of D-penicillamine on the surface of QDs and may effect the interactions between binding species such as cysteamine. To optimize the system for cysteamine sensitivity, the solution pH was varied and the fluorescence of 15.0 mg L<sup>-1</sup> DPA-CdS QDs solutions measured in the presence and absence of 10  $\mu$ M cysteamine. Phosphate buffer was used for the pH range from 6.0-7.0 and Tris-HCl buffer for pHs above 7.0. The results in Fig. 4(a) show that fluorescence intensity of DPA-CdS QDs in the absence of cysteamine decreased when the pH of the solution was increased, nevertheless the DPA-CdS QDs fluorescence was always enhanced in the presence of cysteamine. The efficiency of fluorescence sensitization (F-F<sub>0</sub>) after adding cysteamine is shown in Fig. 4(b). The results show that the best sensing conditions are obtained using 50 mM Tris-HCl buffer at pH 9.0. However, a t-test analysis shows that the fluorescence enhancement at pH 9.0 is not higher than at pH 8.5 at significance level of 0.05. Thus, in order to obtain the best detection sensitivity, solution pH in the range of 8.5-9.0 can be used.

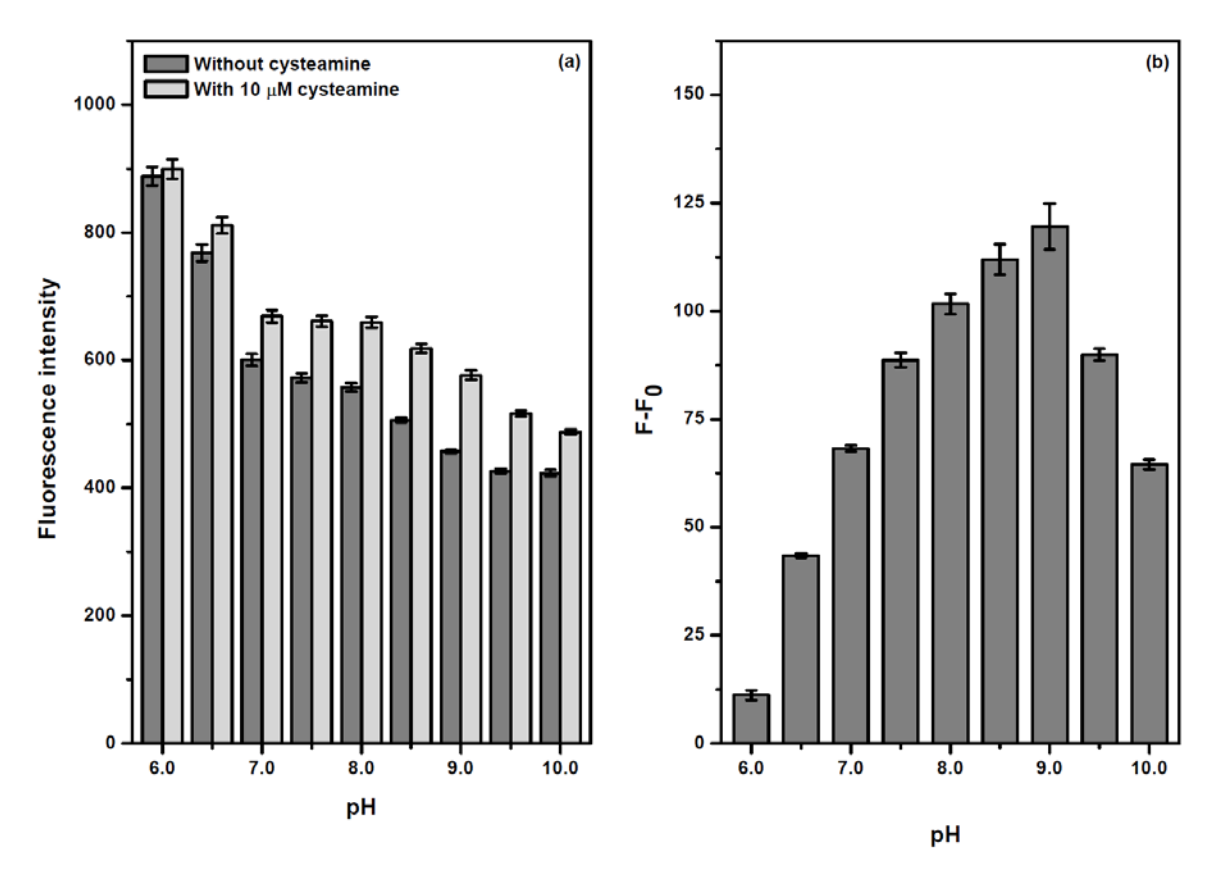


**Fig. 4** (a) Effect of solution pH on the fluorescence intensity of 15.0 mg L<sup>-1</sup> DPA-CdS QDs in 50 mM Tris–HCl buffered (pH 6.0-10.0) in the absence and presence of 10 μM of cysteamine. (b) The comparison of the fluorescence enhancement (F-F<sub>0</sub>) of DPA-CdS QDs under different pH conditions in the presence of 10 μM cysteamine. The slit width for the excitation and emission was 10 nm. Error bars indicate the standard deviation for three measurements.

## 3.5. Effect of the DPA-CdS QDs concentration

The concentration of the sensor probe is a crucial parameter in determining assay sensitivity. We varied the QDs concentration in the range 3.0 to 15.0 mg  $L^{-1}$  in 50 mM Tris-HCl buffer at pH 9.0. Fluorescence spectra of DPA-CdS QDs at different concentrations in the absence cysteamine are depicted in Fig. 5(a). As expected the fluorescence intensities increase with increasing QD concentration, and in the presence of 10  $\mu$ M cysteamine, the QD fluorescence intensity is enhanced at each concentration level. The degree of fluorescence enhancement (F-F<sub>0</sub>) observed upon the addition of cysteamine is compared in Fig. 5(b). These results indicated that the highest fluorescence enhancement was obtained for a DPA-CdS QDs concentration of 15.0 mg  $L^{-1}$ . Thus, 15.0 mg  $L^{-1}$  concentration of DPA-CdS QDs was then applied for further investigation.

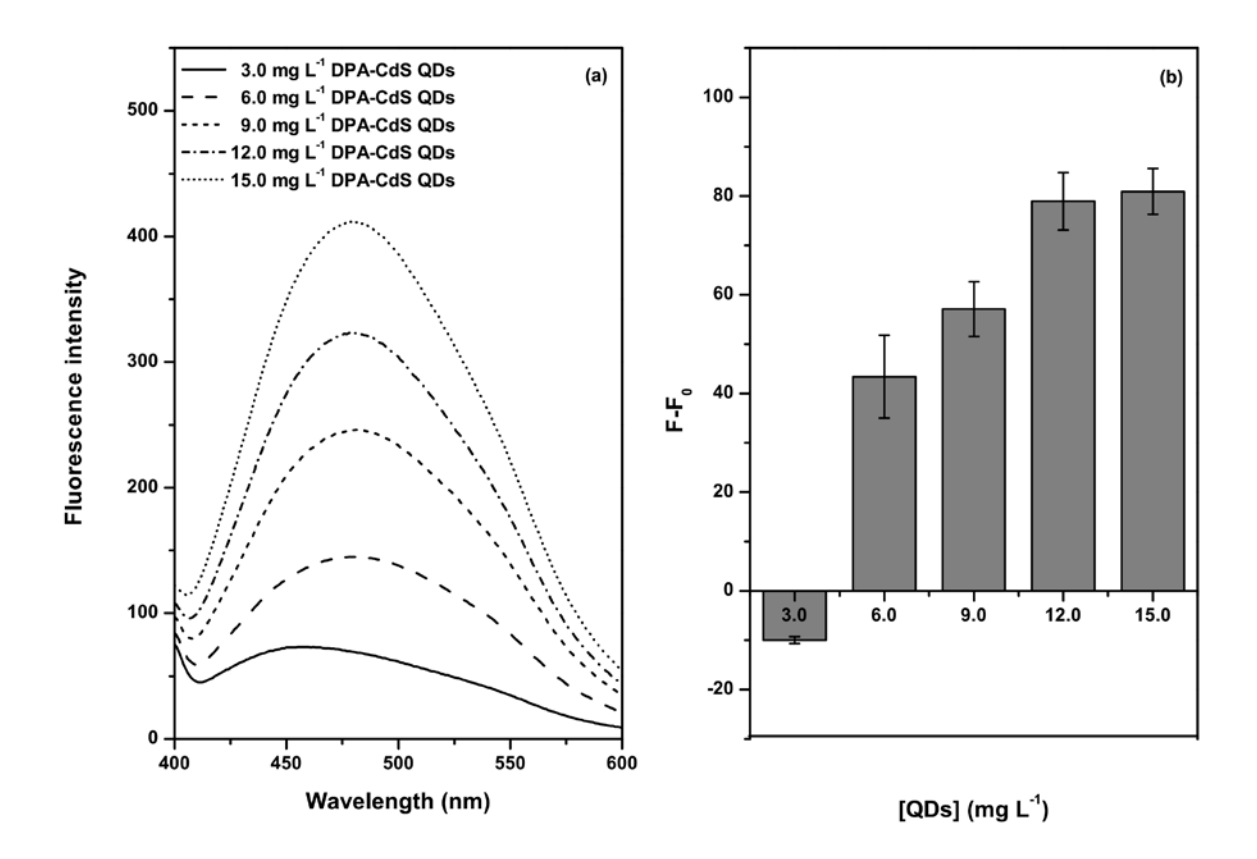


**Fig. 5** (a) Fluorescence spectra of DPA-CdS QDs at different concentrations in 50 mM Tris–HCl buffered solution pH 9.5 (b) The comparison of fluorescence enhancement (F-F<sub>0</sub>) of DPA-CdS QDs after the addition of 10  $\mu$ M cysteamine at different DPA-CdS QDs concentration.

## 3.6. Incubation time

The effect of the incubation time on cysteamine detection efficiency was also investigated. Fluorescence spectra were measured from 0 to 60 minutes, every 5 minutes, after combining DPA-CdS QDs and 10  $\mu$ M cysteamine in 50 mM Tris–HCl buffer solution pH 9.0 at room temperature (Fig. 6 (a)). The fluorescence intensity of an independent DPA-CdS QDs solution was also monitored (Fig. 6(b)). The fluorescence intensities of the DPA-CdS QDs were stable over the whole range studied revealing the photostability of the sensor probe, however in the presence of cysteamine, fluorescence intensity continued to increase over time. To ensure consistency, a standard incubation time of 15 min was employed before recording the fluorescence spectra in all further studies.

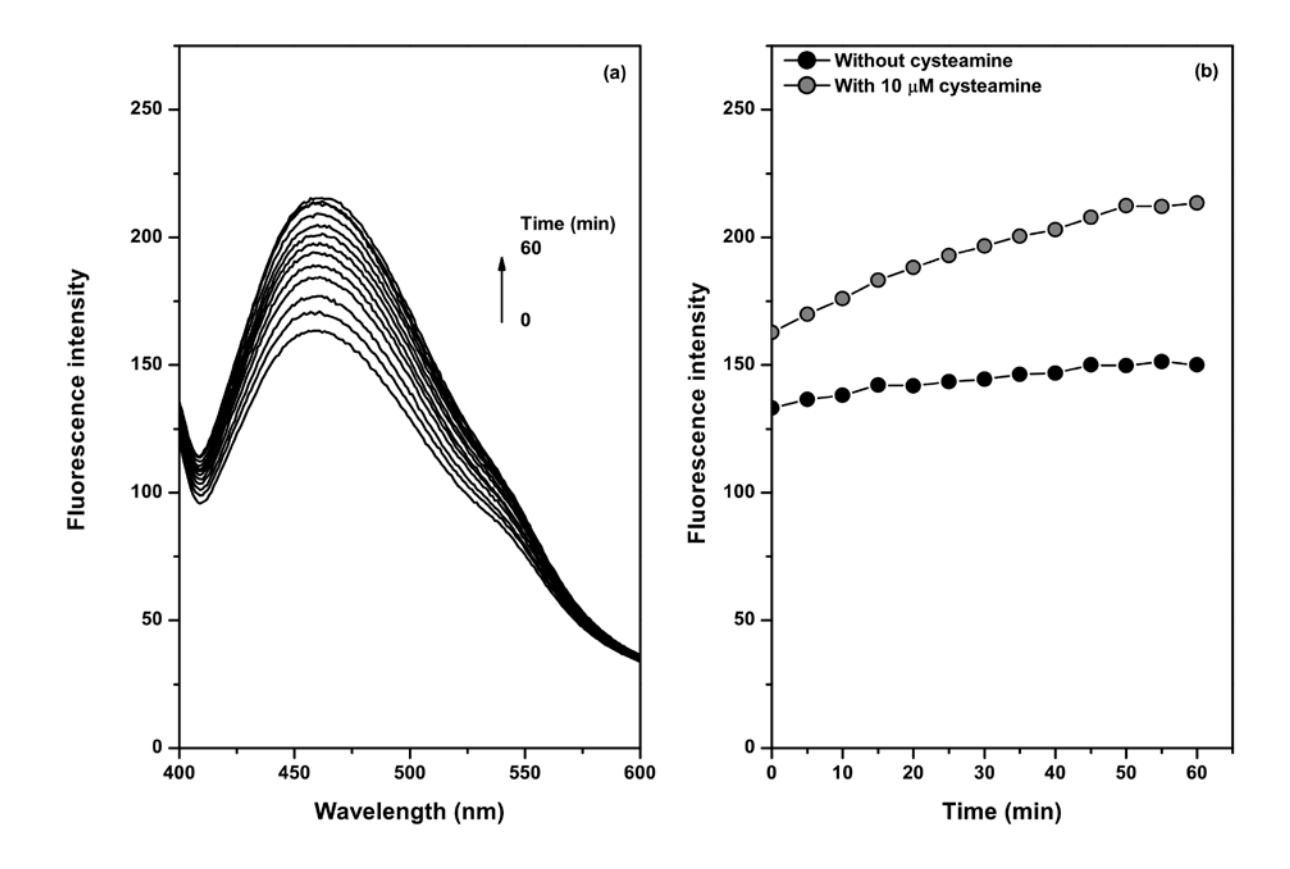


**Fig. 6** (a) Fluorescence spectra of DPA-CdS QDs in the presence of 10 μM cysteamine in 50 mM Tris–HCl buffer solution pH 9.0 at different incubation times (b) Fluorescence intensity of DPA-CdS QDs in the absence and presence of 10 μM cysteamine in 50 mM Tris–HCl buffer solution pH 9.0 at different incubation times

## 3.7. Selectivity

DPA-CdS QDs fluorescence sensing of cysteamine here likely functions by thiol functional group binding to  $Cd^{2+}$  on the surface of the DPA-CdS QDs. Other species that can bind with  $Cd^{2+}$  on the QD surface would thus interfere with cysteamine detection. The selectivity of the sensor was thus evaluated by measuring fluorescence spectra of DPA-CdS QDs before and after adding 10  $\mu$ M of possible interfering species such as amino acids or synthetic amines (Fig. 7(a)). The fluorescence intensity enhancement (F-F<sub>0</sub>) upon addition of the interfering species is compared with that for cysteamine in Fig. 7(b). The results show that the fluorescence intensity of DPA-CdS QDs is dramatically increased only in the presence of cysteamine. Only melamine showed any significant fluorescence enhancement, but still far less than observed for cysteamine. Thus, our system proved to be highly selective towards cysteamine over other amino compounds.

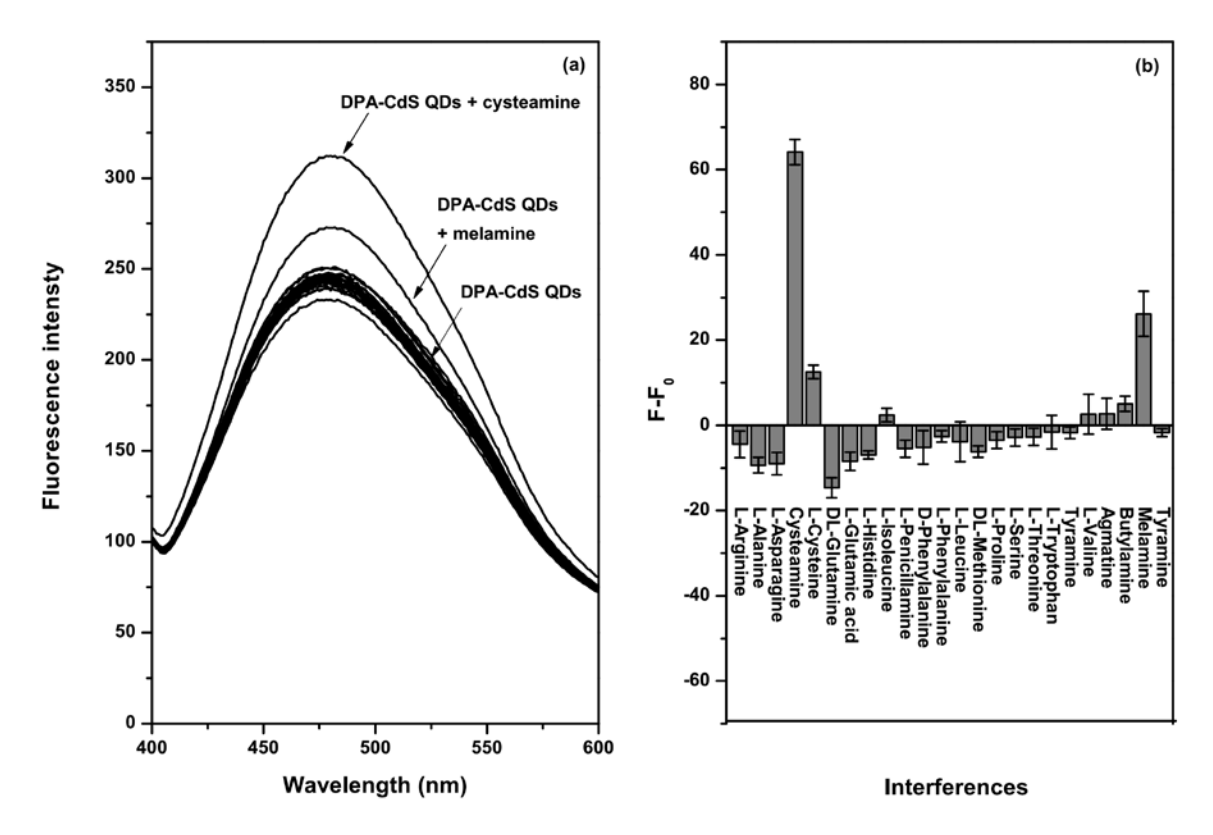


**Fig. 7** (a) Fluorescence spectra of DPA-CdS QDs before and after addition of 10 μM of several amine-containing compounds in 50 mM Tris–HCl buffered solution pH 9.0.(b) The comparison of fluorescence enhancement of DPA-CdS QDs by 10 μM cysteamine or several other amine containing compounds in 50 mM Tris–HCl buffered solution pH 9.0

## 3.8. Analytical performance of the proposed sensor

Sensitivity for cysteamine was assessed under the optimized conditions discussed above. Enhancement of DPA-CdS QDs fluorescence intensity increased linearly with the cysteamine concentration in the concentration range 2-10  $\mu$ M as shown in Fig. 8. The regression equation was observed to be F-F<sub>0</sub> = 15.32 [cysteamine,  $\mu$ M] + 13.11 ( $r^2$  =0.9887). The limit of detection (LOD) and limit of quantitation (LOQ) were then determined to assess sensor performance. The LOD was calculated as the concentration of analyte giving the enhancement of fluorescence intensity (F-F<sub>0</sub>) equal to 3 standard deviations of F<sub>0</sub>, while the LOQ was measured as the concentration of analyte giving a fluorescence intensity enhancement (F-F<sub>0</sub>) equal to 10 standard deviations of F<sub>0</sub>. The LOD and LOQ of the proposed sensor were found to be were 0.07 and 2.23  $\mu$ M, respectively.

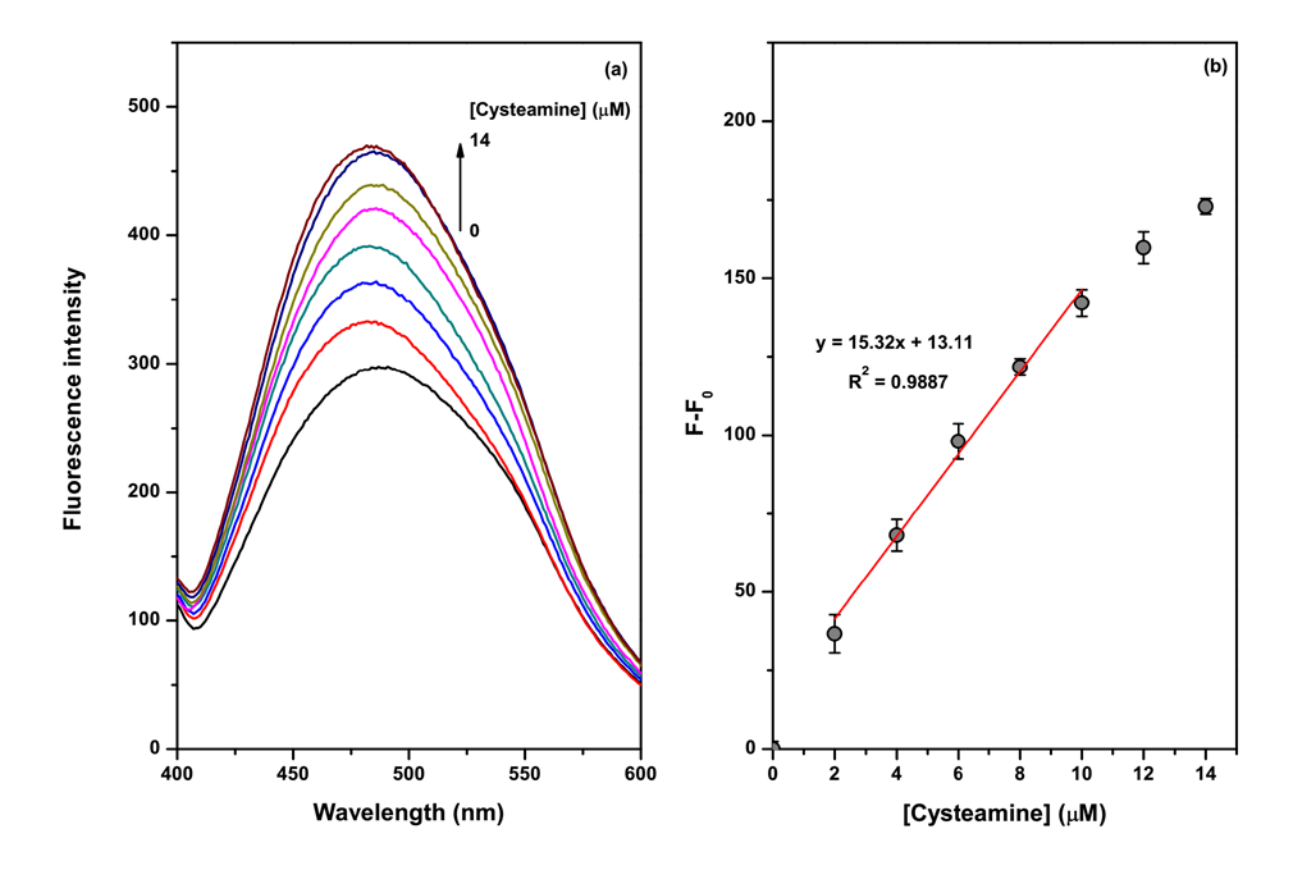


**Fig. 8** (a) The fluorescence spectra of 15.0 mg  $L^{-1}$  DPA-CdS QDs in the presence of cysteamine 0-14  $\mu$ M in 50 mM Tris–HCl buffer solution pH 9.0 (b) The corresponding calibration curve.

## 3.9. Application to human urine samples

In order to demonstrate the feasibility of the proposed sensor in real world applications, it was used to measure the amount of cysteamine in human urine samples by using the standard addition method, and the recoveries were calculated. The results are listed in Table 1. After spiking cysteamine into the urine samples, the average recovery of cysteamine was 92 - 93% and the RSD less than 6.4%. These results confirm that the proposed sensor shows both high accuracy and precision in terms of %RSD and %recovery and that it can be successfully applied to the determination of cysteamine concentration in real urine samples.

**Table 1.** Determination of cysteamine in real urine samples (n=3)

Samples	Spiked (µM)	Found $\pm$ SD $(\mu M)^a$	Recovery (%)	RSD (%)
Sample No. 1	0.0	$0.78 \pm 0.09$	_	_
Swii-pro 1 (ov 2	2.0	$2.64 \pm 0.12$	93	6.4
Sample No. 2	0.0	$0.31 \pm 0.11$	_	_
Sample No. 2	2.0	$2.14 \pm 0.06$	92	3.3

 $a \overline{Mean} \pm SD (n = 3)$ 

## 3.10 Comparison of the merits of the method for cysteamine detection

There are several methods that have been proposed for detection of cysteamine, as summarized in Table 2. Most methods are based on the electrochemistry approach using modified electrodes with appropriate mediators and display detection limits of the same order of magnitude. Although the detection limit of our proposed sensor is not better than those found in previous reports, its selectivity and simplicity is quite remarkable.

**Table 2** Comparison of the merits of methods for cysteamine detection

<b>Detection method</b>	Working range	Detection limit	Type of real samples	Ref.
Electrochemistry with Nq/gold electrode	8-550 μΜ	5.2 μΜ	-	[4]
Electrochemistry with MWCNTPE using 3,4-DHCA as a mediator	0.25-400 μΜ	0.09 μΜ	Capsule and urine	[5]
Electrochemistry with MWCNTPE using <i>p</i> -aminophenol as a mediator	$0.5–300~\mu M$	0.14 μΜ	Capsule and urine	[6]
Electrochemistry with MWCNTPE using ISPT as a mediator	0.3–450 μΜ	0.09 μΜ	Urine and drug	[7]
Electrochemistry with Ferrocene/CNTPE	0.7–200 μΜ	0.30 μΜ	Tablet, serum and urine	[8]
Electrochemistry with NiONPs/CPE	0.09–300.0	µ 0.06 µľ	Urine and capsule	[9]
Electrochemistry with N-4-HP- DNBA/MgONPs/CPE	0.03-600 μΜ	0.009 μΜ	Capsule and serum	[11]
Electrochemistry with DEDE/ NiO/CNTs/CPE	$0.01-250~\mu M$	$0.007~\mu M$	Urine and tablet	[12]
HPLC with fluorescence detection	$2-150  \mu M$	0.5 μΜ	Human serum	[15]
GC with flame photometric detection	0.2–5.0 nmol	0.5 pmol	mouse tissue	[17]
Fluorescence sensor with BSA- Au <sub>25</sub> nanoclusters	5–100 μΜ	0.15 μΜ	Human serum sample	[22]
Fluorescence sensor with DPA-CdS QDs	1.45-10 μΜ	0.23 μΜ	Urine sample	This work

<sup>a</sup>Abbreviations: Nq, 1,2-naphthoquinone-4-sulfonic acid; MWCNTPE, modified multiwall carbon nanotubes paste electrode; 3,4-DHCA, 3,4-dihydroxycinnamic acid; ISPT, isoproterenol; CPE, carbon paste electrode; N-4-HP-DNBA, *N*-(4-hydroxyphenyl)-3,5-dinitrobenzamide; MgONPs, magnesium oxide nanoparticles; CNTPE, carbon nanotube paste electrode; DEDE, (9, 10-dihydro-9, 10-ethanoanthracene-11, 12-dicarboximido)-4-ethylbenzene-1,2-diol and BSA, bovine serum albumin

## 4. Conclusion

In summary, we have successfully developed a sensitive and selective turn-on fluorescence sensor for cysteamine using DPA-CdS QDs. In the presence of cysteamine, the fluorescence intensity enhancement of DPA-CdS QDs increases linearly with increasing cysteamine concentration up to 10  $\mu M$ . The fluorescence enhancement is attributed to the quenching of surface trap states by the binding of the mercapto group of cysteamine at Cd²+ sites on the surface of the DPA-CdS QDs. Our sensor displays excellent selectivity towards

cysteamine and has a limit of detection and limit of quantification of 0.07 and  $2.23~\mu\text{M}$ , respectively. Finally, the potential for real-world application of our sensor is demonstrated by its effective operation in human urine samples.

## References

- [1] T. Khomenko, J. Kolodney, J.T. Pinto, G.D. McLaren, X. Deng, L. Chen, G. Tolstanova, B. Paunovic, B.F. Krasnikov, N. Hoa, A.J.L. Cooper, S. Szabo, Arch. Biochem. Biophys. 525 (2012) 60.
- [2] P. Lochman, T. Adam, D. Friedecký, E. Hlídková, Z. Skopková, Electrophoresis 24 (2003) 1200.
- [3] D.A.M. Zaia, K.C.L. Ribas, C.T.B.V. Zaia, Talanta 50 (1999) 1003.
- [4] J.B. Raoof, R. Ojani, F. Chekin, J. Mater. Sci. 44 (2009) 2688.
- [5] M. Keyvanfard, S. Sami, H. Karimi-Maleh, K.H. Alizad, J. Braz. Chem. Soc. 24 (2013) 32.
- [6] A.A. Ensafi, H. Karimi-Maleh, Electroanalysis 22 (2010) 2558.
- [7] M. Keyvanfard, M. Ahmadi, F. Karimi, K. Alizad, Chin. Chem. Lett. 25 (2014) 1244.
- [8] A. Taherkhani, H. Karimi-Maleh, A.A. Ensafi, H. Beitollahi, A. Hosseini, M.A. Khalilzadeh, H. Bagheri, Chin. Chem. Lett. 23 (2012) 237.
- [9] H. Karimi-Maleh, M. Salimi-Amiri, F. Karimi, M.A. Khalilzadeh, M. Baghayeri, J. Chem. 2013 (2013) 1.
- [10] I.S El-Hallag, A.O. Al-Youbi, A.Y. Obaid, E.H. El-Mossalamy, S.A. El-Daly, A.M. Asiri, J. Chil. Chem. Soc. 56 (2011) 837.
- [11] V. Arabali, H. Karimi-Maleh, Anal. Methods 8 (2016) 5604.
- [12] H. Karimi-Maleh, P. Biparva, M. Hatami, Biosens. Bioelectron. 48 (2013) 270.
- [13] B.D. Soriano, L.T.T. Tam, H.S. Lu, V.G. Valladares, J. Chromatogr. B 880 (2012) 27.
- [14] M.J. Kelly, D. Perrett, S.R. Rudge, Biomed. Chromatogr. 2 (1987) 216.
- [15] M. Stachowicz, B. Lehmann, A. Tibi, P. Prognon, V. Daurat, D. Pradeau, J. Pharm. Biomed. Anal. 17 (1998) 767.
- [16] A.J. Jonas, J.A. Schneider, Anal. Biochem. 114 (1981) 429.
- [17] H. Kataoka, Y. Imamura, H. Tanaka, M. Makita, J. Pharm. Biomed. Anal. 11 (1993) 963.
- [18] H. Kataoka, H. Tanaka, M. Makita, J. Chromatogr. B. 657 (1994) 9.
- [19] D.A.M. Zaia, K.C.L. Ribas, C.T.B.V. Zaia, Talanta 50 (1999) 1003.
- [20] X. Zhang, J. Yin, J. Yoon, Chem. Rev. 114 (2014) 4918.
- [21] K. Ngamdee, T. Tuntulani, W. Ngeontae, Sens. Actuator. B-Chem. 216 (2015) 150.
- [22] T. Shu, L. Su, J. Wang, C. Li, X. Zhang, Biosens. Bioelectron. 66 (2015) 155.
- [23] H. Yao, K. Miki, N. Nishida, A. Sasaki, K.J. Kimura, J. Am. Chem. Soc. 127 (2005) 15536.
- [24] T.G. Schaaff, R.L. Whetten, J. Phys. Chem. B 104 (2000) 2630.
- [25] Y. Xia, Y. Zhou, Z. Tang, Nanoscale 3 (2011) 1374.
- [26] M.V. Mukhina, A.S. Baimuratov, I.D. Rukhlenko, V.G. Maslov, F.P. Milton, Y. K. Gun'ko, A.V. Baranov, A. V. Fedorov, ACS Nano. 10 (2016) 8904.
- [27] J.K. Choi, B.E. Haynie, U. Tohgha, L. Pap, K.W. Elliott, B.M. Leonard, S.V. Dzyuba, K. Varga, J. Kubelka, M. Balaz, ACS Nano. 10 (2016) 3809.
- [28] T. Nakashima, Y. Kobayashi, T. Kawai, J. Am. Chem. Soc. 131 (2009) 10342.
- [29] Y. Zhou, M. Yang, K. Sun, Z. Tang, N.A. Kotov, J. Am. Chem. Soc. 132 (2010) 6006.
- [30] C. Carrillo-Carrión, S. Cárdenas, B.M. Simonet, M. Valcárcel, Anal. Chem. 81 (2009) 4730.
- [31] W. Tedsana, T. Tuntulani, W. Ngeontae, Anal. Chim. Acta 867 (2014) 1.
- [32] S.A. Gallagher, M.P. Moloney, M. Wojdyla, S.J. Quinn, J.M. Kelly, Y.K. Gun'ko, J. Mater. Chem. 20 (2010) 8350.
- [33] M.P. Moloney, Y.K. Gun'ko, J.M. Kelly, Chem. Commun. 38 (2007) 3900.
- [34] T. Noipa, T. Tuntulani, W. Ngeontae, Talanta 105 (2013) 320.
- [35] W. Li, Z. Nie, X. Xu, Q. Shen, C. Deng, J. Chen, S. Yao, Talanta 78 (2009) 954.

- [36] C.R. Tang, Z.H. Su, B.G. Lin, H.W. Huang, Y.L. Zeng, S. Li, H. Huang, Y.J. Wang, C.X. Li, G.L. Shen, R.Q. Yu, Anal. Chim. Acta 678 (2010) 203.
- [37] K. Ngamdee, T. Puangmali, T. Tuntulani, W. Ngeontae, Anal. Chim. Acta 898 (2015) 93.
- [38] S.P. Pawar, A.H. Gore, L.S. Walekar, P.V. Anbhule, S.R. Patil, G.B. Kolekar, Sens. Actuator. B-Chem. 209 (2015) 911.
- [39] T. Khantaw, C. Boonmee, T. Tuntulani, W. Ngeontae, Talanta 115 (2013) 849.
- [40] Y. Lou, Y. Zhao, J. Chen, J. Zhu, J. Mater. Chem. C 2 (2014) 595.
- [41] G.L. Wang, Y.M. Dong, H.X. Yang, Z.J. Li, Talanta 83 (2011) 943.
- [42] R. Mohammad-Rezaei, H. Razmi, H. Abdolmohammad-Zadeh, Luminescence 28 (2013) 503.

# Output

# ผลงานตีพิมพ์ในวารสารระดับนานาชาติจำนวน 7 บทความดังนี้

- 1. Chaiendoo, K., Tuntulani, T., Ngeontae, W. A highly selective colorimetric sensor for ferrous ion based on polymethylacrylic acid-templated silver nanoclusters, *Sens. Actuators B.*, 2015; 207: 658–667. (IF2015 = 4.758)
- 2. Ngamdee, K., Tuntulani, T., Ngeontae, W. L-Cysteine modified luminescence nanomatrials as fluorescence sensor for  $Co^{2+}$ : effects of core nanomaterials in detection selectivity, *Sens. Actuators B.*, 2015; 216, 150-158. (IF2015 = 4.758)
- 3. Tedsana, W., Tuntulani, T., Ngeontae, W. A circular dichroism sensor for Ni<sup>2+</sup> and Co<sup>2+</sup> based on L-Cysteine capped cadmium sulfide quantum dots, *Anal. Chim. Acta*, 2015; 867: 1-8. (IF2015 = 4.712)
- 4. Ngamdee, K., Puangmali, T., Tuntulani, T., Ngeontae, W. Circular dichroism sensor based on cadmium sulfide quantum dots for chiral identification and detection of penicillamine, *Anal. Chim. Acta*, 2015; 898, 93-100. (IF2015 = 4.712)
- 5. Boonme, C., Noipa, T., Tuntulani, T., Ngeontae, W. Cysteamine capped CdS quantum dots as a fluorescence sensor for the determination of copper ion exploiting fluorescence enhancement and long-wave spectral shifts, *Spectroc. Acta Pt. A-Molec. Biomolec. Spectr.*, 2016; 169, 161-168. (IF2015 = 2.653)
- 6. Uppa, Y., Kulchat, S., Ngamdee, K., Pradublai, K., Tuntulani, T., Ngeontae, W. Silver ion modulated CdS quantum dots for highly selective detection of trace Hg<sup>2+</sup>, *J. Lumines.*, 2016; 178, 437-445. (IF2015 = 2.693)
- 7. Ngamdee, K., Kulchat, S., T., Tuntulani, T., Ngeontae, W. Fluorescence sensor based on D-penicillamine capped cadmium sulfide quantum dots for the detection of cysteamine, *J. Lumines.*, 2017; 187, 260–268. (IF2015 = 2.693)

## ภาคผนวก

# ผลงานตีพิมพ์

- 1. Chaiendoo, K., Tuntulani, T., Ngeontae, W. A highly selective colorimetric sensor for ferrous ion based on polymethylacrylic acid-templated silver nanoclusters, *Sens. Actuators B.*, 2015; 207: 658–667. (IF2015 = 4.758)
- 2. Ngamdee, K., Tuntulani, T., Ngeontae, W. L-Cysteine modified luminescence nanomatrials as fluorescence sensor for Co<sup>2+</sup>: effects of core nanomaterials in detection selectivity, *Sens. Actuators B.*, 2015; 216, 150-158. (IF2015 = 4.758)
- 3. Tedsana, W., Tuntulani, T., Ngeontae, W. A circular dichroism sensor for Ni<sup>2+</sup> and Co<sup>2+</sup> based on L-Cysteine capped cadmium sulfide quantum dots, *Anal. Chim. Acta*, 2015; 867: 1-8. (IF2015 = 4.712)
- 4. Ngamdee, K., Puangmali, T., Tuntulani, T., Ngeontae, W. Circular dichroism sensor based on cadmium sulfide quantum dots for chiral identification and detection of penicillamine, *Anal. Chim. Acta*, 2015; 898, 93-100. (IF2015 = 4.712)
- 5. Boonme, C., Noipa, T., Tuntulani, T., Ngeontae, W. Cysteamine capped CdS quantum dots as a fluorescence sensor for the determination of copper ion exploiting fluorescence enhancement and long-wave spectral shifts, *Spectroc. Acta Pt. A-Molec. Biomolec. Spectr.*, 2016; 169, 161-168. (IF2015 = 2.653)
- 6. Uppa, Y., Kulchat, S., Ngamdee, K., Pradublai, K., Tuntulani, T., Ngeontae, W. Silver ion modulated CdS quantum dots for highly selective detection of trace Hg<sup>2+</sup>, *J. Lumines.*, 2016; 178, 437-445. (IF2015 = 2.693)
- 7. Ngamdee, K., Kulchat, S., T., Tuntulani, T., Ngeontae, W. Fluorescence sensor based on D-penicillamine capped cadmium sulfide quantum dots for the detection of cysteamine, *J. Lumines.*, 2017; 187, 260–268. (IF2015 = 2.693)